TECHNIQUES

FOR AUTOMATIC ASSEMBLY

A thesis presented for the degree of

Doctor of Philosophy in Mechanical Engineering

at the

University of Canterbury,

Christchurch, New Zealand

by

C. H. H. WOHLERT-JENSEN

1978

TO MY PARENTS

ACKNOWLEDGEMENTS

My sincere thanks to my supervisor Professor H. McCallion for his guidance and encouragement.

I also extend my gratitude to Professor D. C. Stevenson for the use of the Departmental facilities and to other academic and technical staff, in particular, Messrs. G. Johnson, E. Retallick and O. Bolt.

I wish to thank Mrs. J. Ritchie for both graphic and photographic assistance and Miss B. Nottingham for typing.

ABSTRACT

The objective of the research work carried out was the development of techniques useful in automated assembly. In particular, methods were sought which would allow the extension of simple robot capabilities from the "pick and place" function to the less ordered domain of assembly. Three approaches towards correcting the gross misalignment of a peg and hole are described.

An established method of facilitating assembly involves the vibration of the contacting misaligned components. This technique was studied with respect to the behaviour of an elastically constrained peg under the action of a rotating force. The study was limited initially to a relatively straightforward analysis of simplified situations, then, in order to allow the prediction of the behaviour of practical systems a program was developed which simulated the behaviour of a general nine degree-of-freedom assembly system.

This work led to the second approach where the possibility of using the vibrational motion of the contacting components as feedback for position sensing was investigated.

The third technique involved determining the spatial relationship between the components on the basis of contact forces sensed in their respective coordinate systems.

Finally a six degree-of-freedom force-displacement sensor, able to be used for, either vibratory position sensing, or contact force position sensing, was developed.

CONTENTS

Page

Page

Page

CHAPTER 1

INTRODUCTION

The majority of robots on todays industrial scene are open-loop devices operating in either "point to point" or "continuous motion" modes. The manipulative skills of these robots may be extended by the addition of job-oriented hardware, such as locating pegs, chamfers, or vibrators, or by the incorporation of a sensor-driven feedback loop. Both these approaches are used in this thesis.

Initially, however, the field of robotics is surveyed from both a technical and a social point of view. The technical aspect provides a frame of reference for the content of the thesis. The social view uses, figuratively speaking, a wide angle lens to examine the common justifications for the robot.

In Chapter 3 the general problem of assembly is sketched out and the peg-hole configuration is defended as a case for further study. Work on the geometric and physical interactions of this configuration completes the Chapter and provides a foundation for following work.

Chapters 4 to 8 are grouped together to form Part 1. Here the use of vibrations as a method of facilitating assembly is considered.

In Chapter 4 simple analytic analyses of vibratory assembly are performed to determine the basic conditions under which assembly may occur.

The work of Chapter 4 is then used in the design of a vibratory assembler, the operation of this test rig being described qualitatively and quantitatively in Chapter 5.

Chapter 4 deals with simplified situations; assembly modes are examined in isolation and simple constraints are used. As the assembly process in general is characterized by a wide range of misalignment modes, a full analytical solution would involve an analysis and determination of the limits of application and boundary conditions of each mode. Also more complex manipulator constraints lead to off-diagonal terms in stiffness and damping matrices, complicating analytical solutions. Hence it was decided to use a computer simulation to provide a method whereby the general principles found in Chapter 4 could be employed in the design situation.

The equations of motion of a general nine degree-of-freedom assembly mechanism are developed and two methods of solution described in Chapter 6.

The behaviour of the resulting computer programs is evaluated in Chapter 7 by comparing simulated results with analytical solutions of particular cases.

In Chapter 8 the final program is used to investigate the behaviour of a particular system.

The possibility of using the vibratory motion of components as a method of position sensing is put forward in Part 2 which contains only one chapter, Chapter 9. Limited experimental work indicates the feasibility of this approach.

In Part 3 containing Chapter 10 another position sensing technique utilizing six degree-of-freedom (6 d.o.f.) force sensing is proposed. 6 d.o.f. force sensors based on strain gauge, piezo-electric, or electro-magnetic transducers, are often incorporated into the wrists of manipulators. The contact forces existing between components during assembly therefore may be felt and used to provide feedback. The major effort in this area

has centred on the determination of theoretical or experimental correlations between the sensed force and component misalignment. Essentially therefore the resulting manipulator controlling algorithms are probabilistic. The approach described in Chapter 10, in which we assume forces associated with both components may be sensed, differs in that the forces felt uniquely specify the misalignment.

Finally Part 4, Chapter 11, describes the construction and calibration of two 6 d.o.f. force displacement sensors suitable for either contact force or vibratory position sensing. The calibration accuracy of 6 d.o.f. force sensors is often limited by the accuracy of the calibration loads. A novel method which eliminates the usual problems is described.

CHAPTER 2

PERSPECTIVES

A major feature of mid-twentieth century technology has been the extension of man's computing and controlling powers by electronic technology and the science of cybernetics. This change has affected virtually all areas of business and industry in developed countries with general purpose computers performing data handling, computation, and control.

As the cost of machine intelligence decreases it becomes possible to further extend the use of machines into areas of work previously occupied by humans. One large area potentially open to advanced automation is that of assembly, an activity at present absorbing the efforts of almost half the industrial workforce. In this Chapter we examine both the technical state of, and social justification for, robots.

2.1 TECHNICAL PERSPECTIVE

The scope of assembly work is immense and in this section only major areas of research and application will be mentioned.

Assembly of components where tolerances are carefully maintained may be performed by simple position-controlled manipulators, possibly using jigs, chamfers, and vibratory forces [1]. An impressive example of this approach was the effort of Kawasaki Heavy Industries where a pilot line incorporating 10 Unimate robots, together with work feeders, was developed for the assembly of small petrol engines. The absence of sensors created a heavy reliance on jigging, and as a result the system failed to prove itself cost effective and has since been dismantled [2].

An assembly machine capable of a high level of versatility within a given product family, in this case post office relays, has been successfully developed at the University of Nottingham [3].

For less structured environments some form of feedback is necessary and a second category may be defined. These machines utilize information from tactile, sonic, or visual sensors to provide inputs to a controlling algorithm. A well known example is the Japanese Hi-T-Hand, a sequentially controlled assembly robot, with wrist force sensors, capable of assembling cylindrical components with a clearance of 20 microns [4]. The potential of visual feedback is demonstrated by a system developed at General Motors where the position of studs on an automobile hub is found from a TV picture, using pattern recognition techniques, thus allowing the wheel to be fitted [5]. Manipulators of this type are useful provided the modes of misalignment are limited and the assembly motion is simple.

More complicated situations demand the use of an adaptive controlling program and we may begin to use the adjective "intelligent" in describing machines of this third category. Work in this area falls into the fields of pattern recognition and problem solving. Kinoshita et al. [6] have developed a tactile-sensor equipped hand which is capable of determining the shape of a grasped object from the resulting stress distribution. This scheme, employing a trainable pattern classifier, can discriminate between a cylinder, a trigonal prism, and a square prism. Similar work is reported by Okada and Tsuchiya [7] and Stojiljkovic and Saletic [8]. Both pattern recognition and problem solving abilities are present in a program developed by Ejiri et al. [9]; a line drawing and a disordered scene containing building blocks are analyzed and a strategy to build the object in the drawing is developed by the program. Related work has been performed at Edinburgh and at MIT. [10], however at this stage these third

generation systems only exist within the laboratory environment.

At the Stark Draper Laboratories efforts have been made to examine the problem of assembly from a theoretical viewpoint. At the macro level work has concentrated on a detailed analysis of the assembly sequence, tools, and jig requirements etc. [11]. The micro view deals with the mechanics of assembly, the interaction of components, and the forces and trajectories required for assembly [12].

Assuming the continuation of the present industrial order, the future development of robotic automation is likely to continue along the following paths. The improving utility of simple position controlled robots should make them an evermore attractive proposition to industry. Both modular assembly systems and more general 6 d.o.f. manipulators are contenders in this market [13]. The decreasing price and increasing power of electronic hardware should continue to stimulate the development of 2nd and 3rd generation robots [14] [15].

2.2 SOCIAL PERSPECTIVE

Possession of the technical ability to build new machinery does not automatically justify its employment, therefore in this section we shall examine the raison d'être of robots in the wider context of the overall sociotechnical system.

The arguments advanced by the proponents of robotic automation may be divided into two categories. Firstly, economic grounds, often expressed in the economic concepts of cost accounting, where robots are seen as being able to provide profitable reliable labour in an industrial scene increasingly plagued by unrest and rising labour costs. [16] [17] [18] [19] [20] [21].

Secondly, social arguments are put forward; the robot excels at dangerous or monotonous work and therefore is capable of freeing workers for the more pleasant tasks of supervision, maintenance, and programming. [1] [17] [22] [23].

The first of these arguments is based on the assumption that the cost-benefit analysis is a sufficiently accurate method with which to judge the worth of advanced automation systems. Although convenient, and amenable to the economic calculus, this approach by necessity deals only with the readily quantifiable elements of the situation. The results, according to Schumacher [24], are that short term costs are given vastly more weight than long term costs, and also that the free component of goods such as air, water, and raw materials is by definition excluded from the analysis. In the light of modern day environmental crises, namely pollution, energy and raw material shortages, such analyses must offer a distorted picture. Efforts to sophisticate the economic procedures, to incorporate the intangibles, are based on the premise that everything has a price, and again the conclusion fails to reflect reality.

Obviously economic analyses have an important role, however, the fact must be realized that they are only true within a defined and artificial framework and thus can only be considered as data for a human judgement.

The second argument put forward for the robot, that of work improvement, may be criticized on the basis of studies performed by sociologists in automated industries since the mid-sixties.

Adam Smith in 1776 predicted that the division of labour made possible by factory mechanization would render work trivial, repetitive, and dull. This perspective has persisted until the present day where it finds expression in the word alienation. Peterson [25] describes several

variations of alienation which he considers relevant to people in today's industrial setting. One of these is the powerlessness of men in modern industries where job performance is largely dictated by the system, for example in highly automated plants where men may function simply as machine minders. Another aspect of alienation is meaninglessness, this resulting from the fragmentation of the production process into small areas, thus removing the worker from the end product of his labours. Again, this separation of the worker from his work could be aggravated by the installation of robots.

Erich Fromm [26] fears that automation has isolated the worker psychologically from his colleagues; the reduction in labour requirements made possible by robots could promote a loss of camaraderie in traditionally non-automated industries. A further effect of automation has been a general reduction in the skill demanded of the worker, according to James Bright [26].

In a paper presented to leading British and European roboticists, M. J. Cooley [27] examines these social difficulties and concludes "These problems are widespread and growing in their generality".

Therefore, although it is a fact that robots have eased the burden of industrial work in such areas as forging, welding, and the handling of hot or dangerous materials, it does not automatically follow that their introduction leads to work enrichment, but possibly the reverse, unless the attendant problems are dealt with.

Thus neither of the two arguments tendered is capable of justifying the robot per se. This situation exemplifies two traps which snare modern man, according to the British cybernetician Stafford Beer [28].

Firstly, the dominance of money as a measure of value and secondly the narrowness of his perceptual scale.

H. Ozbekhan, quoted by H. W. Bruck [29], describes the effects of these traps in the technological system, "Confronted with what appears inevitable, people tend to abdicate their role as creators of new and different events and abide by the dimensions and measurements which current technology has imposed upon their vision. Further, once imprisoned within such a restricted outlook they tend automatically to act so as to make the prediction come true. The present is thus perpetuated by techniques which become strengthened and more elaborate at each step of the way - as does the feeling of impotence and irrelevance experienced by those who manipulate them. Technique-derived imperatives multiply and increasingly restrict the areas of free choice".

From this we must conclude that decision making, to be effective at all, must consider as many different viewpoints as possible. The decision maker is in effect called upon to assume a variety of roles, these dictated by the decision situation. For example a factory engineer considering the installation of new plant should view the decision confronting him in turn through the eyes of a worker, a shareholder, a sociologist, a conservationist etc.

The difficulties of such a stance are apparent. Decision makers at all levels are constrained to conformity simply for day-to-day survival. The complexity of what H. W. Bruck [29] calls "The Great Gloppata-Gloppata Machine" makes difficult the prediction of the effects of a specific part of technology in such diverse areas as the trade balance, the environment, agriculture, and health. In addition, many of today's problems are only identifiable in terms of symptoms such as urban transport congestion, crime, or land erosion.

Nevertheless despite these constraints the exercise of effective decision making is essential, if man is to assume control over the technological order and hence over the technologically shaped problems confronting him.

CHAPTER 3

THE ASSEMBLY PROCESS

In this Chapter we shall attempt to gain a closer view of the assembly process, in particular the importance of the final fitting stage. As a prelude to further studies, the contact modes of an unchamfered peg and hole are considered, as well as the impact and friction characteristics.

3.1 THE ASSEMBLY PROCESS

The assembly process is a complex task, involving the selection, transfer, orientation, and fitting of components comprising the final product [30]. Whitney [31] defines assembly as "a staged process of removal of uncertainty until positions and orientations are known with enough certainty so that assembly can occur".

Robot manipulator systems in general have the functional flexibility required to cope with the wide variety of operations demanded by the assembly process. However, because of structural deflections, wear, and limitations in positioning control, the locating accuracies are restricted to the range 1-.1 mm [31]. As the clearances existing between components may be ten times less than these limits, obviously the final stages of positioning are most critical.

The study of the mechanics of assembly will be centred around the case of a peg and hole for the following reasons:-

(i) It has been shown that this configuration forms the basis of many mechanical assemblies [11], e.g. shafts and bearings, bolts and nuts, plugs, washers and spacers.

(ii) The geometric analysis is relatively straightforward and the modes of misalignments are limited.

Given the peg-hole configuration we may define the assembly process more rigorously, as shown in Fig. 3.1.

(i) Stage 1 involving the transfer of the peg to the hole. This gross motion typically is achieved by the robot and will have a final positioning error of several millimetres.

(ii) Stage 2 is defined as beginning when contact occurs between the edge of the peg, and the edge of the hole at either one or two points. This stage involves the sensing and correction of the peg position in readiness for Stage 3.

(iii) Stage 3 is the final assembly stage and in this case may conveniently be defined as beginning when the peg edge lies within the projected hole cylinder. In this stage fine manipulation is required in order to avoid jamming or wedging.

Although considerable work has been done on the insertion of a peg into a hole [4] [11] [12], i.e. Stage 3, the initial positioning, Stage 2, has been a relatively neglected area considering the large number of modes of misalignment possible. Therefore in this thesis the problems associated with Stage 2 of peg-hole assembly only will be dealt with.

3.2 PEG-HOLE CONTACT

Wong [32] has summarized the possible interactions between a peg and hole. In this work the unchamfered peg and hole are examined, the following three cases only being considered;

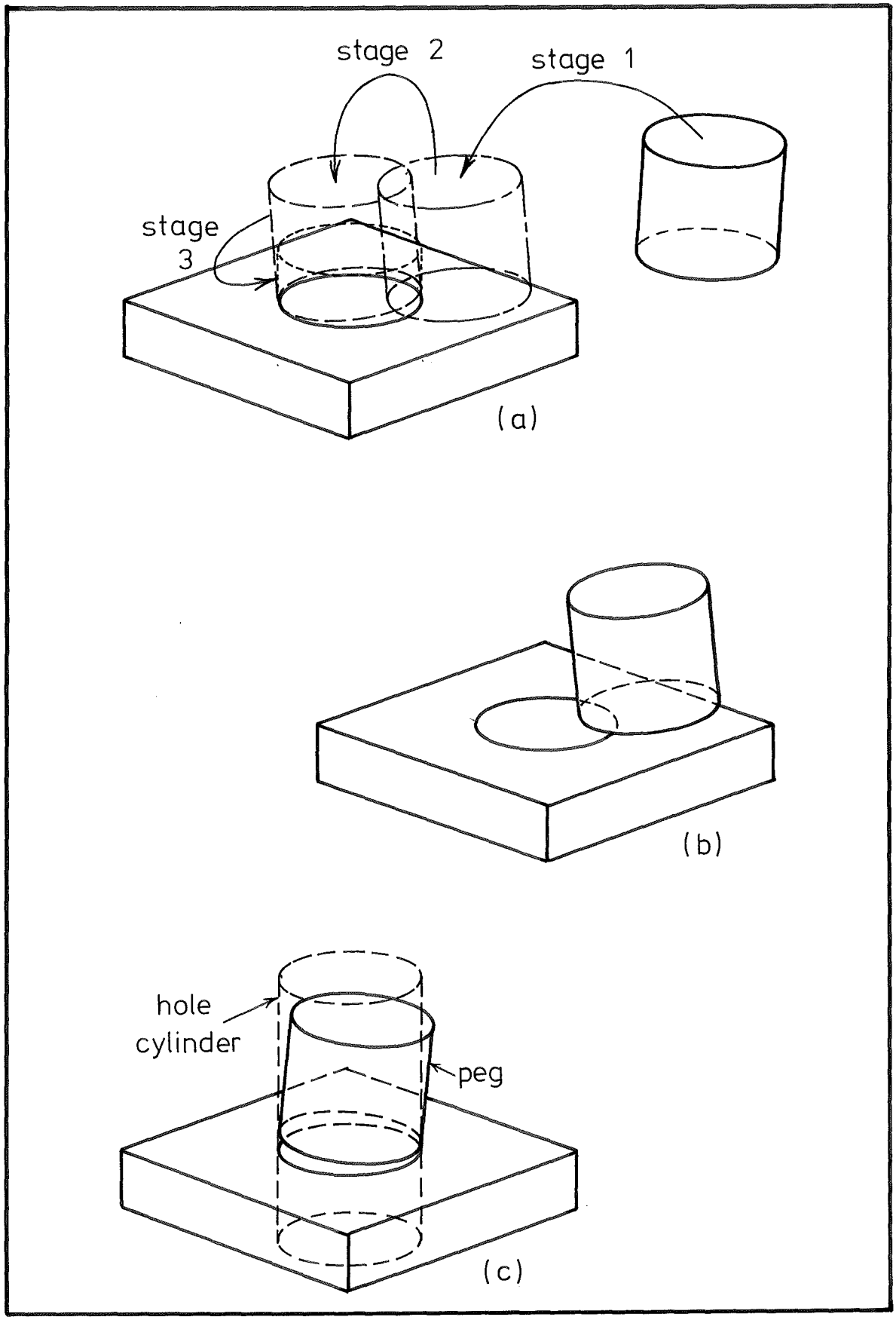

FIG. 3.1 (a) THE ASSEMBLY PROCESS.

(b) EDGE EDGE CONTACT COMMENCEMENT OF STAGE TWO.

(c) COMMENCEMENT OF STAGE THREE.

(i) Peg edge - hole edge single point contact.

(ii) Peg edge - hole edge double point contact.

(iii) Peg edge - hole plane single point contact.

3.2.1 Peg Edge-Hole Edge Single Point Contact

Contact occurs as shown in Fig. 3.2. Limited rotation of the peg may occur about the contact point and sliding may occur on the contact plane.

McCallion and Wong [33] give the direction of the contact normal in the hole centred ijk coordinate system as

$$\underline{n} = \frac{c}{\sqrt{(b^2 + c^2)}}\ \underline{j} - \frac{b}{\sqrt{(b^2 + c^2)}}\ \underline{k} \qquad (3.1)$$

where the tangent vector i' of the peg circumference is

$$\underline{i}' = a\underline{i} + b\underline{j} + c\underline{k},$$

and the vector $\underline{i}$ is tangential to the hole circumference.

The assumption is made that the contact normal lies in the radial planes of both peg and hole cylinders.

Because the peg edge cannot intersect the hole plane the tangent vector i' must have components in the quadrants shown in Fig. 3.3, i.e. b +ve and c -ve, or vice versa. As a result the +ve unit normal vector always contains the component

$$\frac{b}{\sqrt{(b^2 + c^2)}}\ \underline{k}$$

lying toward the hole centre. In other words, single point contact occurs on a plane inclined at an angle

$$\alpha = \sin^{-1} \frac{b}{\sqrt{(b^2 + c^2)}} \qquad (3.2)$$

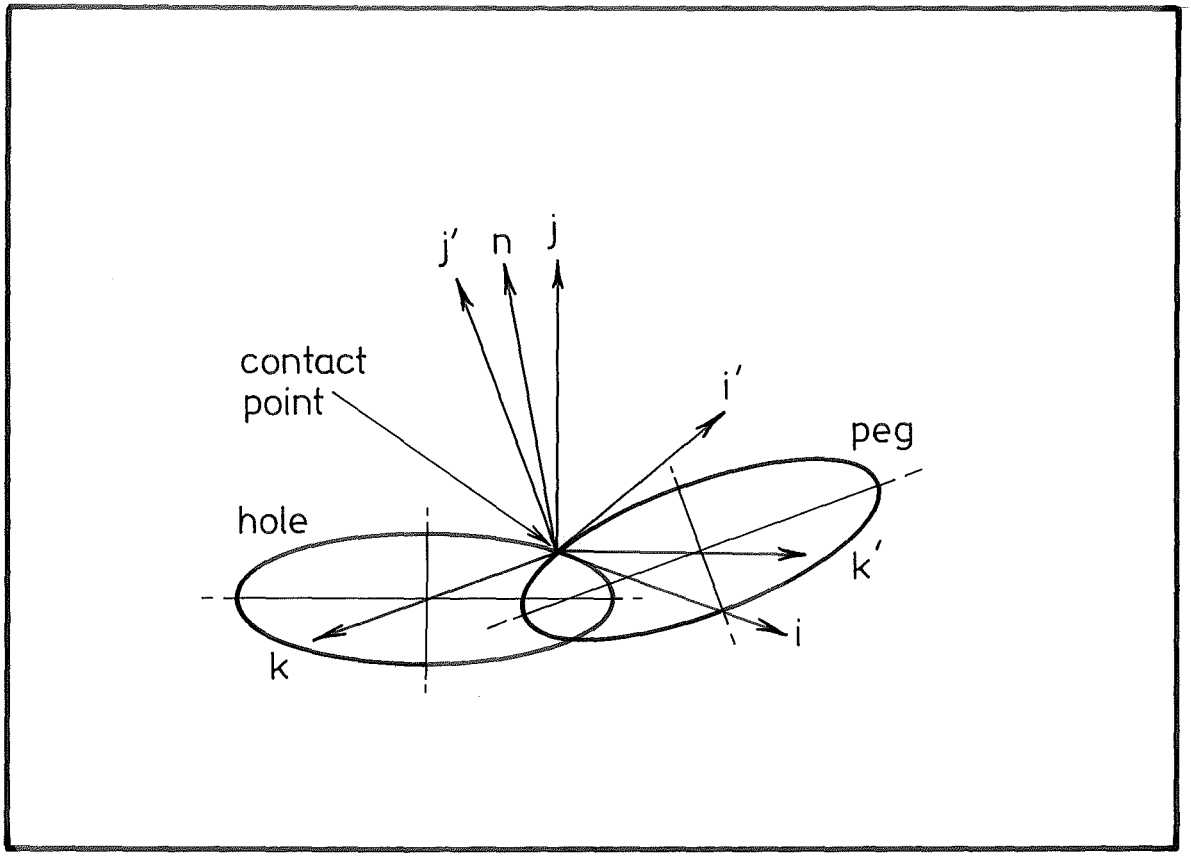

FIG. 3.2 SINGLE POINT CONTACT

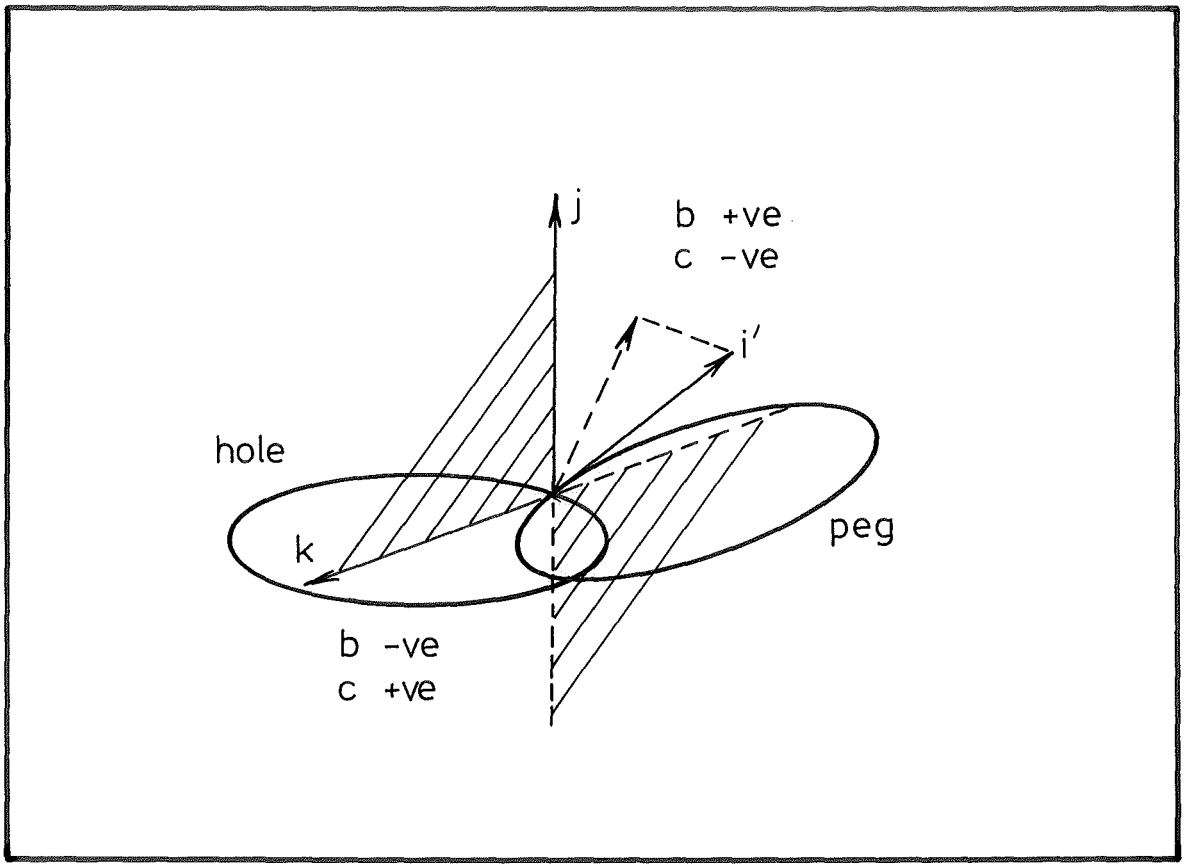

FIG. 3.3 POSITION OF PEG TANGENT VECTOR

to the horizontal, Fig. 3.4. The effect of this is that a chamfer effect exists as a result of the angular misalignment.

It may be seen from Equation 3.1 that in cases of small angular misalignment, i.e. as

$$b \rightarrow 0$$

the normal $\underline{n}$ becomes aligned with the vertical $\underline{j}$ axis.

3.2.2 Peg Edge-Hole Edge Double Point Contact

When contact occurs at two points, A and B, as shown in Fig. 3.5, rotation may occur about the chord connecting the contact points and sliding may occur at either contact point.

With reference to Fig. 3.5, the triad of unit vectors $\underline{i}\ \underline{j}\ \underline{k}$ is centred at A, $\underline{i}$ and $\underline{k}$ lie in the plane of the hole circumference, $\underline{i}$ being collinear with chord AB. The triad $\underline{i}'\ \underline{j}'\ \underline{k}'$ is again centred at A and is similarly aligned with respect to the peg edge. The two coordinate systems are rotated with respect to each other by the angle α, about the AB axis, and the length of AB is 2a.

The tangent vectors to the hole circle radius R at A and B may be written as

$$\underline{TA} = -\sqrt{(R^2-a^2)}\ \underline{i} + a\ \underline{k} \tag{3.3}$$

$$\underline{TB} = \sqrt{(R^2-a^2)}\ \underline{i} + a\ \underline{k} \tag{3.4}$$

The tangent vectors to the peg circle, radius r, transformed to the i j k system becomes

$$\underline{tA} = \sqrt{(r^2-a^2)}\ \underline{i} + a(\cos\alpha\underline{k} - \sin\alpha\underline{j}) \tag{3.5}$$

$$\underline{tB} = -\sqrt{(r^2-a^2)}\ \underline{i} + a(\cos\alpha\underline{k} - \sin\alpha\underline{j}) \tag{3.6}$$

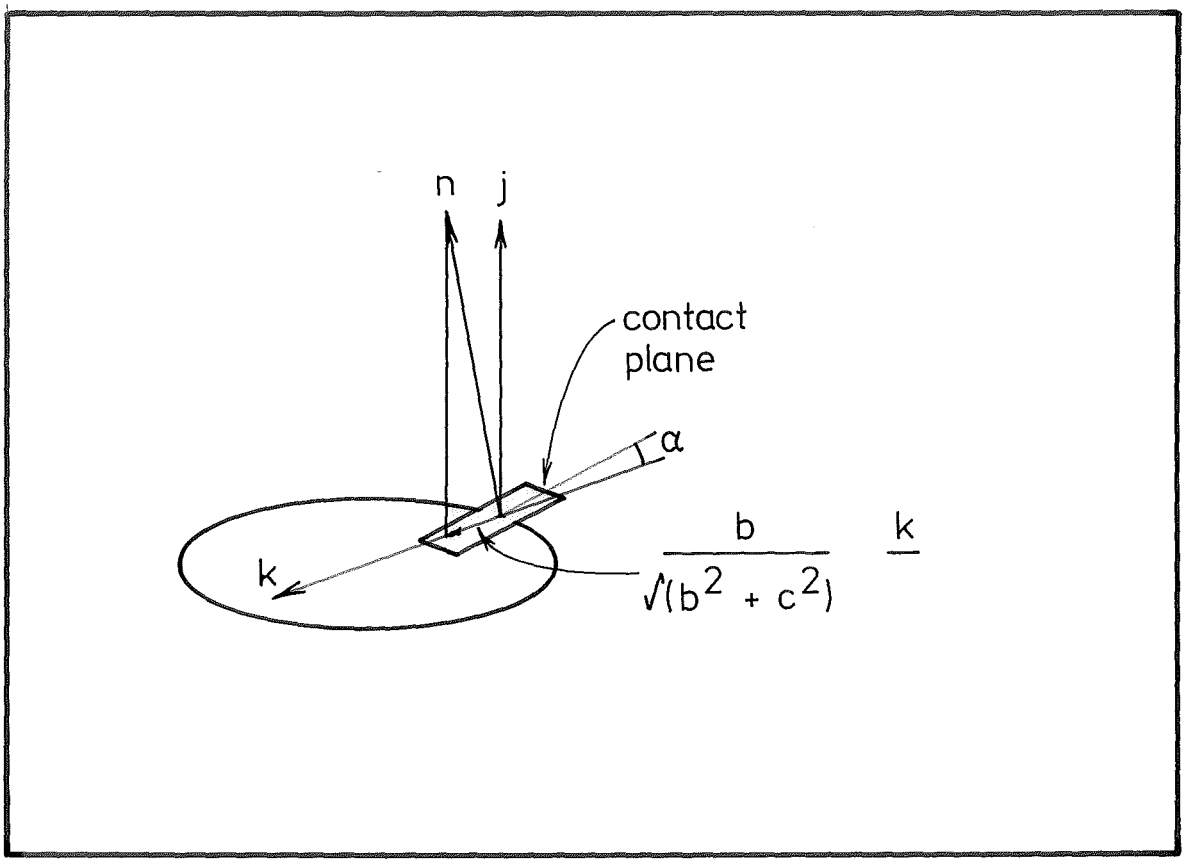

FIG. 3.4 CONTACT PLANE

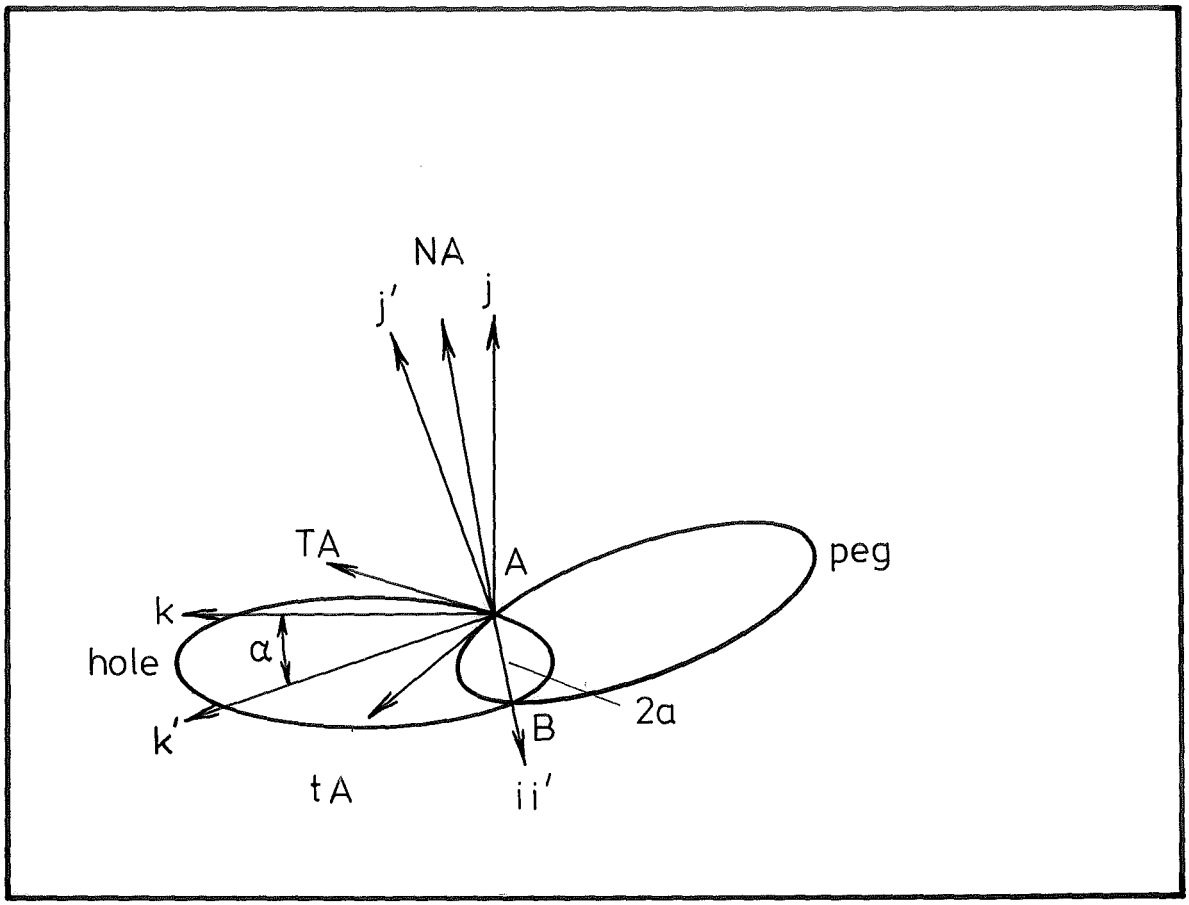

FIG. 3.5 DOUBLE POINT CONTACT

The tangent vectors of the peg and hole circumferences are normal to their respective radial planes, hence we may write the contact normal vectors as,

$$\underline{NA} = (\underline{TA} \times \underline{tA})$$

$$\underline{NB} = (\underline{TB} \times \underline{tB})$$

i.e.

$$\underline{NA} = a\sin\alpha\underline{i} + (\sqrt{(r^2-a^2)} + \sqrt{(R^2-a^2)}\cos\alpha)\,\underline{j} + \sqrt{(R^2-a^2)}\sin\alpha\underline{k} \qquad (3.7)$$

$$\underline{NB} = -a\sin\alpha\underline{i} + (\sqrt{(r^2-a^2)} + \sqrt{(R^2-a^2)}\cos\alpha)\,\underline{j} + \sqrt{(R^2-a^2)}\sin\alpha\underline{k} \qquad (3.8)$$

Sliding may occur on the contact planes at either A or B, so the instantaneous direction at sliding $\underline{s}$, without rotation, is given thusly

$$\underline{s} = \underline{NA} \times \underline{NB}$$

$$\underline{s} = -\sqrt{(R^2-a^2)}\sin\alpha\underline{j} + (\sqrt{(r^2-a^2)} + \sqrt{(R^2-a^2)}\cos\alpha)\underline{k} \qquad (3.9)$$

If the peg and hole radii are equal then

$$\underline{s} = \tan\tfrac{\alpha}{2}\,\underline{j} + \underline{k} \qquad (3.10)$$

i.e. the instantaneous direction of sliding is perpendicular to chord AB and lies midway between the peg and hole planes as shown in Fig. 3.6.

As previously, we see that for small misalignments, i.e. as

$\alpha \rightarrow 0$

both $\underline{NA}$ and $\underline{NB}$ become aligned with $\underline{j}$.

3.2.3 Peg Edge-Hole Plane Single Point Contact

The contact between the peg edge and hole plane is similar to that discussed in Section 3.2.1 except in this case, the normal direction is independent of the peg orientation, lying normal to the hole plane.

3.3 IMPACT DURING ASSEMBLY

Impact between the component surfaces occurs during the final fitting stage and in general the contacts made will be either

i Edge - edge contact

ii Edge - plane contact.

Contacts involving edges are characterized by low area and high pressures.

The commonly accepted view of contact between surfaces [34] involves the progressive plastic deformation of asperities with underlying elastic deformation, as illustrated in Fig. 3.7. In high pressure situations, such as occur during assembly, we would expect the contacts to be largely plastic.

Evidence exists suggesting that the presence of a lubricant film is capable of introducing a viscous damping component into the contact force [35].

3.4 FRICTION DURING ASSEMBLY

The friction existing between contacting components during assembly is complicated by the high local pressures causing surface deformation and mechanical locking. The results of tests carried out by Simunovic [12] are shown in Fig. 3.8. These show a considerable variation in the coefficient of friction occurring on the first sweep. Presumably the components become bedded in on this run.

The presence of vibration causes an apparent reduction in the coefficient of friction [36], which effect may be used to aid assembly.

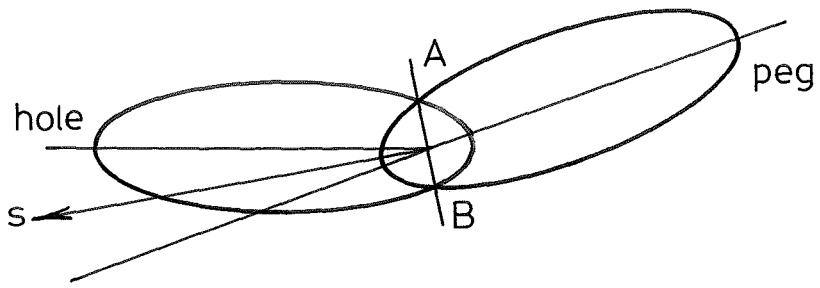

FIG. 3.6 DOUBLE POINT CONTACT INSTANTANEOUS DIRECTION OF SLIDING.

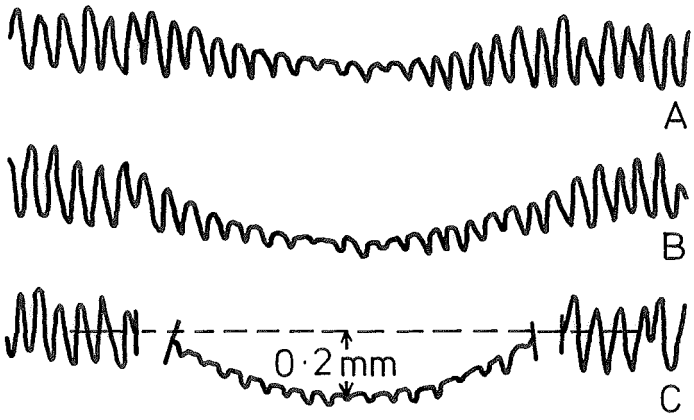

a) Plastic deformation of asperities and underlying elastic deformation.

b) Intermediate stage.

c) Overall plastic deformation.

FIG. 3.7 CONTACT BETWEEN SURFACES (after Bowden & Tabor)

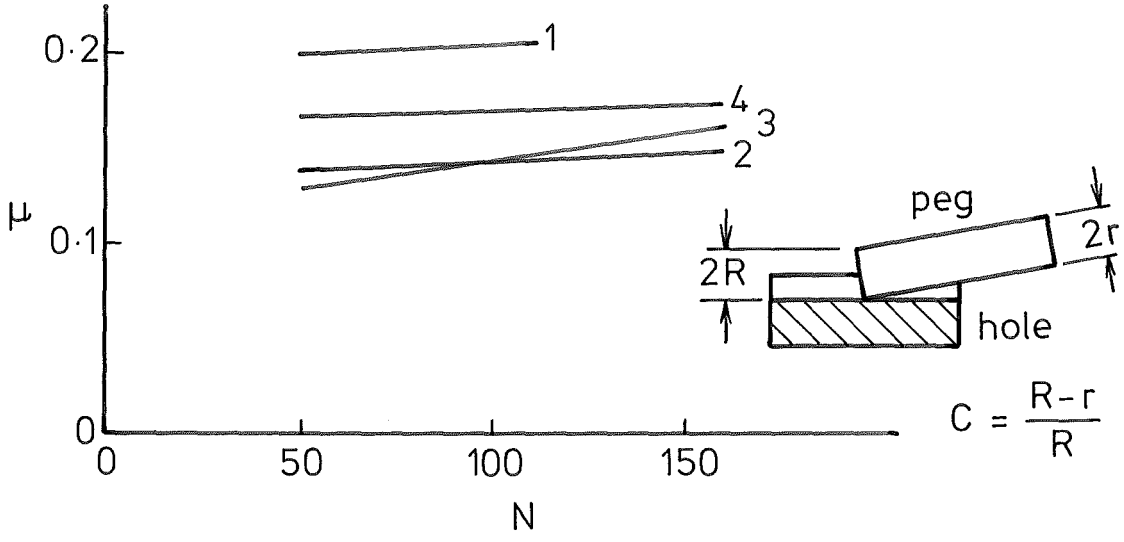

Friction at tip of peg

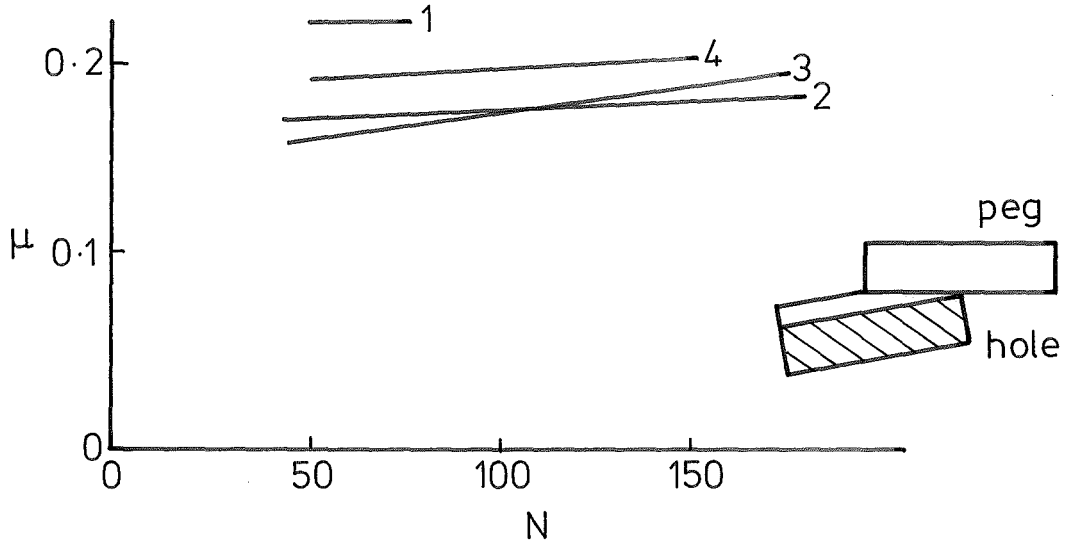

Friction at mouth of hole

1. Steel on steel $C = 9 \times 10^{-3}$ - 1st sweep
2. Steel on steel $C = 9 \times 10^{-3}$
3. Steel on steel $C = 3 \times 10^{-3}$
4. Steel on al $C = 3 \times 10^{-3}$

FIG. 3.8 FRICTION IN PEG-HOLE CONTACTS
(after Simunovic)

PART ONE

VIBRATORY ASSEMBLY

CHAPTER 4

VIBRATORY ASSEMBLY

This Chapter examines the use of vibration to facilitate the assembly process, in particular the behaviour of a simple spring-constrained peg-hole system under a periodic force.

A variety of assembly movements are studied, and the results evaluated with regard to practical applications.

4.1 VIBRATORY ASSEMBLY

During assembly a wide range of contact modes may occur between the mating components before the final assembled state is achieved. The contact forces existing between the components are dependent on the misalignment and therefore may, under certain circumstances, be used to aid assembly. Aligning contact forces may be produced, for example by chamfers. Contact forces aiding assembly may also be produced by the application of a periodic force.

In the initial stages of assembly the oscillatory motion of the vibrated component acts as a searching movement. This principle is used by Karelin & Girel [37] and Andreev [38], where cylindrical parts are oscillated in a 50 Hz rotating magnetic field to find a mating recess, significant radial misalignments being dealt with. Karelin and Girel [39] and Savischenko [40] also report successful assembly, using mechanical oscillators.

The apparent reduction in friction due to vibration has the effect of preventing jamming in the final stages of assembly [41]. Yakhimovich and Ponomarchuk [42] successfully have used vertical vibrations of

ultrasonic frequencies to achieve the assembly of a peg into a hole.

The motion of a peg during vibratory assembly is complex, influenced by manipulator constraints, the exciting force and the type of contact. Consequently, a comprehensive analytical approach is difficult. However, it is still advantageous to examine some simplified situations in order to gain insight into the possible types of behaviour.

4.2 VIBRATORY ASSEMBLY DEVICE

The phenomena occurring in vibratory assembly are discussed with reference to the peg-hole manipulator system shown in Fig. 4.1. The unchamfered peg, of height 2h, radius r, mass m is supported in elastic constraints, acting at a height l above its top surface. Contact between the peg and hole edges occurs at either one or two points and the peg edge may also contact the hole plane. A force of magnitude F rotates about the peg vertical axis as shown, and gravity acts at the centre of mass.

4.3 PEG EDGE - HOLE EDGE SINGLE POINT CONTACT WITH NO SLIDING

The first case to be examined is that shown in Fig. 4.2 where contact between the peg edge and hole edge occurs at a single point. In the case where no sliding occurs the peg may be treated as an elastically-constrained body rotating about the contact point.

It is convenient to define axes θ_x θ_y θ_z centred at the contact point which are aligned with the principal axes of inertia through this point. The elastic constraints may be described in terms of three principal rotational stiffnesses about axes passing through the contact

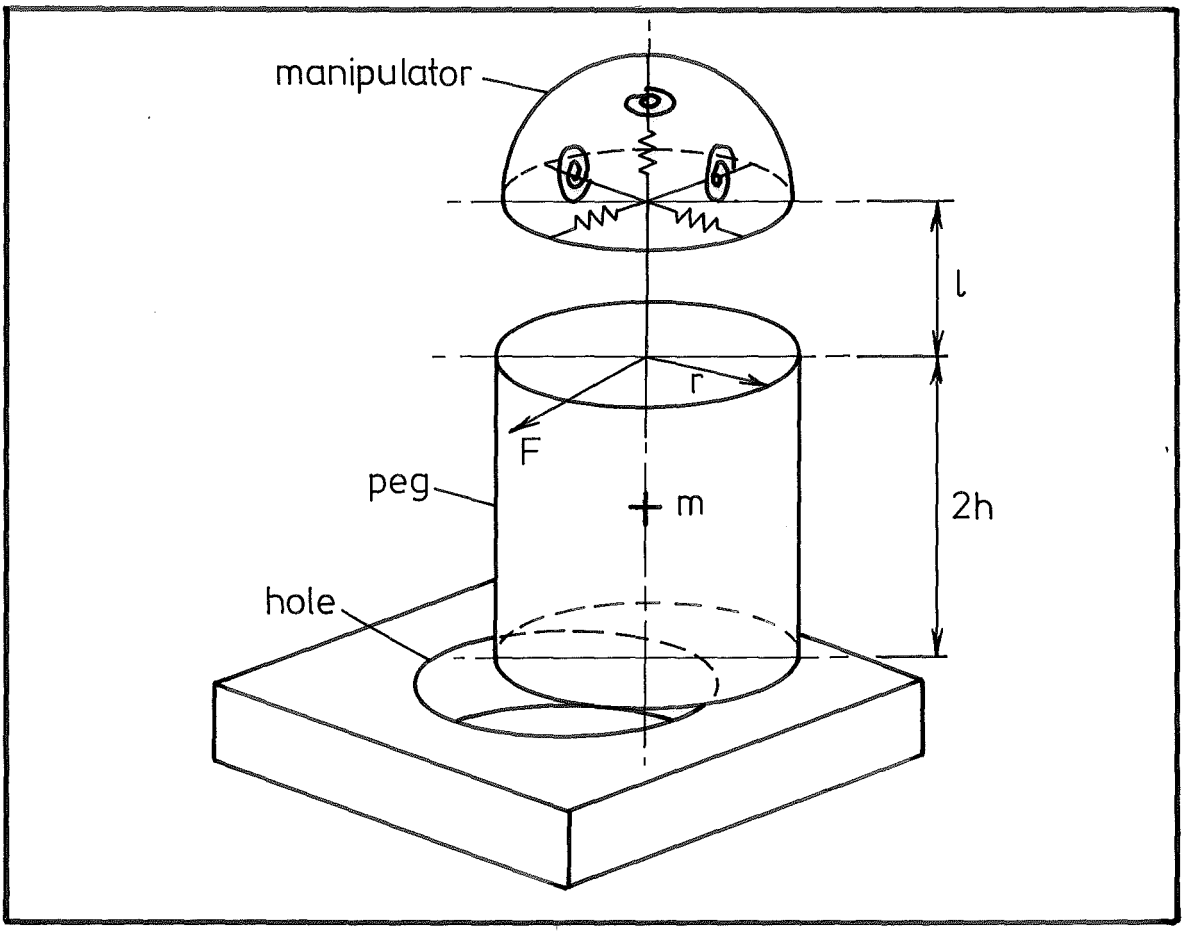

FIG. 4.1 VIBRATORY ASSEMBLY DEVICE

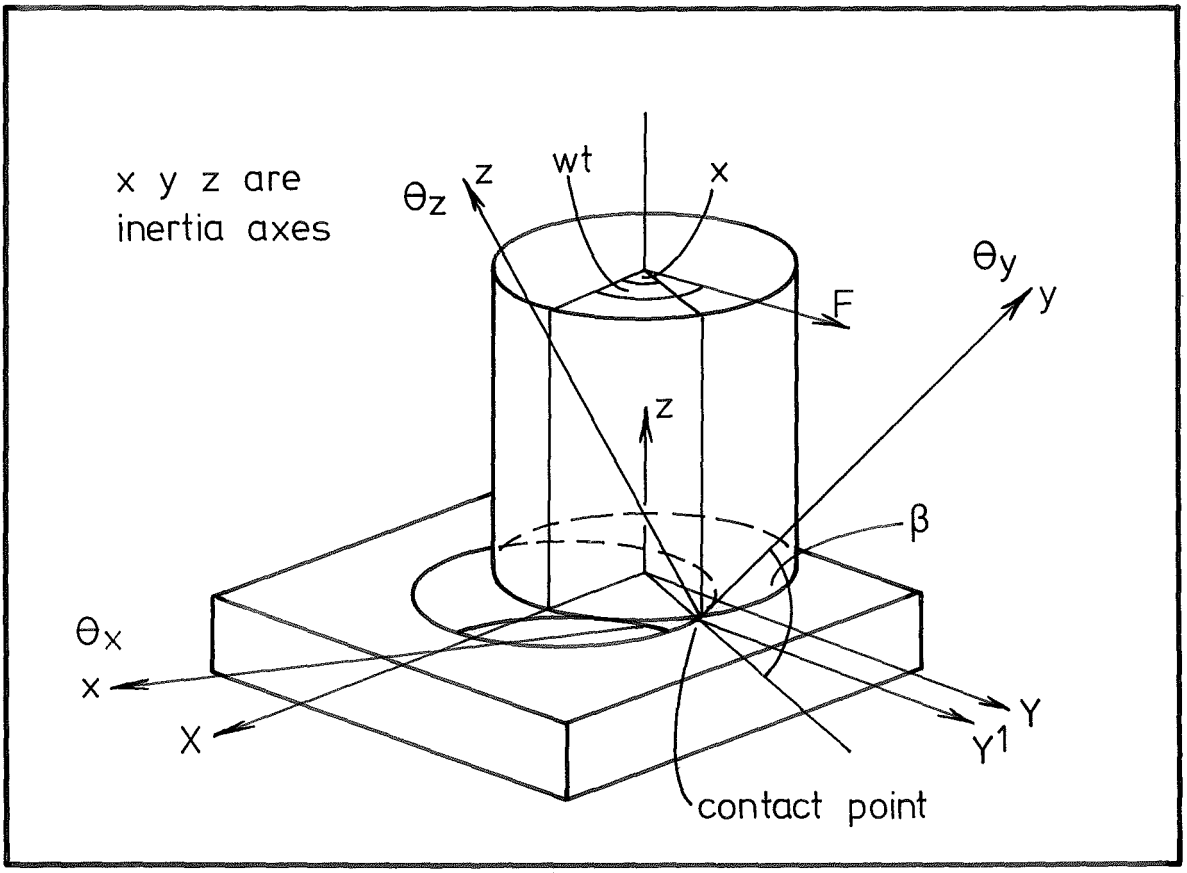

FIG. 4.2 SINGLE POINT CONTACT NO SLIDING.

point. For convenience of analysis we shall assume that the three principal rotational stiffnesses are equal.

The equations of motion for small rotational movements of the peg about the θ_x θ_y θ_z axes are

$$I_x\ddot{\theta}_x + K\theta_x = M_x \tag{4.1}$$

$$I_y\ddot{\theta}_y + K\theta_y = M_y \tag{4.2}$$

$$I_z\ddot{\theta}_z + K\theta_z = M_z \tag{4.3}$$

where I_x I_y I_z are the moments of inertia about the θ_x θ_y θ_z axes and K is the rotational stiffness about those axes. The moments about the θ_x θ_y θ_z axes due to the applied force are

$$M_x = -2Fh\cos(\omega t-\alpha) \tag{4.4}$$

$$M_y = -F(r\sin\beta +2h\cos\beta)\ \sin(\omega t-\alpha) \tag{4.5}$$

$$M_z = -F(r\cos\beta -2h\sin\beta)\ \sin(\omega t-\alpha) \tag{4.6}$$

The angle α describes the position of the contact point on the peg edge with respect to the peg centred XYZ coordinate system. The angle between the y axis and the XY plane is β.

The steady state solution of the equations of motion becomes

$$\theta_x = \frac{-2Fh\ \cos(\omega t-\alpha)}{K-I_x\omega^2} \tag{4.7}$$

$$\theta_y = \frac{-F(r\sin\beta +2h\cos\beta)\ \sin(\omega t-\alpha)}{K-I_y\omega^2} \tag{4.8}$$

$$\theta_z = \frac{-F(r\cos\beta -2h\sin\beta)\ \sin(\omega t-\alpha)}{K-I_z\omega^2} \tag{4.9}$$

Equations 4.8 and 4.9 describe a net rotation about axis P in the y-z plane, Fig. 4.3.

$$\underline{\theta}_p = \underline{\theta}_y + \underline{\theta}_z \tag{4.10}$$

Thus the resulting motion of the peg is a non-symmetric clockwise or anti-clockwise wobble about an axis Q, perpendicular to both x and P and passing through the contact point as shown in Fig. 4.3.

4.4 PEG EDGE - HOLE EDGE SINGLE POINT CONTACT WITH SLIDING

The combination of exciting force and spring force, acting approximately parallel to the contact plane, may cause slippage at the contact point.

In the previous section, Section 4.3, it was shown that the symmetrically constrained peg under the action of a rotating force executed a wobble about the axis Q through the contact point. Referring to Fig. 4.4, the movement of the constraint attachment point G in the X*Y*Z* system for small movements may be expressed in terms of the wobble displacements.

$$X^* = -\theta_x \, l \, \sin\theta_2 \tag{4.11}$$

$$Y^* = -\theta_p \, l \, \sin\theta_1 \tag{4.12}$$

$$Z^* = -\theta_x \, l \, \cos\theta_2 \tag{4.13}$$

Assuming the transverse stiffnesses k to be equal in all directions, then clearly the peg will experience a force proportional to and opposing the displacement at G.

The force causing sliding for small angular misalignments, F_s, is due to the rotating exciting force F, and the reaction force F_{Gs} of the transverse constraint springs at G, both in the X*Y* plane. In vector notation

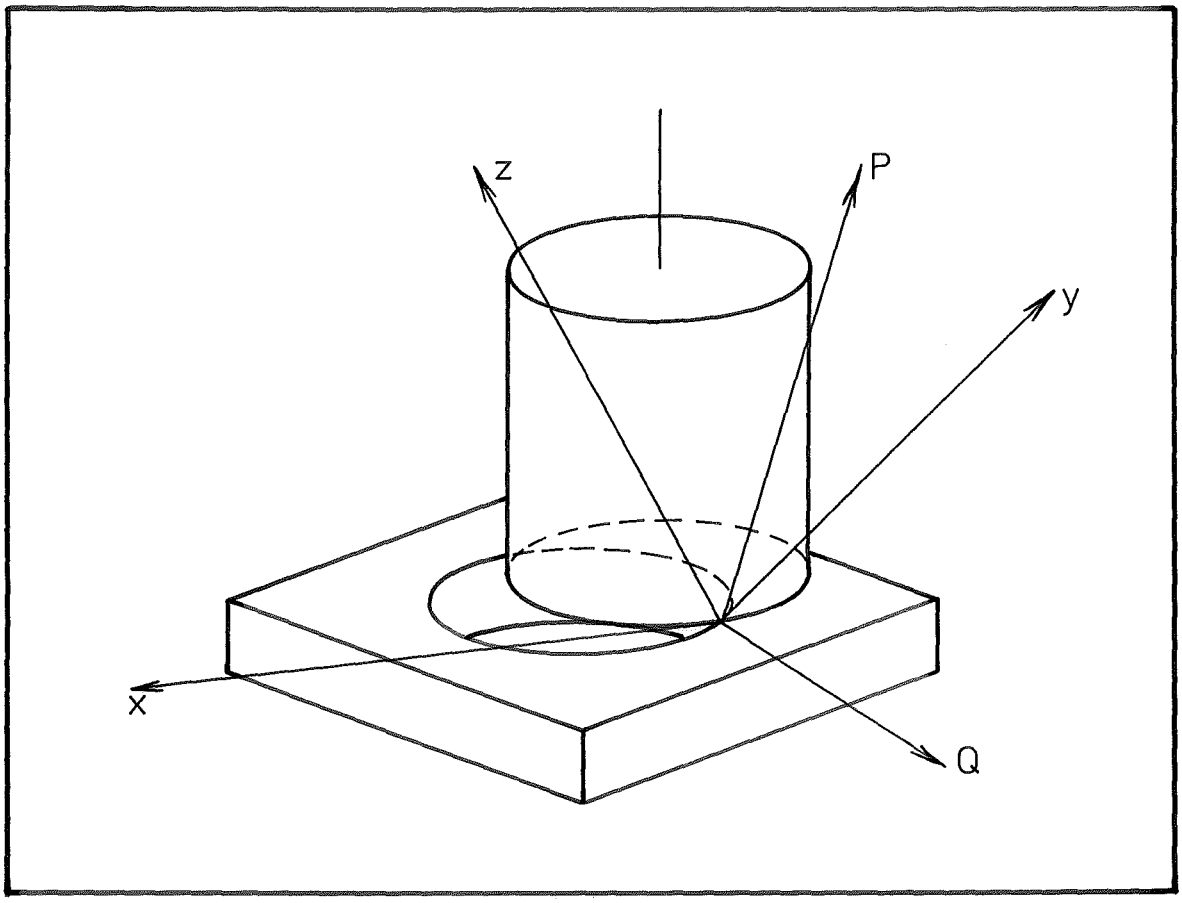

FIG. 4.3 SINGLE POINT CONTACT WOBBLE AXIS Q

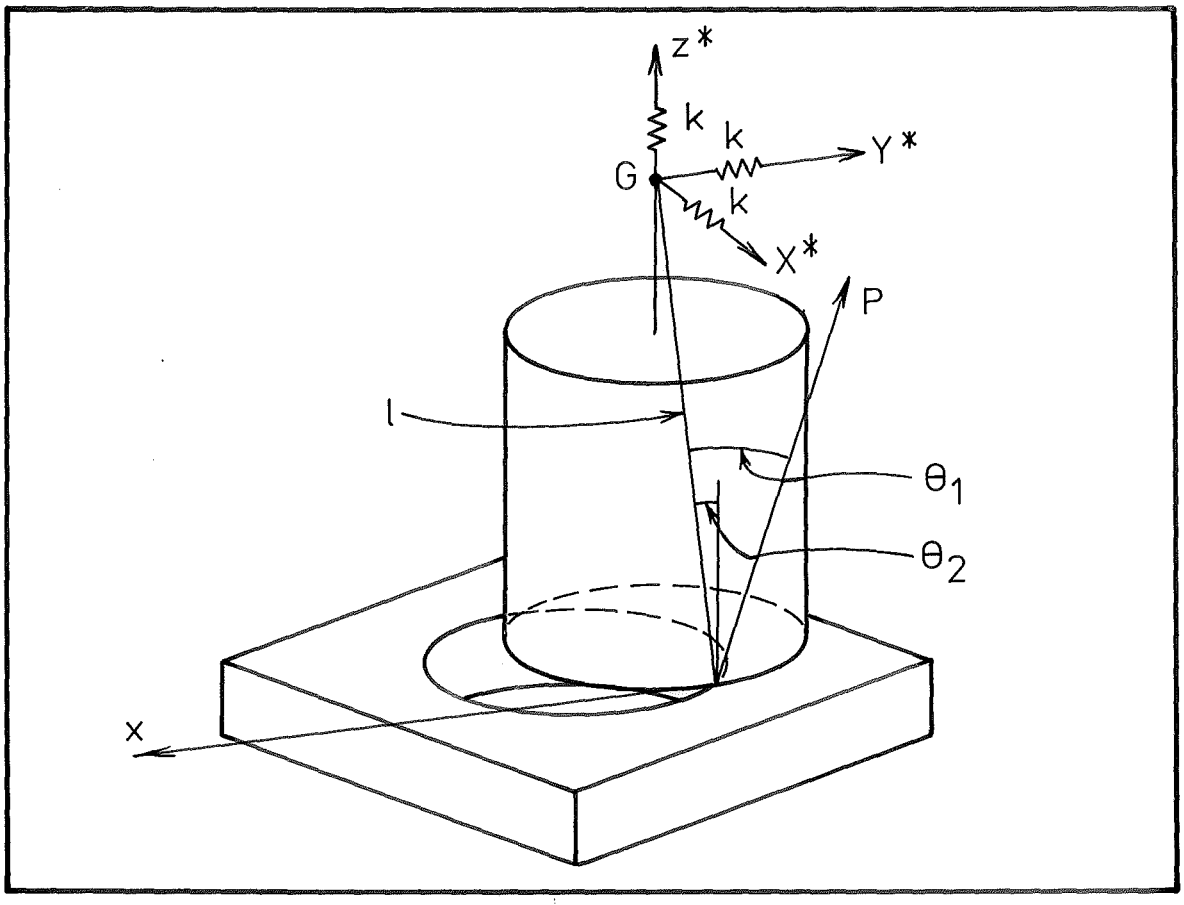

FIG. 4.4 MOVEMENT AT CONSTRAINT ATTACHMENT POINT G.

$$\underline{F_S} = (F\cos(\omega t-\alpha) + k1\theta_x \sin\theta_2)\ \underline{i}$$

$$+(F\sin(\omega t-\alpha) + k1\theta_p \sin\theta_1)\ \underline{j} \qquad (4.14)$$

This force is shown diagramatically in Fig. 4.5. F is of constant magnitude and rotates in an anti-clockwise direction, whereas F_{Gs}, which follows an elliptical path rotates either clockwise or anti-clockwise. Clearly the maximum sliding force occurs when the two force vectors are coincident.

The normal force F_N is altered by the vertical constraint force F_{GN} at G, i.e.

$$F_N = mg - k.1.\theta_x \cos\theta_2 \qquad (4.15)$$

Obviously as the vertical force approaches the magnitude of the peg mass sliding will occur. If the resultant horizontal force on the peg is toward the hole at this stage, assembly will occur.

Clearly for single point contact the final motion is subject to a host of variables such as the peg dimensions, constraint stiffness and exciting force. Two simple cases will be dealt with in the following sections.

4.4.1 Single Point Sliding, Solid Cylindrical Peg h >> r

For a long thin cylindrical peg, Fig. 4.6

$h >> r$

$\beta \ \underline{\Omega}\ 0$

From Equations 4.7 - 4.9 we see that θ_z is much smaller than θ_x and θ_y, and as a result the wobble axis Q is approximately aligned with z.

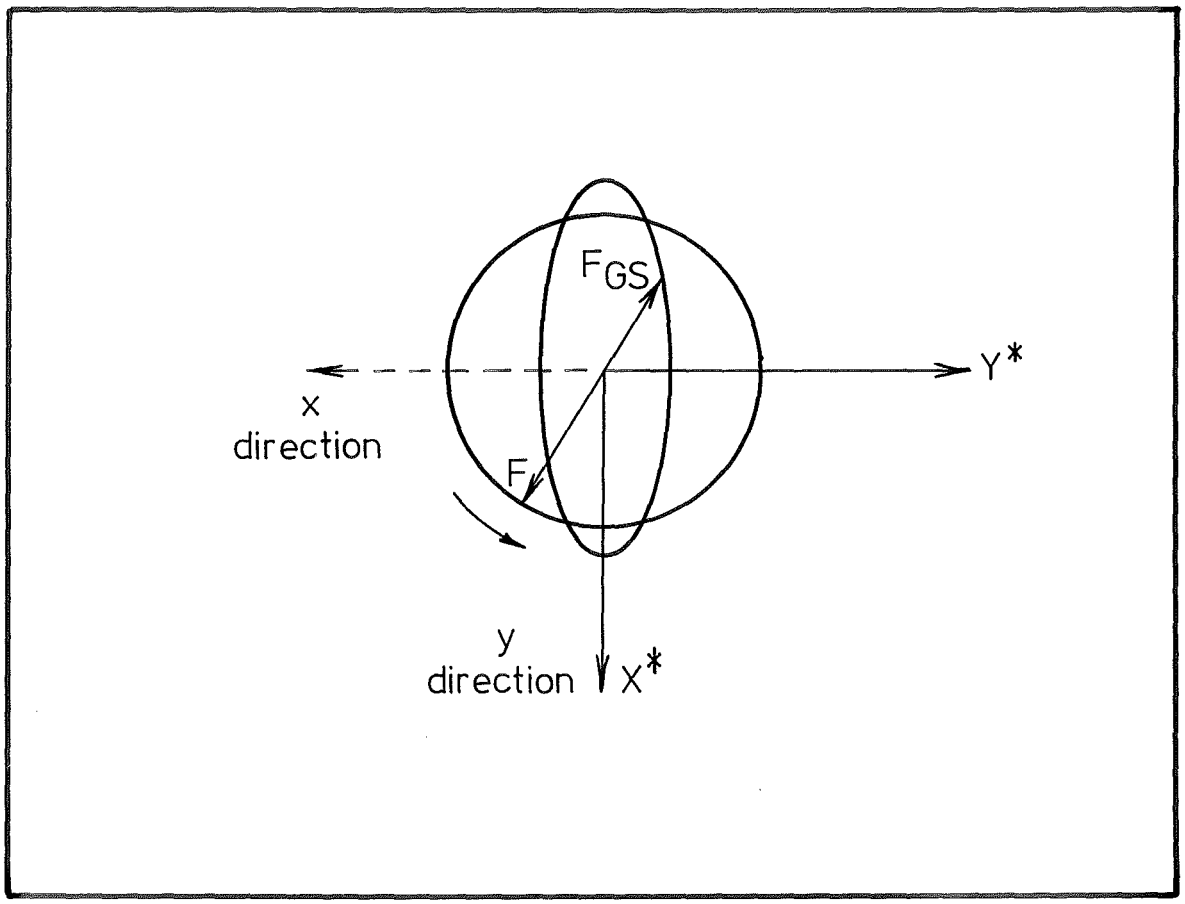

FIG. 4.5 FORCES ACTING ON PEG - X* Y* PLANE

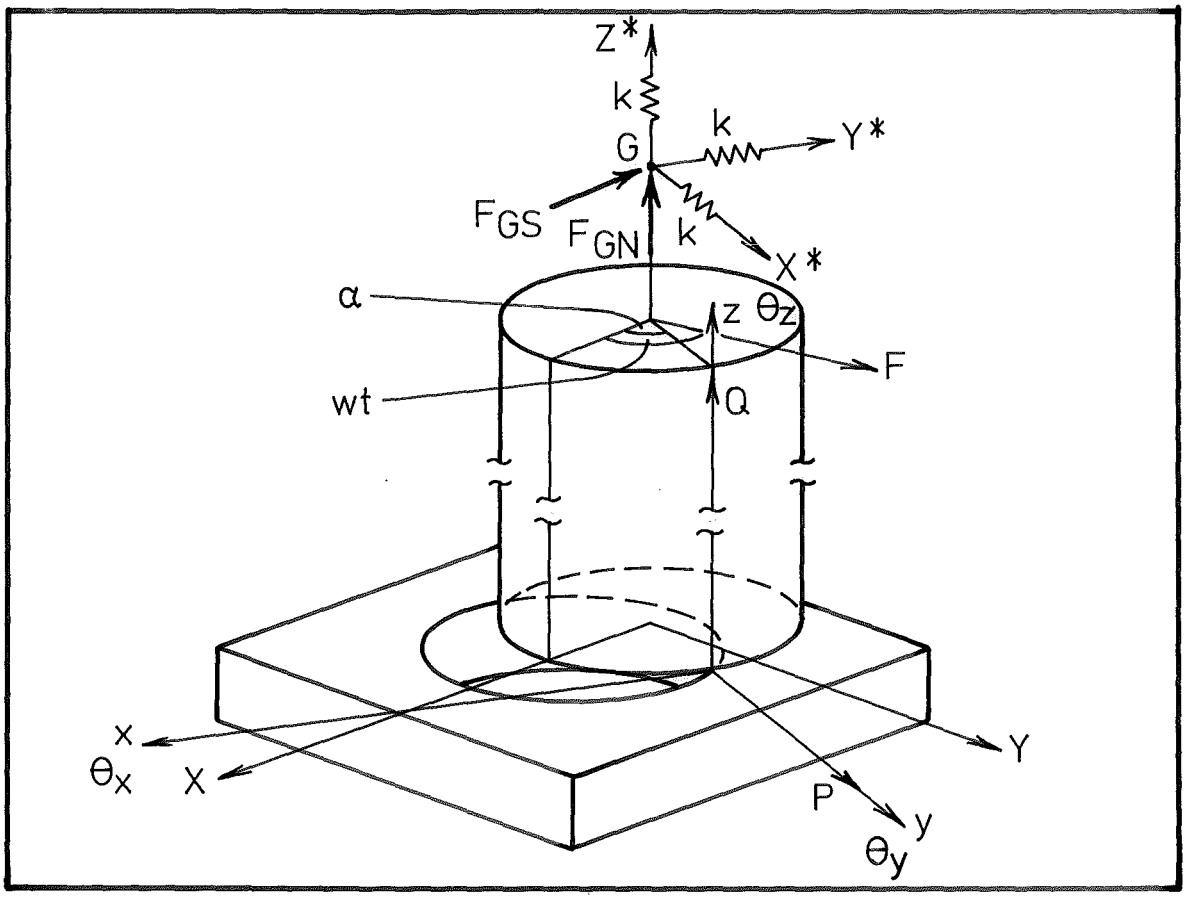

FIG. 4.6 SINGLE POINT CONTACT h >> r

At low frequencies

$$|\theta_x| \Omega |\theta_y| \Omega \frac{2F.h.}{K}$$

and as a result there is a symmetrical clockwise wobble about the vertical z axis. Equation 4.14 states that the resulting reaction force F_{Gs} acts in opposition to the applied exciting force, thus reducing the nett sliding force F_s. The normal force F_N is not affected overly by the movement of the peg as the radius is small, Equation 4.15.

When the exciting frequency lies between the two resonant frequencies, ω_x and ω_y, of motions in the θ_x and θ_y direction the wobble becomes anti-clockwise, and the spring reaction force and exciting force combine to give a high sliding force, twice per cycle. For a peg of the dimensions considered the moments of inertia, I_x and I_y, and thus the natural frequencies, ω_x and ω_y, are quite close.

At high frequencies, above either ω_x or ω_y, and also well removed from the natural frequency of motion in the θ_z direction, the wobble again becomes anti-clockwise. However as the inertia forces are now dominant, the spring constraint and exciting forces are aligned. Sliding may be likely in this case. Possibly the chamfer effect referred to in Section 3.2.1 may bias sliding toward the hole.

4.4.2 Single Point Sliding, Solid Cylindrical Peg r >> h

In the case of a short cylinder

$r >> h$

$\beta \Omega 0$

and when the exciting frequency is not close to any of the resonant frequencies, θ_y predominates over θ_z, and θ_x is also small as can be seen from the Equations 4.7 - 4.9.

As a result the motion of the peg consists essentially of an oscillation about the vertical z axis, Fig. 4.7.

At low frequencies the spring constraint force opposes the exciting force and above resonance, ω_y, the forces are in phase.

Near the resonance frequency ω_x the increased amplitude of motion about the θ_x axis combined with the large radius of the peg will cause considerable translation movements of the spring constraint attachment point in the vertical direction. The effect of this displacement acting on the vertical constraint spring will be to cause the normal contact force to fluctuate. Sliding may occur in this case.

In the peg types considered in this and the previous section, sliding may be expected at high rather than low frequencies and the chamfer effect described in Section 3.2.1 may then cause sliding assembly to occur.

4.5 PEG EDGE - HOLE EDGE DOUBLE POINT CONTACT WITH NO SLIDING

We will now examine the case where contact between the edge of the peg and the edge of the hole occurs at two points as shown in Fig. 4.8.

If the condition

$$mg\, r\sin\alpha \geq 2\, Fh$$

holds, double point contact is maintained throughout the force cycle, and if no sliding occurs the situation simplifies to a simple spring-inertia system rotating about the contact chord Y' axis.

The steady state solution for small oscillations $\theta_{Y'}$ about equilibrium is

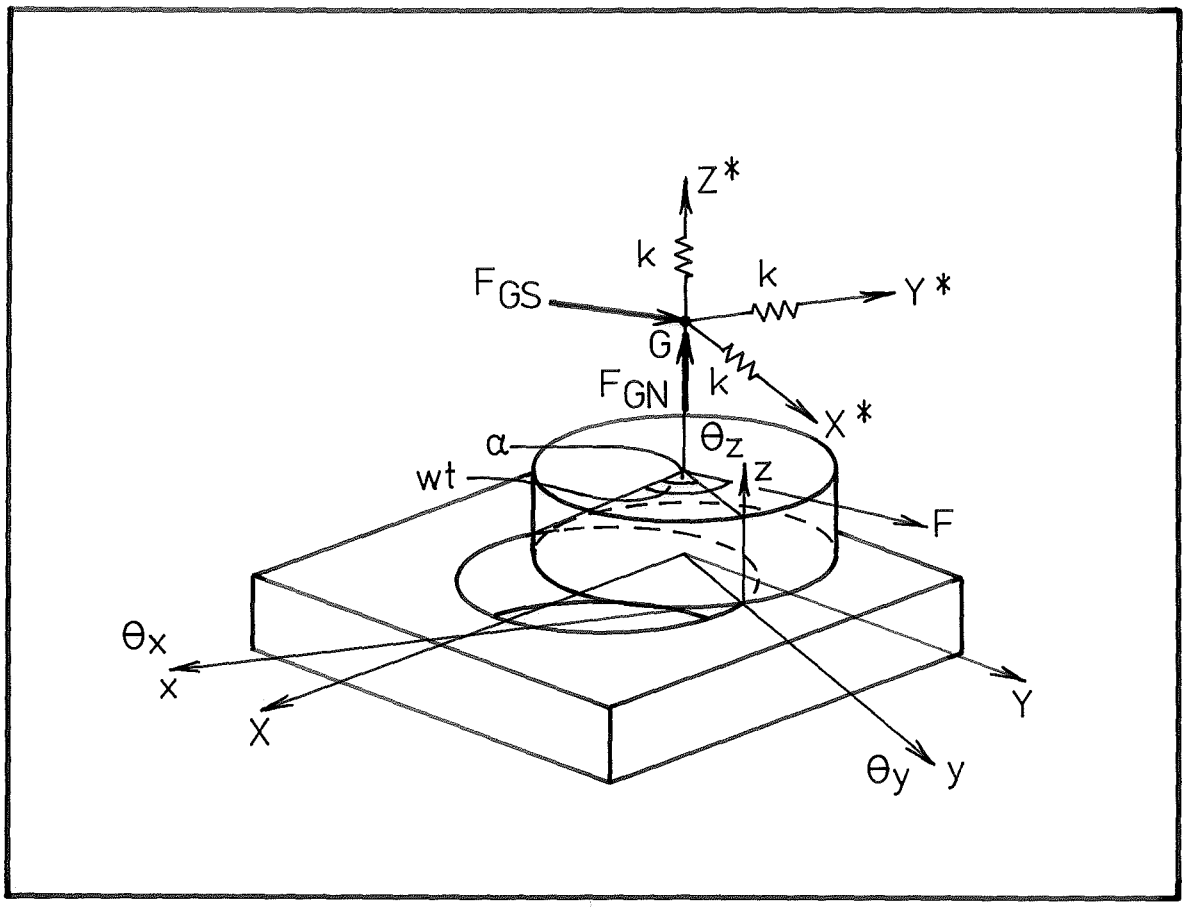

FIG. 4.7 SINGLE POINT CONTACT r >> h

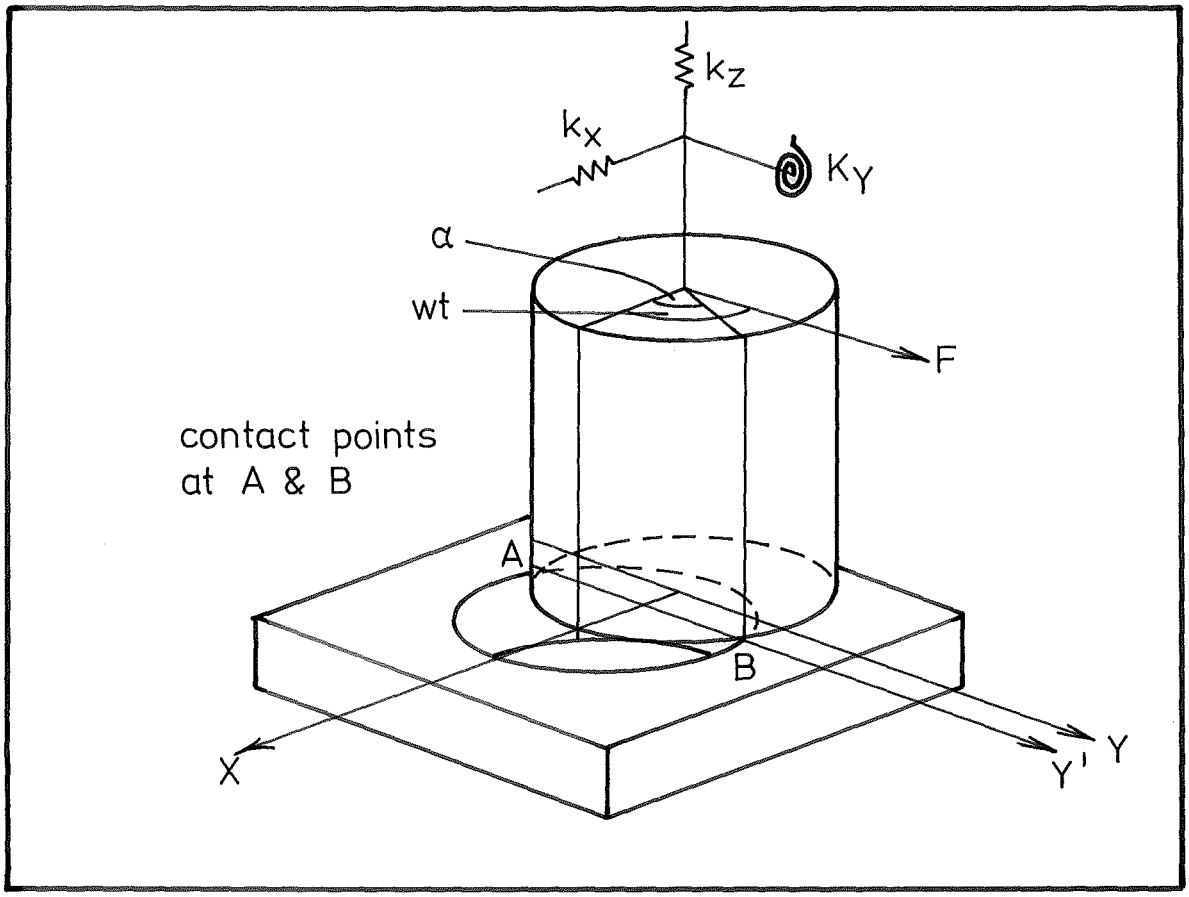

FIG. 4.8 PEG EDGE-HOLE EDGE DOUBLE POINT CONTACT

$$\theta_{Y'} = \frac{2Fh\ \cos\omega t}{(K_{Y'} - I_{Y'}\omega^2)} \tag{4.16}$$

where the rotational stiffness about the Y' axis is

$$K_{Y'} = k_x(2h+1)^2 + K_Y + k_z\, r^2(1-\cos\alpha)^2 \tag{4.17}$$

and the inertia is

$$I_{Y'} = \frac{m}{12}(16h^2 + (3+12\cos^2\alpha)r^2) \tag{4.18}$$

4.6 PEG EDGE - HOLE EDGE DOUBLE POINT CONTACT WITH SLIDING

As in the single point contact case the combined exciting and reaction forces may cause sliding. The limiting conditions for sliding will be developed below under the assumption that Equation 4.16 remains valid.

At frequencies below the natural i.e. when

$$K_{Y'} - I_{Y'}\omega^2 > 0$$

the exciting moment is in phase with the peg displacement and hence the exciting force F and spring reaction force F_x act in opposition.

Consideration of the static case shows that at low frequencies, the exciting force exceeds the spring force, and therefore sliding into the hole is most likely to occur when the peg is positioned as shown in Fig. 4.9a. Recalling the previous result in Section 3.2.2, giving the instantaneous direction of sliding for a peg and hole of equal radius and ignoring the wedging effect of the peg and hole edges, we may write the surface reaction forces of the equivalent system, Fig. 4.9b, in terms of the applied forces, i.e.

$$F_N = mg\ \cos\left(\frac{\alpha+\theta}{2}\right) + (F-F_x)\ \sin\left(\frac{\alpha-\theta}{2}\right) \tag{4.19}$$

$$F_x = mg\ \sin\left(\frac{\alpha+\theta}{2}\right) + (F-F_x)\ \cos\left(\frac{\alpha-\theta}{2}\right) \tag{4.20}$$

The peg slips into the hole when

$$\frac{F_s}{F_N} > \mu$$

i.e. when the coefficient of friction at the contact point is exceeded. Rewriting Equation 4.16

$$F = \frac{(K_Y'-I_Y'\omega^2)\theta}{2h} \tag{4.21}$$

and from Fig. 4.9a, it can be seen that the spring force

$$F_x = k_x (2h+1)\theta \tag{4.22}$$

Thus, substituting Equations 4.21 and 4.22 into Equations 4.19 and 4.20, the contact force ratio p_1 may be written in terms of the initial misalignment α, and the amplitude of excitation θ.

$$p_1 = \frac{mg \sin(\frac{\alpha+\theta}{2}) + (\frac{K_Y'-I_Y'\omega^2}{2h} - k_x(2h+1))\theta\cos(\frac{\alpha-\theta}{2})}{mg \cos(\frac{\alpha+\theta}{2}) + (\frac{K_Y'-I_Y'\omega^2}{2h} - k_x(2h+1))\theta\sin(\frac{\alpha-\theta}{2})} \tag{4.23}$$

Clearly if p_1 exceeds μ, slipping into the hole occurs.

Slipping out of the hole is most probable when the peg is aligned as in Fig. 4.10a, and we may write the surface reaction forces for the equivalent system, Fig. 4.10b, as

$$F_N = mg \cos(\frac{\alpha-\theta}{2}) - (F-F_x)\sin(\frac{\alpha+\theta}{2})$$

$$F_x = -mg \sin(\frac{\alpha-\theta}{2}) + (F-F_x)\cos(\frac{\alpha-\theta}{2})$$

As previously the ratio p_2 of sliding to normal contact force is given by

$$p_2 = \frac{-mg \sin(\frac{\alpha-\theta}{2}) + (\frac{K_Y'-I_Y'\omega^2}{2h} - k_x(2h+1))\theta\cos(\frac{\alpha+\theta}{2})}{mg \cos(\frac{\alpha-\theta}{2}) - (\frac{K_Y'-I_Y'\omega^2}{2h} - k_x(2h+1))\theta\sin(\frac{\alpha+\theta}{2})} \tag{4.24}$$

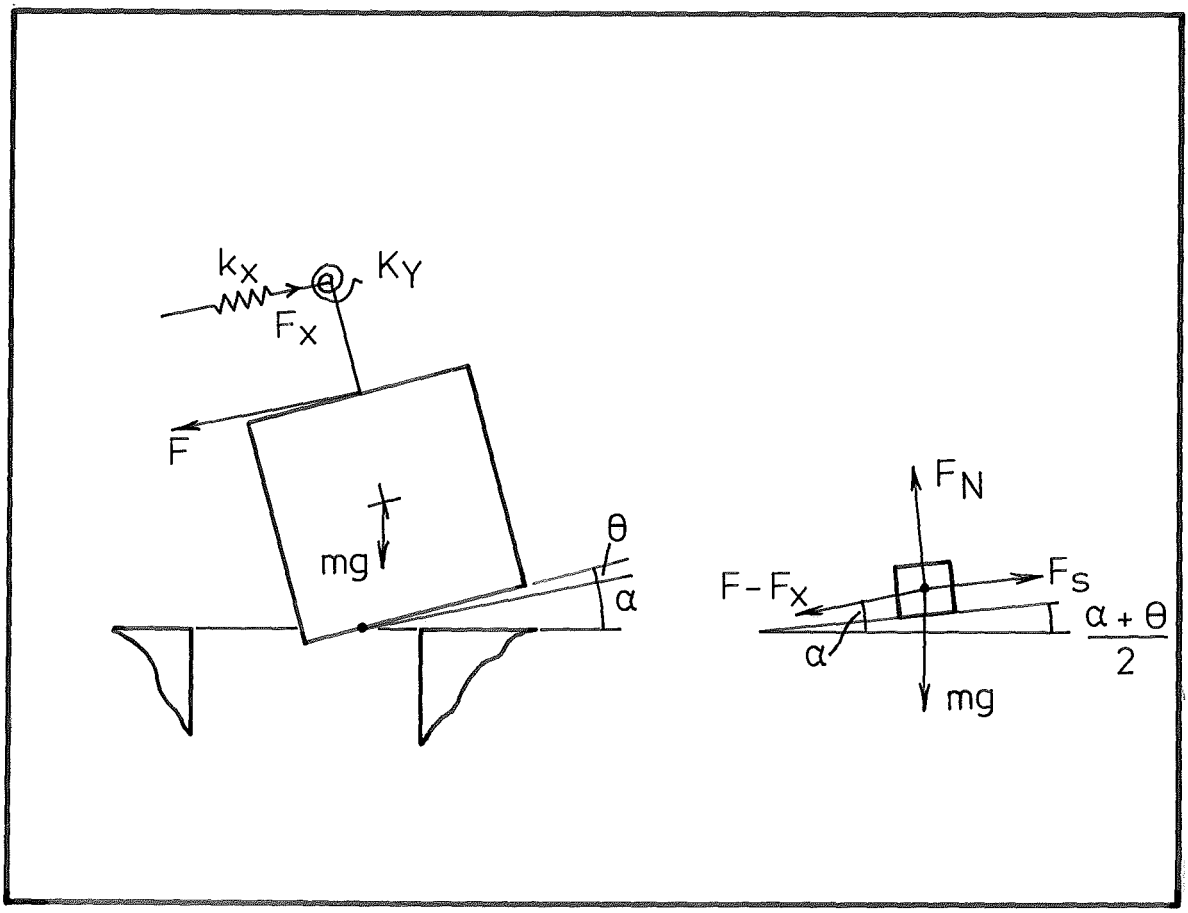

FIG. 4. 9 (a) SLIDING INTO HOLE (b) EQUIVALENT SYSTEM

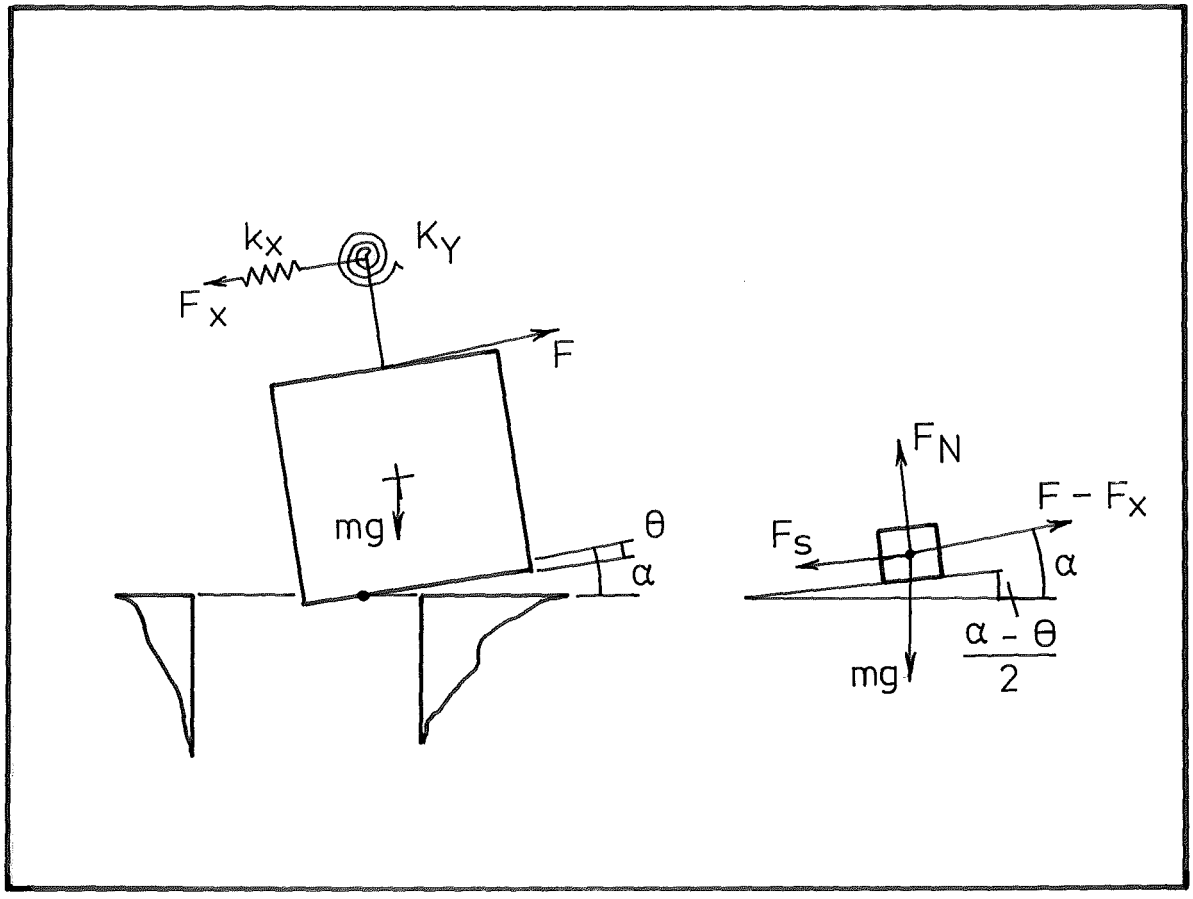

FIG. 4.10 (a) SLIDING OUT OF HOLE (b) EQUIVALENT SYSTEM

Equations 3.23 and 3.24 are shown in Fig. 4.11 for a typical system, Table 4.1. Clearly successful assembly will occur if the peg slides only toward the hole during a force cycle. The condition for this is that the force ratio p_1 for movement into the hole, should exceed μ and p_2, for movement out of the hole, should be less than μ. Obviously, where p_2 is negative and exceeds μ in magnitude, sliding will occur into the hole also. Even if p_2 exceeds μ and movement occurs out of the hole, the generally greater value of p_1 indicates that overall net sliding into the hole will take place.

From Equations 4.21 and 4.22 it is apparent that the spring reaction force increases relative to the exciting force as the system approaches its natural frequency. The spring reaction force F_x exceeds the exciting force when ω lies in the range

$$\sqrt{\left(\frac{k_x\, l(2h+l) + K_Y}{I_Y'}\right)} < \omega < \sqrt{\left(\frac{K_Y'}{I_Y'}\right)}$$

Sliding into the hole occurs in the case shown in Fig. 4.12a. The surface reaction force ratio is

$$p_1 = \frac{mg\,\sin\left(\frac{\alpha-\theta}{2}\right) + \left(k_x(2h+l)\,\frac{-K_Y'-I_Y'\omega^2}{2h}\right)\theta\cos\left(\frac{\alpha+\theta}{2}\right)}{mg\,\cos\left(\frac{\alpha-\theta}{2}\right) + \left(k_x(2h+l)\,\frac{-K_Y'-I_Y'\omega^2}{2h}\right)\theta\sin\left(\frac{\alpha+\theta}{2}\right)} \qquad (4.25)$$

Fig. 4.13a shows sliding out of the hole and the force ratio p_2 is

$$p_2 = \frac{-mg\,\sin\left(\frac{\alpha+\theta}{2}\right) - \left(k_x(2h+l)\,\frac{-K_Y'-I_Y'\omega^2}{2h}\right)\theta\cos\left(\frac{\alpha-\theta}{2}\right)}{mg\,\cos\left(\frac{\alpha+\theta}{2}\right) - \left(k_x(2h+l)\,\frac{-K_Y'-I_Y'\omega^2}{2h}\right)\theta\sin\left(\frac{\alpha-\theta}{2}\right)} \qquad (4.26)$$

Fig. 4.14 shows values of Equations 4.25 and 4.26 for a typical case.

At high frequencies

$$K_Y' - I_Y'\omega^2 < 0$$

the applied moment and displacement are out of phase by π. Fig. 4.15a

TABLE 4.1

SYSTEM PARAMETERS

DOUBLE POINT SLIDING CONTACT

m	=	.766 Kg
g	=	9806.6 mm/s^2
$K_{Y'}$	=	10^7 mN-mm
h	=	25 mm
r	=	25 mm
$I_{Y'}$	=	877 Kg-mm^2
$\Omega_{Y'}$	=	107 rad/s

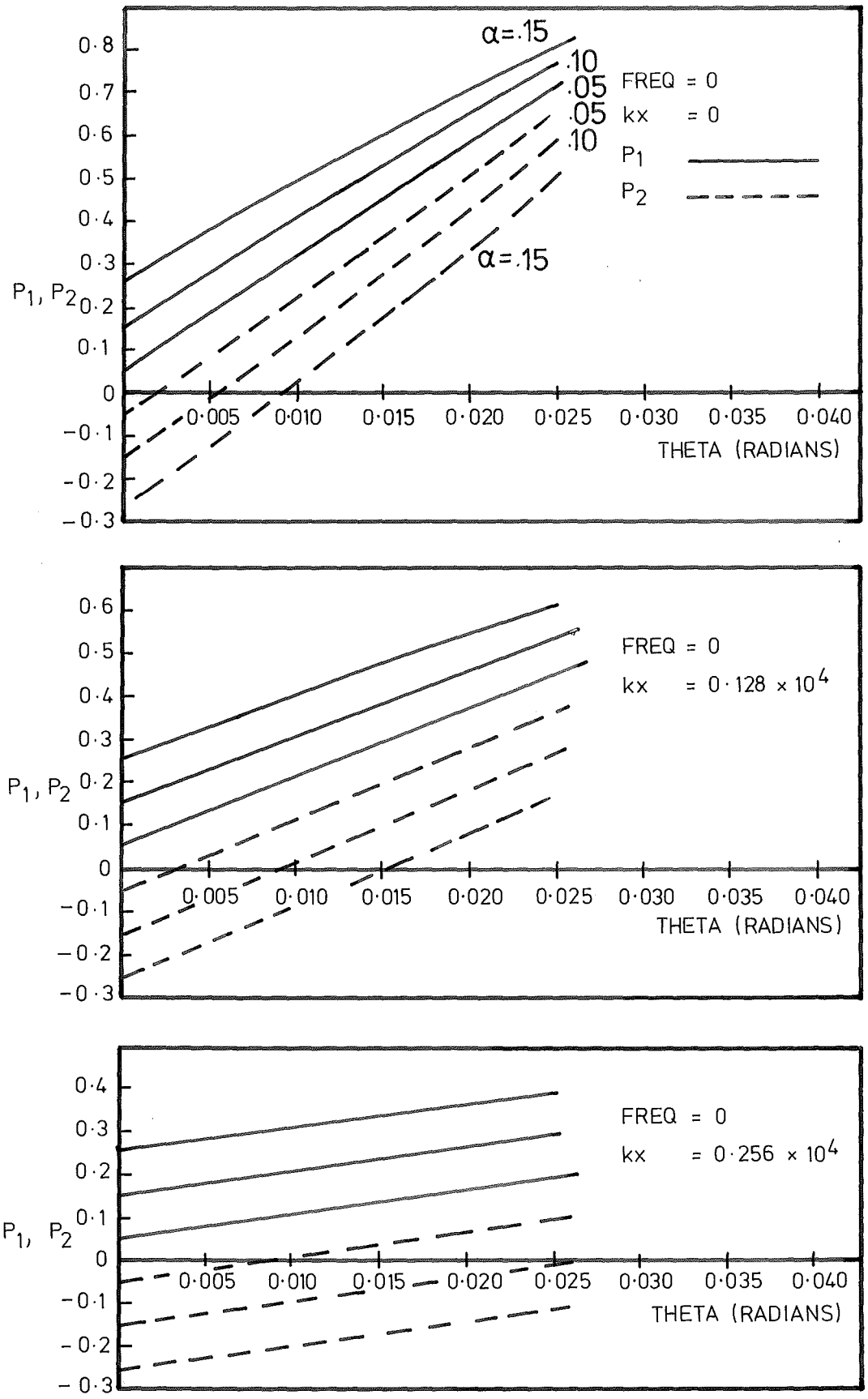

FIG. 4.11 ASSEMBLY AT LOW FREQUENCIES

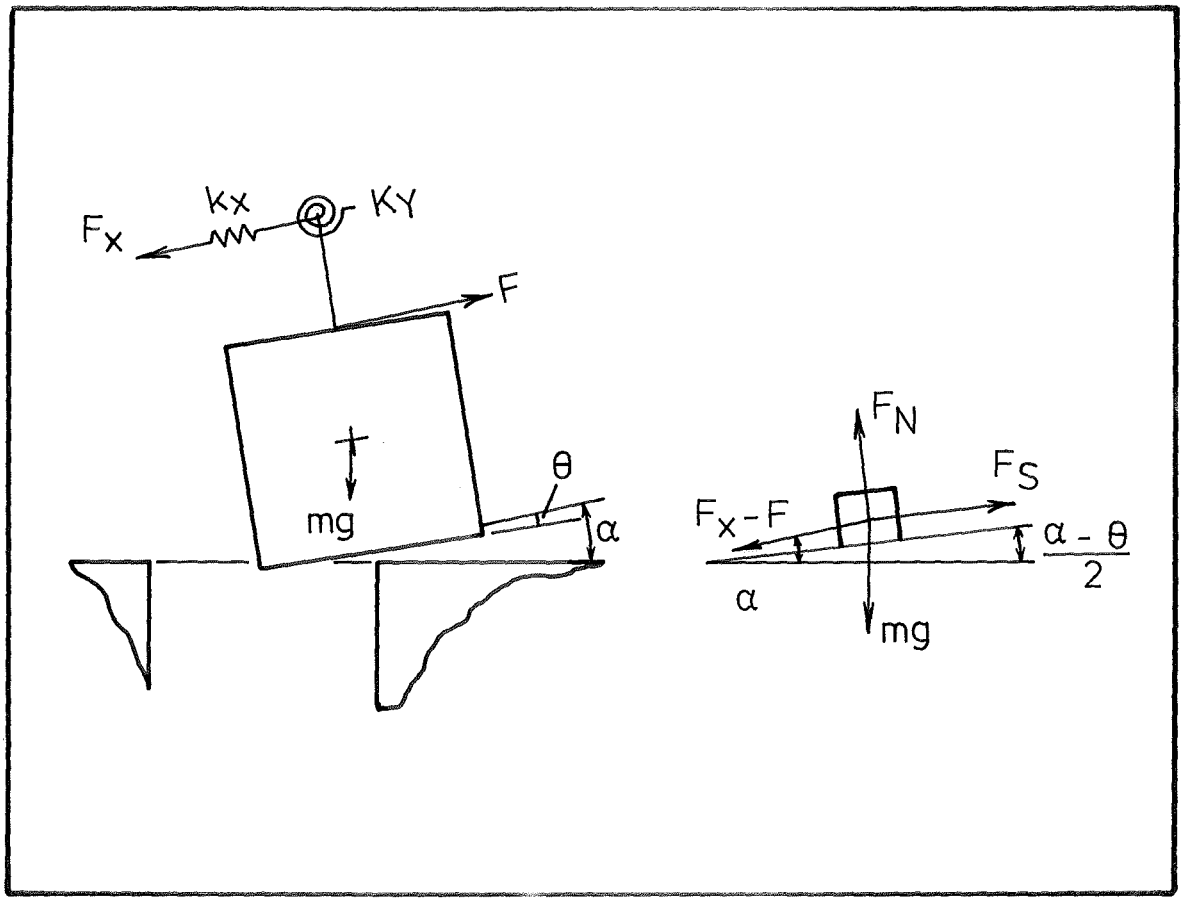

FIG. 4.12 (a) SLIDING INTO HOLE (b) EQUIVALENT SYSTEM

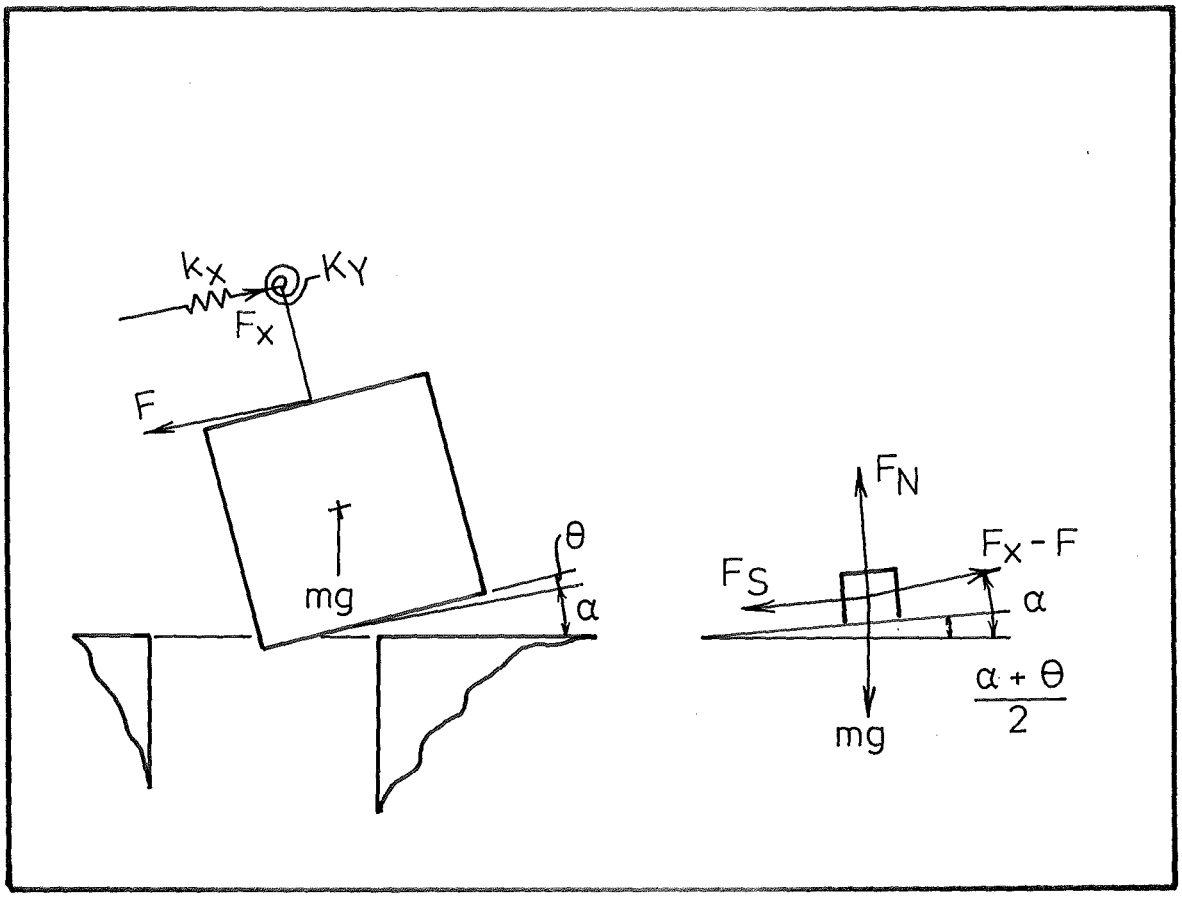

FIG. 4.13 (a) SLIDING OUT OF HOLE (b) EQUIVALENT SYSTEM

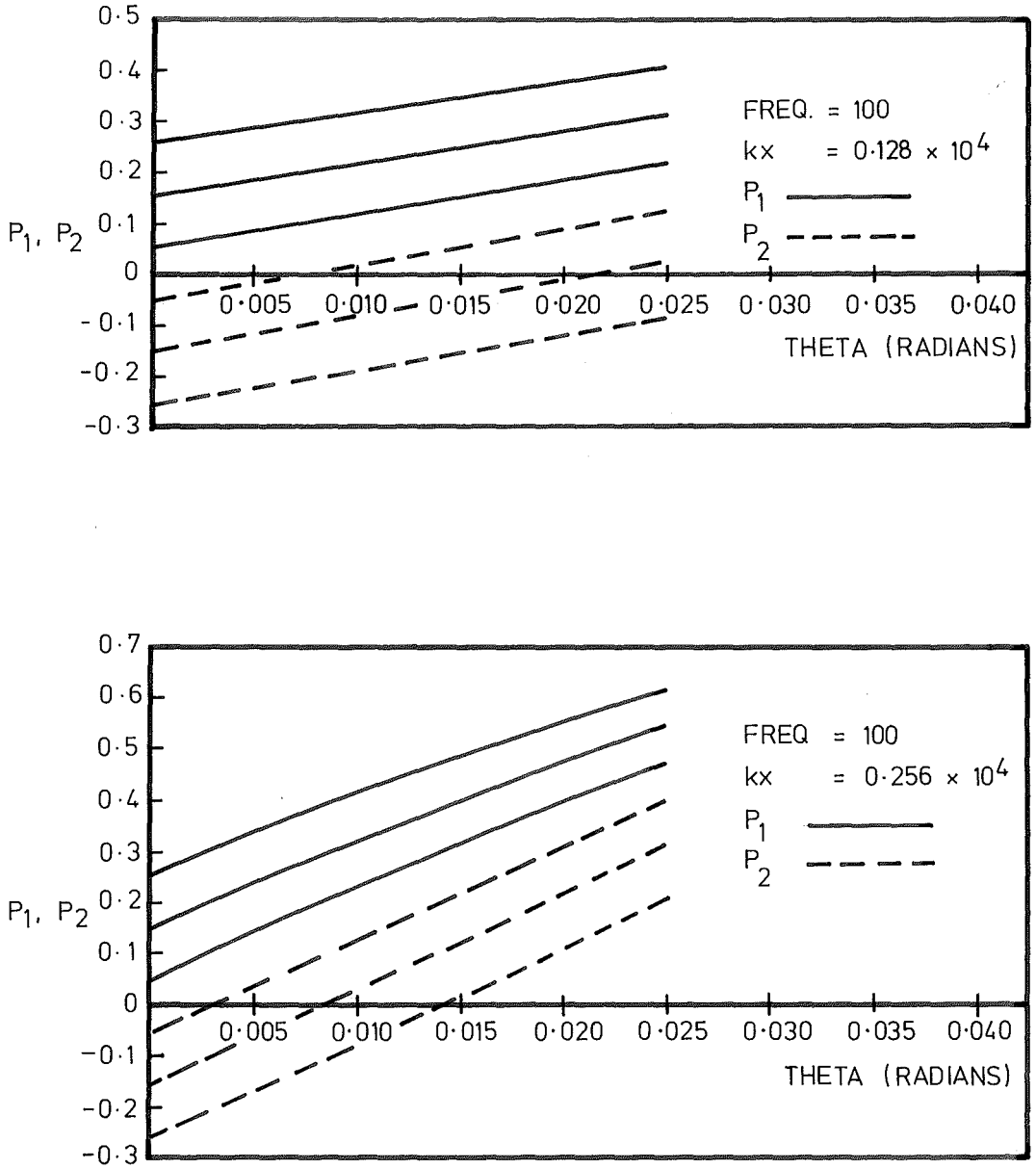

FIG. 4.14 ASSEMBLY AT INTERMEDIATE FREQUENCIES

shows when slipping into the hole is most probable, the force ratio in this case being

$$p_1 = \frac{mg \sin(\frac{\alpha-\theta}{2}) + (K_Y'-I_Y\omega^2 + k_x(2h+l))\theta\cos(\frac{\alpha-\theta}{2})}{mg \cos(\frac{\alpha-\theta}{2}) + \frac{(K_Y'-I_Y'\omega^2}{2h} + k_x(2h+l))\theta\sin(\frac{\alpha+\theta}{2})} \tag{4.27}$$

and finally referring to Fig. 4.16a the force ratio p_2 for sliding out of the hole is

$$p_2 = \frac{-mg \sin(\frac{\alpha+\theta}{2}) + \frac{(K_Y'-I_Y'\omega^2}{2h} + k_x(2h+l))\theta\cos(\frac{\alpha-\theta}{2})}{mg \cos(\frac{\alpha+\theta}{2}) + \frac{(K_Y'-I_Y'\omega^2}{2h} + k_x(2h+l))\theta\sin(\frac{\alpha-\theta}{2})} \tag{4.28}$$

Equations 4.27 and 4.28 are shown in Fig. 4.17. Referring to Figs. 4.11, 4.14 and 4.17 it can be seen in general that there is a tendency for the peg to vibrate into the hole. At higher frequencies and high exciting amplitudes the action of the translational constraint reverses this trend, as is apparent in Fig. 4.17c.

In general the method of two point contact sliding offers good assembly, operative under a wide range of frequencies and amplitudes, provided there is an initial misalignment toward the hole.

4.7 PEG EDGE - HOLE EDGE DOUBLE POINT - SINGLE POINT CONTACT WITH NO SLIDING

As the magnitude of F is increased, the weight of the peg becomes insufficient to maintain two point contact and the peg lifts onto a single contact point. Referring to Fig. 4.18, this may be expected when

$$F = \frac{mg\ r\sin\alpha}{2h}$$

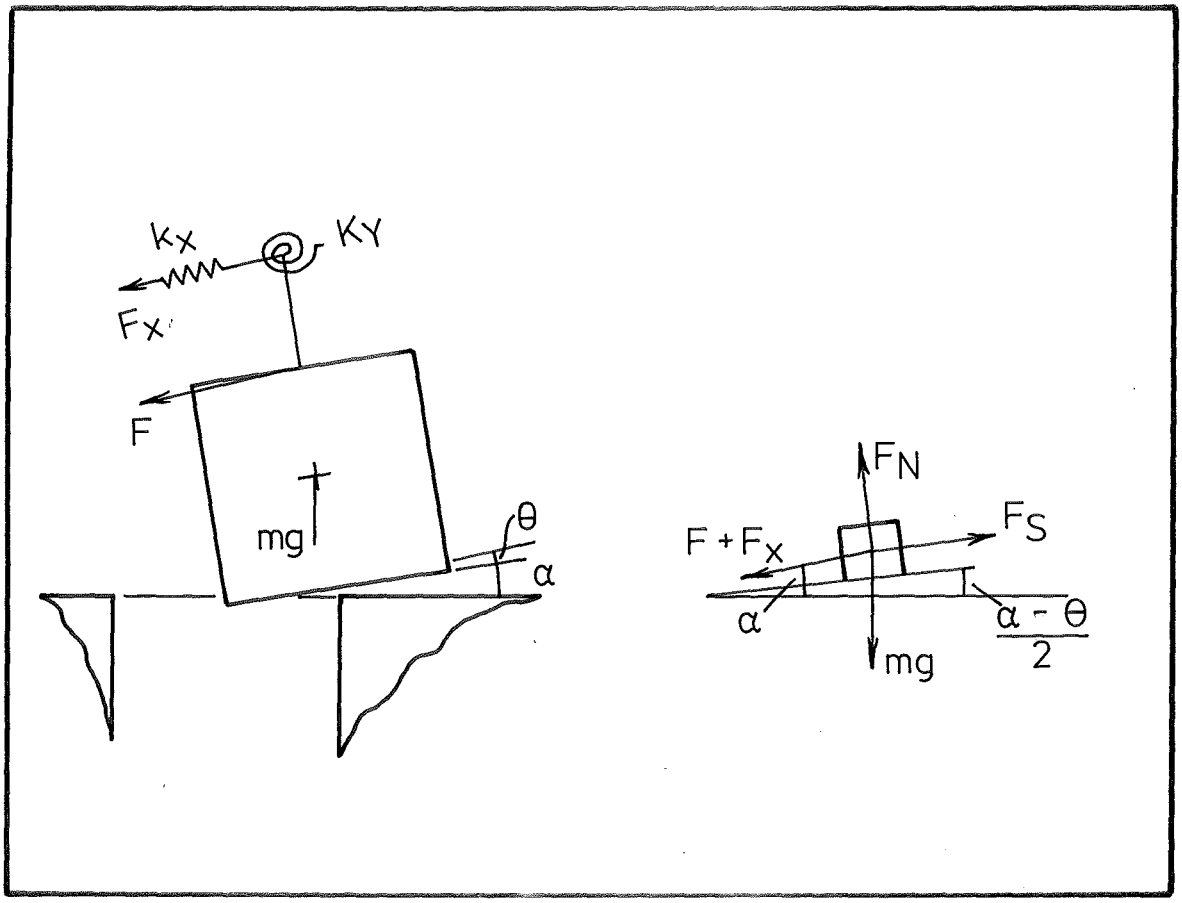

FIG. 4.15 (a) SLIDING INTO HOLE (b) EQUIVALENT SYSTEM

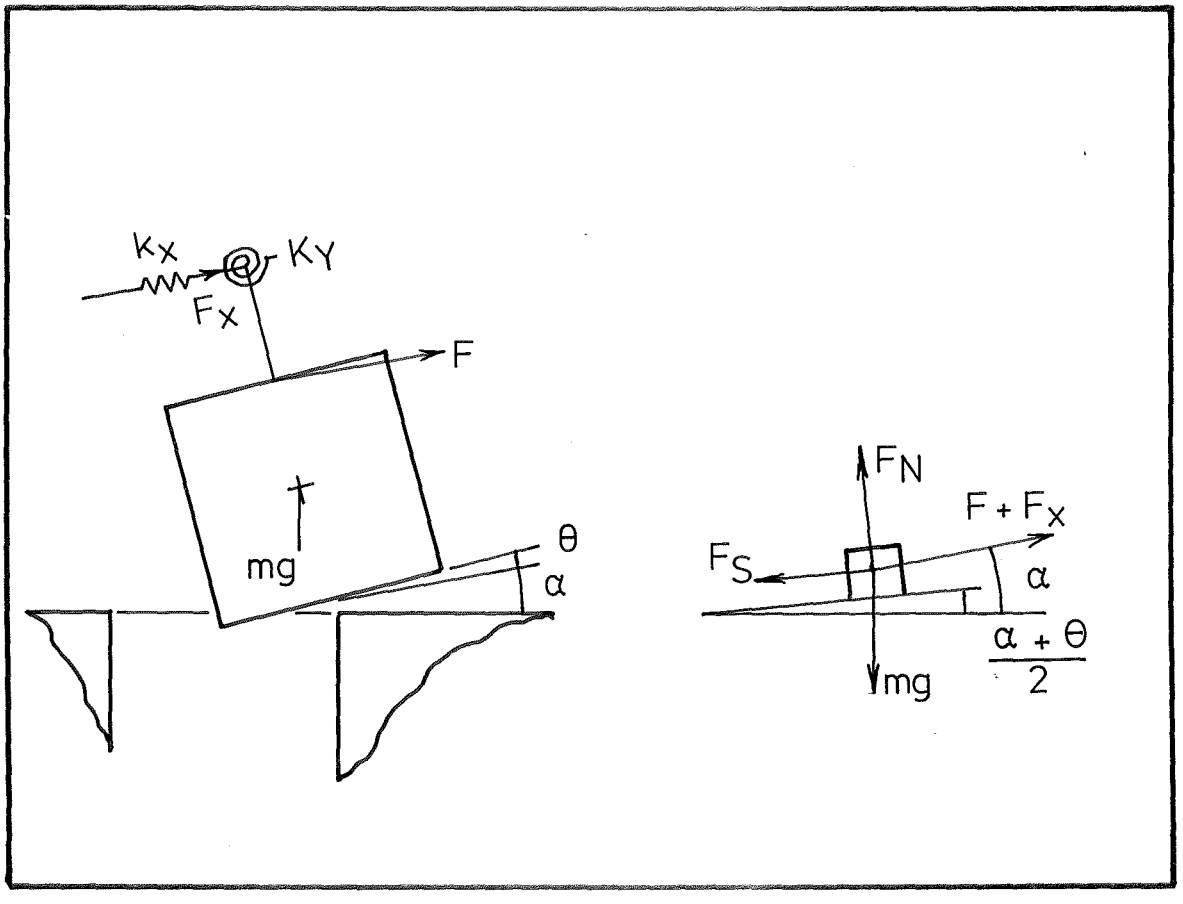

FIG. 4.16 (a) SLIDING OUT OF HOLE (b) EQUIVALENT SYSTEM

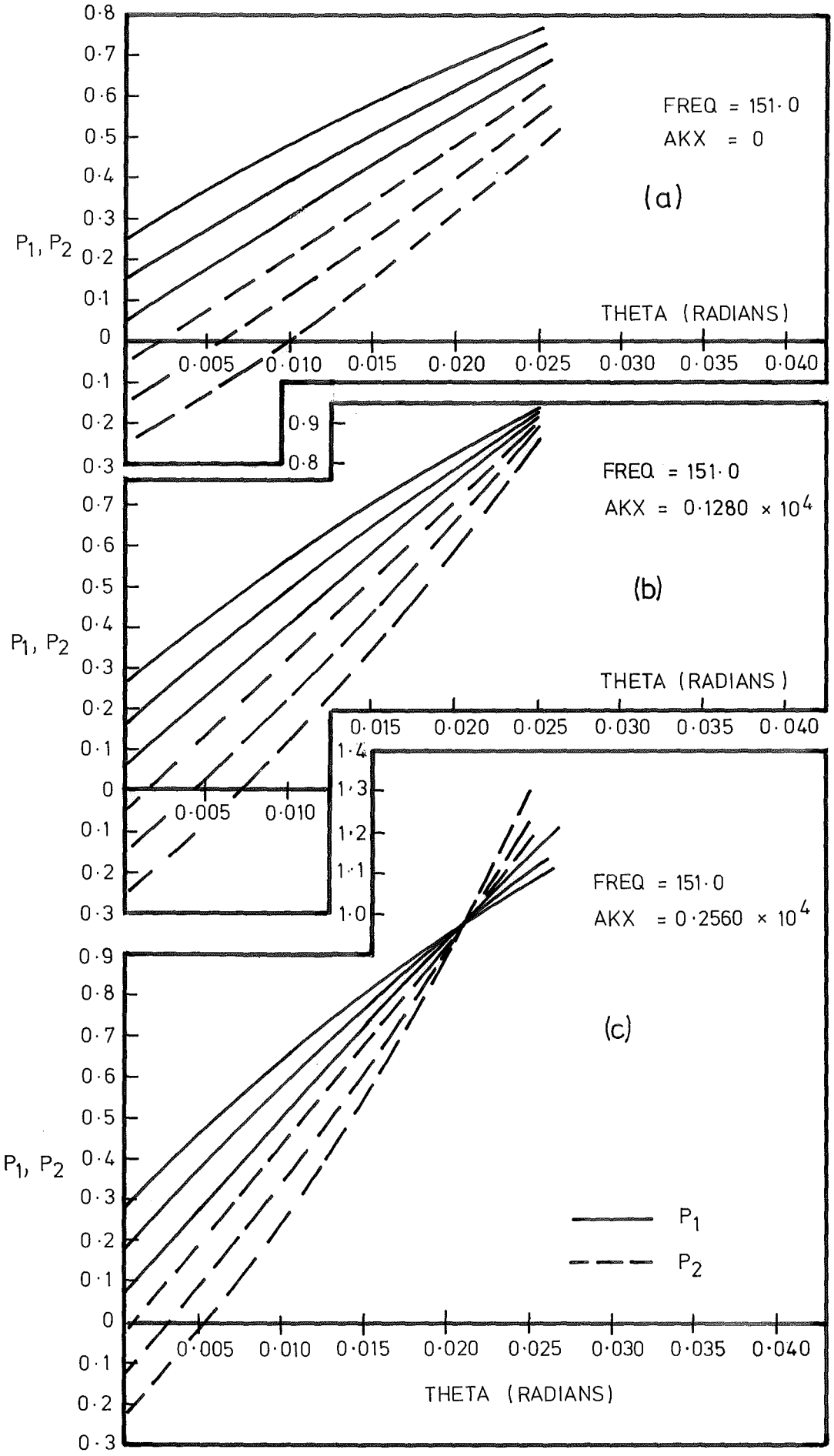

FIG. 4.17 ASSEMBLY AT HIGH FREQUENCIES

As the two modes of contact, i.e. single and double point contact, may occur alternately several times during each force cycle, the initial response of the system in each mode to the applied force and starting conditions is of interest. For the sake of simplicity, we will assume the rotational stiffnesses about the set of axes through the contact point to be equal.

4.7.1 Equations of Motion for Double Point Contact

It can be shown that the response of an initially quiescent spring-mass system, Fig. 4.19, to a time-varying force, F(t), may be written as [43]

$$x = \int_{t_1}^{t_2} \frac{F(t)\ \sin\Omega(t_2-t)}{M\Omega}\,dt$$

where $\Omega = \sqrt{\frac{K}{M}}$

The equation of motion for small movements of the peg about the Y' axis passing through the contact points, Fig. 4.20, is

$$I_{Y'}\,\ddot{\theta}_{Y'} + K_{Y'}\theta_{Y'} = M_{Y'}$$

The stiffness and inertia terms are identical to those used in Sec. 4.5, and the moment $M_{Y'}$ of the applied forces about the Y' axis is expressed as

$$M_{Y'} = 2Fh\cos\omega t - mgr(1-\cos\alpha)$$

The response of the quiescent system to this forcing function becomes

$$\theta_{Y'} = \int_{t_1}^{t_2} \frac{(2Fh\cos\omega t - mgr(1-\cos\alpha))\sin\Omega_{Y'}(t_2-t)}{I_{Y'}\,\theta_{Y'}}\,dt \qquad (4.29)$$

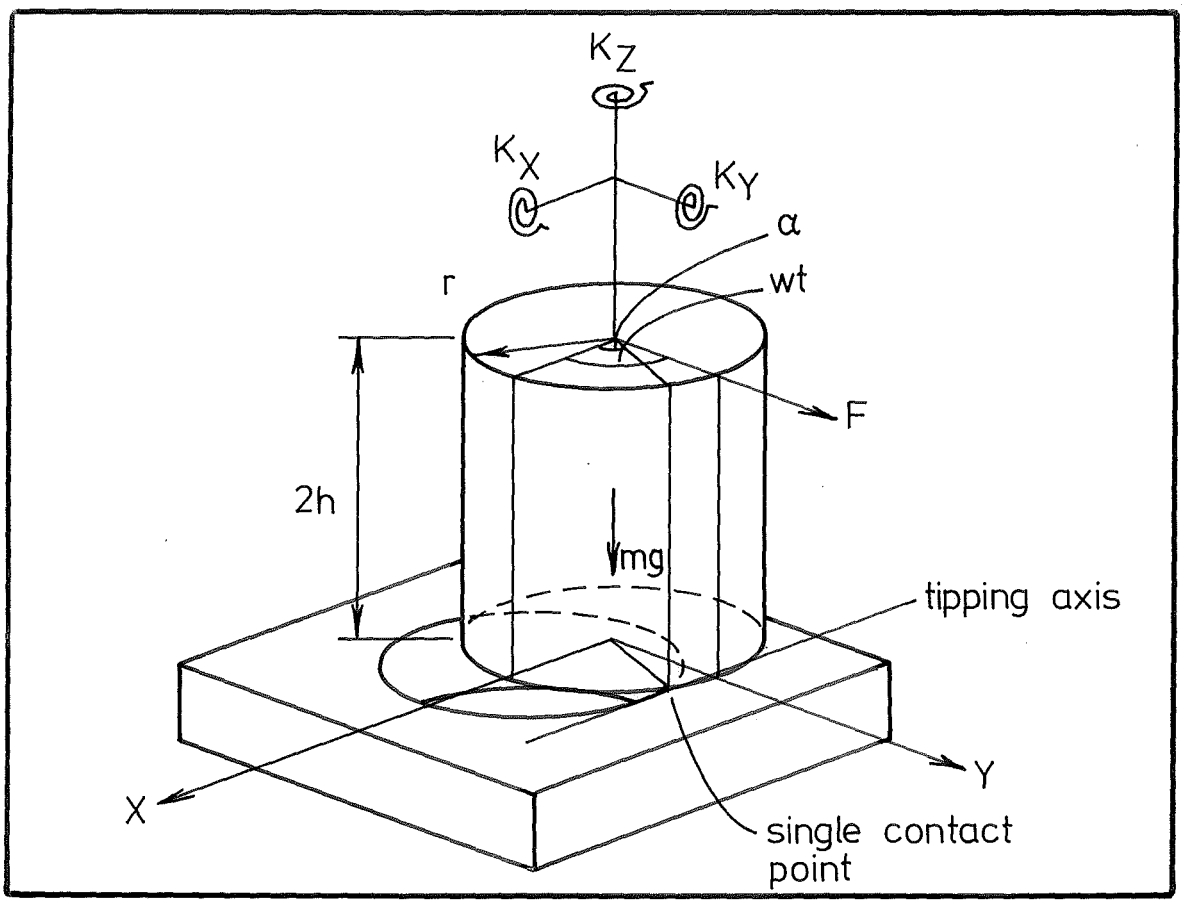

FIG. 4.18 SINGLE POINT CONTACT

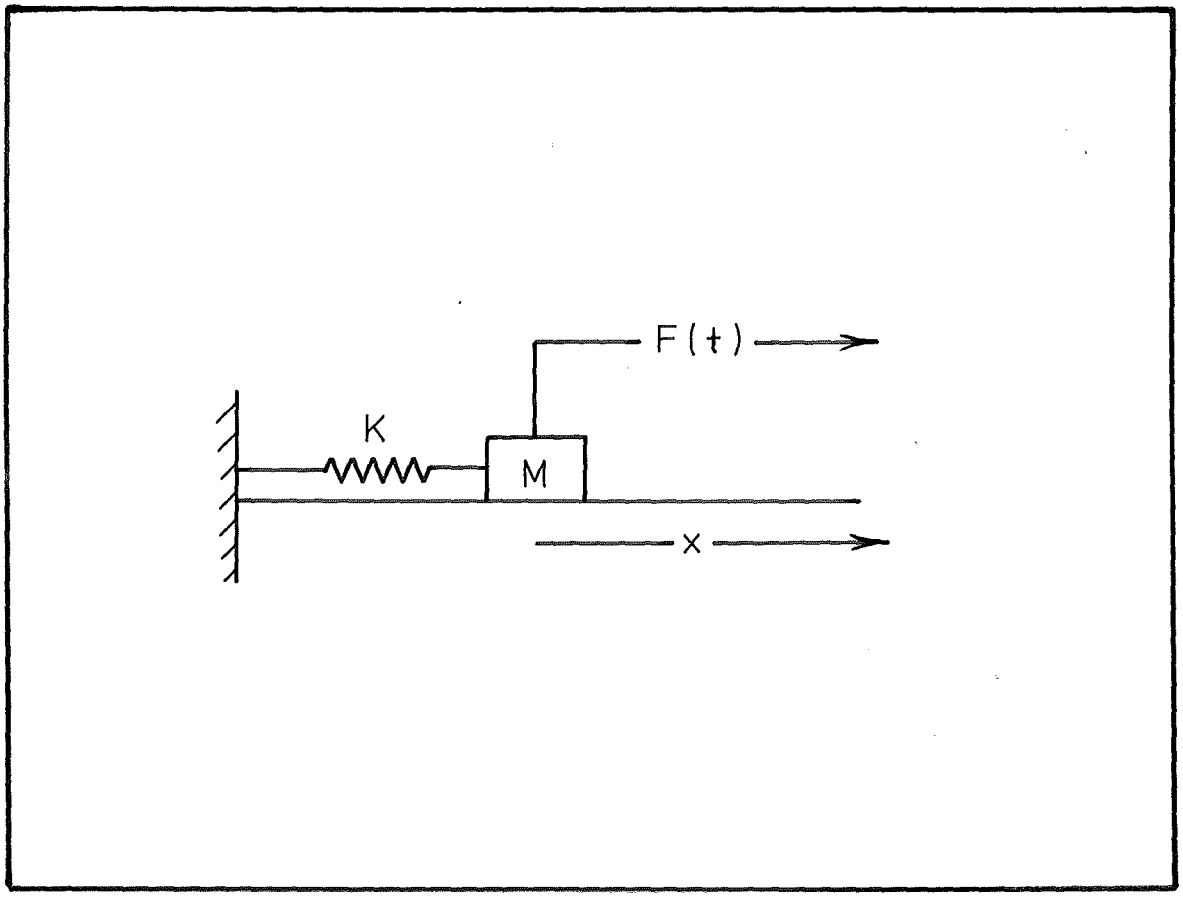

FIG. 4.19 SPRING MASS SYSTEM

where

$$\Omega_{Y'} = \sqrt{\left(\frac{K_{Y'}}{I_{Y'}}\right)}$$

Evaluating this integral and incorporating the responses due to initial conditions $\dot{\theta}^{i}_{Y'}$, $\theta^{i}_{Y'}$, we obtain

$$\theta_{Y'} = \frac{2Fh}{I_{Y'}\Omega_{Y'}} \sin\Omega_{Y'}t_2 \left[\frac{\sin\alpha t}{2\alpha} + \frac{\sin\beta t}{2\beta} \right]_{t_1}^{t_2}$$

$$- \frac{2Fh}{I_{Y'}\Omega_{Y'}} \cos\Omega_{Y'}t_2 \left[\frac{\cos\alpha t}{2\alpha} - \frac{\cos\beta t}{2\beta} \right]_{t_1}^{t_2}$$

$$\frac{-mgr(1-\cos\alpha)}{I_{Y'}\Omega_{Y'}^2} \left[1 - \cos\Omega_{Y'}(t_2-t_1) \right]$$

$$+ \frac{\dot{\theta}^{i}_{Y'}}{\Omega_{Y'}} \sin\Omega_{Y'}(t_2-t_1) + \theta^{i}_{Y'}\cos\Omega_{Y'}(t_2-t_1) \qquad (4.30)$$

where

$$\alpha = \omega - \Omega_{Y'}$$

$$\beta = \omega + \Omega_{Y'}$$

4.7.2 Equations of Motion for Single Point Contact

The peg lifts onto a single contact point when

$$2Fh\sin\omega t > mgr\sin\alpha \qquad (4.31)$$

Equations 4.1 - 4.6 in Sec. 4.3 describe the motion of the system in single point contact, Fig. 4.21. In this case the response of the quiescent system is required.

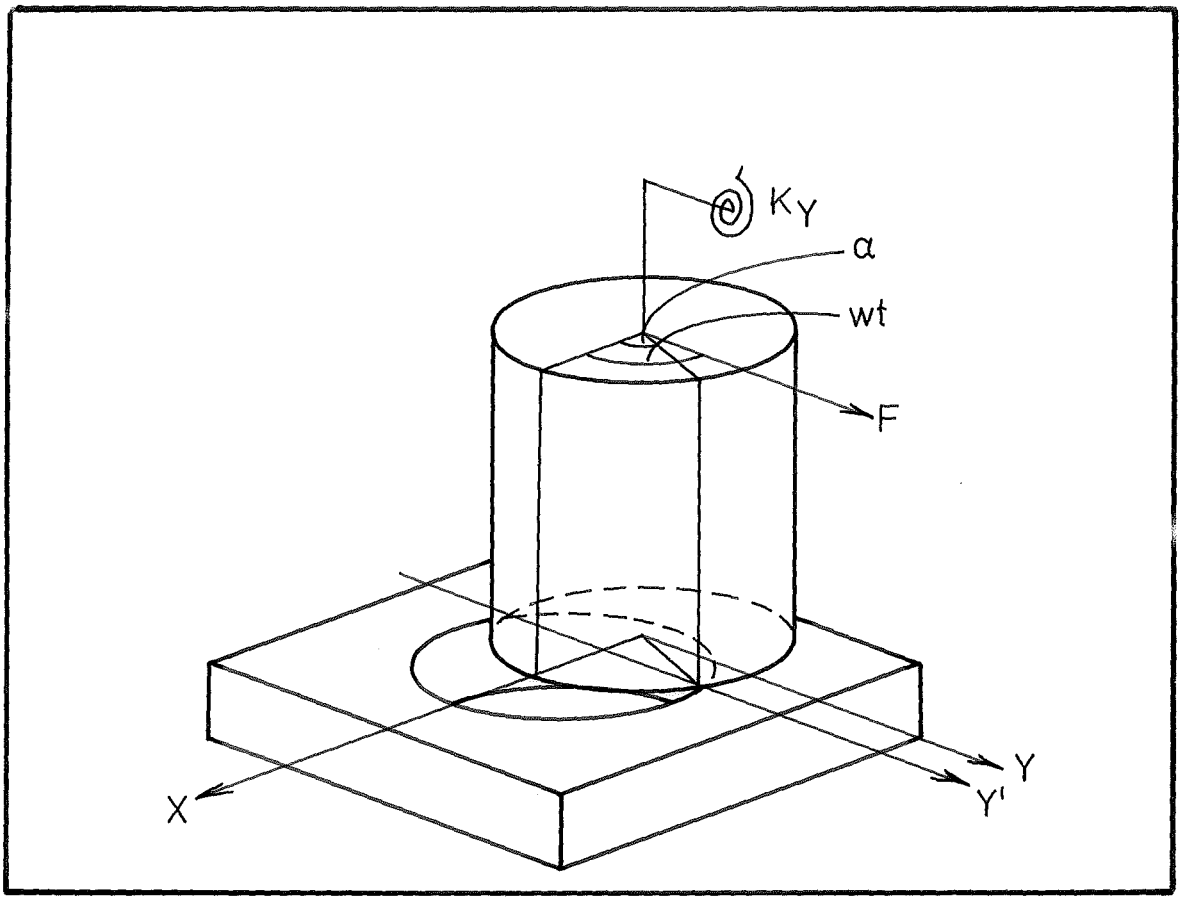

FIG. 4.20 PEG-EDGE HOLE-EDGE DOUBLE POINT CONTACT

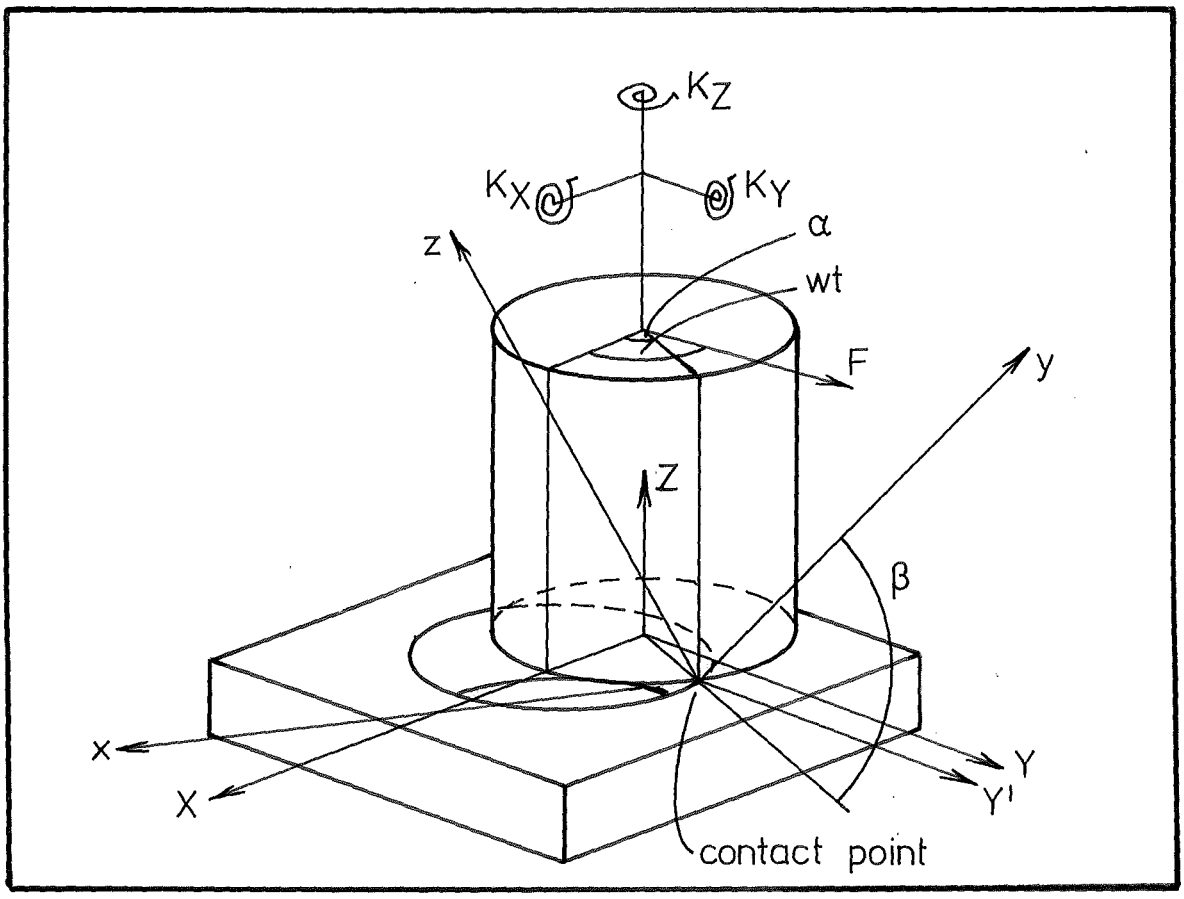

FIG. 4.21 SINGLE POINT CONTACT

$$\theta_x = \int_{t_1}^{t_2} \frac{(-2Fh\cos(\omega t-\alpha) + mgr)\sin\Omega_x(t_2-t)dt}{I_x\Omega_x} \tag{4.32}$$

$$\theta_y = \int_{t_1}^{t_2} \frac{-F\sin(\omega t-\alpha)(r\sin\beta+2h\cos\beta)\sin\Omega_y(t_2-t)dt}{I_y\Omega_y} \tag{4.33}$$

$$\theta_z = \int_{t_1}^{t_2} \frac{-F\sin(\omega t-\alpha)(r\cos\beta-2h\sin\beta)\sin\Omega_z(t_2-t)dt}{I_z\Omega_z} \tag{4.34}$$

Evaluating and inserting initial values we have

$$\theta_x = \frac{-2FhA_x}{I_x\Omega_x}\left[\frac{\sin\alpha_x t}{2\alpha_x} + \frac{\sin\beta_x t}{2\beta_x}\right]_{t_1}^{t_2}$$

$$\frac{-2Fh\,B_x}{I_x\Omega_x}\left[\frac{\cos\alpha_x t}{2\alpha_x} - \frac{\cos\beta_x t}{2\beta_x}\right]_{t_1}^{t_2}$$

$$\frac{-2FhC_x}{I_x\Omega_x}\left[\frac{-\cos\alpha_x t}{2\alpha_x} - \frac{\cos\beta_x t}{2\beta_x}\right]_{t_1}^{t_2}$$

$$\frac{-2FhD_x}{I_x\Omega_x}\left[\frac{\sin\alpha_x t}{2\alpha_x} - \frac{\sin\beta_x t}{2\beta_x}\right]_{t_1}^{t_2}$$

$$\frac{+mgr}{I_x\Omega_x^2}\left[1 - \cos\Omega_x(t_2-t_1)\right]$$

$$\frac{+\dot{\theta}_x^i}{\Omega_x}\sin\Omega_x(t_x-t_1)$$

$$+\theta_x^i\cos\Omega_x(t_2-t_1) \tag{4.35}$$

$$\theta_y = \frac{-FpA_y}{I_y\Omega_y}\left[\frac{-\cos\alpha_y t}{2\alpha_y} - \frac{\cos\beta_y t}{2\beta_y}\right]_{t_1}^{t_2}$$

$$\frac{-FpB_y}{I_y\Omega_y}\left[\frac{\sin\alpha_y t}{2\alpha_y} - \frac{\sin\beta_y t}{2\beta_y}\right]_{t_1}^{t_2}$$

$$\frac{-FpC_y}{I_y\Omega_y}\left[\frac{\sin\alpha_y t}{2\alpha_y} + \frac{\sin\beta_y t}{2\beta_y}\right]_{t_1}^{t_2}$$

$$\frac{-FpD_y}{I_y\Omega_y}\left[\frac{\cos\alpha_y t}{2\alpha_y} - \frac{\cos\beta_y t}{2\beta_y}\right]_{t_1}^{t_2}$$

$$+ \frac{\dot{\theta}_y^i}{\Omega_y}\sin\Omega_y(t_2-t_1) + \theta_y^i\cos\Omega_y(t_2-t_1) \qquad (4.36)$$

$$\theta_z = \frac{-FqA_z}{I_z\Omega_z}\left[\frac{-\cos\alpha_z t}{2\alpha_z} - \frac{\cos\beta_z t}{2\beta_z}\right]_{t_2}^{t_1}$$

$$\frac{-FqB_z}{I_z\Omega_z}\left[\frac{\sin\alpha_z t}{2\alpha_z} - \frac{\sin\beta_z t}{2\beta_z}\right]_{t_2}^{t_1}$$

$$+ \frac{FqC_z}{I_z\Omega_z}\left[\frac{\sin\alpha_z t}{2\alpha_z} + \frac{\sin\beta_z t}{2\beta_z}\right]_{t_2}^{t_1}$$

$$\mp \frac{FqD_z}{I_z\Omega_z}\left[\frac{\cos\alpha_z t}{2\alpha_z} - \frac{\cos\beta_z t}{2\beta_z}\right]_{t_2}^{t_1}$$

$$+\frac{\dot{\theta}_z^i}{\Omega_z}\sin\Omega_z(t_2-t_1) + \theta_z^i\cos\Omega_z(t_2-t_1) \qquad (4.37)$$

where $\Omega_r = \frac{K_r}{I_r}$

$\alpha_r = \omega - \Omega_r$

$\beta_r = \omega + \Omega_r$

$p = r\sin\beta + 2h\cos\beta$

$q = r\cos\beta - 2h\sin\beta$

$A_r = \cos\alpha \sin\Omega_r t_2$

$B_r = -\cos\alpha \cos\Omega_r t_2$

$C_r = \sin\alpha \sin\Omega_r t_2$

$D_r = -\sin\alpha \cos\Omega_r t_2$

4.7.2.1 Transformation of Rotations About Principal Axes

The rotations about the principal axes of inertia can be expressed in terms of the rotations about the main XYZ system, using the fact that small rotational displacements may be added vectorially.

The angular relationship between the main, XYZ, and principal inertia axes systems for small angular displacements may be expressed in terms of the variables α and β. Referring to Fig. 4.22

$$\begin{bmatrix} X \\ Y \\ Z \end{bmatrix} = [R_1] \begin{bmatrix} X' \\ Y' \\ Z' \end{bmatrix} = \begin{bmatrix} \sin\alpha & \cos\alpha & 0 \\ -\cos\alpha & \sin\alpha & 0 \\ 0 & 0 & 1 \end{bmatrix} \begin{bmatrix} x' \\ y' \\ z' \end{bmatrix}$$

$$\begin{bmatrix} x' \\ y' \\ z' \end{bmatrix} = [R_2] \begin{bmatrix} x \\ y \\ z \end{bmatrix} = \begin{bmatrix} 1 & 0 & 0 \\ 0 & \cos\beta & -\sin\beta \\ 0 & \sin\beta & \cos\beta \end{bmatrix} \begin{bmatrix} x \\ y \\ z \end{bmatrix}$$

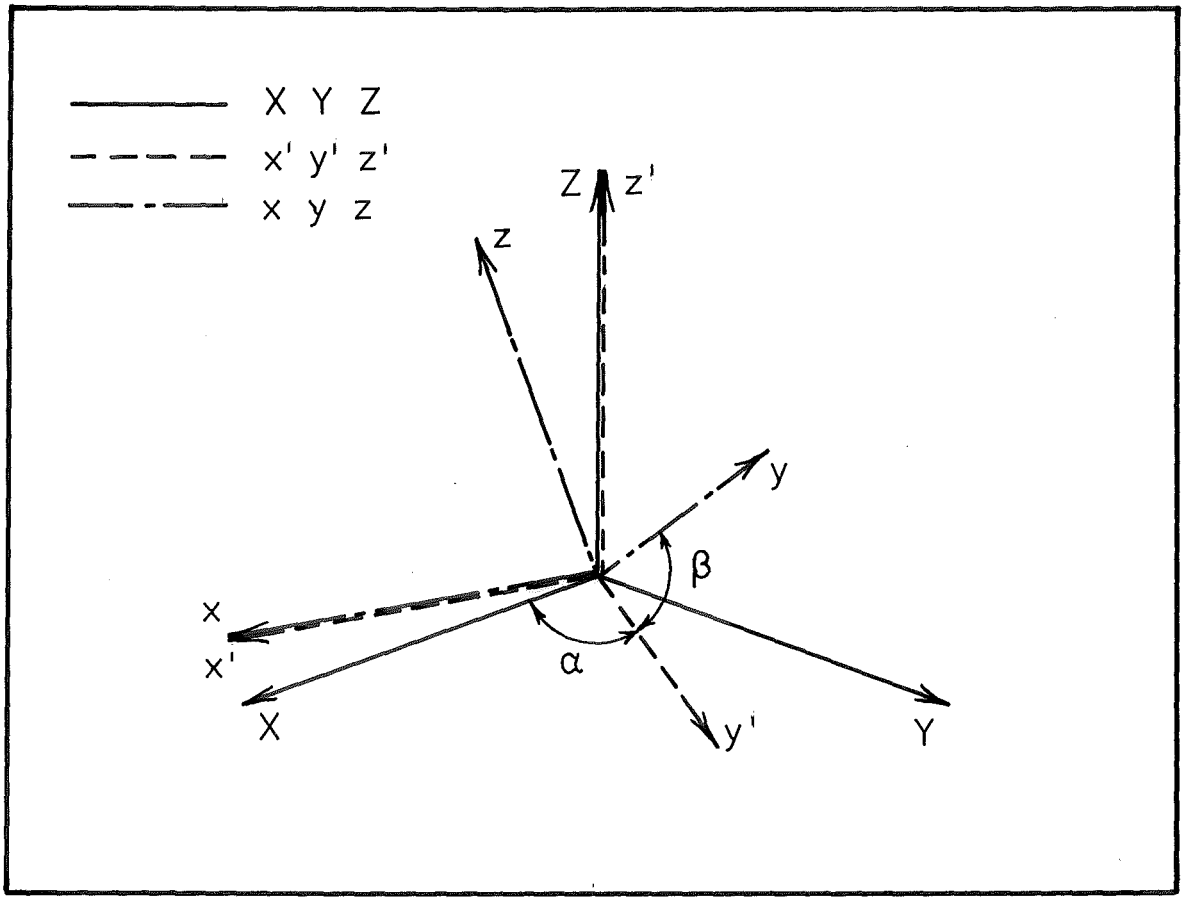

FIG 4.22 TRANSFORMATION BETWEEN COORDINATE SYSTEMS

so

$$\begin{bmatrix} X \\ Y \\ Z \end{bmatrix} = [R_1][R_2] \begin{bmatrix} x \\ y \\ z \end{bmatrix} = [R] \begin{bmatrix} x \\ y \\ z \end{bmatrix}$$

i.e.

$$\begin{bmatrix} X \\ Y \\ Z \end{bmatrix} = \begin{bmatrix} \sin\alpha & \cos\alpha\cos\beta & -\cos\alpha\sin\beta \\ -\cos\alpha & \sin\alpha\cos\beta & -\sin\alpha\sin\beta \\ 0 & \sin\beta & \cos\beta \end{bmatrix} \begin{bmatrix} x \\ y \\ z \end{bmatrix} \tag{4.37}$$

The angle α describes the position of the contact point, with respect to the main coordinate system, and β is the angle between the XY plane and the y principal axis. For a solid cylinder it may easily be shown that

$$\beta = \tfrac{1}{2} \tan^{-1} \frac{12rh}{(16\ h^2 - 15\ r^2)}$$

4.7.3 Total Solution

In general, both the single and double point edge-edge contacts occur, and the starting conditions for each case are obtained from the final state of the peg in the previous contact mode.

The transition to single point contact from double point contact occurs when the inequality 4.31 holds. In the double point contact mode, by definition, rotation about the Y' axis only exists, and so the initial conditions for the single point contact Equations 4.35 - 4.37 are obtained from the final position $\theta_{fY'}$, and final velocity $\dot{\theta}_{fY'}$ of the peg in the double point contact mode. Also the θ_{fZ} position existing when two point contact was first established must be considered. The initial conditions then are

$$\begin{bmatrix} \theta_x^i \\ \theta_y^i \\ \theta_z^i \end{bmatrix} = [R^{-1}] \begin{bmatrix} 0 \\ \theta_{fY'} \\ \theta_{fZ} \end{bmatrix} \tag{4.39}$$

$$\begin{bmatrix} \dot{\theta}_x^i \\ \dot{\theta}_y^i \\ \dot{\theta}_z^i \end{bmatrix} = [R^{-1}] \begin{bmatrix} 0 \\ \dot{\theta}_{fY'} \\ 0 \end{bmatrix} \tag{4.40}$$

Two point contact is re-established when θ_x becomes zero again. It is assumed that inelastic contact occurs, and as the new contact point through which the contact impulse is applied lies on the Y' axis, no change in the rotational velocity about the Y' axis occurs whilst, the values of $\dot{\theta}_x$ and $\dot{\theta}_z$ become zero. The values of $\dot{\theta}_y$ and θ_y therefore become the initial values $\dot{\theta}_{Y'}^i$, and $\theta_{Y'}^i$, in Equation 4.30, describing double point contact motion.

Equations 4.30 and 4.35 - 4.37 have been evaluated for a typical system, Table 4.2, the results being shown in Fig. 4.23. It is apparent from considering the rotation about the vertical Z axis occurring at each single contact point, that the peg exhibits a tendency to "walk" out of the hole. In other words the final position θ_{fZ} when double point contact is re-established, is such that a net rotation out of the hole has occurred during the single point contact phase.

As this analysis assumes non-sliding contact it may be useful to determine briefly under what circumstances intermittent contact occurs.

TABLE 4.2

SYSTEM PARAMETERS

SINGLE POINT DOUBLE POINT INTERMITTENT CONTACT

m	=	.766 Kg
g	=	9806.6 mm/s^2
K_x	=	10^7 mN-mm
K_y	=	10^7 mN-mm
K_z	=	10^7 mN=mm
$K_{Y'}$	=	10^7 mN-mm
h	=	25 mm
r	=	25 mm
I_x	=	1237 Kg-mm^2
I_y	=	1217 Kg-mm^2
I_z	=	259 Kg-mm^2
$I_{Y'}$	=	1199 Kg-mm^2
F	=	1500 mN
Ω_x	=	89 rad/s
Ω_y	=	90 rad/s
Ω_z	=	196 rad/s
$\Omega_{Y'}$	=	91 rad/s

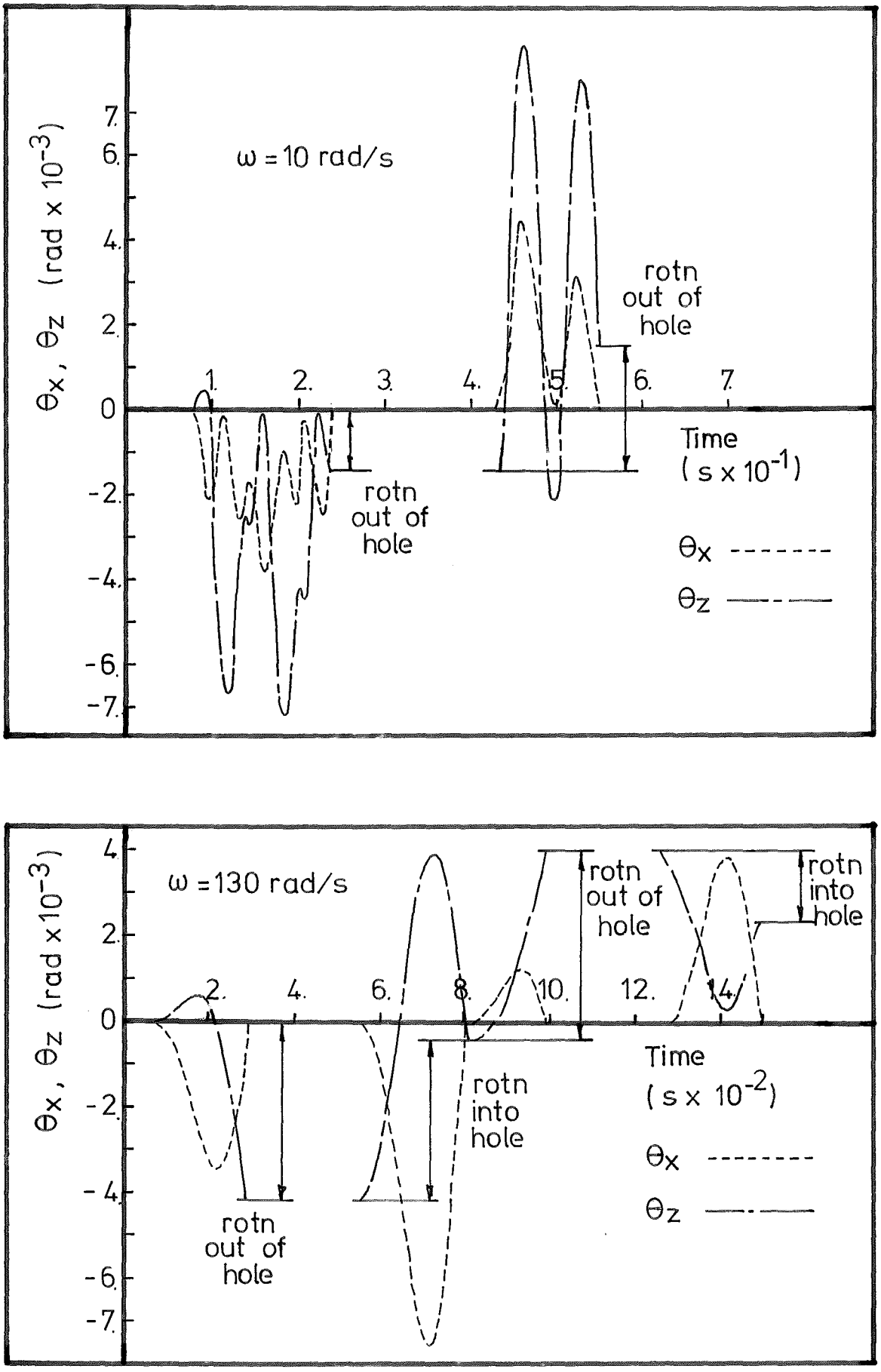

FIG. 4.23 DOUBLE AND SINGLE POINT CONTACT

Assuming the normal contact force

$$F_N = mg$$

and the friction force

$$F_s = \mathbf{F}$$

then combining the conditions for single point contact, Inequality 4.31, with the simple friction relationship we get

$$\mu > \frac{r \sin\alpha}{2h} \tag{4.41}$$

This inequality must hold for non sliding single point contact. If we further assume that for a typical system

$$r = h$$

then from 4.41 the limiting value of α is

$$\alpha = \sin^{-1}(2\mu)$$

and the overlap as defined in Fig. 4.24 becomes

$$2r(1-\sqrt{(1-4\mu^2)})$$

i.e. for a value $\mu = .2$ the maximum overlap for the walking motion to be possible is only 8.35% of the peg radius. It would seem therefore that walking is not an important mode of behaviour and occurs under the following conditions.

(i) In badly misaligned cases,

(ii) Where high friction exists.

(iii) The peg height h is large compared with the radius r.

4.8 PEG EDGE - HOLE EDGE HOLE PLANE CONTACT

So far we have considered only edge-hole edge contacts. In this section the effects of interaction between the peg edge and hole plane are studied.

Initially two point edge-edge contact occurs and the peg is at rest on the hole plane as depicted in Fig. 4.25. The rotating force F is insufficient to cause tipping about the peg edge on the hole plane however tipping occurs about the Y' axis when

$$2Fh\sin\omega t > mgr\cos\alpha \tag{4.42}$$

When $\theta_{Y'}$ becomes zero again impact occurs and two possibilities exist. If the impact is totally inelastic the system returns to its quiescent state. If elasticity exists, as is possible in the impact of flat surfaces, an impulse is imparted to the peg, and the subsequent free flight motion is determined by the mass and inertia of the peg, and the system constraints. This second possibility is examined in Sec. 4.82.

4.8.1 Equations of Motion for Peg Edge - Hole Edge Contact

The movement of the peg in double point contact, Fig. 4.26, is governed by the equation

$$I_{Y'}\ddot{\theta}_{Y'} + K_{Y'}\theta_{Y'} = M$$

where $I_{Y'}$ and $K_{Y'}$ are as defined in Sec. 4.5 and in this case

$$M = 2Fh\sin\omega t - mgr\cos\alpha \tag{4.43}$$

From the quiescent state therefore

$$\theta_{Y'} = \int_{t_1}^{t_2} \frac{(2Fh\sin\omega t - mgr\cos\alpha)}{I_{Y'}\Omega_{Y'}} \sin\Omega_{Y'}(t_2-t)\,dt$$

which becomes

$$\theta_{Y'} = \frac{2Fh}{I_{Y'}\Omega_{Y'}} \sin\Omega_{Y'}t_2 \left[\frac{-\cos(2-\Omega_{Y'})t}{2(\omega-\Omega_{Y'})} \quad \frac{-\cos(\omega+\Omega_{Y'})t}{2(\omega+\Omega_{Y'})} \right]_{t_1}^{t_2}$$

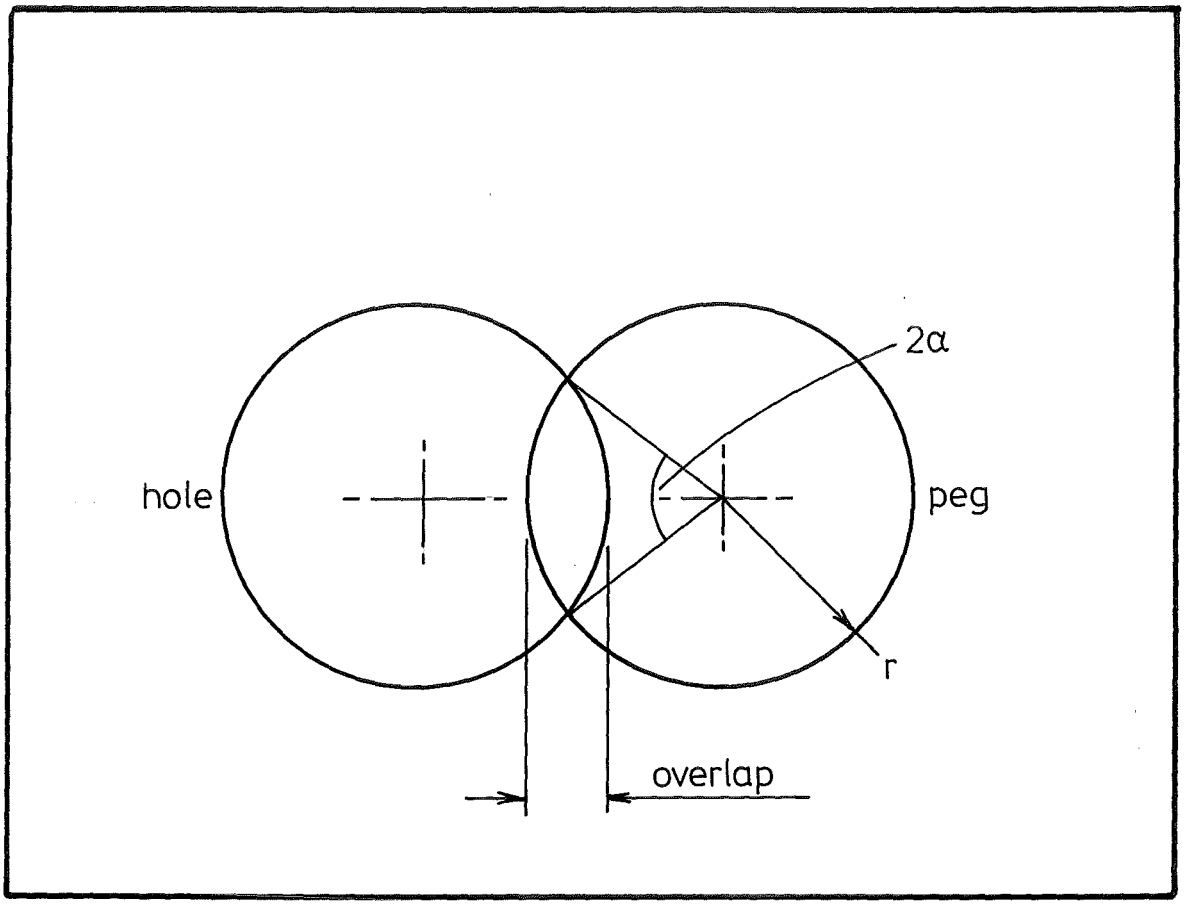

FIG. 4.24 DEFINITION OF OVERLAP

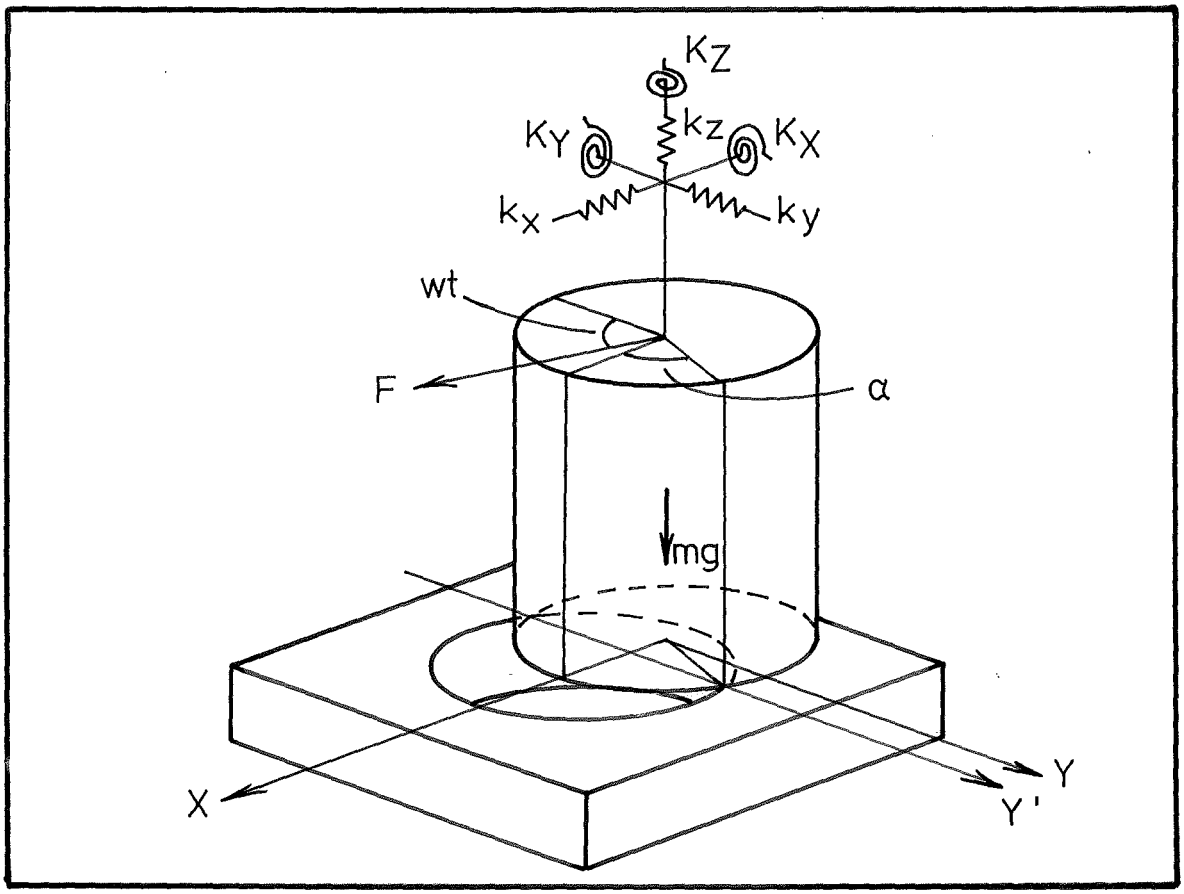

FIG. 4.25 PEG EDGE-HOLE EDGE/HOLE PLANE CONTACT.

$$\frac{-2Fh}{I_{Y'}\Omega_{Y'}} \cos\Omega_{Y'}t_2 \left[\frac{\sin(\omega-\Omega_{Y'})t}{2(\omega-\Omega_{Y'})} - \frac{\sin(\omega+\Omega_{Y'})t}{2(\omega+\Omega_{Y'})} \right]_{t_1}^{t_2}$$

$$\frac{-mgr\cos\alpha}{I\Omega_{Y'}^2} \left[1 - \cos\Omega_{Y'}(t_2-t_1) \right] \tag{4.44}$$

4.8.2 Equations of Motion for Peg Edge - Hole Plane Contact

The free flight motion of the peg due to the impulse $\mathcal{J}$ caused by the elastic contact of the peg edge and hole plane is examined. It is assumed that the impulse $\mathcal{J}$ is applied at the peg edge and that motion occurs only in the XZ plane appearing in Fig. 4.27. The action of the rotating force F is neglected, as the impulse provides a more significant force over the small time period under consideration. The equations of motion for movement in the X, Z, θ_Y coordinate system are

$$m\ddot{Z} + k_x X + (1+h)k_x\theta_Y = 0 \tag{4.45}$$

$$m\ddot{Z} = -mg \tag{4.46}$$

$$I_Y\ddot{\theta}_Y + K_Y\theta_Y + (1+h)k_x X = 0 \tag{4.47}$$

The solution of Equation 4.46 is

$$Z = -\tfrac{1}{2}gt^2 + \frac{\mathcal{J}}{m}t \tag{4.46}$$

Equations 4.45 and 4.47 contain static coupling terms and the solutions are of the form

$$X = A\sin\omega t + B\sin\Omega t \tag{4.47}$$

$$\theta_Y = C\sin\omega t + D\sin\Omega t \tag{4.48}$$

where

$$\omega = \frac{p_1 + \sqrt{(p_1^2-4p_2)}}{2}$$

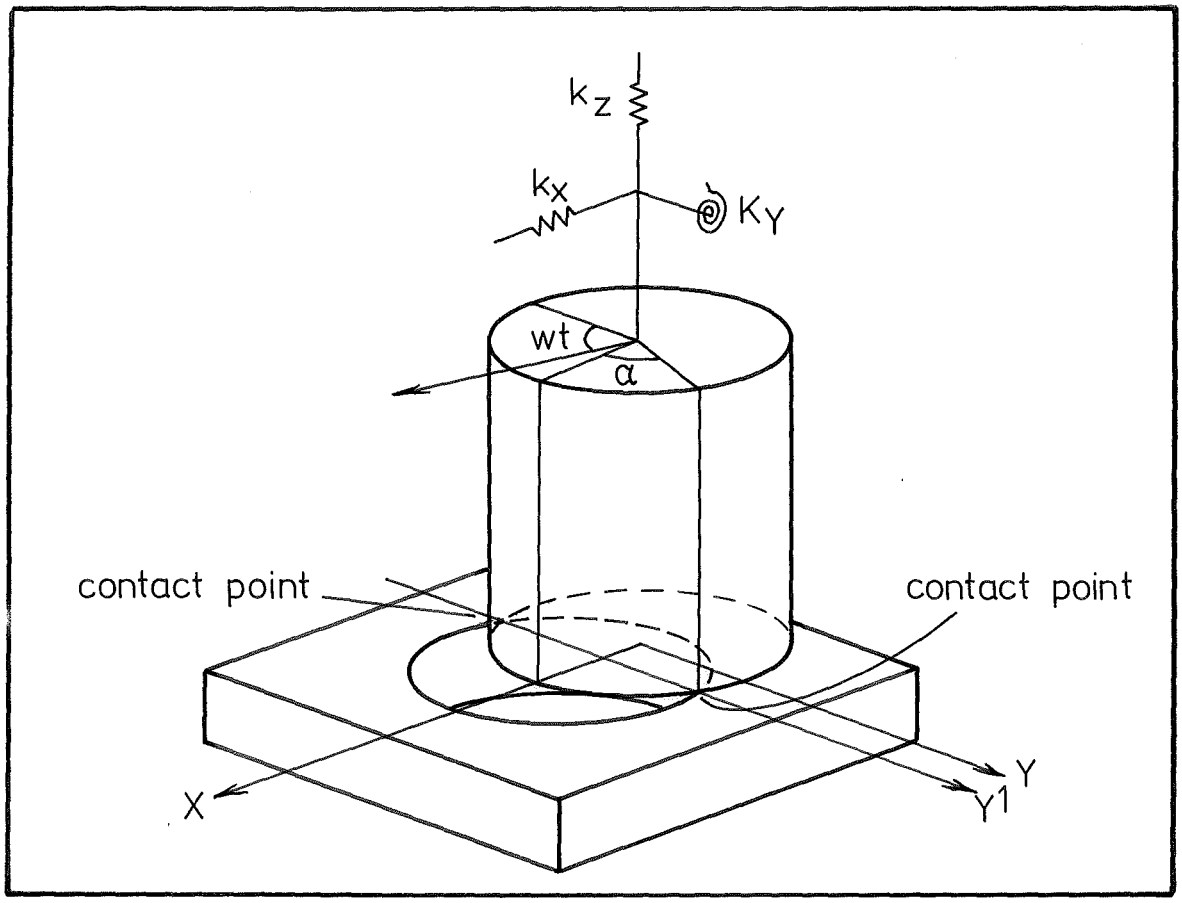

FIG. 4.26 PEG EDGE-HOLE EDGE DOUBLE POINT CONTACT

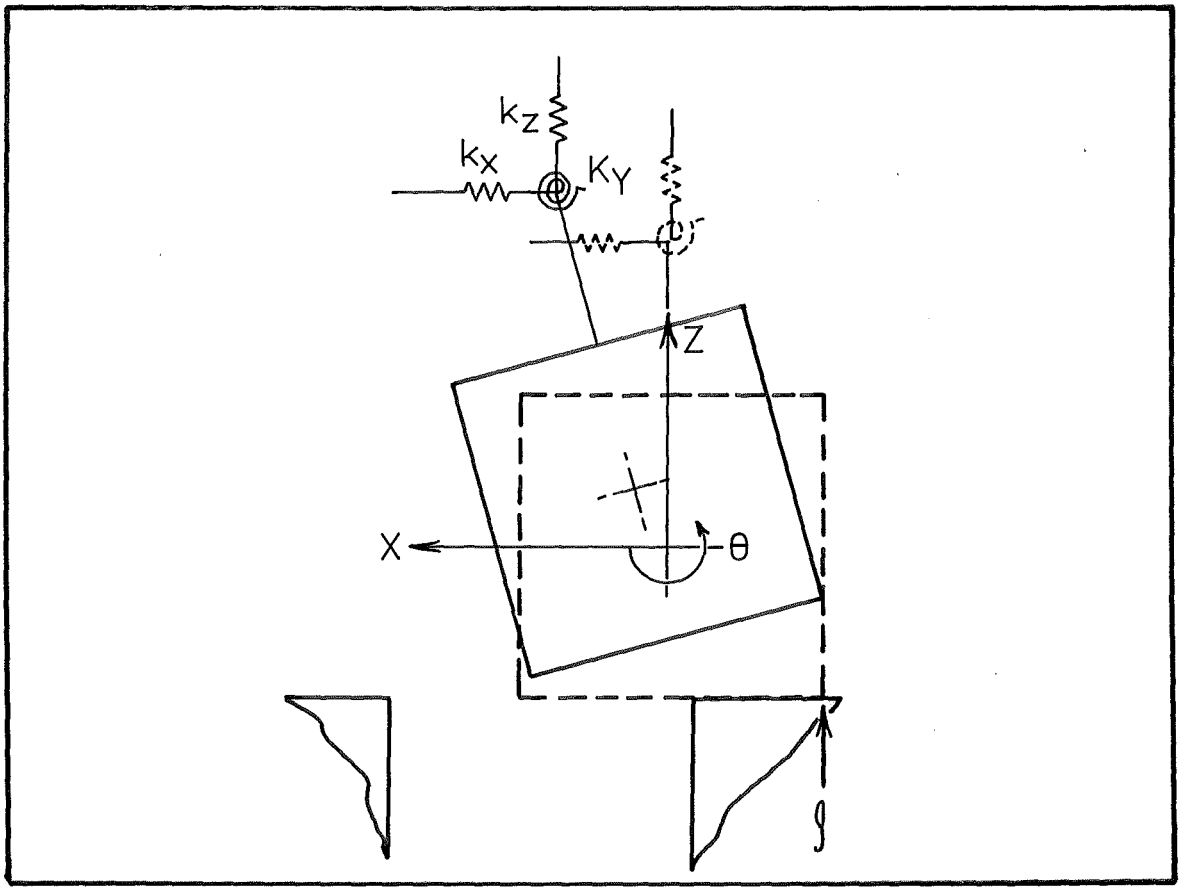

FIG. 4.27 PEG EDGE HOLE PLANE CONTACT

$$\Omega = \frac{p_1 - \sqrt{(p_1^2 - 4p_2)}}{2}$$

$$p_1 = -\left[\frac{k_x}{m} + \frac{K_Y}{I_Y}\right]$$

$$p_2 = \frac{k_x K_Y - (1+h)^2 k_x^2}{I_Y\, m}$$

$$A = \frac{(1+h)\, k_x \int r}{\omega m I\ (\omega^2 - \Omega^2)}$$

$$B = \frac{-(1+h)\, k_x \int r}{\Omega m I\ (\omega^2 - \Omega^2)}$$

$$C = \frac{\int r}{I\omega}\left[1 - \frac{(k_x - m\Omega^2)}{m(\omega^2 - \Omega^2)}\right]$$

$$D = \frac{(k_x - m\Omega^2) \int r}{\Omega m I\ (\omega^2 - \Omega^2)}$$

4.8.3 Total Solution

The two point contact movement Equation 4.44 is evaluated till impact occurs. When the peg edge contacts the hole plane, the value of the impulse imparted to the peg edge is obtained from the rotational momentum of the peg in the two point contact mode.

$$\int = \frac{C\ I_{Y'} \dot{\theta}_{Y'}}{r(1+\cos\alpha)}$$

where C is the coefficient of restitution.

For free flight clearly the following conditions must be met.

(i) The peg edge may not contact the hole edge, referring to Fig. 4.28 this condition may be written as

$$Z\cos\theta - a\sin\theta + X\sin\theta > r\sin\theta - Z$$

(ii) The peg edge may not contact the hole plane, i.e.

$$h\cos\theta + r\sin\theta > h+Z$$

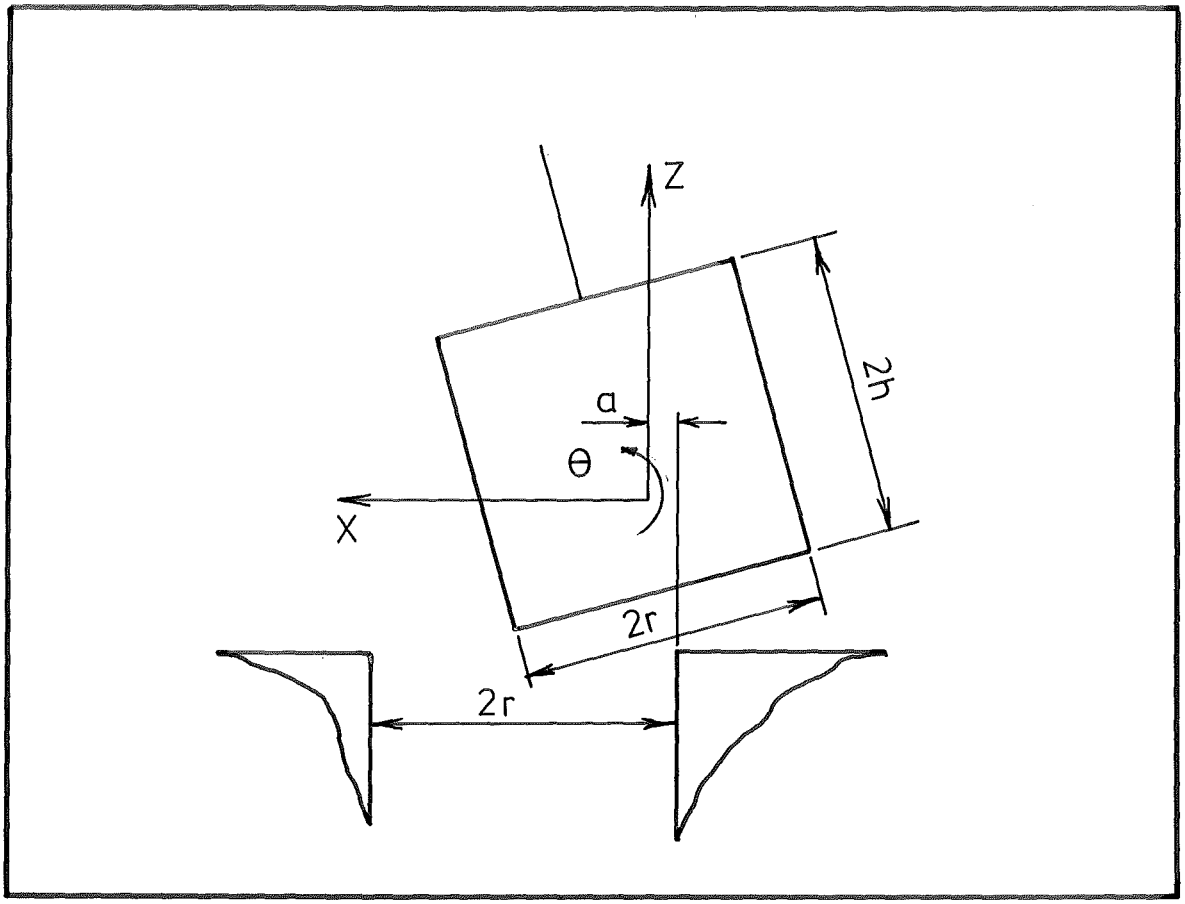

FIG. 4.28 CONDITIONS FOR FREE FLIGHT

During the free flight mode movement of the peg toward the hole is possible, this was examined by evaluating Equations 4.44 and 4.46 - 4.48 in turn. As Equations 4.46 - 4.48 describe the movement of the peg from the equilibrium position the first bounce only was considered.

The results are shown in Fig. 4.29 for a variety of constraints, in all cases the peg flight movement was short lived and no strong tendency either to assemble or disassemble appears to exist.

4.9 SUMMARY

The work of this chapter may be summarized by the following points.

(i) Sliding assembly of the peg into the hole is possible under single point contact, however the complex dynamics of the situation can lead to erroneous behaviour.

(ii) When two point contact exists the peg under certain circumstances is capable of sliding toward the hole under gravitational action.

(iii) Factors including high friction and excessive misalignment are capable of causing the peg to oscillate from one contact point to the other and walk out of the hole.

(iv) The existence of peg edge hole plane contacts appears to have a negligible effect on the translational misalignment of the peg.

(v) Two point sliding seems to possess the most potential as an assembly method however any solution based on this approach must also be capable of dealing with single point contacts as these form the majority of initial contacts.

TABLE 4.3

SYSTEM PARAMETERS

PEG EDGE - HOLE EDGE, HOLE PLANE CONTACT

m	=	.766 Kg
g	=	9806.6 mm/s^2
$K_{Y'}$	=	10^7 mN-mm
$I_{Y'}$	=	877 Kg-mm^2
I_Y	=	279 Kg-mm^2
l	=	12.5 mm
h	=	25.0 mm
r	=	25.0 mm

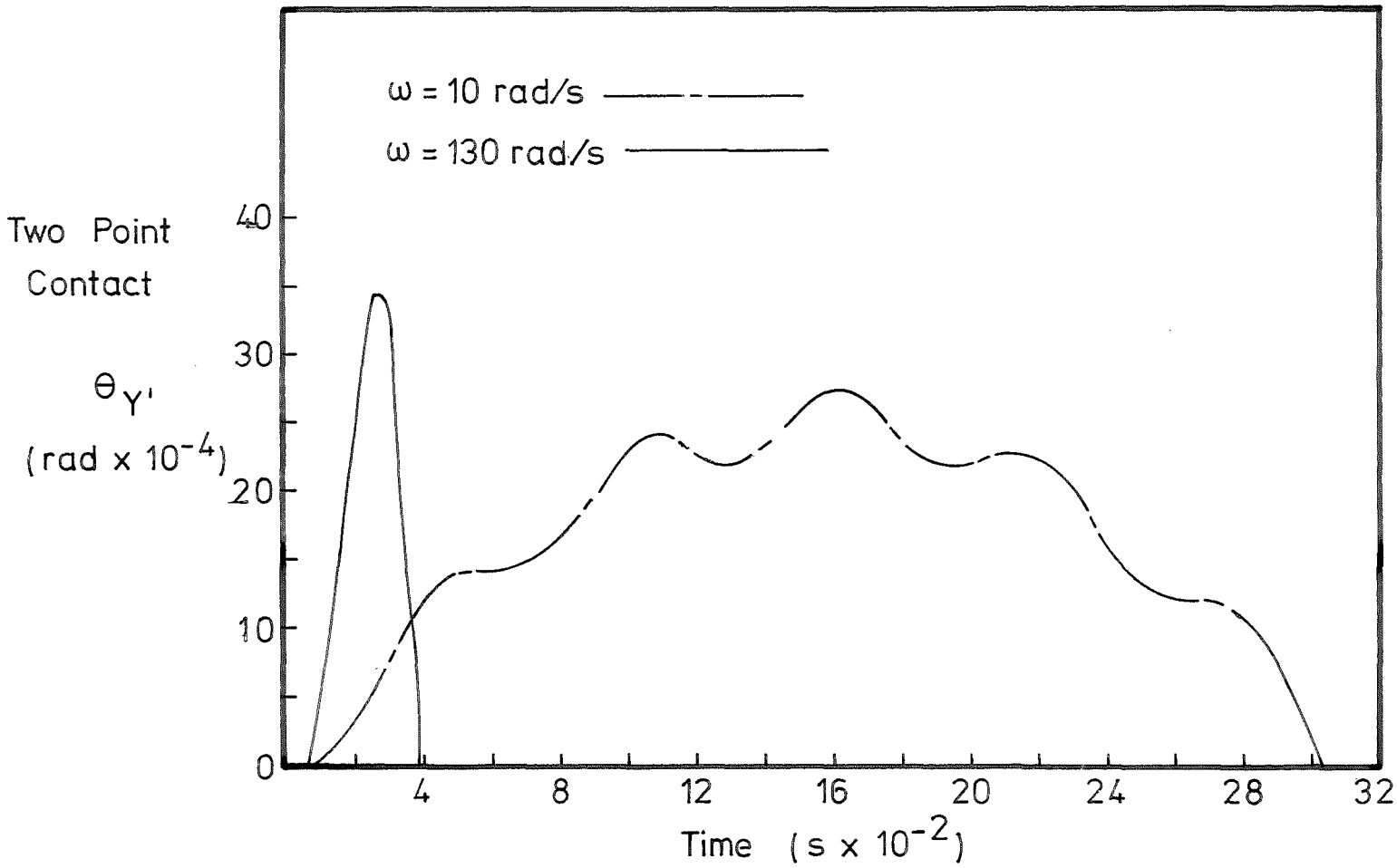

Single Point Contact X movement is less than 10^{-7} mm. in following cases

$k_X = k_Z =$
$.23 \times 10^4$ mN/mm.
$.128 \times 10^4$ " "
$.20 \times 10^4$ " "

$K_{Y'} = 10^7$ mN–mm.

FIG. 4.29 PEG EDGE HOLE EDGE HOLE PLANE CONTACT

CHAPTER 5

VIBRATORY ASSEMBLY TEST RIG

In order to demonstrate the feasibility of two point contact sliding assembly, a simple rig based on the work of the previous chapter was built and tested.

5.1 VIBRATORY ASSEMBLY TEST RIG

The test rig shown in Plate 5.1 and Fig. 5.1, uses the method of two point contact sliding to assemble a peg into a hole.

The manipulator body is carried in a quadrifilar suspension, which for small movements, allows approximately planar motion and rotation about the vertical axis.

The steel test peg is mounted on a universal joint centred swash mechanism actuated by six circumferentially arranged air cylinders. The peg may be wobbled by sequentially pressurizing the air cylinders.

The hole plate is located beneath the manipulator and offset to the desired misalignment.

In order to achieve two point contact under all circumstances, the manipulator is endowed with a high degree of rotational flexibility about the horizontal axes passing through the universal joint. Single point contact is therefore eliminated.

The flexibility of the manipulator also leads to the occurrence of peg edge-hole plane contacts, however the results of the previous chapter suggest that this mode of contact has little effect on the assembly process.

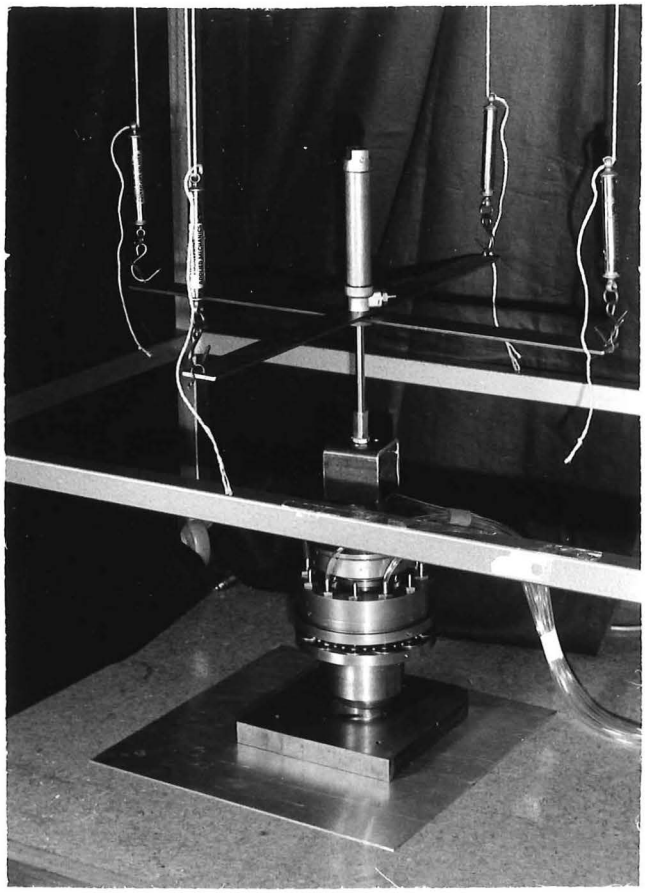

PLATE 5.1

VIBRATORY ASSEMBLY TEST RIG

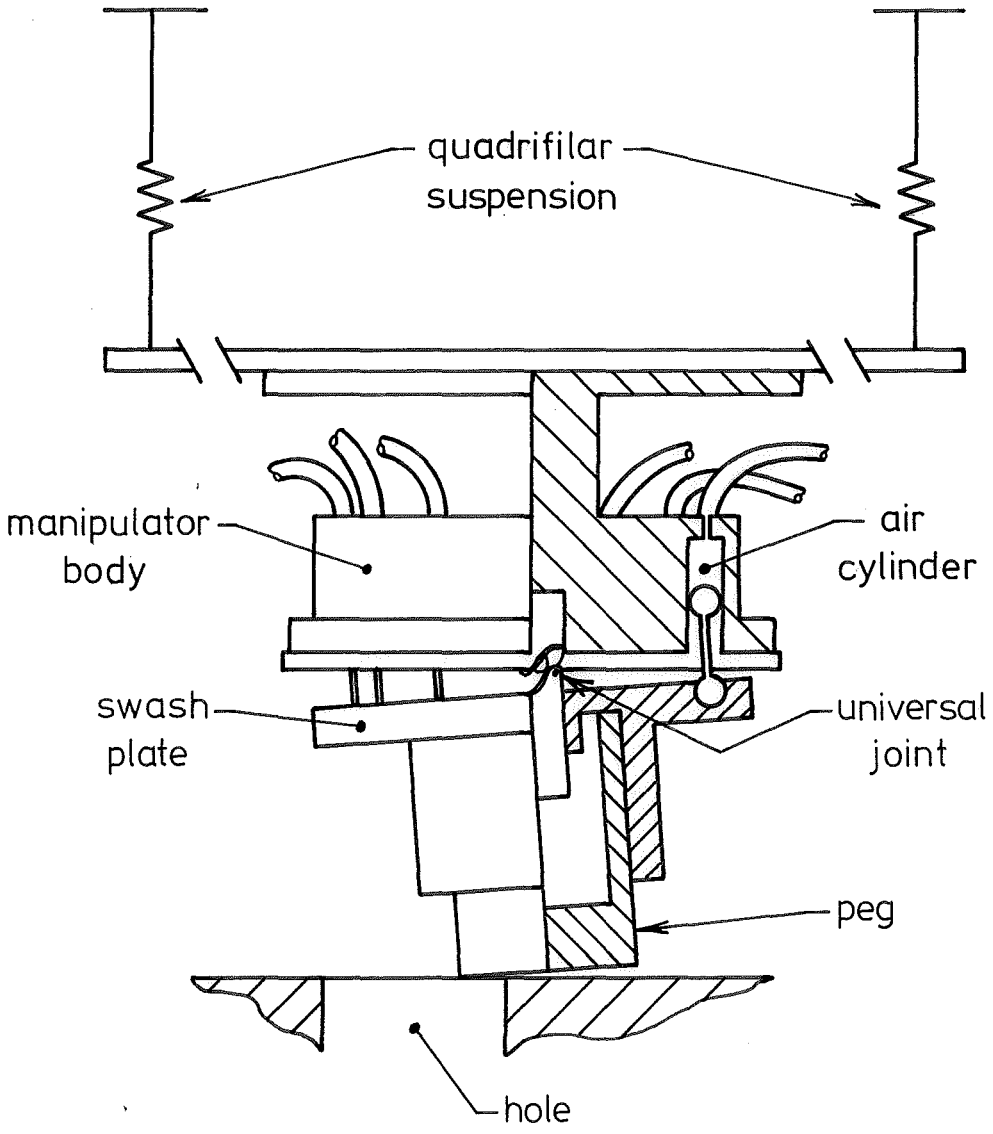

FIG. 5.1 VIBRATORY ASSEMBLY TEST RIG.

5.2 THEORETICAL ANALYSIS

Referring to Fig. 5.2 a peg at radius r, height 2h, rests on the hole plane. A vertical load L acts through the peg centre and a moment M rotates about the vertical axis. The moment M is insufficient to cause lifting at the peg edge on the hole plane, however rotation does occur about the two point contact chord when

$$M \cos\beta = \frac{LX}{2} \tag{5.1}$$

We assume the peg tips toward the hole centre, and the resulting displacement coupled with the inherent disturbances in the system causes the peg to slide into the hole under the action of gravity, for as long as the peg remains in the tipped position.

If the initial misalignment is x_o and sliding starts at t_o the position of the moment at t_o is given by

$$\beta_o = \cos^{-1} \frac{Lx_o}{2M} \tag{5.2}$$

and if sliding stops at x, t, then we can write

$$\begin{aligned}(x_o - x_1) &= \tfrac{1}{2}kg(t_o - t_1)^2 \\ &= \tfrac{1}{2}kg\Delta t^2\end{aligned} \tag{5.3}$$

where k is a factor depending upon the slope and friction of the contact. Now

$$x_1 = \frac{2M\cos\beta_1}{L} \tag{5.4}$$

and $$\beta_1 = \omega\Delta t - \beta_o \tag{5.5}$$

where ω is the frequency of the rotating moment. Combining 5.4 and 5.5, and substituting into 5.3 we get

$$\Delta t = \frac{-4M\cos(\omega\Delta t - \beta_o)}{LKg} + \frac{2x_o}{Kg} \tag{5.6}$$

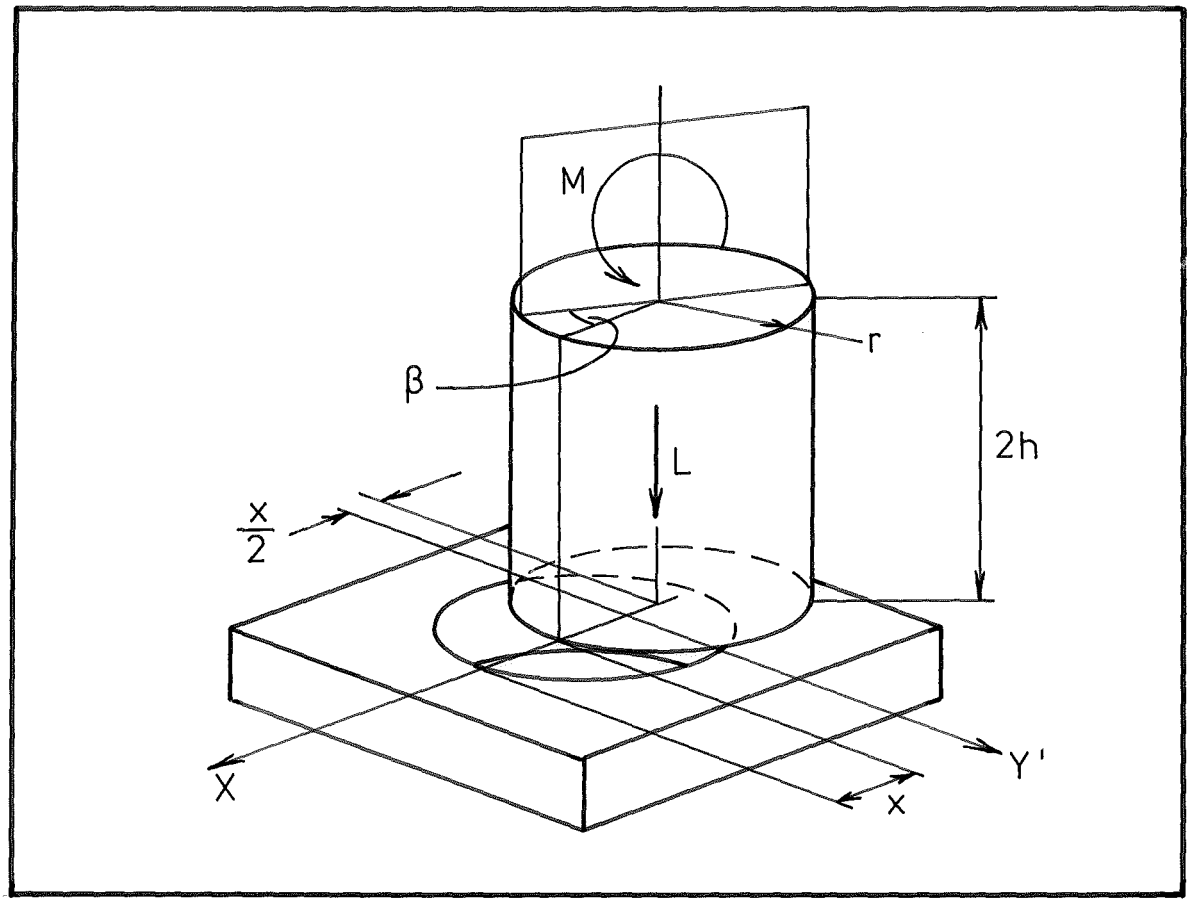

FIG. 5.2

IDEALIZED ASSEMBLY RIG

Solving this equation numerically, and substituting the sliding time Δt back into Equation 5.3, allows the sliding distance and hence the new misalignment to be computed. Repeating the process till the translational misalignment is eliminated allows the total time for assembly to be obtained.

5.3 EXPERIMENTAL WORK

The peg support head was misaligned with respect to the hole, and the time taken for assembly was measured by stop watch.

Two series of tests were performed; the first involved finding the minimum assembly time, for a given misalignment at various swash plate air cylinder pressures. The air pressure provided a convenient measure of the moment applied to the peg.

The second test investigated the effect of wobble frequency upon the minimum assembly time at various pressures.

5.4 RESULTS

The results of the first experiment are shown in Fig. 5.3, together with the theoretical results of Sec. 5.2.

The Equations 5.6 and 5.3 were evaluated using a value

$$r = 25$$

to correspond with the test peg radius. Horizontal scaling was achieved by equating the air pressure, when edge-plane tipping occurred, to the theoretical result

$$M = Lr.$$

Thus an air pressure at 40 psi corresponded to

$$\left(\frac{M}{L}\right)_{max} = 25$$

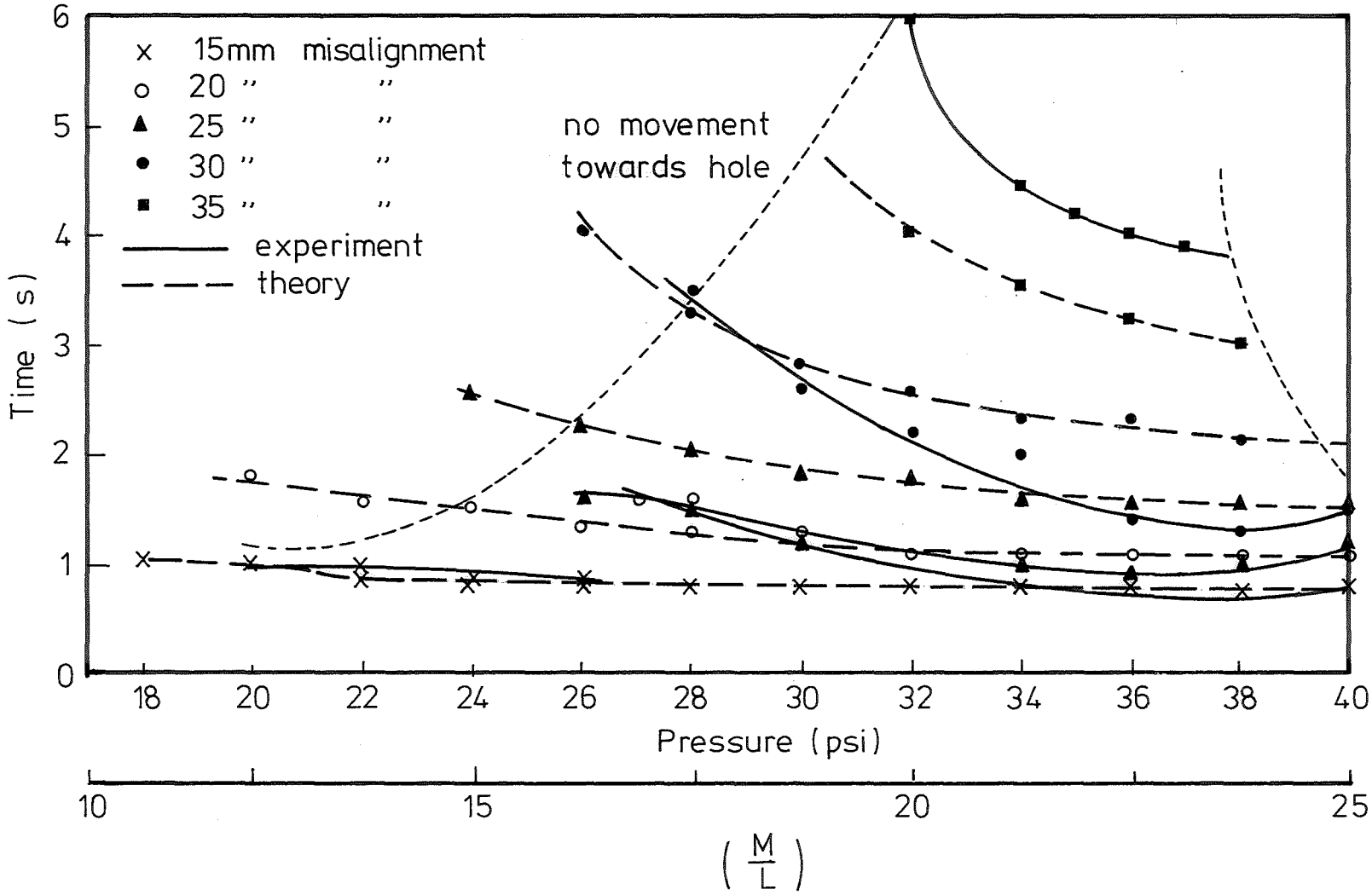

FIG. 5.3 MINIMUM ASSEMBLY TIME vs WOBBLE MOMENT. FREQUENCY = 4 Hz.

The slope factor K was arrived at by trial and error, and a value

$$K = .075$$

gave a reasonable correlation.

The results of the second tests are shown in Fig. 5.4.

5.5 DISCUSSION

It can be seen firstly, considering the simple theoretical model, that there is a reasonable agreement between the experimental and the theoretical results of the first test. In both cases the following points emerge.

(i) The minimum time of assembly increases markedly with misalignments greater than 50%.

(ii) An increase in the magnitude of the rotating-moment causes the assembly time to decrease. The maximum moment of course being limited by peg edge - hole plane contact.

There is a poor agreement between the results of the second test and the theoretical results. At low frequencies, the theoretical model predicts that, the peg will slide into the hole within the time period for which the peg remains cocked. This leads to a large difference between the theoretical results at the different frequencies. By contrast the minimum assembly time of the experimental rig seems independent of frequency. One possible explanation is that the value of K varies with the assembly frequency. At lower frequencies the smoother operation of the rig causes less disturbance hence increases the effective friction.

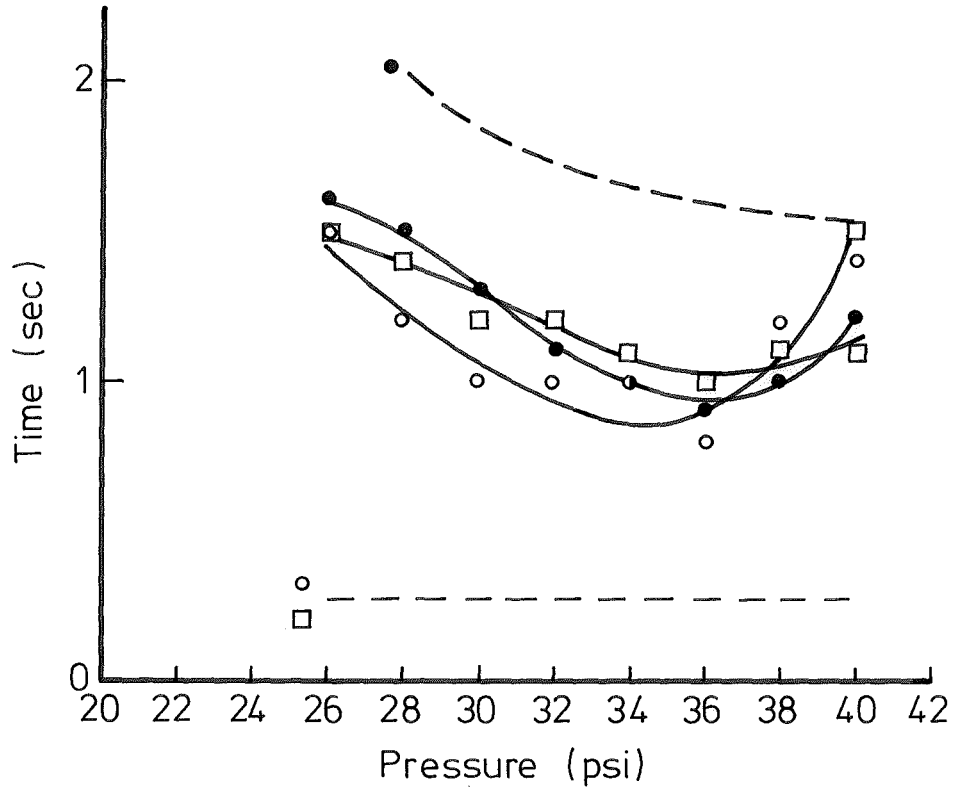

FIG. 5.4 THE EFFECT OF FREQUENCY UPON MINIMUM ASSEMBLY TIME.

5.6 CONCLUSION

Although the operation of the rig left something to be desired the use of two point contact as the basis of an assembly technique appears feasible.

The addition of a vertical vibration to reduce the effective friction would be useful in two ways. Firstly the speed of assembly would be improved, secondly a smaller tilt angle would be needed, this allowing the peg to be more favourably inclined prior to final insertion.

CHAPTER 6

COMPUTER SIMULATION OF AN ASSEMBLY SYSTEM

In this chapter an attempt is made to set up a realistic computer model of a manipulator peg-hole assembly system. The equations of motion are developed using Lagranges method, and two solution schemes are outlined.

6.1 SIMULATION OF AN ASSEMBLY SYSTEM

The variety of constraints, exciting forces, and contact modes possible in an assembly situation suggested that a simulation approach would be an appropriate extension to the study of vibratory assembly.

Simulation is a problem solving technique which draws inferences about the behaviour of a system by performing experiments on a model of the system. The advantage of the approach is its ability to deal with large systems of highly interrelated components. Obviously disadvantages also exist; firstly, simulation is based on assumptions about the real system, this limits its application to systems whose components are reasonably well understood. Secondly, unlike analytical techniques, the results of a simulation are not given in terms of general relationships, hence simulation is suited for the study of systems whose approximate operating point is known, i.e. simulation is a finishing rather than exploratory tool.

Neither of the above disadvantages presents a barrier to the use of simulation in predicting the performance of an assembly system for design purposes, hence it was decided to develop a model of the system

shown in Fig. 6.1 having the following features:

(i) The peg and hole edges may touch at either one or two points, both sliding and stationary contacts being permissible.

Peg edge and hole plane contacts are not considered for two reasons. Firstly edge-plane contact is difficult to describe accurately as the resultant contact force is influenced greatly by the micro-configuration of the components. Secondly, whereas the peg-hole configuration can be relied upon to possess two contacting and well defined edges the surface of the surrounding plane can, in reality, not be generalized so easily.

Likewise peg edge-hole cylinder contacts are also ignored. This type of contact only occurs in final fitting, Stage 3 as defined in Sec. 3.1.

(ii) The actuator situated above the peg applies a time varying force through the point G.

(iii) The peg and actuator are fixed at the end of a flexible coupling which in turn is fastened to an elastically constrained carrier, with rotational and translational degrees of freedom.

6.1.1 System Generalized Coordinates

An idealized representation of the system is shown in Fig. 6.2. The peg is free to translate and rotate, and its position in the 0-centred coordinate system is described by the coordinates of its centre of mass, x_1^p x_2^p x_3^p, and the three Euler angles, ϕ θ ψ, which define the orientation of the peg-centred 0_p coordinate system, with respect to the 0 system.

The carrier block is able to move in the x_2 x_3 plane and rotate about the vertical x_1 axis direction. The generalized coordinates are x_2^c x_3^c and γ.

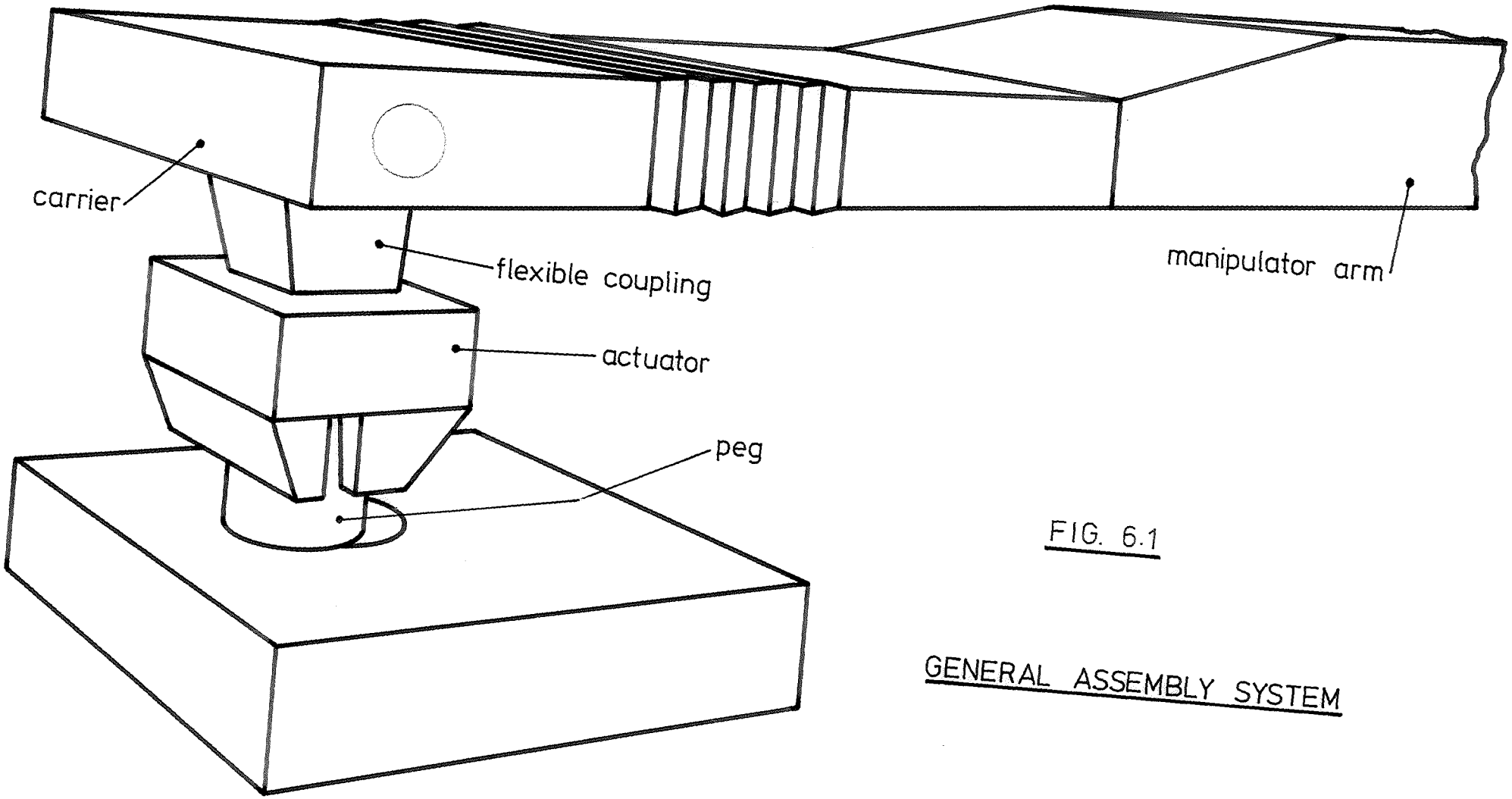

FIG. 6.1

GENERAL ASSEMBLY SYSTEM

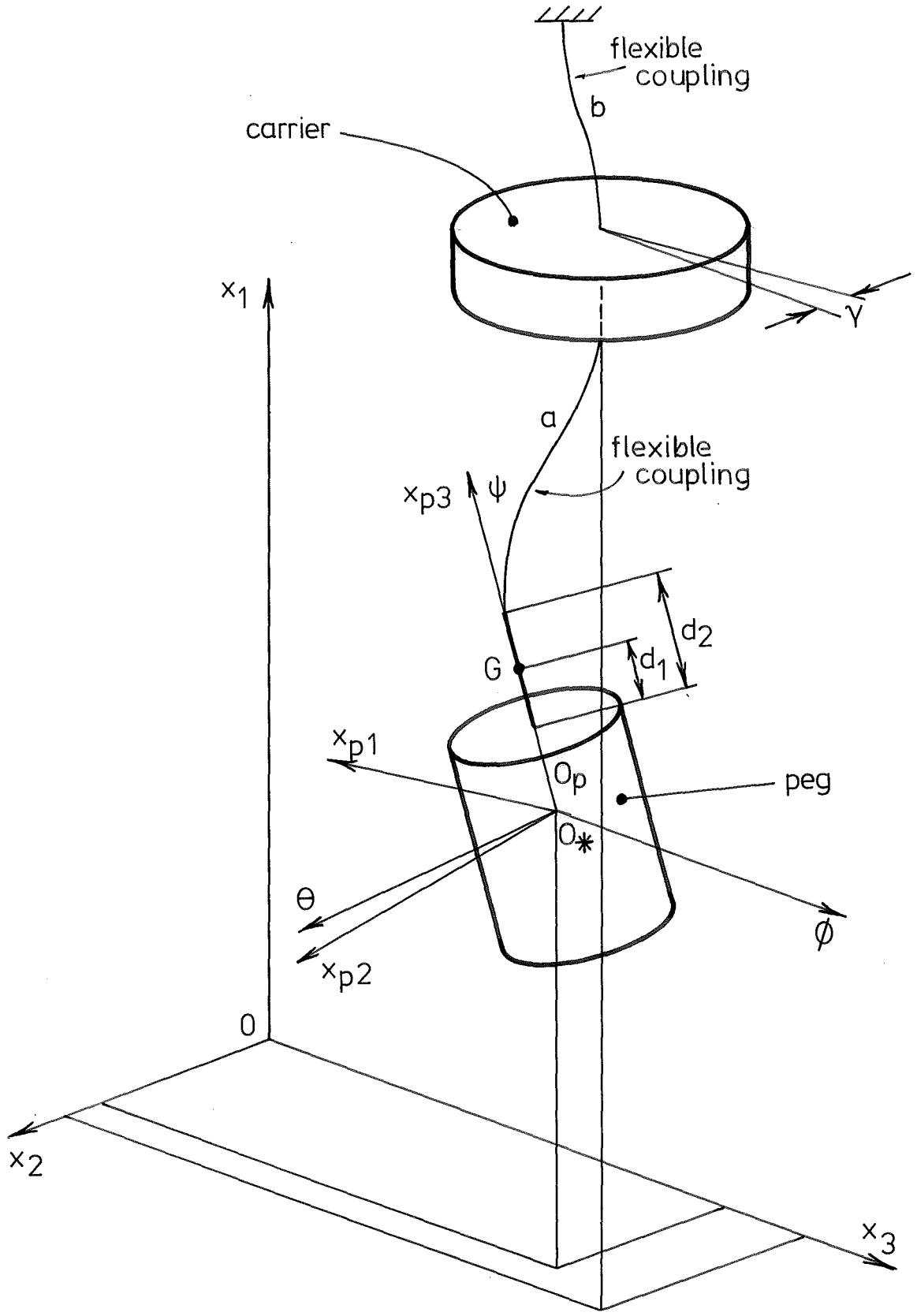

FIG. 6.2 IDEALIZED ASSEMBLY SYSTEM

6.1.2 Coordinate System Transformation

For convenience the transformation between the 0, 0_p and Euler system 0_e will be written below as reference is made to them later.

Firstly, the transformation between the peg-centred 0_p system and the manipulator-centred 0 system is

$$\begin{bmatrix} x_{p1} \\ x_{p2} \\ x_{p3} \end{bmatrix} = \begin{bmatrix} \cos\phi\cos\theta\cos\psi & \sin\phi\cos\theta\cos\psi & -\sin\theta\cos\psi \\ -\sin\phi\sin\psi & +\cos\phi\sin\psi & \\ -\cos\phi\cos\theta\sin\psi & -\sin\phi\cos\theta\sin\psi & \sin\theta\sin\psi \\ -\sin\phi\cos\psi & +\cos\phi\cos\psi & \\ -\sin\phi\cos\psi & \cos\phi\cos\psi & \cos\theta \\ +\cos\phi\sin\theta & \sin\phi\sin\theta & \end{bmatrix} \begin{bmatrix} x_1-x_1^p \\ x_2-x_2^p \\ x_3-x_3^p \end{bmatrix} \tag{6.1}$$

i.e. $[x_p] = [R]\ [x-x^p] = [R][x_*]$

The relationship between the 0 coordinate system and the Euler axes is

$$\begin{bmatrix} x_1 \\ x_2 \\ x_3 \end{bmatrix} = \begin{bmatrix} 0 & -\sin\phi & \cos\phi\sin\theta \\ 0 & \cos\phi & \sin\phi\sin\theta \\ 1 & 0 & \cos\theta \end{bmatrix} \begin{bmatrix} x_\phi \\ x_\theta \\ x_\psi \end{bmatrix} + \begin{bmatrix} x_1^p \\ x_2^p \\ x_3^p \end{bmatrix} \tag{6.2}$$

$$[x] = [R_e]\ [X_e] + [x^p]$$

and between the 0_p system and the Euler axes

$$\begin{bmatrix} x_{p1} \\ x_{p2} \\ x_{p3} \end{bmatrix} = \begin{bmatrix} -\sin\theta\cos\psi & \sin\psi & 0 \\ \sin\theta\sin\psi & \cos\psi & 0 \\ \cos & 0 & 1 \end{bmatrix} \begin{bmatrix} x_\psi \\ x_\theta \\ x_\psi \end{bmatrix} \tag{6.3}$$

$$[x_p] = [R_{pe}]\ [x_e]$$

6.1.3 System Inertias and Masses

The inertia of the peg about its principal, 0_p centred, axes in tensor notation is

$$[I^p] = \begin{bmatrix} I^p & 0 & 0 \\ 0 & I^p & 0 \\ 0 & 0 & I^p{}_3 \end{bmatrix}$$

The peg mass is M^p and the carrier block has inertia I^c about its centre of mass, and mass M^c.

6.1.4 System Stiffnesses and Damping

The stiffness and damping characteristics of the flexible coupling, a, and the carrier constraints, b, shown in Fig. 6.2, with respect to the 0 centred coordinate system, are

$$[K^a] = \begin{bmatrix} K_1^a & & & & & \\ & K_2^a & & 0 & & K_{26}^a \\ & & K_3^a & & K_{35}^a & \\ & 0 & & K_4^a & & 0 \\ & & K_{53}^a & & K_5 & \\ & K_{62}^a & & 0 & & K_6^a \end{bmatrix}$$

$$[C^a] = \begin{bmatrix} C_1^a & & & & & \\ & C_2^a & & 0 & & C_{26}^a \\ & & C_3^a & & C_{35}^a & \\ & 0 & & C_4^a & & 0 \\ & & C_{53}^a & & C_5^a & \\ & C_{62}^a & & 0 & & C_6^a \end{bmatrix}$$

and

$$[K^b] = \begin{bmatrix} K_2^b & 0 & \\ & K_3^b & \\ 0 & & K_4^b \end{bmatrix} \quad [C^b] = \begin{bmatrix} C_2^b & 0 & \\ & C_3^b & \\ 0 & & C_4^b \end{bmatrix}$$

6.1.5 System Forces and Moments

Forces are applied to the system by the actuator and by contact with the hole edge. The actuator force acts in the peg-centred coordinate system at the point G and is designated as F_p^G. The contact forces F^{c1} F^{c2} are described in terms of the 0 coordinate system and contact occurs at points x^{c1} x^{c2} on the peg edge.

6.2 EQUATIONS OF MOTION

Having defined the system components, the equations of motion may be developed using Lagrange's approach.

6.2.1 Kinetic Energy

The kinetic energy due to rotational and translational velocities in terms of the generalized coordinates is

$$\begin{aligned} 2T = {} & [\dot\phi\dot\theta\dot\psi][R_{pe}]^T[I^p][R_{pe}]\begin{bmatrix}\dot\phi\\ \dot\theta\\ \dot\psi\end{bmatrix} \\ & + M^p[\dot x_1^p \quad \dot x_2^p \quad \dot x_3^p]\begin{bmatrix}\dot x_1^p\\ \dot x_2^p\\ \dot x_3^p\end{bmatrix} \\ & + M^c[\dot x_2^c \quad \dot x_3^c]\begin{bmatrix}\dot x_2^c\\ \dot x_3^c\end{bmatrix} + I^c\dot\gamma^2 \end{aligned} \tag{6.4}$$

6.2.2 Potential Energy

Potential energy is stored in the system due to gravity and elastic deformation of the constraints (a) and (b). The deflection of the constraints may be written in terms of the system generalized coordinates.

i. Element (a) translational deflections

$$[R^T]\begin{bmatrix}0\\0\\d_2\end{bmatrix}+\begin{bmatrix}x_1^p\\x_2^p\\x_3^p\end{bmatrix}-\begin{bmatrix}x_1^e\\x_2^c\\x_3^c\end{bmatrix}=[d_T^a] \tag{6.5}$$

ii. Element (a) rotational deflections. For small rotations about equilibrium (ϕ , $\psi \underline{\Omega} 0$, $\theta \simeq \frac{\pi}{2}$), we assume the rotations about the Euler axis to be equal to rotations about the 0 axes, so

$$\begin{bmatrix}\psi\\\theta\\\phi\end{bmatrix}-\begin{bmatrix}\gamma\\\theta_2^e\\\theta_3^e\end{bmatrix}=[d_R^a] \tag{6.6}$$

iii. Element (b) translational deflections.

$$\begin{bmatrix}x_2^c\\x_3^e\end{bmatrix}-\begin{bmatrix}x_2^e\\x_3^e\end{bmatrix}=[d_T^b] \tag{6.7}$$

iv. Element (b) rotational deflections.

$$[\gamma-\theta_1^e]=[d_R^b] \tag{6.8}$$

Thus the potential energy of the system becomes

$$2V=\left[d^a_T\,;\,d^a_R\right]K^a\left[\begin{matrix}d^a_T\\---\\d^a_R\end{matrix}\right]+\left[d^b_T\,;\,d^b_R\right]K^b\left[\begin{matrix}d^b_T\\---\\d^b_R\end{matrix}\right]+M^p g x_1^p \tag{6.9}$$

6.2.3 Energy Dissipation

Energy is dissipated by damping in the constraint elements, the damping force being proportional to velocity.

Equations 6.5, 6.7 - 6.8 may be differentiated to obtain the deflection velocities. The rotational velocity of the peg about the axes of the 0 system may be written as

$$\left[\dot{d}_R^a\right] = \left[R_e\right] \begin{vmatrix} \dot{\phi} \\ \dot{\theta} \\ \dot{\psi} \end{vmatrix}$$

and so the dissipation function D is

$$2D = \left[D_T^a \,;\, d_R^a\right]\left[C^a\right]\begin{bmatrix} d_T^a \\ \hline d_R^a \end{bmatrix} + \left[d_T^b \,;\, d_R^b\right]\left[C^b\right]\begin{bmatrix} d_T^b \\ \hline d^b \end{bmatrix} \tag{6.10}$$

6.2.4 Applied Forces and Moments

The forces and moments applied to the peg, Fig. 6.3, must be expressed in terms of the generalized coordinates.

The direct forces are simply

$$\left[\underline{F}\right] = \left[R^T\right]\left[\underline{F}_p^G\right] + \left[\underline{F}^{c1}\right] + \left[\underline{F}^{c2}\right] \tag{6.11}$$

and the moments acting about the Euler axes due to contact and applied forces are

$$\left[\underline{M}^e\right] = \left[R_e\right]^{-1}\left[\underline{x}_*^{c1} \times \underline{F}^{c1}\right] + \left[R_e\right]^{-1}\left[\underline{x}_*^{c2} \times \underline{F}^{c2}\right]$$

$$+ \left[R_{pe}\right]^{-1}\left[\underline{x}_p^G \times \underline{F}_p^G\right] \tag{6.12}$$

where $\underline{x}_*^{c1}$ $\underline{x}_*^{c2}$ describe the contact points onto the 0_* coordinate system

$$\left[Q\right] = \begin{bmatrix} F \\ \hline M^e \end{bmatrix}$$

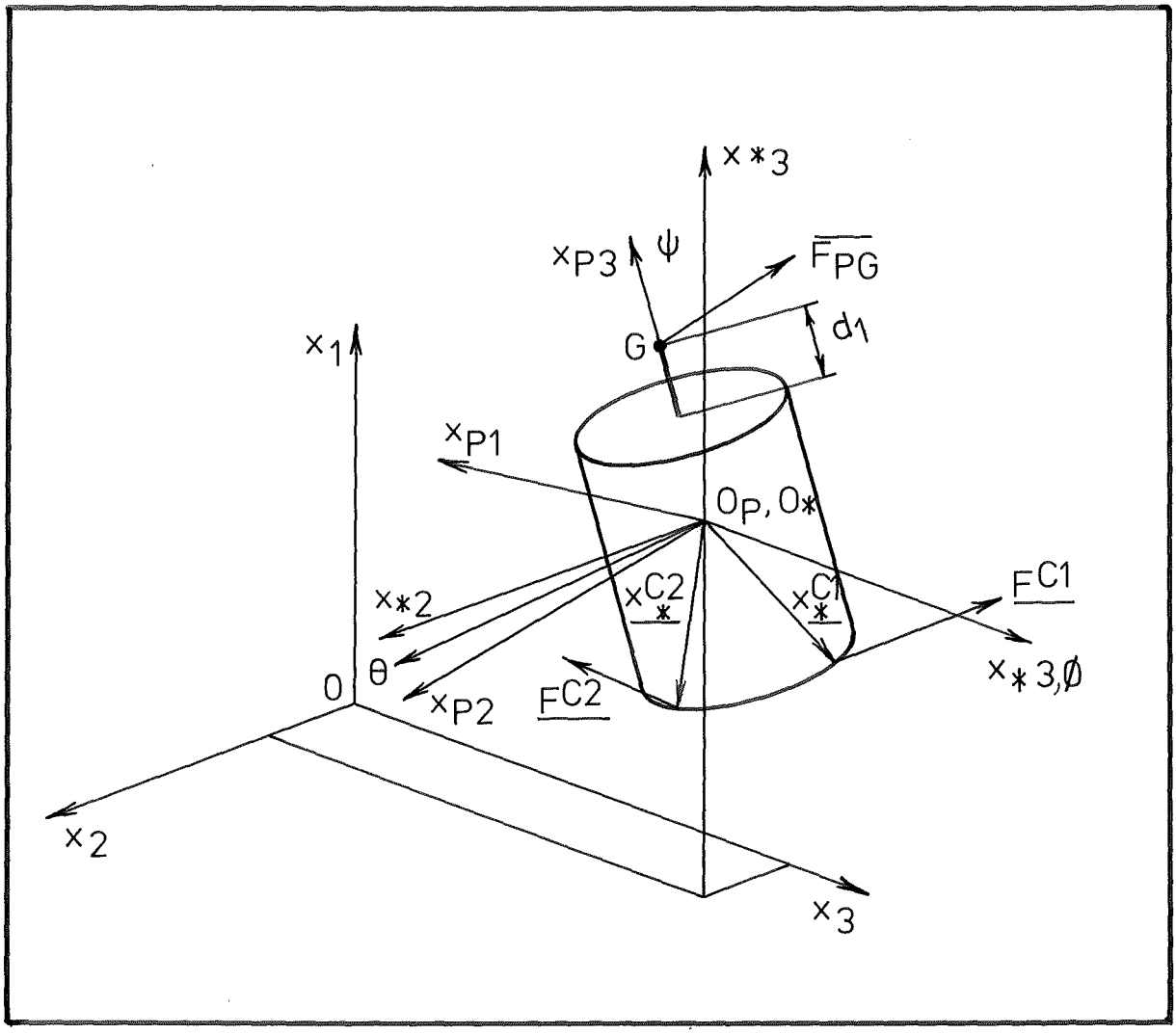

FIG 6.3 FORCES AND MOMENTS ACTING ON THE SYSTEM.

6.2.5 General Form of Lagrange's Equation

The Lagrangean formulation of the equations of motion is

$$\frac{d}{dt}\frac{\partial T}{\partial \dot{q}_K} - \frac{\partial T}{\partial q_K} + \frac{\partial D}{\partial \dot{q}_K} + \frac{\partial V}{\partial q_K} = Q_K$$

Differentiating and substituting the various terms, we obtain the 9 equations of motion describing the movement of the system

$$\begin{aligned} & M^p \ddot{x}1^p + K^a_{11}(d_2\cos\phi\sin\theta + x^p_1 - x^e_1) \\ & \quad + C^a_{11}(-d_2\dot{\phi}\sin\phi\sin\theta + d_2\dot{\theta}\cos\phi\cos\theta + \dot{x}^p_1) \\ & \quad + M^p g x^p_1 \\ & = \begin{bmatrix} \cos\phi\cos\phi\cos\psi \\ -\sin\phi\sin\psi \end{bmatrix} F^G_{p1} + \begin{bmatrix} -\cos\phi\cos\theta\sin\psi \\ -\sin\phi\cos\psi \end{bmatrix} F^G_{p2} \\ & \quad + \left[\cos\phi\sin\theta\right] F^G_{p3} + F^{c1}_1 + F^{c2}_1 \end{aligned} \tag{6.13}$$

$$\begin{aligned} & M^p \ddot{x}^p_2 + K^a_{22}(d_2\sin\phi\sin\theta + x^p_2 - x^c_2) \\ & \quad + \frac{K^a_{26} + K^a_{62}}{2}(\phi - \theta^e_3) \\ & \quad + C^a_{22}(d_2\dot{\phi}\cos\phi\sin\theta + d_2\dot{\theta}\sin\phi\cos\theta + \dot{x}^p_2 - \dot{x}^c_2) \\ & \quad + \frac{C^a_{26} + C^a_{62}}{2}(\dot{\phi} + \dot{\psi}\cos\theta) \\ & = \begin{bmatrix} \sin\phi\cos\theta\cos\psi \\ +\cos\phi\sin\psi \end{bmatrix} F^G_{p1} + \begin{bmatrix} -\sin\phi\cos\theta\sin\psi \\ +\cos\phi\cos\psi \end{bmatrix} F^G_{p2} \\ & \quad + \left[\sin\phi\sin\theta\right] F^G_{p3} + F^{c1}_2 + F^{c2}_2 \end{aligned} \tag{6.14}$$

$$M\ddot{x}_3^p + K_{33}^a(d_2\cos\theta + x_3^p - x_3^c)$$

$$+ \frac{K_{35} + K_{53}}{2}(\theta - \theta_2^e)$$

$$+ C_{33}^a(-d_2\dot{\theta}\sin\theta + \dot{x}_3^p - \dot{x}_3^c)$$

$$+ \frac{C_{35} + C_{53}}{2}(\dot{\theta}\cos\phi + \dot{\psi}\sin\phi\sin\theta)$$

$$= [-\sin\theta\cos\psi]\, F_{p1}^G + [\sin\theta\sin\psi]\, F_{p2}^G + [\cos\theta]\, F_{p3}^G$$

$$+ F_3^{c1} + F_3^{c2} \qquad (6.15)$$

$$I(\ddot{\phi}\sin^2\theta + 2\dot{\phi}\dot{\theta}\cos\theta\sin\theta)$$

$$+ I_3(\ddot{\phi}\cos^2\theta - 2\dot{\phi}\dot{\theta}\cos\theta\sin\theta + \ddot{\psi}\cos\theta - \dot{\theta}\dot{\psi}\sin\theta)$$

$$+ K_{11}^a(d_2\cos\phi\sin\theta + x_1^p - x_1^e)(-d_2\sin\phi\sin\theta)$$

$$+ K_{22}^a(d_2\sin\phi\sin\theta + x_2^p - x_2^c)(d_2\cos\phi\sin\theta)$$

$$+ K_{66}^a(\phi - \theta_3^e)$$

$$+ \frac{K_{26} + K_{62}}{2}((d_2\sin\phi\sin\theta + x_2^p - x_2^c) + (d_2\cos\phi\sin\theta)(\phi - \theta_3^e))$$

$$+ C_{11}^a(-d_2\dot{\phi}\sin\phi\sin\theta + d_2\dot{\theta}\cos\phi\cos\theta + \dot{x}_1^p)(-d_2\sin\phi\sin\theta)$$

$$+ C_{22}^a(d_2\dot{\phi}\cos\phi\sin\theta + d_2\dot{\theta}\sin\phi\cos\theta + \dot{x}_2^p - \dot{x}_2^c)(d_2\cos\phi\sin\theta)$$

$$+ C_{66}^a(\dot{\phi} + \dot{\psi}\cos\theta)$$

$$+ \frac{C_{26} + C_{62}}{2}((d_2\dot{\phi}\cos\phi\sin\theta + d_2\dot{\theta}\sin\phi\cos\theta + \dot{x}_2^p - \dot{x}_2^c)$$

$$+ (\dot{\phi} + \dot{\psi}\cos\theta)(d_2\cos\phi\sin\theta))$$

$$= \frac{-1}{\sin\theta}(\cos\phi\cos\theta(x_{*2}^{ci}F_3^{ci} - x_{*3}^{ci}F_2^{ci}) + \sin\phi\cos\theta(x_{*3}^{ci}F_1^{ci} - x_{*1}^{ci}F_3^{ci})$$

$$- \sin\theta(x_{*1}^{ci}F_2^{ci} - x_{*2}^{ci}F_1^{ci}))$$

$$\frac{-1}{\sin\theta}(\cos\psi(x_{p2}^G F_{p3}^G - x_{p3}^G F_{p2}^G) - \sin\psi(x_{p3}^G F_{p1}^G - x_{p1}^G F_{p3}^G)) \qquad (6.16)$$

$$
\begin{aligned}
&I\ddot{\theta} + I\dot{\phi}^2\sin\theta\cos\theta \\
&+ I_3(-\dot{\phi}^2\cos\theta\sin\theta - \dot{\phi}\dot{\psi}\sin\theta) \\
&+ K_{11}^a(d_2\cos\phi\sin\theta + x_1^p - x_1^e)(d_2\cos\phi\cos\theta) \\
&+ K_{22}^a(d_2\sin\phi\sin\theta + x_2^p - x_2^c)(d_2\sin\phi\cos\theta) \\
&+ K_{33}^a(d_2\cos\theta + x_3^p - x_3^c)(-d_2\sin\theta) \\
&+ K_{55}^a(\theta - \theta_2^e) \\
&+ \frac{K_{35} + K_{53}}{2}((d_2\cos\theta + x_3^p - x_3^c) + (-d_2\sin\theta)(\theta - \theta_2^e)) \\
&+ C_1(-d_2\dot{\phi}\sin\phi\sin\theta + d_2\dot{\theta}\cos\phi\cos\theta + \dot{x}_1^p)(d_2\cos\phi\cos\theta) \\
&+ C_2(d_2\dot{\phi}\cos\phi\sin\theta + d_2\dot{\theta}\sin\phi\cos\theta + \dot{x}_2^p - \dot{x}_2^c)\ (d_2\sin\phi\cos\theta) \\
&+ C_3(-d_2\dot{\theta}\sin\theta + \dot{x}_3^p - \dot{x}_3^c)(-d_2\sin\theta) \\
&+ C_4(-\dot{\theta}\sin\phi + \dot{\psi}\cos\phi\sin\theta - \dot{\gamma})(-\sin\phi) \\
&+ C_5(\dot{\theta}\cos\phi + \dot{\psi}\sin\phi\sin\theta)(\cos\phi) \\
&+ \frac{(C_{35} + C_{53})}{2}((-d_2\dot{\theta}\sin\theta + \dot{x}_3^p - \dot{x}_3^c) + (\dot{\theta}\cos\phi + \dot{\psi}\sin\phi\sin\theta)(-d_2\sin\theta)) \\
&= \frac{-1}{\sin\theta}(\sin\phi\sin\theta(x_{*2}^{ci}F_3^{ci} - x_3^{ci}F_2^{ci}) - \cos\phi\sin\theta(x_{*3}^{ci}F_1^{ci} - x_{*1}^{ci}F_3^{ci})) \\
&\quad \frac{-1}{\sin\theta}(-\sin\theta\sin\psi(x_{p2}^G F_{p3}^G x_{p3}^G F_{p2}^G) - \sin\theta\cos\psi(x_{p3}^G F_{p1}^G - x_{p1}^G F_{p3}^G)) \qquad (6.17)
\end{aligned}
$$

$$
\begin{aligned}
&I_3(\ddot{\phi}\cos\theta - \dot{\phi}\dot{\theta}\sin\theta + \ddot{\psi}) \\
&+ K_4(\psi - \gamma) \\
&+ C_4(-\dot{\theta}\sin\phi + \dot{\psi}\cos\phi\sin\theta - \dot{\gamma})(\cos\phi\sin\theta) \\
&+ C_5(\dot{\theta}\cos\phi - \dot{\psi}\sin\phi\sin\theta)(\sin\phi\sin\theta) \\
&+ C_6(\dot{\phi} + \dot{\psi}\cos\theta)(\cos\theta) \\
&+ \frac{(C_{35} + C_{53})}{2}(-d_2\dot{\theta}\sin\theta + \dot{x}_3^p - \dot{x}_3^c)(\sin\phi\sin\theta) \\
&+ \frac{(C_{26} + C_{62})}{2}(d_2\dot{\phi}\cos\phi\sin\theta + d_2\dot{\theta}\sin\phi\cos\theta + \dot{x}_2^p - \dot{x}_2^c)(\cos\theta)
\end{aligned}
$$

$$= \frac{-1}{\sin\theta} \left(-\cos\phi\left(x^{ci}_{*2}F^{ci}_{3} - x^{ci}_{*3}F^{ci}_{2}\right) - \sin\phi\left(x^{ci}_{*3}F^{ci}_{1} - x^{ci}_{*1}F^{ci}_{3}\right)\right.$$

$$\frac{-1}{\sin\theta} \left(-\cos\theta\cos\psi\left(x^{G}_{p2}F^{G}_{p3} - x^{G}_{p3}F^{G}_{p2}\right) + \cos\theta\sin\psi\left(x^{G}_{p3}F^{G}_{p1} - x^{G}_{p1}F^{G}_{p3}\right)\right.$$

$$\left. - \sin\theta\left(x^{G}_{p1}F^{G}_{p2} - x^{G}_{p2}F^{G}_{p1}\right)\right. \tag{6.18}$$

$$M^{c\cdot\cdot c}x^{c}_{2} + K^{b}_{22}\left(x^{c}_{2} - x^{e}_{2}\right)$$

$$- K^{a}_{22}\left(d_{2}\sin\phi\sin\theta + x^{p}_{2} - x^{c}_{2}\right)$$

$$- \frac{K^{a}_{26} + K^{a}_{62}}{2}\left(\phi - \theta^{e}_{3}\right)$$

$$+ C^{b}_{77}\left(\dot{x}^{c}_{2}\right)$$

$$+ C^{a}_{22}\left(d_{2}\dot{\phi}\cos\phi\sin\theta + d_{2}\dot{\theta}\sin\phi\cos\theta + \dot{x}^{p}_{2} - \dot{x}^{c}_{2}\right)$$

$$- \frac{C^{a}_{26} + C^{a}_{62}}{2}\left(\dot{\phi} + \dot{\psi}\cos\theta\right)$$

$$= 0 \tag{6.19}$$

$$M^{c\cdot\cdot c}x^{c}_{3} + K^{b}_{33}\left(x^{c}_{3} - x^{e}_{3}\right)$$

$$- K^{a}_{33}\left(d_{2}\cos\theta + x^{m}_{3} - x^{c}_{3}\right)$$

$$- \frac{K^{a}_{35} + K^{a}_{53}}{2}\left(\theta - \theta^{e}_{2}\right)$$

$$+ C^{b}_{33}\left(\dot{x}^{c}_{3}\right)$$

$$- C^{b}_{33}\left(-d_{2}\dot{\theta}\sin\theta + \dot{x}^{m}_{3} - \dot{x}^{c}_{3}\right)$$

$$- \frac{\left(C_{35} + C_{53}\right)}{2}\left(\dot{\theta}\cos\phi + \dot{\psi}\sin\phi\sin\theta\right)$$

$$= 0 \tag{6.20}$$

$$I\ddot{\gamma} + K_{44}^{b}(\gamma - \theta_{1}^{e}) - K_{44}^{a}(\psi - \gamma) + C_{44}^{b}(\dot{\gamma}) - C_{44}^{a}(-\dot{\theta}\sin\phi + \dot{\psi}\cos\phi\sin\theta - \dot{\gamma}) = 0 \qquad (6.21)$$

6.3 SOLUTION OF EQUATIONS OF MOTION

The equations of motion for the peg and carrier were solved numerically using a subroutine, HPCG, developed by the IBM Corporation, based on Hamming's modified predictor-corrector method for solving systems of general, first order, differential equations. A simplified flow diagram of the solution procedure is shown in Fig. 6.4.

At each step in the procedure it is necessary to determine the type of contact occurring, and the resulting contact forces acting on the peg. These operations will now be described in detail.

6.3.1 Peg-Hole Contact

Six different modes of contact between the peg and hole edges were considered.

(i) No contact.

(ii) Single point contact - sliding.

(iii) Single point contact - stationary.

(iv) Double point contact - both sliding.

(v) Double point contact - sliding and stationary.

(vi) Double point contact - both stationary.

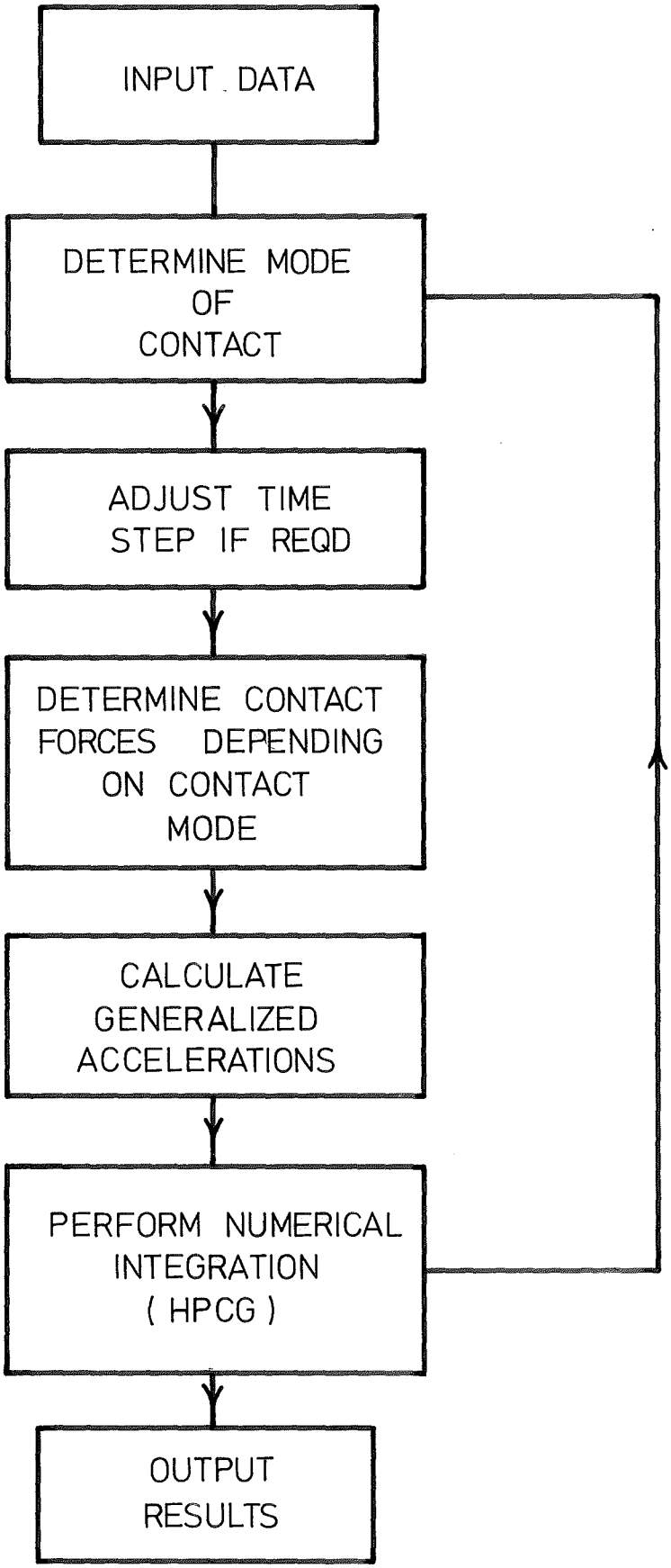

FIG. 6.4 SOLUTION PROCEDURE

6.3.1.1 Location of Contact Points

A procedure suggested by Comba [46] was used to determine the location of the point(s) on the peg edge where contact occurred.

In this approach, the expressions representing the bounding surfaces of the objects are combined into a single pseudo-characteristic (p/c) function G, which has the property $G \leq 0$ in a region approximating the region of intersection of the objects. The problem of determining whether or not intersection occurs becomes one of determining whether $G \leq 0$ at any point.

The p/c function G is defined as follows; objects are considered as being the intersection of regions R_i where R_i is given by the inequality.

$$g_i(x_j) \leq 0$$

and $$v_i = (g_i^2 + t^2)^{\frac{1}{2}} + g_i \quad 0<t<<1 \tag{6.22}$$

and summing all v_i

$$V = \sum v_i$$

the p/c function G is

$$G = \tfrac{1}{2}(V - t^2/V) + C \tag{6.23}$$

In the case considered, the possible contact modes are limited to small interpenetrations at either one or two points on the peg and hole edges. The search for a minimum of G was therefore carried out around the circumference of the peg base for the intersections of the regions R_1 and R_2, defining the hole cylinder and hole plane, Fig. 6.5

i.e. $$g_1 = \frac{(-x_2^2 - x_3^2 + r_h^2)}{r_h} \tag{6.24}$$

$$g_2 = x_1 + h \tag{6.25}$$

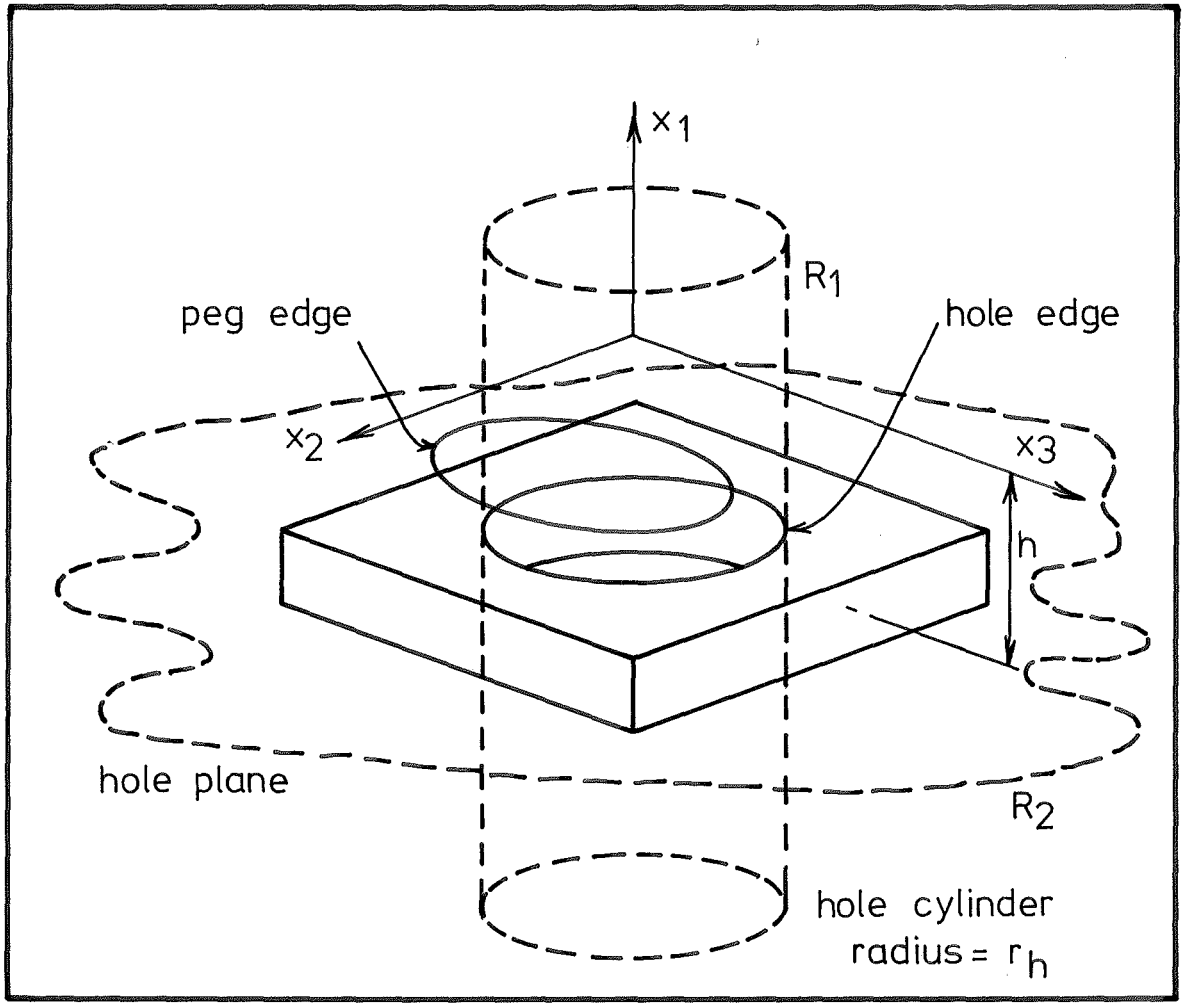

FIG. 6.5 PEG EDGE-HOLE EDGE CONTACT.

Fig. 6.6 shows the value of G along the peg edge for a typical case of single point contact. Generally two minima exist which, if negative, indicate that interpenetration occurs. The minima are found using a simple bisection method, the slope being used as a criterion for increment halving. The positions of the previous minima are stored and used as starting points for each search. This method iterates to the solution reliably.

6.3.1.2 Velocity at Contact Points

Having found the contact points the next step involves finding the velocity of the peg at the contact point to determine the normal and sliding velocities.

The velocity at the first contact point for example is

$$\begin{bmatrix} \dot{x}_1^{cl} \\ \dot{x}_2^{cl} \\ \dot{x}_3^{cl} \end{bmatrix} = \begin{bmatrix} & x_{*3}^{cl} & -x_{*2}^{cl} \\ -x_{*3}^{cl} & 0 & x_{*1}^{cl} \\ x_{*2}^{cl} & -x_{*1}^{cl} & 0 \end{bmatrix} R_e \begin{bmatrix} \dot{\phi} \\ \dot{\theta} \\ \dot{\psi} \end{bmatrix} + \begin{bmatrix} \dot{x}_1^{p} \\ \dot{x}_2^{p} \\ \dot{x}_3^{p} \end{bmatrix} \tag{6.26}$$

Using the work of Sec. 3.2.1 to obtain the contact point normal n^{cl}, the velocity in the normal direction is simply

$$\underline{\dot{x}}^{ncl} = (\underline{\dot{x}}^{cl} \cdot \underline{n}^{cl})\, \underline{n}^{cl} \tag{6.27}$$

and the sliding velocity on the contact planes is

$$\underline{\dot{x}}^{pcl} = \underline{\dot{x}}^{cl} - \underline{\dot{x}}^{ncl} \tag{6.28}$$

6.3.1.3 Misalignment Modes

For the purposes of computing, the criteria shown in Fig. 6.7 were used to determine the type of contact.

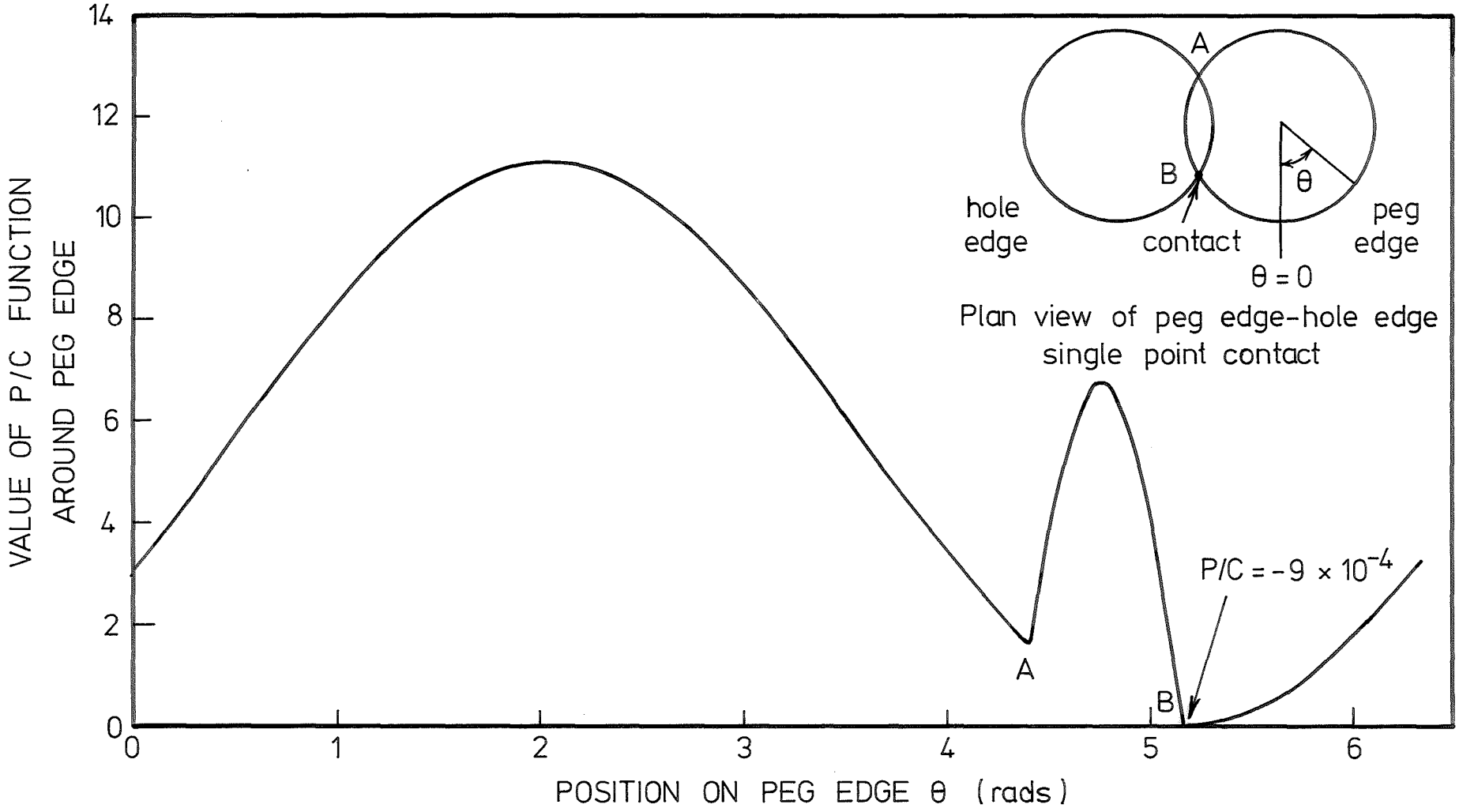

FIG 6.6 TYPICAL P/C FUNCTION G VALUES

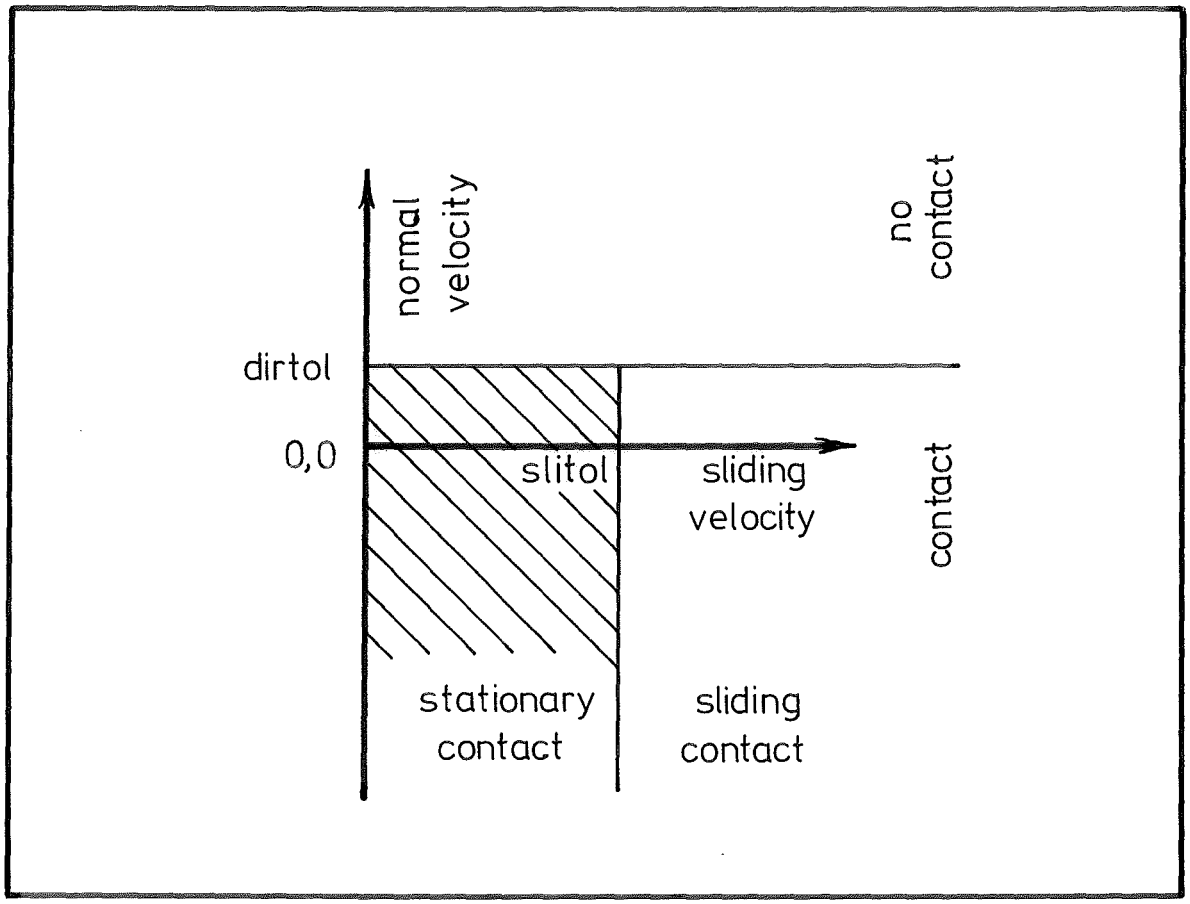

FIG. 6.7 CONTACT MODES

6.3.2 Contact Forces

Two approaches were used to find the contact forces generated between the peg and hole, and although in practice only the second proved successful both are described here.

6.3.2.1 First Approach

This approach involved making assumptions regarding the stiffness, damping and frictional characteristics of the contact point. This allowed the contact forces to be calculated directly as a function of peg position and velocity. It was assumed that

(i) the normal force/deformation characteristic could be modelled by a linear over-damped spring-dashpot system as shown in Fig. 6.8a i.e.

$$\underline{F}^{ncl} = (-K.r. + C|\dot{\underline{x}}^{ncl}|)\ \underline{n}^{cl} \tag{6.29}$$

(ii) the following friction conditions applied; with reference to Fig. 6.9, the friction force opposing the plane contact velocity direction has magnitudes given by

$$|\underline{F}^{pcl}| = \mu_{ST} \frac{\dot{x}^{pcl}}{V_{ST}} |\underline{F}^{ncl}| \tag{6.30}$$

when $\dot{x}^{pcl} \leqslant V_{ST}$

and $$|\underline{F}^{pcl}| = \mu_{SL} |\underline{F}^{ncl}| \tag{6.31}$$

V_{ST} the limiting velocity, is small compared with the usual values of $\dot{x}^{pcl}$, and in the first case, above, the static friction force, dependent upon the creep at the peg, is allowed to adjust itself over successive iterations to react against the applied force.

In the second case when sliding occurs the simple friction theory holds.

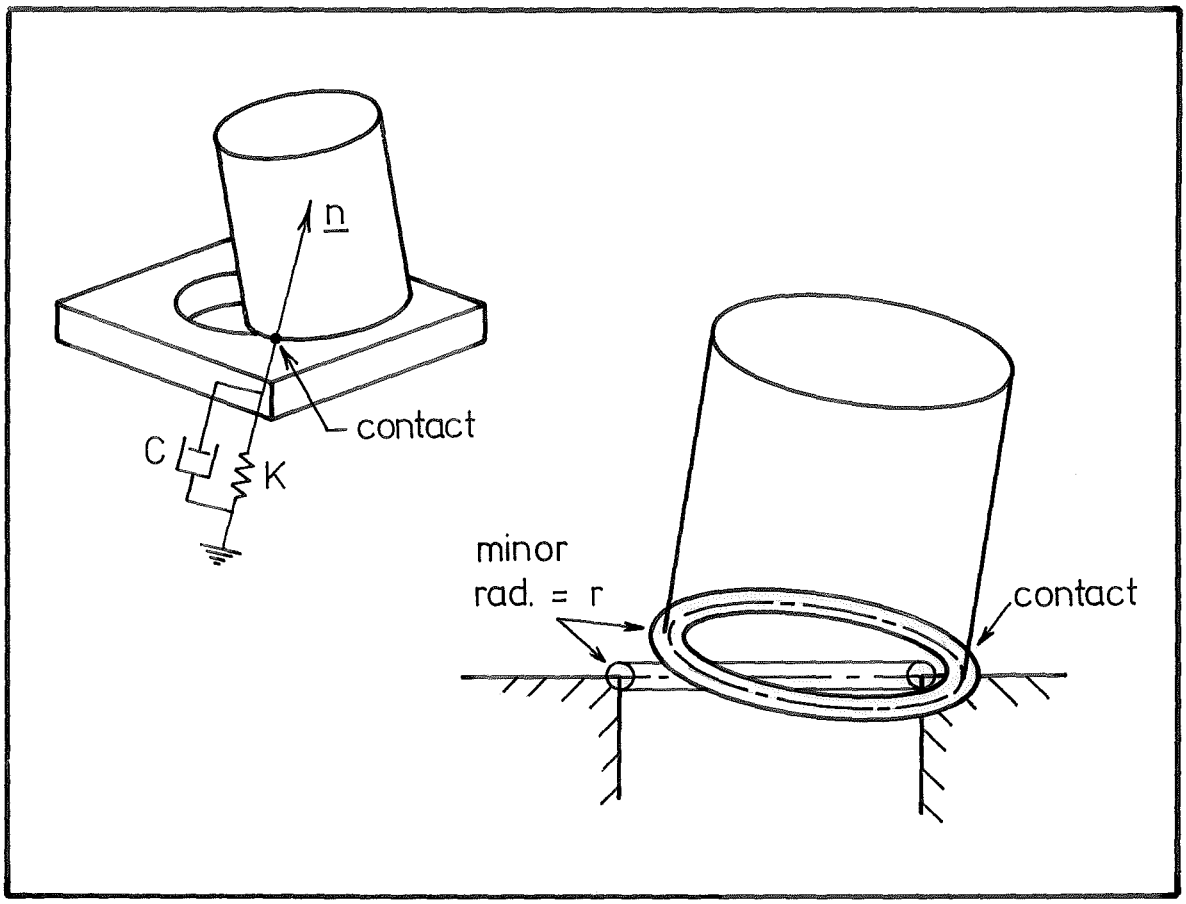

FIG. 6.8 (a) SPRING DASHPOT MODEL OF CONTACT. (b) COMPUTATION OF INTERPENETRATION.

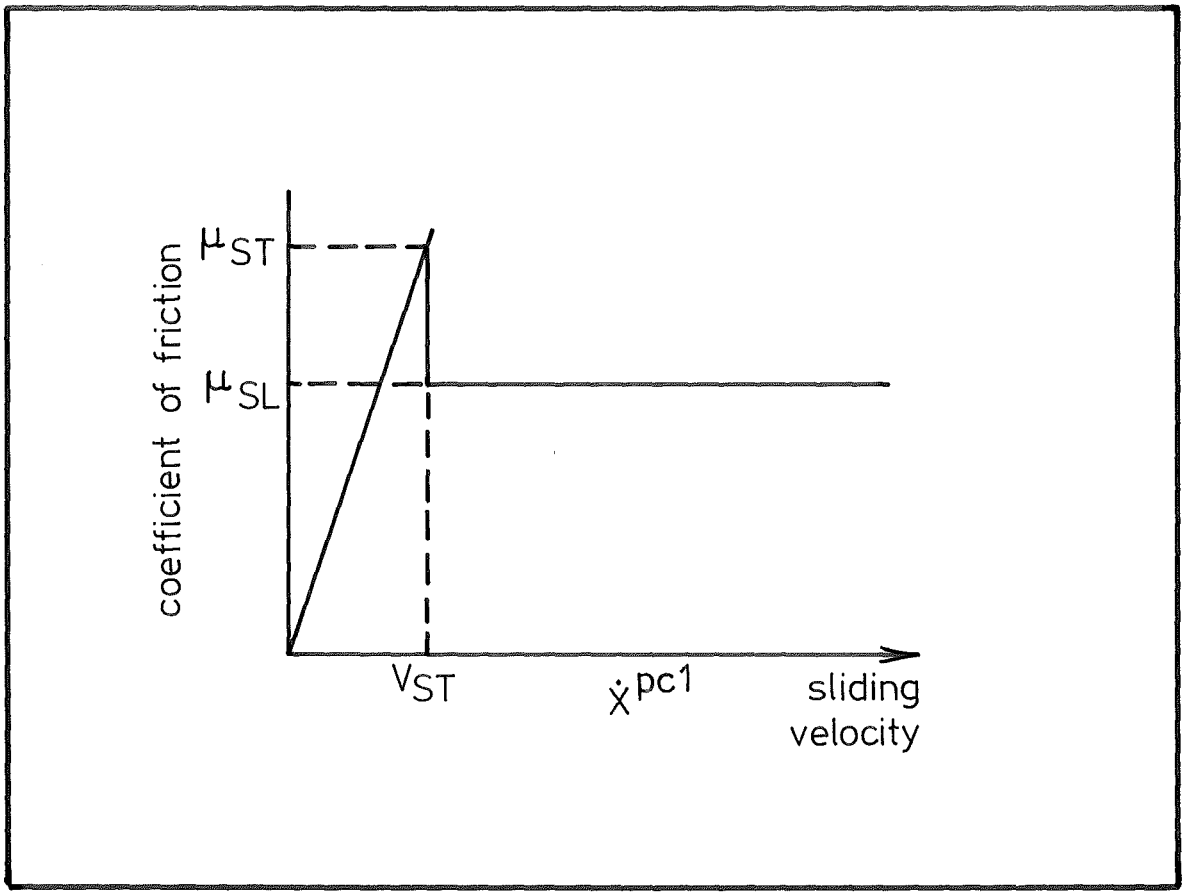

FIG. 6.9 FRICTION CONDITIONS

This approach, although direct, suffered a number of drawbacks.

(i) The computation of the deformation r as shown in Fig. 6.8b required considerable effort.

(ii) The high stiffness and damping necessary to simulate contact demanded small time increments, this leading to slow runs and round off errors.

6.3.2.2 Second Approach

The second method used the relationships between the accelerations and velocities at the contact point, together with the simple friction theory, to obtain the contact forces acting on the peg. The assumptions were that;

(i) The normal acceleration of the peg away from the hole surface at the contact point was proportional to the normal velocity, i.e. viscous damping

$$\underline{n}^{cl} \cdot \ddot{\underline{x}}^{cl} = -k(\underline{n}^{cl} \cdot \dot{\underline{x}}^{cl}) \tag{6.32}$$

(ii) If movement occurred on the plane i.e. if

$$\dot{x}^{pcl} > V_{ST}$$

then the following conditions are assumed.

(a) The simple friction relation applies

$$\underline{F}^{cl} \cdot (\underline{p}^{cl} + \mu \underline{n}^{cl}) = 0 \tag{6.33}$$

where the vectors n^{cl}, p^{cl} q^{cl} are defined in Fig. 6.10.

(b) The friction force acts in opposition to the direction of sliding

$$\underline{F}^{cl} \cdot \underline{q}^{cl} = 0 \tag{6.34}$$

(iii) If the plane velocity is lower than the limiting velocity V_{ST} then the following conditions hold;

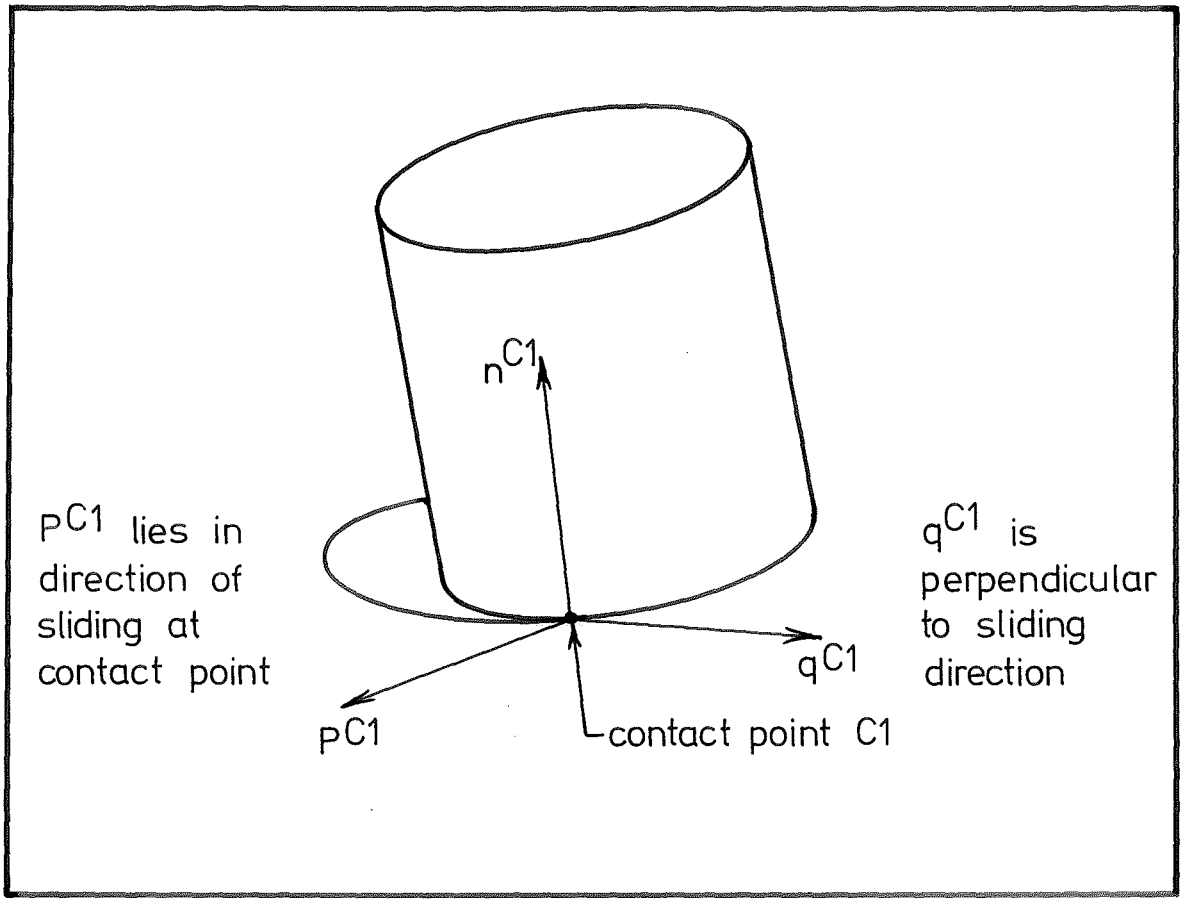

FIG. 6.10 DEFINITION OF CONTACT VECTORS

(a) The acceleration of the peg in the direction of the contact plane vector $\underline{p}^{cl}$ is zero

$$\underline{p}^{cl} \cdot \ddot{\underline{x}}^{cl} = 0 \tag{6.35}$$

(b) The acceleration in the direction of the contact plane vector $\underline{q}^{cl}$ is zero

$$\underline{q}^{cl} \cdot \ddot{\underline{x}}^{cl} = 0 \tag{6.36}$$

The equations of motion, Equations 6.13 to 6.21, involving contact force terms may be written together with the contact conditions developed above, in the following general form.

$$\begin{bmatrix} A_{11} & A_{12} & A_{13} \\ A_{21} & A_{22} & A_{23} \\ A_{31} & A_{32} & A_{33} \end{bmatrix} \begin{bmatrix} U_1 \\ U_2 \\ U_3 \end{bmatrix} = \begin{bmatrix} B_1 \\ B_2 \\ B_3 \end{bmatrix}$$

B_1: Equations of Motion; B_2, B_3: Contact Conditions

where U_1 is the submatrix of the 6 unknown generalized accelerations of the peg,

U_2 is the 3 x 1 submatrix of the first contact point force components,

U_3 is the 3 x 1 submatrix of the second contact point force components,

B_1 is the 6 x 1 submatrix of generalized forces due to stiffness, damping, and applied forces,

and B_2 and B_3 are the RHS values of the appropriate conditions.

Essentially the method involves solving the 6 equations of motion of the peg, and the appropriate contact conditions, to find the unknown accelerations and contact forces U. The form of matrix A will be examined for different contact conditions.

(i) No contact - In this case no forces exist so we may write

$$\begin{bmatrix} A_{11} \end{bmatrix} \begin{bmatrix} U_1 \end{bmatrix} = \begin{bmatrix} B_1 \end{bmatrix}$$

which is easily solved to obtain the peg generalized accelerations U_1.

(ii) Single point sliding contact - The elements of U_3 are zero so the equations have the following form,

$$\left[\begin{array}{c|c} A_{11} & A_{12} \\ \hline A_{21} & A_{22} \end{array}\right] \left[\begin{array}{c} U_1 \\ \hline U_2 \end{array}\right] = \left[\begin{array}{c} B_1 \\ \hline B_2 \end{array}\right] \tag{6.37}$$

Submatrices A_{11} A_{12} simply contain the coefficients of the accelerations and forces in the equations of motion. The elements of A_{21} and A_{22} are obtained from the conditions described in Equations 6.32 - 6.34.

Recalling Equation 6.26 giving the velocities at the first contact point, we differentiate to obtain the acceleration components.

$$\begin{aligned} \ddot{x}_1^{cl} = {} & \ddot{x}_1^{p} - x_{*2}^{cl}\ddot{\phi} + x_{*3}^{cl}\cos\phi\ddot{\theta} + (x_{*3}^{cl}\sin\phi\sin\theta - x_{*2}^{cl}\cos\theta)\ddot{\psi} \\ & + x_{*3}^{cl}(-\dot{\phi}\dot{\theta}\sin\phi + \dot{\phi}\dot{\psi}\cos\phi\sin\theta + \dot{\theta}\dot{\psi}\sin\phi\cos\theta) \\ & + x_{*2}^{cl}(-\dot{\theta}\dot{\psi}\sin\theta) \end{aligned} \tag{6.38}$$

$$\begin{aligned} \ddot{x}_2^{cl} = {} & \ddot{x}_2^{p} + x_{*1}^{cl}\ddot{\phi} + x_{*3}^{cl}\sin\phi\ddot{\theta} + (x_{*1}^{cl}\cos\theta - x_{*3}^{cl}\cos\phi\sin\theta)\ddot{\psi} \\ & + x_{*1}^{cl}(-\dot{\theta}\dot{\psi}\sin\theta) \\ & - x_{*3}^{cl}(-\dot{\phi}\dot{\theta}\cos\phi - \dot{\phi}\dot{\psi}\sin\phi\sin\theta + \dot{\theta}\dot{\psi}\cos\phi\cos\theta) \end{aligned} \tag{6.39}$$

$$\begin{aligned} \ddot{x}_3^{cl} = {} & \ddot{x}_3^{p} + (-x_{*2}^{cl}\sin\phi - x_{*1}^{cl}\cos\phi)\ddot{\theta} \\ & + (x_{*2}^{cl}\cos\phi\sin\theta - x_{*1}^{cl}\sin\phi\sin\theta)\ddot{\psi} \\ & + x_{*2}^{cl}(\dot{\phi}\dot{\theta}\cos\phi - \dot{\phi}\dot{\psi}\sin\phi\sin\theta + \dot{\theta}\dot{\psi}\cos\phi\cos\theta) \\ & - x_{*1}^{cl}(-\dot{\phi}\dot{\theta}\sin\phi + \dot{\phi}\dot{\psi}\cos\phi\sin\theta + \dot{\theta}\dot{\psi}\sin\phi\cos\theta) \end{aligned} \tag{6.40}$$

Substituting these expressions into the following form of Equation 6.32

$$n_1^{cl}\,\ddot{x}_1^{cl} + n_2^{cl}\,\ddot{x}_2^{cl} + n_3^{cl}\,\ddot{x}_3^{cl}$$

$$= -k\,(n_1^{cl}\,x_1^{cl} + n_2^{cl}\,x_2^{cl} + n_3^{cl}\,x_3^{cl} \qquad (6.41)$$

gives an equation from which the first row of elements of submatrices A_{21} A_{22} and B_2 may be found.

The Equations 6.33 6.34 may be expanded and rewritten as

$$(\mu n_1^{cl} + p_1^{cl})F_1^{cl} + (\mu n_2^{cl} + p_2^{cl})F_2^{cl} + (\mu n_3^{cl} + p_3^{cl})F_3^{cl} = 0 \qquad (6.42)$$

and

$$q_1^{cl}F_1^{cl} + q_2^{cl}F_2^{cl} + q_3^{cl}F_3^{cl} = 0 \qquad (6.43)$$

thus giving all the elements of A_{21} A_{22} and B_2. Hence Equations 6.37 may be solved to yield the contact forces and accelerations.

It should be noted that Equations 6.42 and 6.43 are ambiguous in that both $\pm \underline{F}^{cl}$ satisfy them. In practice the sense of $\underline{F}^{cl}$ was checked and the acceleration values recalculated if necessary.

(iii) Single point stationary contact - Equation 6.41 is again imposed upon the peg accelerations at the contact point and Equations 6.35 and 6.36 applied. The expanded form of these equations is

$$p_1^{cl}\ddot{x}_1^{cl} + p_2^{cl}\ddot{x}_2^{cl} + p_3^{cl}\ddot{x}_3^{cl} = 0 \qquad (6.44)$$

$$q_1^{cl}\ddot{x}_2^{cl} + q_2^{cl}x_2^{cl} + q_3^{cl}x_3^{cl} = 0 \qquad (6.45)$$

Again these equations provide the elements of A_{21} A_{22} and B_2, allowing the accelerations and forces to be found.

(iv) Double point sliding contact - Equations 6.41 to 6.43 are applied at both contact points to provide the elements in the equations

$$\begin{bmatrix} A_{11} & A_{12} & A_{13} \\ A_{21} & A_{22} & A_{23} \\ A_{31} & A_{32} & A_{33} \end{bmatrix} \begin{bmatrix} U_1 \\ U_2 \\ U_3 \end{bmatrix} = \begin{bmatrix} B_1 \\ B_2 \\ B_3 \end{bmatrix}$$

If the peg and hole axes are parallel, the vectors $\underline{n}^{cl}\ \underline{p}^{cl}\ \underline{q}^{cl}$ at the first contact point become collinear with those of the second contact point, thus making A singular. It is assumed then that the first and second point contact forces are equal.

(v) Double point sliding and stationary contact - The stationary conditions, Equations 6.41, 6.44 and 6.45, are applied at the first contact point and the sliding conditions, Equations 6.41 - 6.43, are applied at the second contact point.

(vi) Double point stationary contact - Both contact points have the stationary conditions, Equations 6.41 6.44 and 6.45 applied at them.

CHAPTER 7

PROGRAM DESCRIPTION AND EVALUATION

In this chapter two computer programs modelling the system described in the previous chapter are described. Their numerical validity is checked by comparison with simple analytical models. Specifically the behaviour of the programs in simulating impact and friction is examined.

7.1 COMPUTER PROGRAMS

The two programs developed differed only in the approach taken toward finding the contact forces. The methods described in Sec. 3.2.1 and Sec. 3.2.2 being used respectively in Programs A and B.

The structure of the programs are shown in Fig. 7.1 and the function of the subroutines is described below.

Main Program: The system parameters are input, printed, and control passed to HPCG.

Subroutine HPCG: This subroutine developed by I.B.M. as part of their Scientific Subroutine package uses Hamming's modified predictor-corrector method to solve the equations of motion.

Subroutine FCT: For a given set of generalized displacements and velocities the system accelerations are determined from the equations of motion. The contact forces are also calculated in this subroutine.

Subroutine STATE: The misalignment mode as defined in Sec. 6.3.1.3. is specified here. The contact normal and velocity at the contact point(s) are found initially.

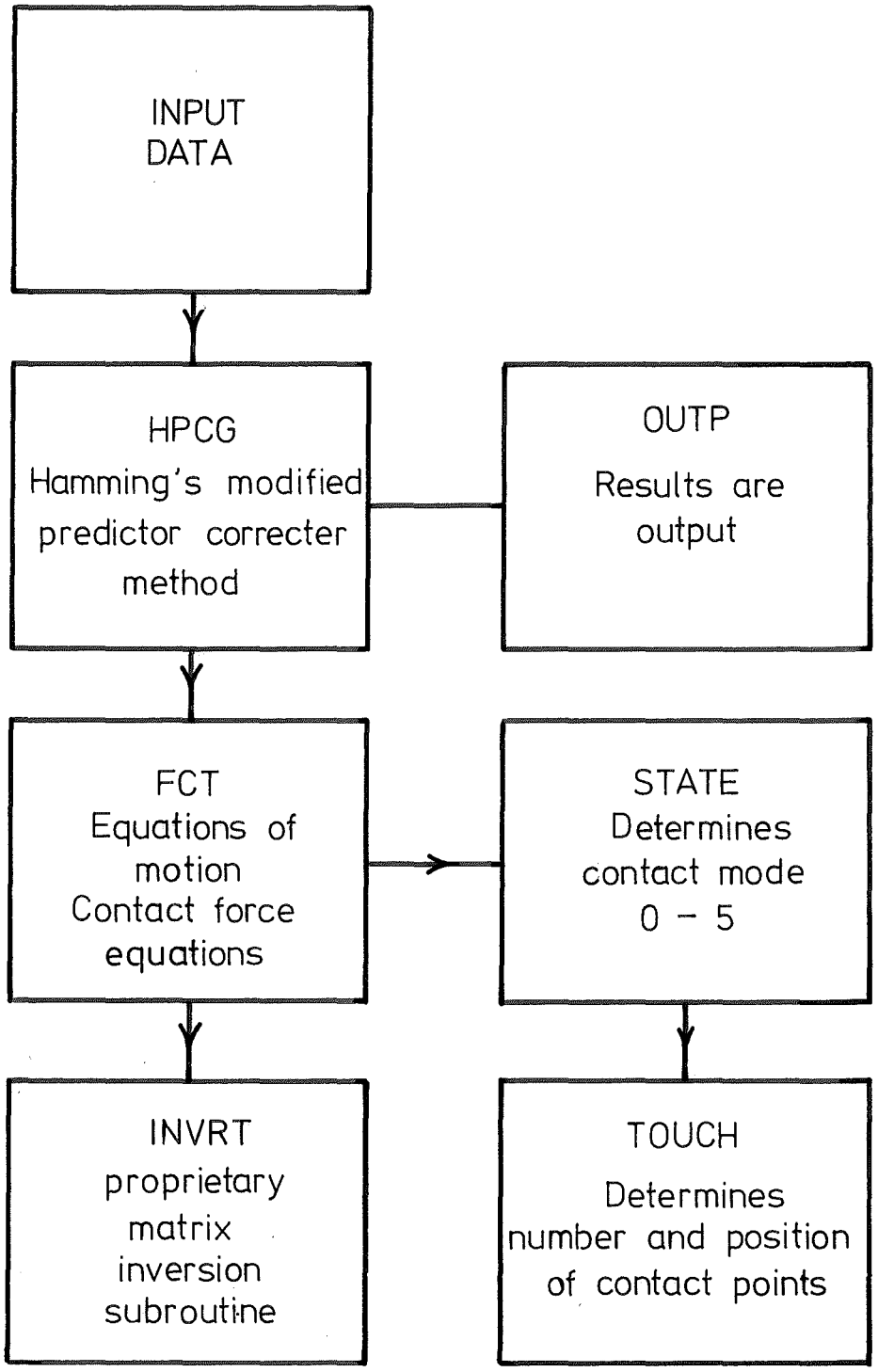

FIG. 7.1 PROGRAM STRUCTURE

Subroutine TOUCH: This subroutine uses Comba's approach, Sec. 6.3.1.1. to find the position of the contact point(s) on the peg edge.
Subroutine INVRT: This is a proprietary Burroughs matrix inversion subroutine used in Program B to solve the equations of motion and contact conditions, for the unknown peg accelerations and contact forces.
Subroutine OUTP: The results of the program, namely the values of the system generalized coordinates and the first and second derivatives at successive time intervals, are output here.

7.2 PROGRAM EVALUATION

The accuracy with which the programs will reproduce the behaviour of an actual physical system depends upon

(i) The assumptions made in the model i.e. the friction and impact characteristics of contact, the stiffness and damping characteristics of the constraints and the masses and inertias of the system components.

(ii) The numerical evaluation of the equations of motion.

The assumptions in the model have been dealt with in Chapter 3 and so here we shall only concern ourselves with the accuracy of the numerical methods used in Programs A and B.

The scarcity of information on the behaviour of vibratory assembly mechanisms made it necessary to adopt the following approach where analytically verifiable situations were simulated by the programs. Two situations were chosen which would test the program's abilities to simulate impact and friction.

(i) The peg was accelerated onto the hole edges.

(ii) The inclined peg was slid across the hole.

7.2.1 Impact

The program was given the initial conditions shown in Fig. 7.2, effectively this accelerated the peg for about 2 mm onto the hole edges. A simple model of this situation is shown in Fig. 7.3 where a mass M with a single vertical degree of freedom is dropped toward the surface S.

i.e. $M\ddot{x} = -k_x$

$x = X\cos\omega t$

$\dot{x} = X\omega\sin\omega t$

where

$\omega = \sqrt{\frac{K}{M}}$

The resulting motion of the peg is shown in Fig's 7.4 to 7.6. During the free flight phase there was very close agreement between the analytical result and the results of both Programs A and B.

At contact it can be seen that the numerical methods depart from the analytical solution. The displacement curves are significant, both numerical solutions overshooting the contact point.

The overshoot of Program A although initially less than that of Program B fails to flatten out; the result is that the peg continues to sink into the hole edge.

The results of Program B show the peg, overshooting the contact point by .25 mm, rebounding slightly, probably because of elasticity in the system, and then remaining stable. The amount of overshoot was considered acceptable being approximately 1% of the peg radius.

The velocity curves in Fig. 7.5 again reveal the differing behaviour of the two programs.

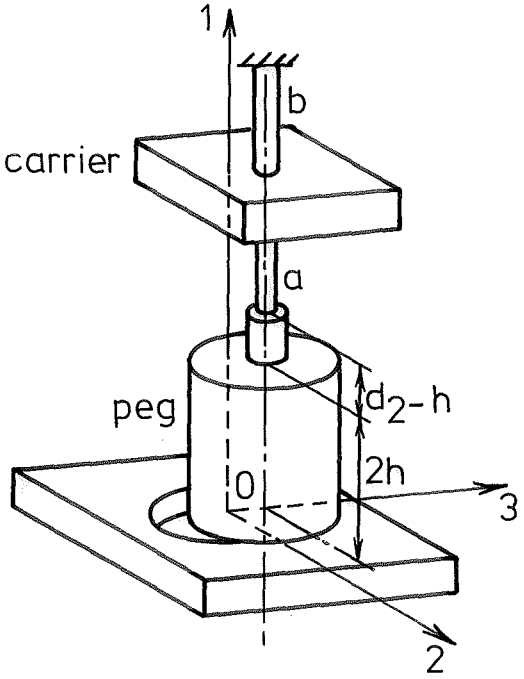

FIG. 7.2 IMPACT MODEL SYSTEM PARAMETERS

$d_1 = 56$

$d_2 = 50$

$2h = 60$

$r_p = 25$

$r_h = 25$

$\mu_{ST} = .2$

$\mu_{SL} = .2$

$M^c = .395$

$I^c = .81E5$

$M^p = .395$

$$I^p = \begin{bmatrix} .25E3 & & \\ & .25E3 & \\ & & .10E3 \end{bmatrix}$$

Units

Kg, mm, s

$x_1^p = 31.96 \quad \dot{x}_1^p = 0 \quad x_1^e = 73.46$

$x_2^p = 0 \quad \dot{x}_2^p = 0$

$x_3^p = 20 \quad \dot{x}_3^p = 0$

$\phi = 0 \quad \dot{\phi} = 0 \quad \theta_3^e = 0$

$\theta = 1.58 \quad \dot{\theta} = 0 \quad \theta_2^e = 1.58$

$\psi = 0 \quad \dot{\psi} = 0$

$x_2^c = 0 \quad \dot{x}_2^c = 0 \quad x_2^e = 0$

$x_3^c = 19.54 \quad \dot{x}_3^c = 0 \quad x_3^e = 19.54$

$\gamma = 0 \quad \dot{\gamma} = 0 \quad \theta_1^e = 0$

$$[K^a] = \begin{bmatrix} .45E3 & & & \\ & .46E5 & & .17E7 \\ & & .46E5 & -.17E7 \\ & & & .24E8 \\ & & -.17E7 & .27E9 \\ & .17E7 & & .27E9 \end{bmatrix}$$

$$[K^b] = \begin{bmatrix} .13E2 & & \\ & .13E2 & \\ & & .26E6 \end{bmatrix}$$

$$[C^a] = \begin{bmatrix} 0 & & & & & \\ & .67E2 & & & & \\ & & .67E2 & & & \\ & & & .25E5 & & \\ & & & & .13E6 & \\ & & & & & .13E6 \end{bmatrix} \qquad [C^b] = \begin{bmatrix} 0 \end{bmatrix}$$

FIG. 7.2 contd.

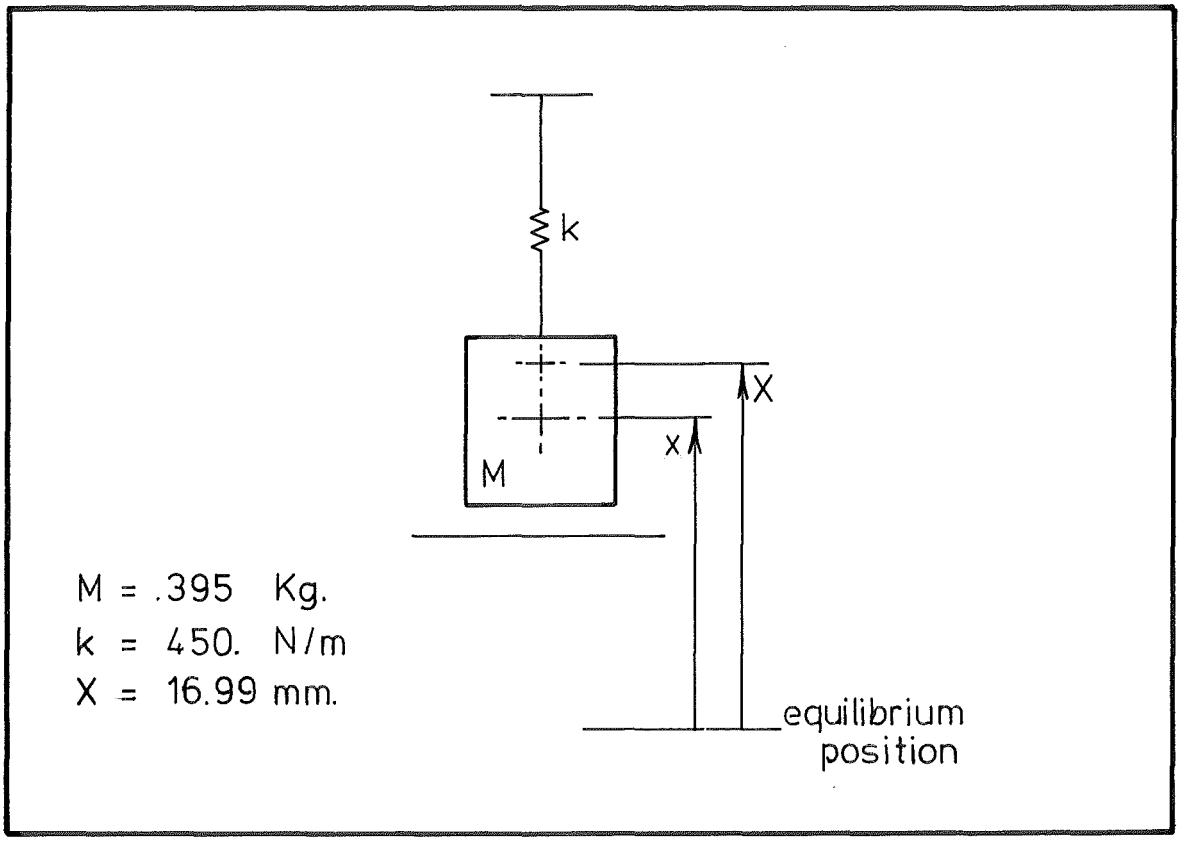

FIG. 7.3 MODEL OF IMPACT

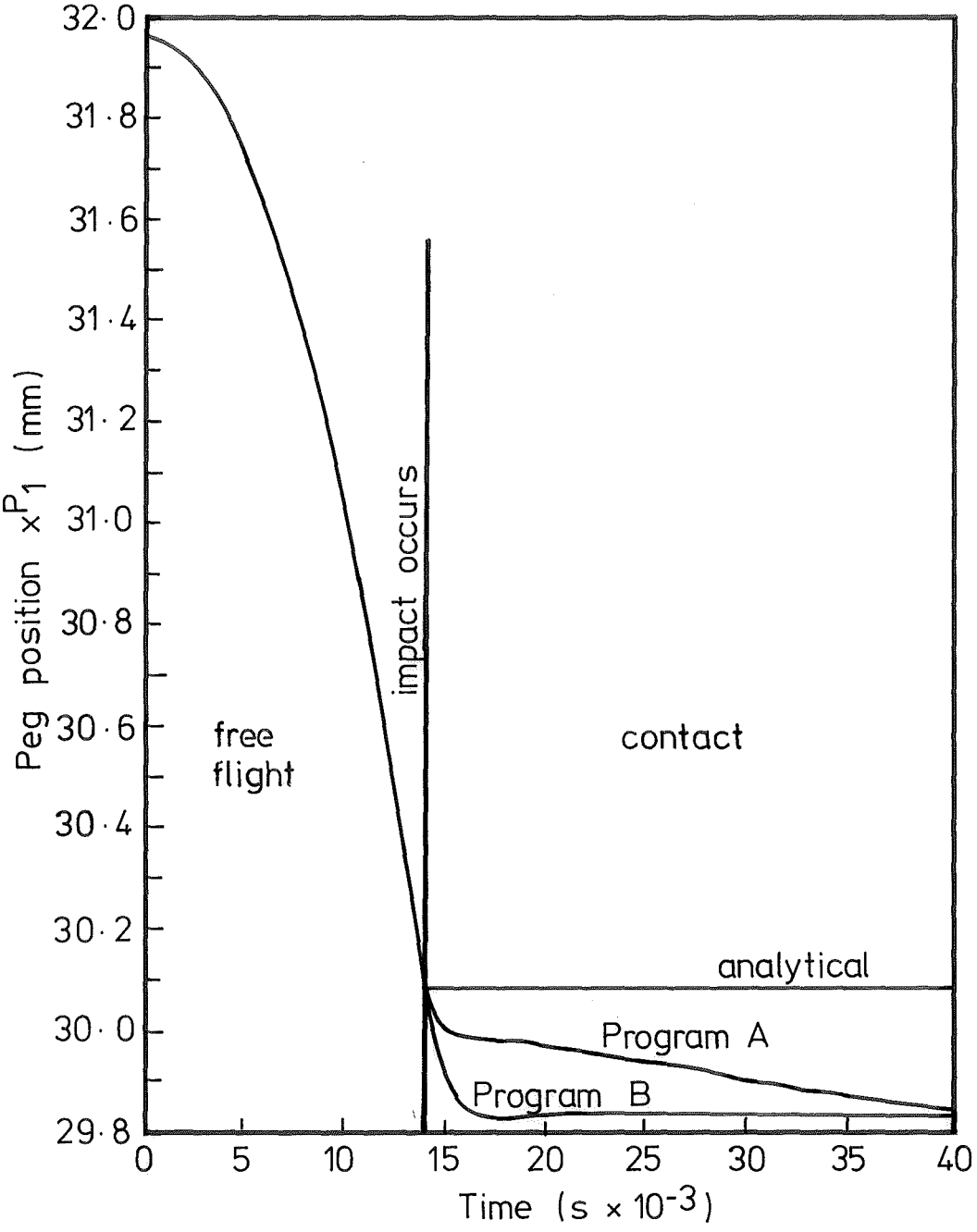

FIG. 7.4 IMPACT TEST DISPLACEMENT

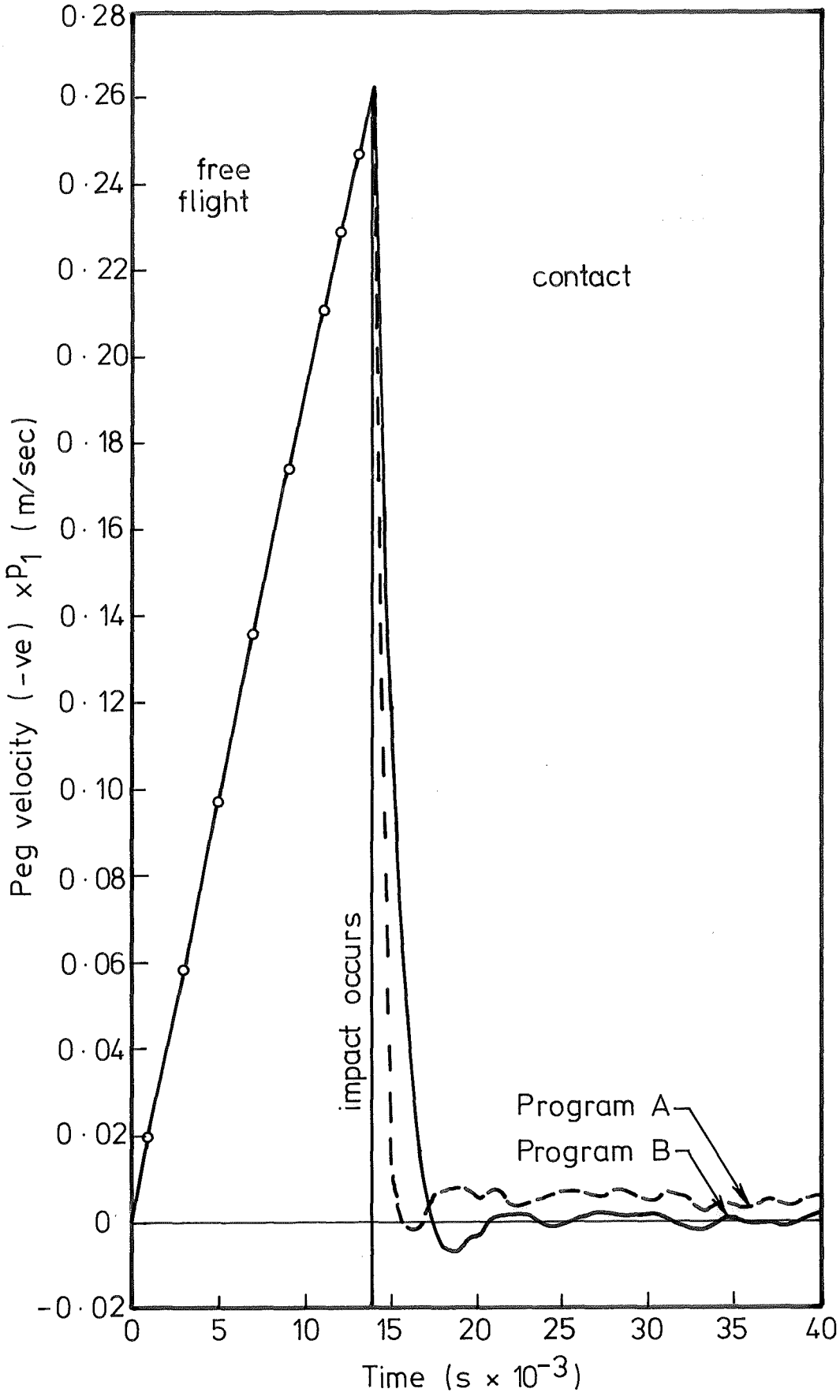

FIG. 7.5 IMPACT TEST VELOCITY

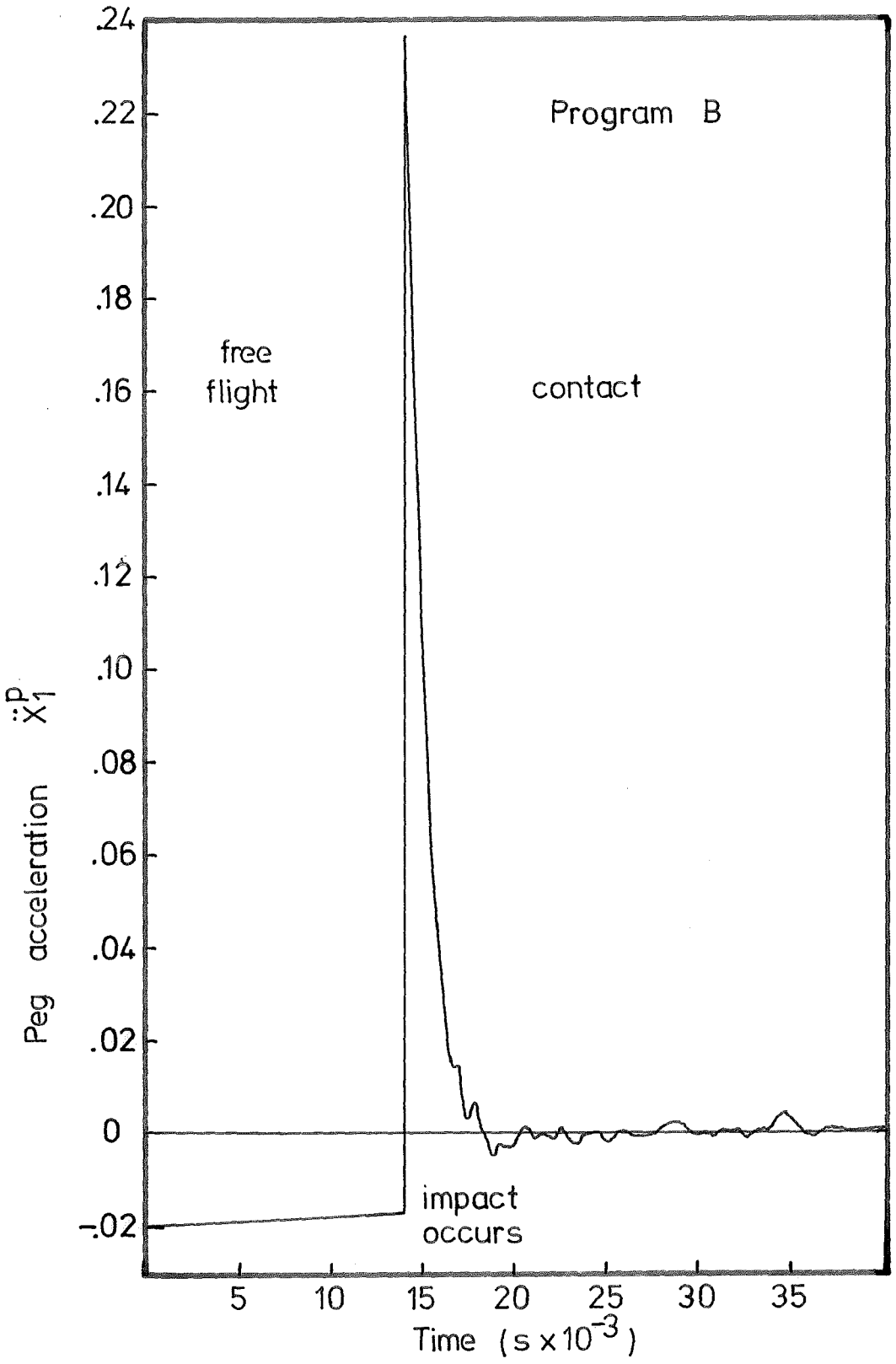

FIG. 7.6 IMPACT TEST ACCELERATION

The acceleration curve of Program B is shown in Fig. 7.6. The numerical difficulties in modelling impact are demonstrated by the sharpness of the contact acceleration curve.

7.2.2 Sliding

The behaviour of both programs under sliding conditions was studied by giving them the initial conditions shown in Fig. 7.7. The peg, contacting the hole at two points and tilted into the hole, was acted on by a direct force acting toward the hole centre.

The simple model representing this case is shown in Fig. 7.8.

$$M\ddot{y} = F_N\cos\theta + F_s\sin\theta - F\sin2\theta - Mg$$

$$2M\ddot{x} = F\cos2\theta + F_N\sin\theta - F_s\cos\theta$$

Also

$$\ddot{y} = -\ddot{x}\tan\theta$$

$$\mu F_N = F_s.$$

Substituting to eliminate $\ddot{y}$, F_N, F_s we get

$$\ddot{x} = \frac{F\cos2\theta(\cos\theta + \mu\sin\theta) + (F\sin2\theta + M_g)(\sin\theta - \mu\cos\theta)}{2(\cos\theta + \mu\sin\theta) + \tan\theta(\sin\theta - \mu\cos\theta)}$$

Using the values in Fig. 7.7 we get

$$\ddot{x} = 357.65 \text{ mm/s}^2$$

$$\dot{x} = 357.65t \text{ mm/s}$$

$$x = \frac{357.62t^2}{2} \text{ mm}$$

The behaviour of the programs as compared to the simple model is shown in Fig's 7.9 and 7.10.

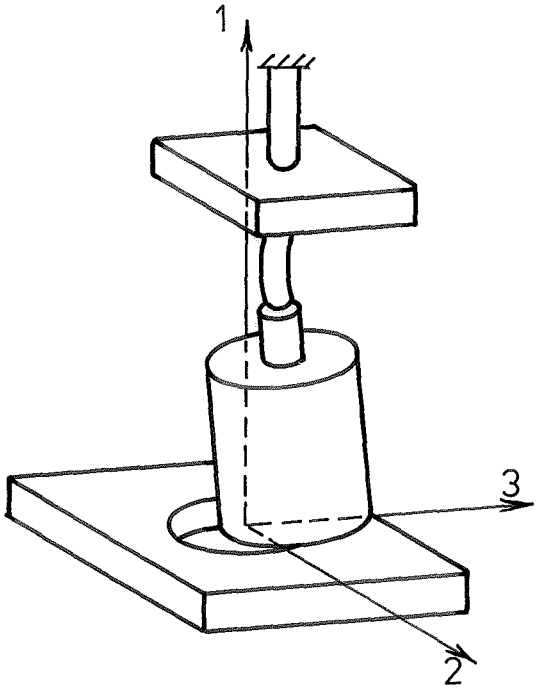

FIG. 7.7 SLIDING MODEL SYSTEM PARAMETERS

$d_1 = 56$

$d_2 = 50$

$h = 30$

$r_p = 25$

$rh = 25$

$\mu_{SL} = .2$

$\mu_{ST} = .2$

$M^c = .395$

$I^c = .81E5$

$M^p = .395$

$$I^p = \begin{bmatrix} .25E3 & & \\ & .25E3 & \\ & & .10E3 \end{bmatrix}$$

x_1^p	= 34.02	$\dot{x}_1^p$	= 0	x_1^e	= 75.0	Units
x_2^p	= 0	$\dot{x}_2^p$	= 0			Kg, mm, s
x_3^p	= 40.0	$\dot{x}_3^p$	= 0			
ϕ	= 0	ϕ	= 0	θ_3^e	= 0	
θ	= 1.771	θ	= 0	θ_2^e	= 1.771	
ψ	= 0	ψ	= 0			
x_2^c	= 0	x_2^c	= 0	x_2^e	= 0	
x_3^c	= 30.07	x_3^c	= 0	x_3^e	= 30.07	
γ	= 0	γ	= 0	θ_3^e	= 0	

$$K^a = \begin{bmatrix} 0 & & & \\ & .46E5 & & .17E7 \\ & & .46E5 & -.17E7 \\ & & & .24E8 \\ & & -.17E7 & .27E9 \\ & .17E7 & & .27E9 \end{bmatrix} \qquad Kb = \begin{bmatrix} 0 & & \\ & 0 & \\ & & 0 \end{bmatrix}$$

$$[C^a] = \begin{bmatrix} 0 & & & & \\ & .67E2 & & & \\ & & 0 & & \\ & & & .25E5 & \\ & & & & .13E6 \\ & & & & & .13E6 \end{bmatrix} \qquad [C^b] = \begin{bmatrix} 0 \end{bmatrix}$$

FIG. 7.7 contd.

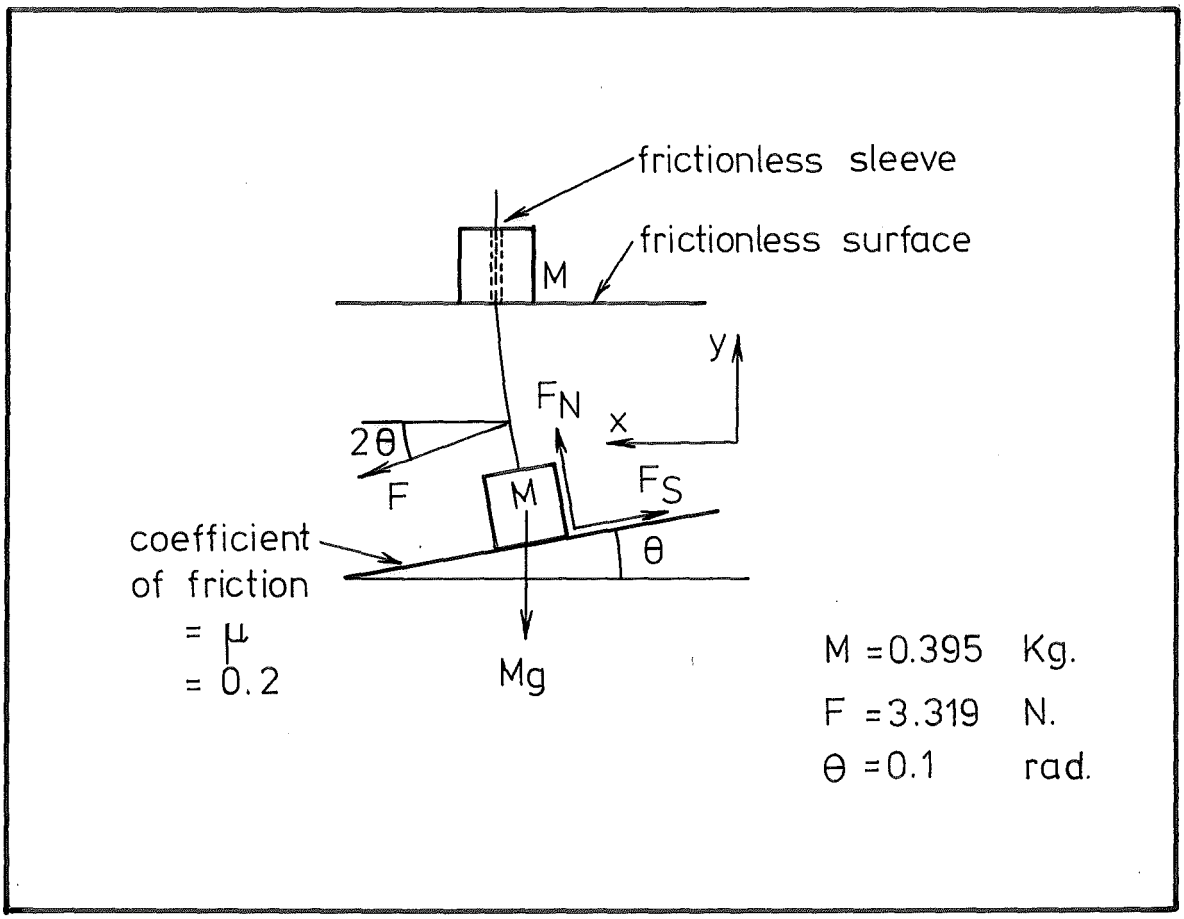

FIG. 7.8 MODEL OF SLIDING.

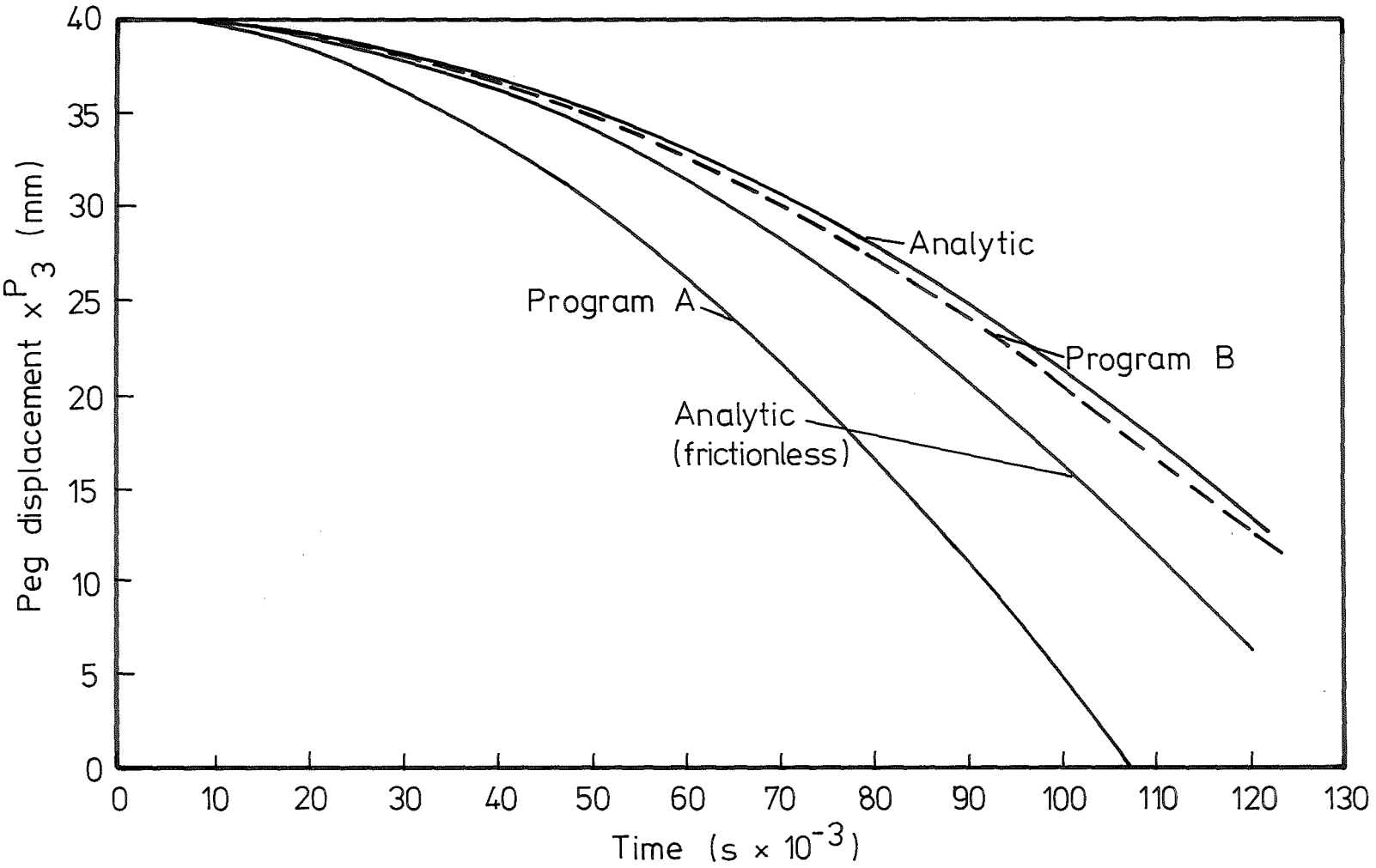

FIG. 7.9 SLIDING TEST DISPLACEMENT

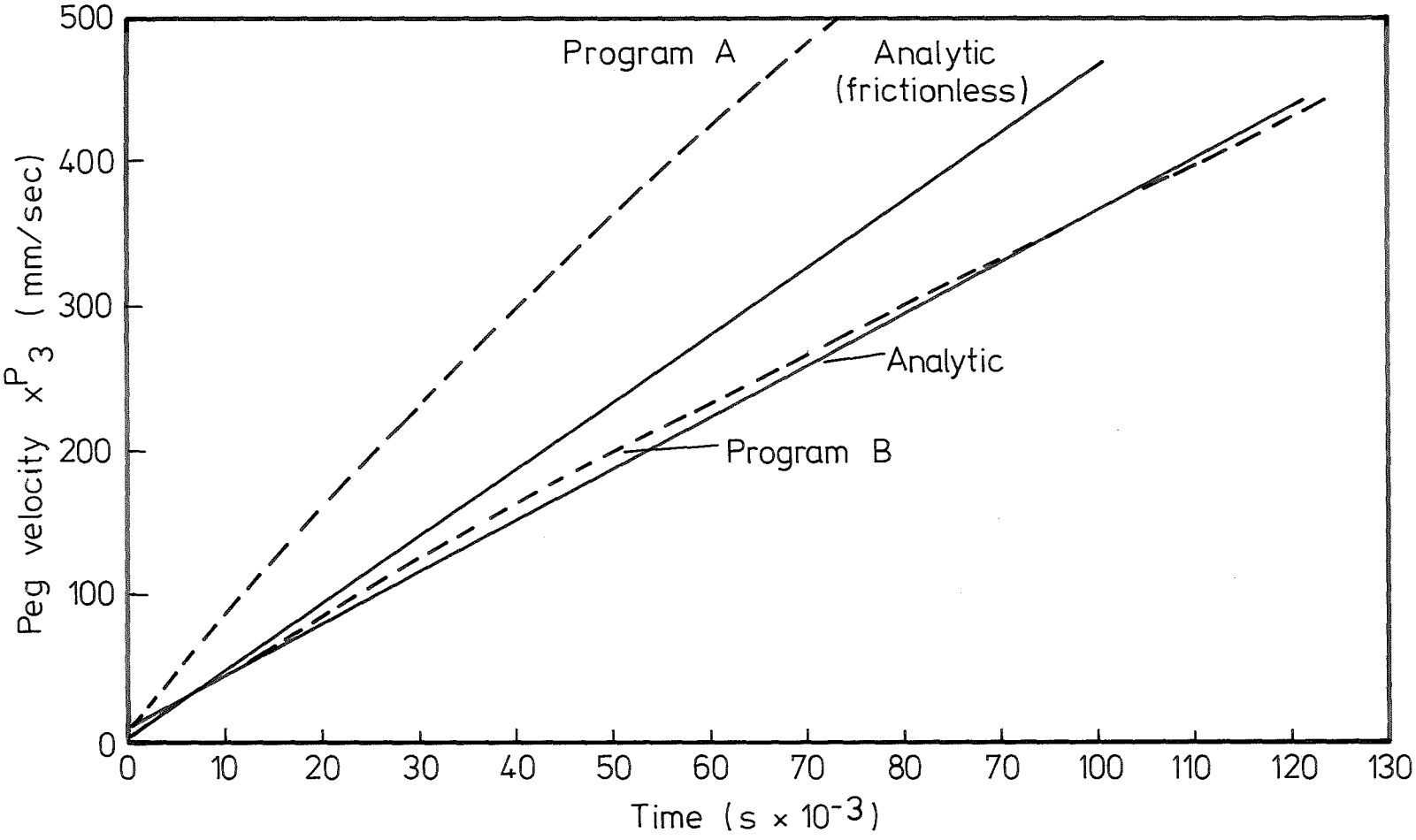

FIG. 7.10 VELOCITY

SLIDING TEST

It is obvious from the displacement and velocity graphs that Program B agrees closely with the analytical results.

Program A on the other hand reveals a marked tendency toward instability. The kinetic energy of the system toward the end of the run is approximately 3.5 times that predicted by the analytical solution and over twice that predicted by the analytical solution for the frictionless case. The latter fact rules out the possibility of the variation in kinetic energy being due to the bouncing of the peg in the program, the effect of this being the creation of near frictionless conditions.

7.3 SUMMARY

The result of the second test rules out the use of Program A. The results of both tests indicate Program B however to be sufficiently accurate for simulation work.

A listing of Program B appears in Appendix 1.

CHAPTER 8

SIMULATION RESULTS

In this chapter the effects of variations in system parameters on the behaviour of a typical system are examined using Program B.

8.1 SYSTEM PARAMETERS

Using the simulation program to indicate general trends in vibratory assembly requires a large number of computer runs and is therefore expensive. Hence the study of vibratory assembly techniques is centralized around the fairly typical arrangement shown in Fig. 8.1, with a view to indicating the effect of important parameters such as coupling stiffness and damping, exciting force magnitude, and contact force on the second stage of assembly as defined in Sec. 3.1. The movement of the peg's centre of mass and changes in the orientation of the peg are of interest.

8.2 COUPLING STIFFNESS

An important characteristic of any assembly system is the stiffness of the coupling connecting the peg and the carrier. We will therefore, firstly, simulate systems with high, intermediate, and low stiffnesses in this coupling.

It is assumed that there is a relatively low interaction between the translational and rotational displacements of the coupling. In this case the off-diagonal stiffness elements are related to the diagonal rotational and translational elements by the relationship

$$K_{ij} = \pm .5 \sqrt{(K_{ii} \times K_{jj})}$$

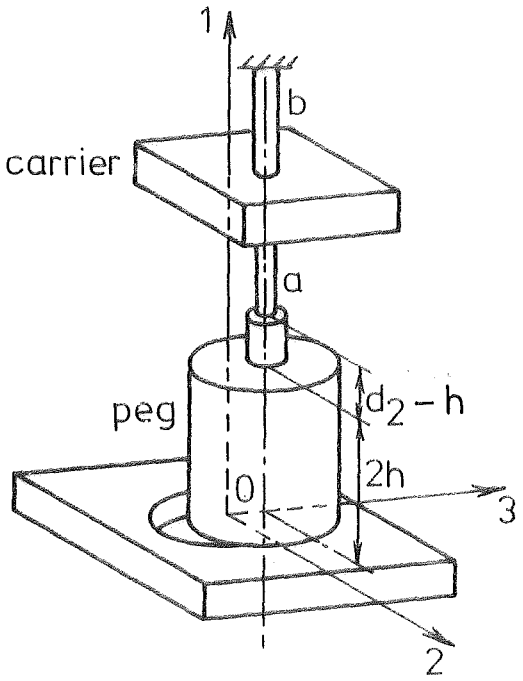

FIG 8.1 SYSTEM PARAMETERS

$d_1 = 56$ mm

$d_2 = 50$ mm

$h = 30$ mm

$r_p = 25$ mm

$r_h = 25$ mm

$\mu_{SL} = .3$

$\mu_{ST} = .35$

$M^c = .396$ Kg

$I^c = 1000$ Kg-mm^2

$M^p = .395$ Kg

$$I^p = \begin{bmatrix} .25E3 & & \\ & .25E3 & \\ & & .10E3 \end{bmatrix}$$

Single Point Contact

x_1^p	= 34.85	$\dot{x}_1^p$	= 0	x_1^e	= 0	
x_2^p	= -.25	$\dot{x}_2^p$	= 0			
x_3^p	= 40.0	$\dot{x}_3^p$	= 0			
ϕ	= .1	$\dot{\phi}$	= 0	θ_3^e	= .1	
θ	= 1.771	$\dot{\theta}$	= 0	θ_2^e	= 1.771	
ψ	= 0	$\dot{\psi}$	= 0			
x_2^c	= 46.0	$\dot{x}_2^c$	= 0	x_2^e	= 46	
x_3^c	= 30.07	$\dot{x}_3^c$	= 0	x_3^e	= 30.07	
γ	= 0	$\dot{\gamma}$	= 0	θ_1^e	= 0	

Double Point Contact

x_1^p	= 34.02	$\dot{x}_1^p$	= 0	x_1^e	= 0	
x_2^p	= 0	$\dot{x}_2^p$	= 0			
x_3^p	= 40.0	$\dot{x}_3^p$	= 0			
ϕ	= 0	$\dot{\phi}$	= 0	θ_3^e	= 0	
θ	= 1.771	$\dot{\theta}$	= 0	θ_2^e	= 1.771	
ψ	= 0	$\dot{\psi}$	= 0			
x_2^c	= 0	$\dot{x}_2^c$	= 0	x_2^e	= 0	
x_3^c	= 30.07	$\dot{x}_3^c$	= 0	x_2^e	= 30.07	
γ	= 0	$\dot{\gamma}$	= 0			

By comparison, in a uniform beam the relationship is

$$K_{ij} = \pm .866 \sqrt{(K_{ii} \times K_{jj})}$$

The stiffness matrix for the coupling is shown in Fig. 8.2 together with other relevant parameters. Damping is assumed to be negligible and the carrier is unconstrained.

8.2.1 Results

The behaviour of the assembly system under different coupling stiffnesses and in single and double point contact modes is shown in Fig's 8.3 to 8.6. The main trends are summarized below.

(i) Generally comparing the graphs for single point contact with those describing the peg movement in two point contact the greater freedom of the peg in the former case is evident.

(ii) In all cases the peg tends to lean back under the influence of the edge-edge contact force. Fig's 8.4b and 8.6b clearly show the change in the orientation of the peg.

(iii) In single point contact, and to a lesser extent in two point contact, a slight rotation of the peg about the vertical axis and toward the hole occurs.

(iv) There appears to be little difference between the behaviour of the system under intermediate or high stiffness constraints.

(v) Peg edge-hole plane contact occurred in the intermediate and low stiffness systems in single point contact. This situation is outside the bounds of the present program.

FIG. 8.2 COUPLING STIFFNESS $[K^a]$ MATRICE's

$$\begin{bmatrix} 1E2 & & \\ & 5E2 & 1.58E3 \\ & 5E2 & 1.58E3 \\ & 5E5 & \\ 1.58E3 & & 5E5 \\ 1.58E3 & & 5E5 \end{bmatrix}$$

Low Stiffness

$$\begin{bmatrix} 1E2 & & \\ & 5E3 & 1.58E4 \\ & 5E3 & 1.58E4 \\ & 5E3 & \\ 1.58E4 & & 5E6 \\ 1.58E4 & & 5E6 \end{bmatrix}$$

Medium Stiffness

$$\begin{bmatrix} 1E2 & & \\ & 5E4 & 1.58E5 \\ & 5E4 & 1.58E5 \\ & 5E7 & \\ 1.58E5 & & 5E7 \\ 1.58E5 & & 5E7 \end{bmatrix}$$

High Stiffness

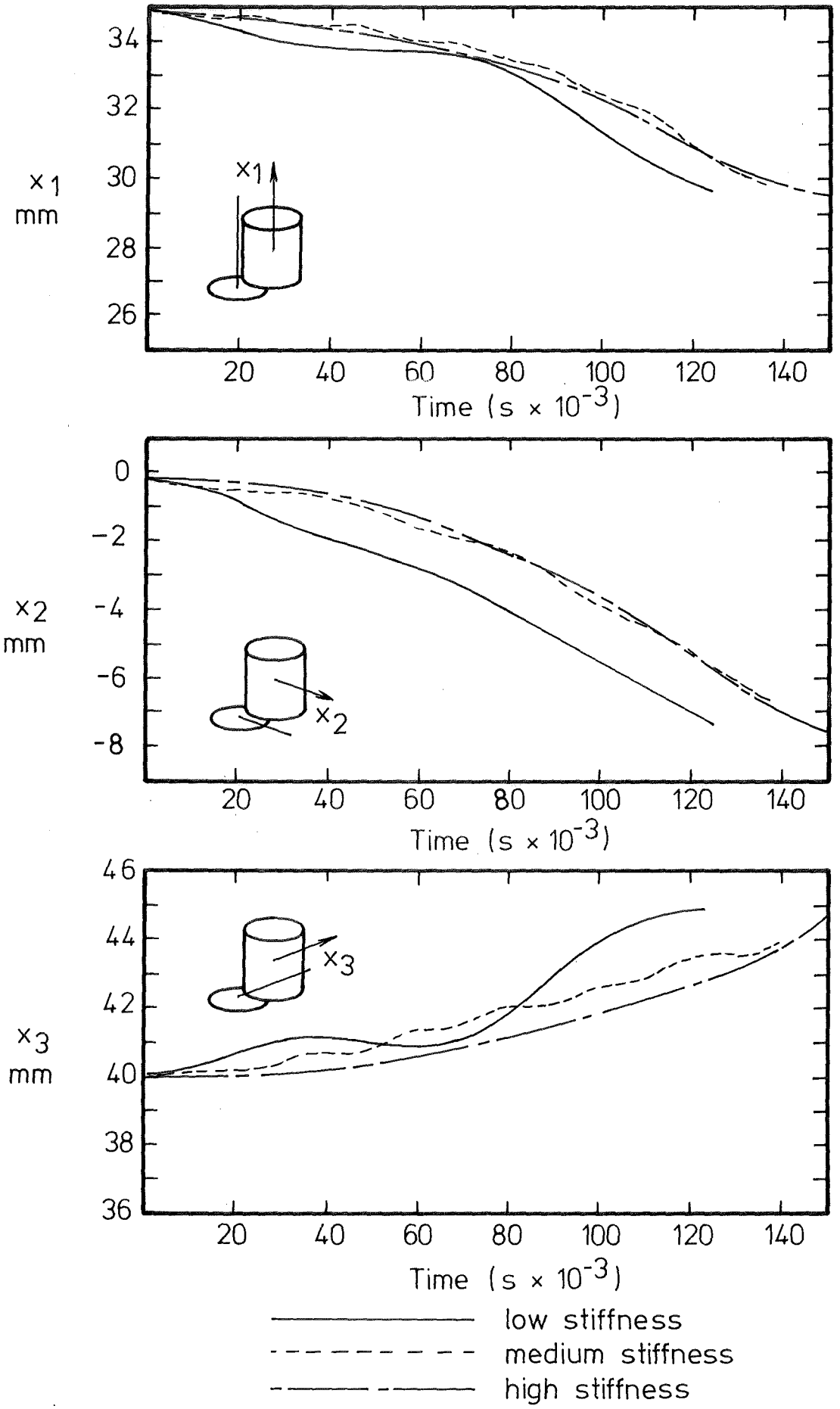

FIG. 8.3 VARIATION OF COUPLING STIFFNESSES. SINGLE POINT CONTACT.

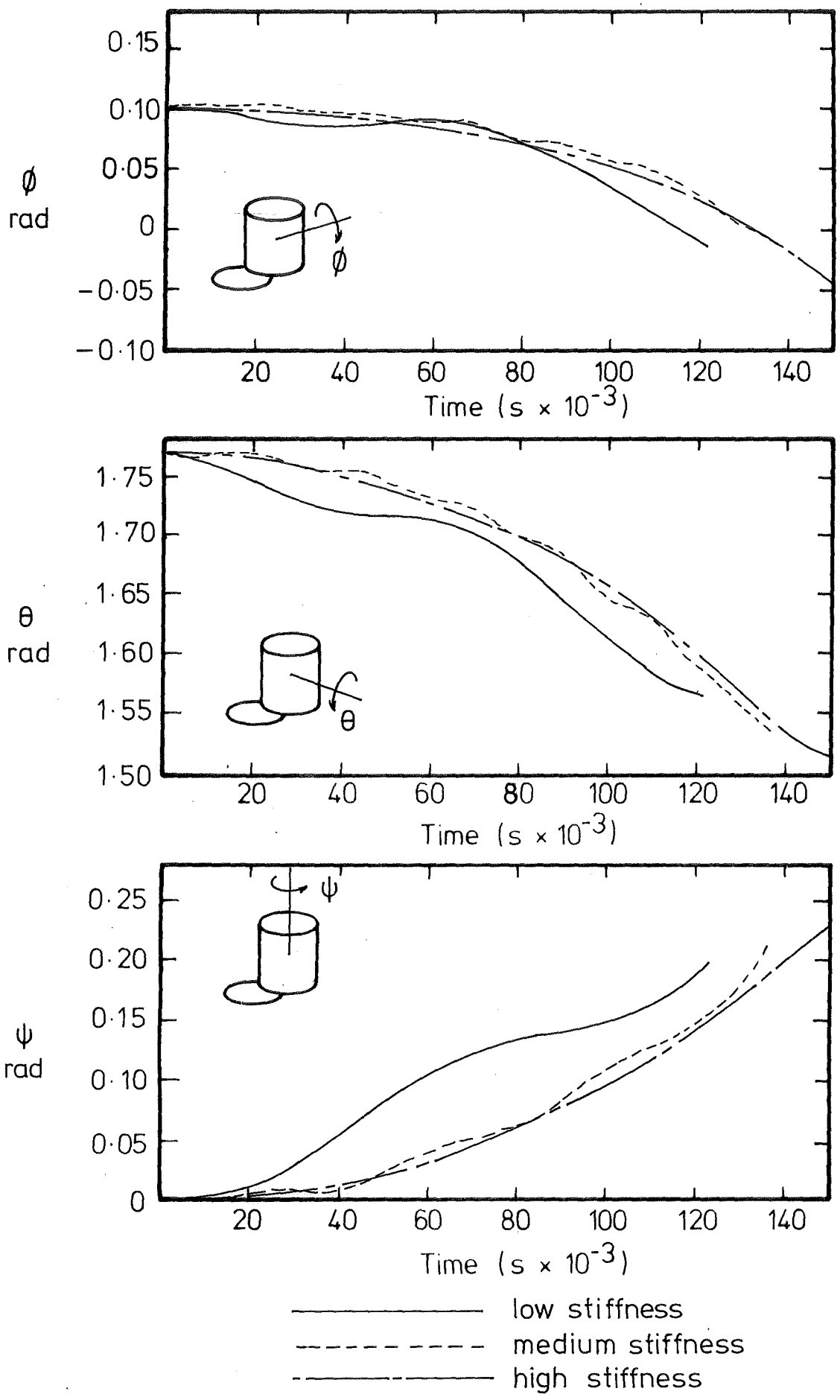

FIG. 8.4 VARIATION OF COUPLING STIFFNESSES. SINGLE POINT CONTACT.

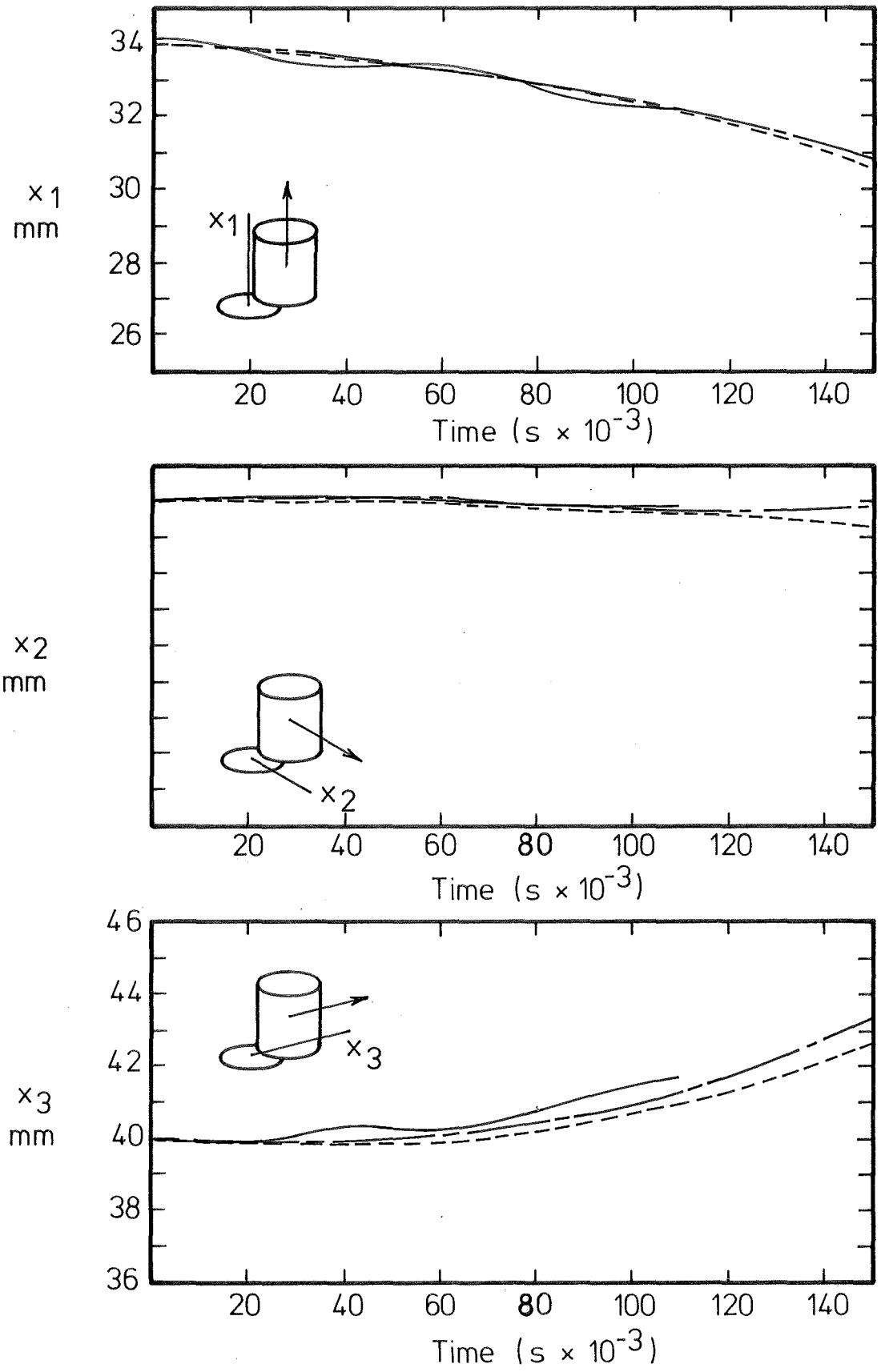

FIG 8.5 VARIATION OF COUPLING STIFFNESSES DOUBLE POINT CONTACT.

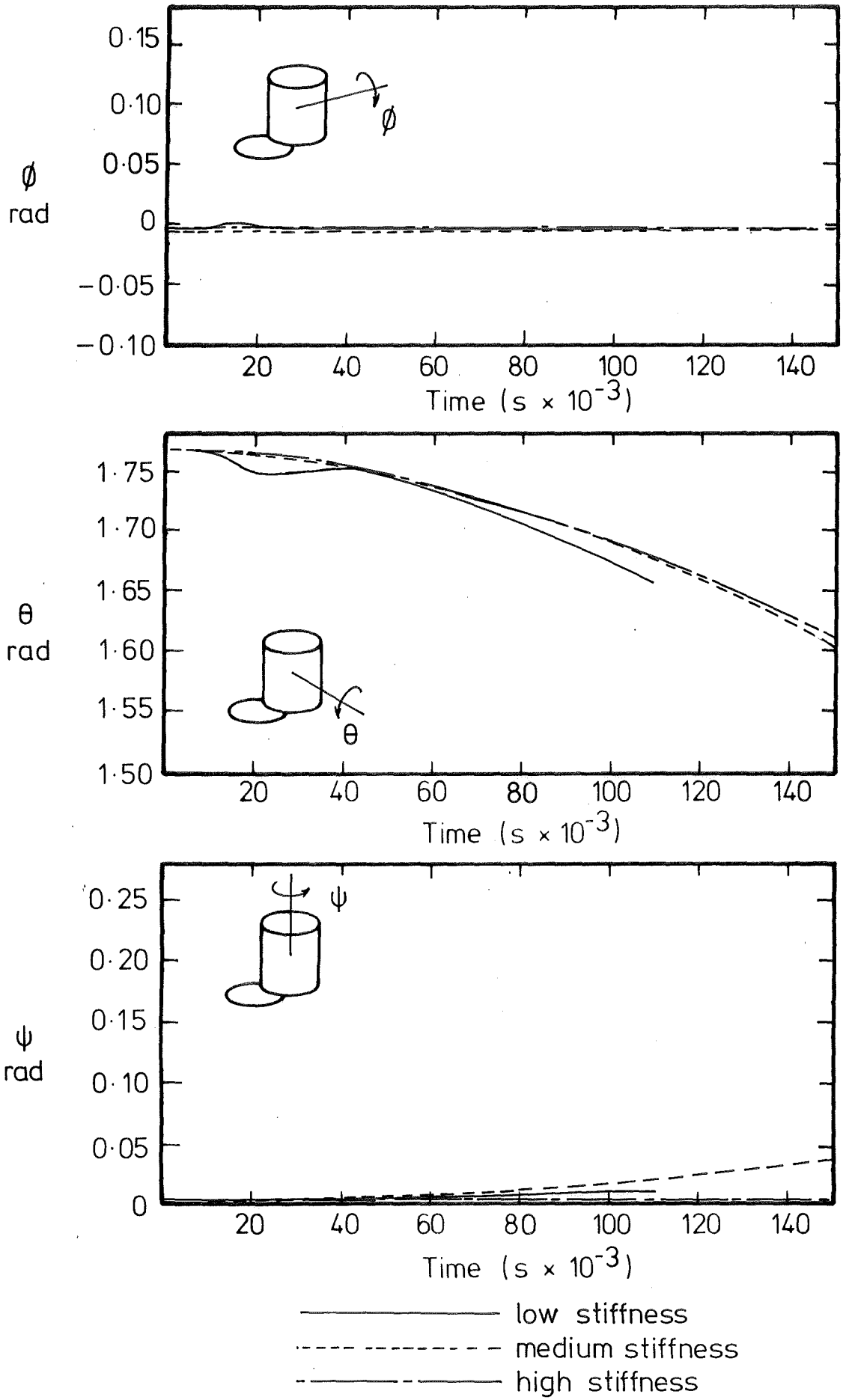

FIG.8.6 VARIATION OF COUPLING STIFFNESSES. DOUBLE POINT CONTACT.

8.3 COUPLING DAMPING

In reality some form of damping will exist in all assembly systems. An important effect of this is that the amplitude of vibrations is limited when the exciting frequency approaches a natural frequency of the system. Adequate separation of exciting and natural frequencies is difficult in the type of system considered, as the natural frequencies are dependent upon the kinematic constraints introduced by contact as well as by the contact forces.

The high stiffness system described in the previous section was operated under conditions of medium and high damping.

The damping coefficients used are shown in Fig. 8.7 and were related to their associated inertia's and stiffnesses by the expression.

$C = 0\ \sqrt{(\text{Inertia} \times \text{Stiffness})/10}$

$C = 0\ \sqrt{(\text{Inertia} \times \text{Stiffness})}$

where 0 denotes "the order of".

8.3.1 Results

The results of the simulations are shown in Fig's 8.8 to 8.14.

(i) In single point contact an increase in damping appears to be beneficial in so far as assembly is concerned. Fig. 8.10a in particular showing a marked movement of the peg toward the hole in the highly damped case. The locus of the peg in the x_2 x_3 plane is shown in Fig. 8.10 this indicates rotation about the vertical axis through the contact point as the principal mechanism of assembly.

(ii) In two point contact the peg movement is more restrained however the same trends as in single point contact emerge, i.e. increased damping promotes assembly by rotation about a single contact point.

FIG. 8.7 COUPLING DAMPING $[C^a]$ MATRICES'

$$\begin{bmatrix} 0 & & & & \\ & 2.8E1 & & & \\ & & 2.8E1 & & \\ & & & 1.5E4 & \\ & & & & 1.5E4 \\ & & & & & 1.5E4 \end{bmatrix}$$

Medium Damping

$$\begin{bmatrix} 0 & & & & \\ & 2.8E2 & & & \\ & & 2.8E2 & & \\ & & & 1.5E5 & \\ & & & & 1.5E5 \\ & & & & & 1.5E5 \end{bmatrix}$$

High Damping

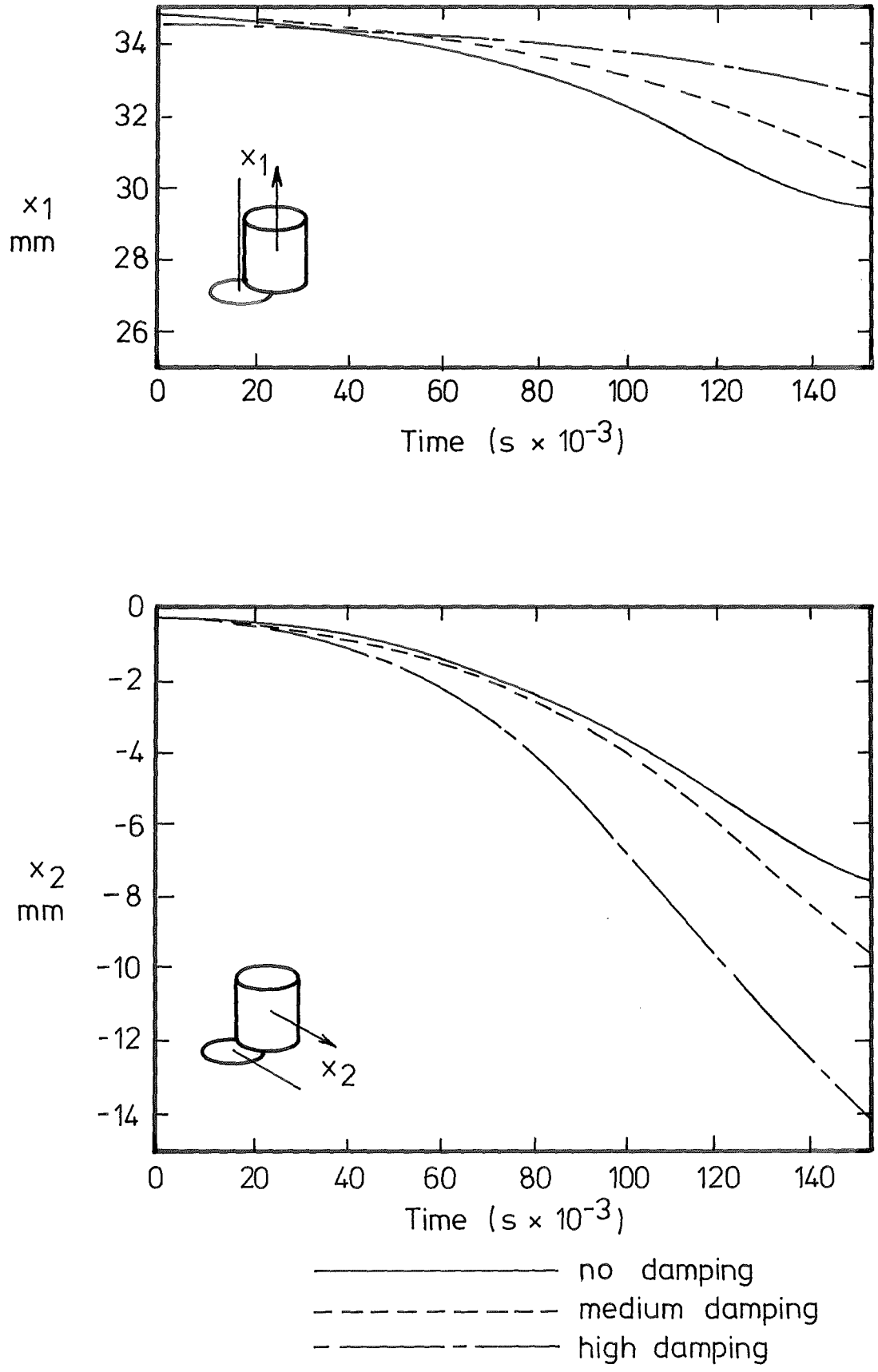

FIG. 8.8 VARIATION OF COUPLING DAMPING. SINGLE POINT CONTACT.

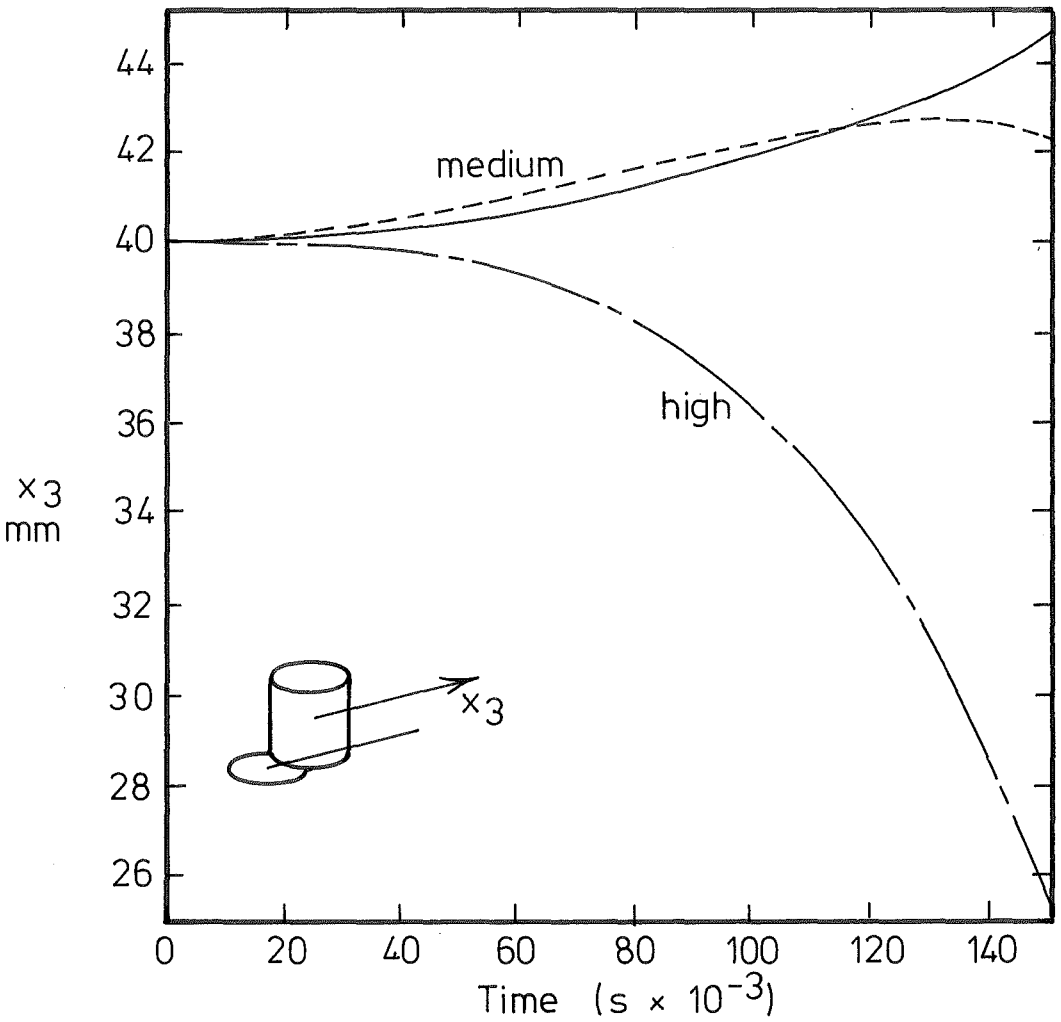

FIG. 8.9 VARIATION OF COUPLING DAMPING. SINGLE POINT CONTACT.

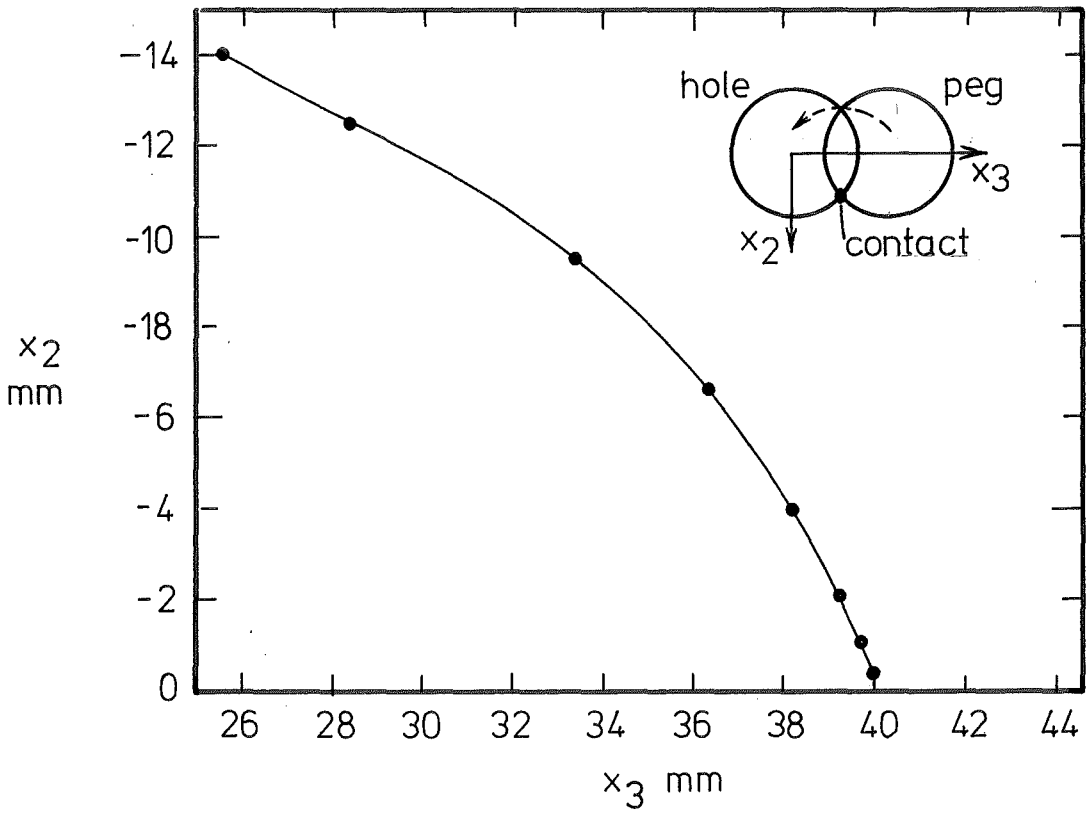

FIG. 8.10 LOCUS OF PEG CENTRE OF MASS IN x_2, x_3 PLANE HIGH DAMPING.

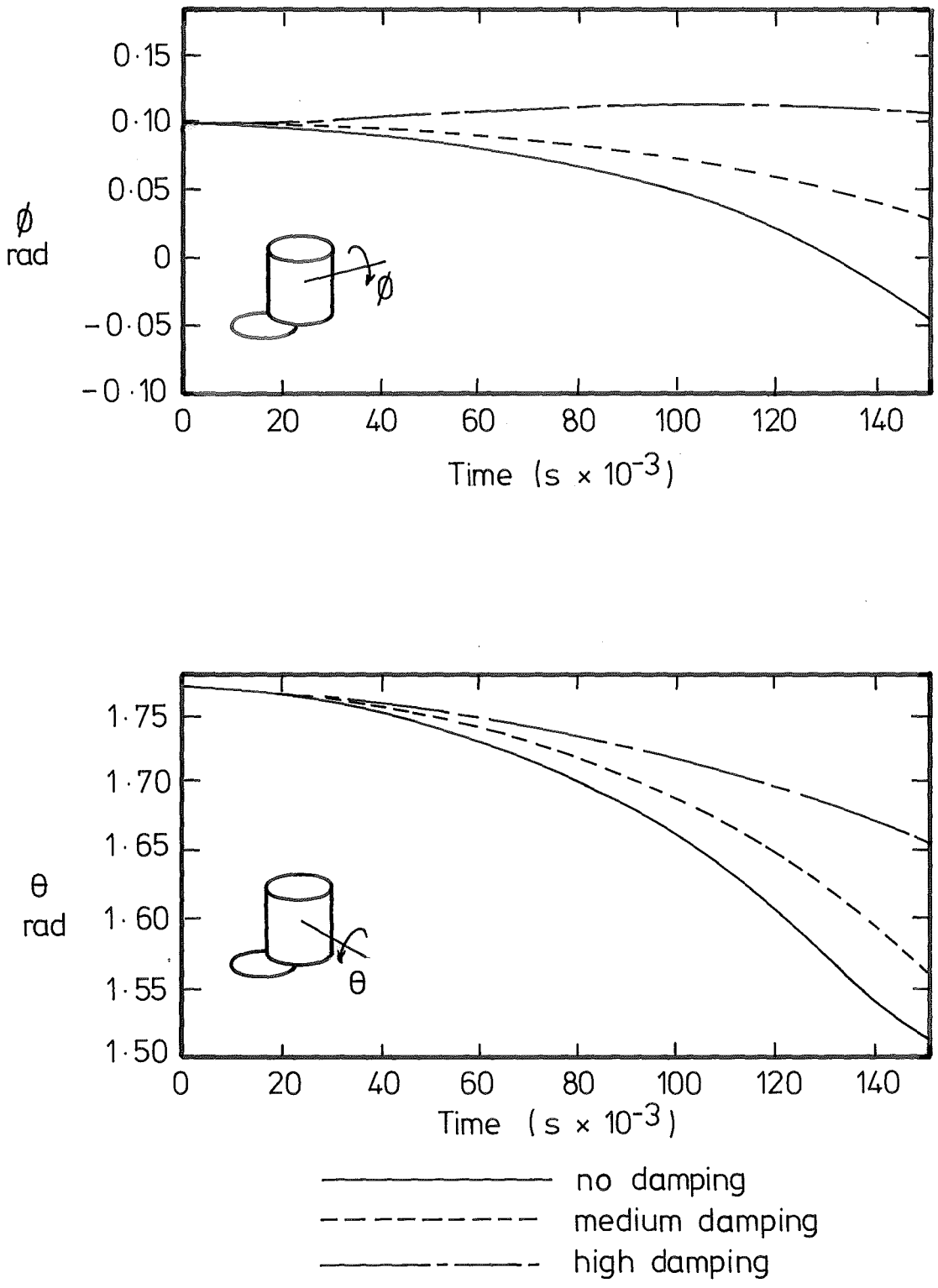

FIG. 8.11 VARIATION OF COUPLING DAMPING. SINGLE POINT CONTACT

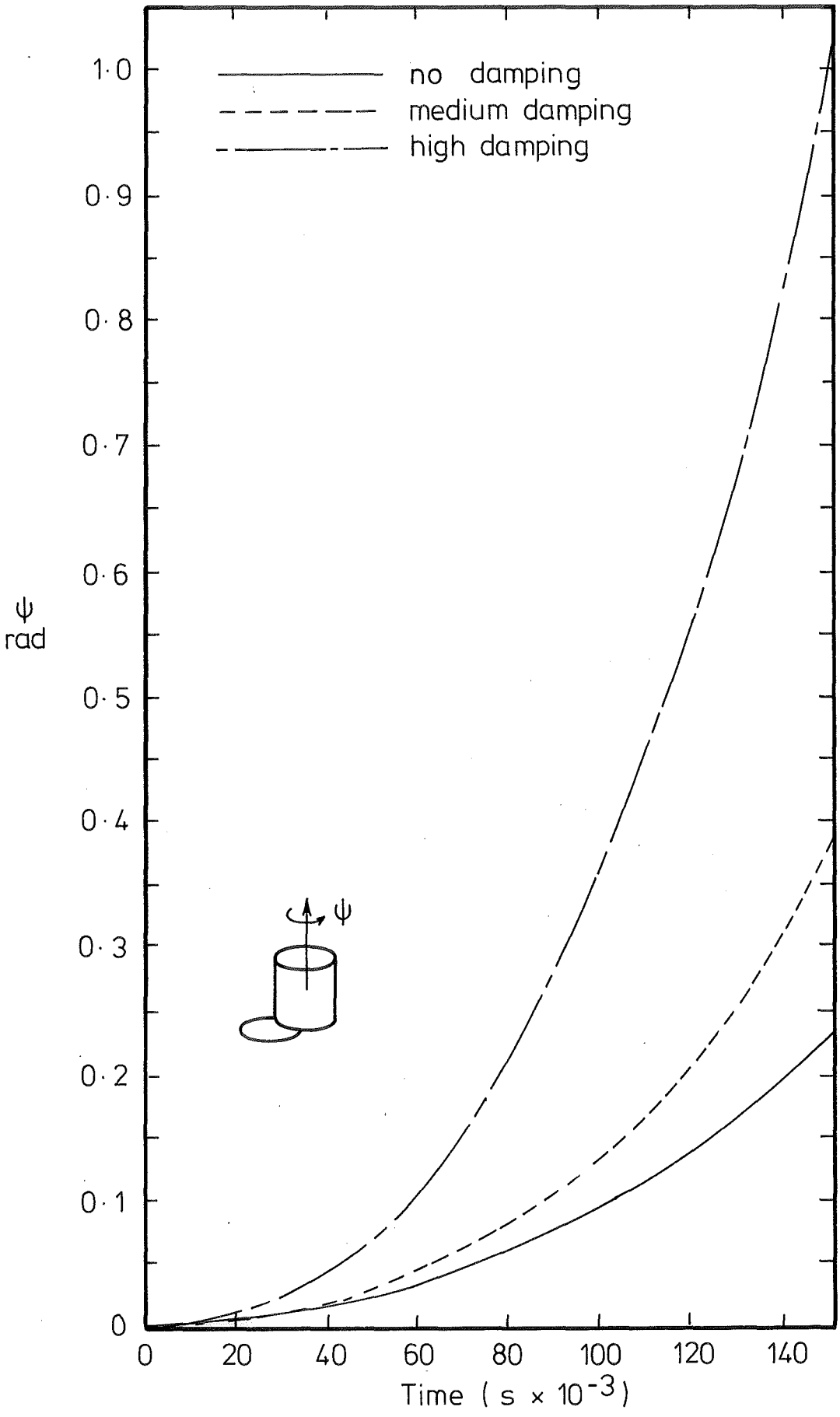

FIG. 8.12 VARIATION OF COUPLING DAMPING. SINGLE POINT CONTACT.

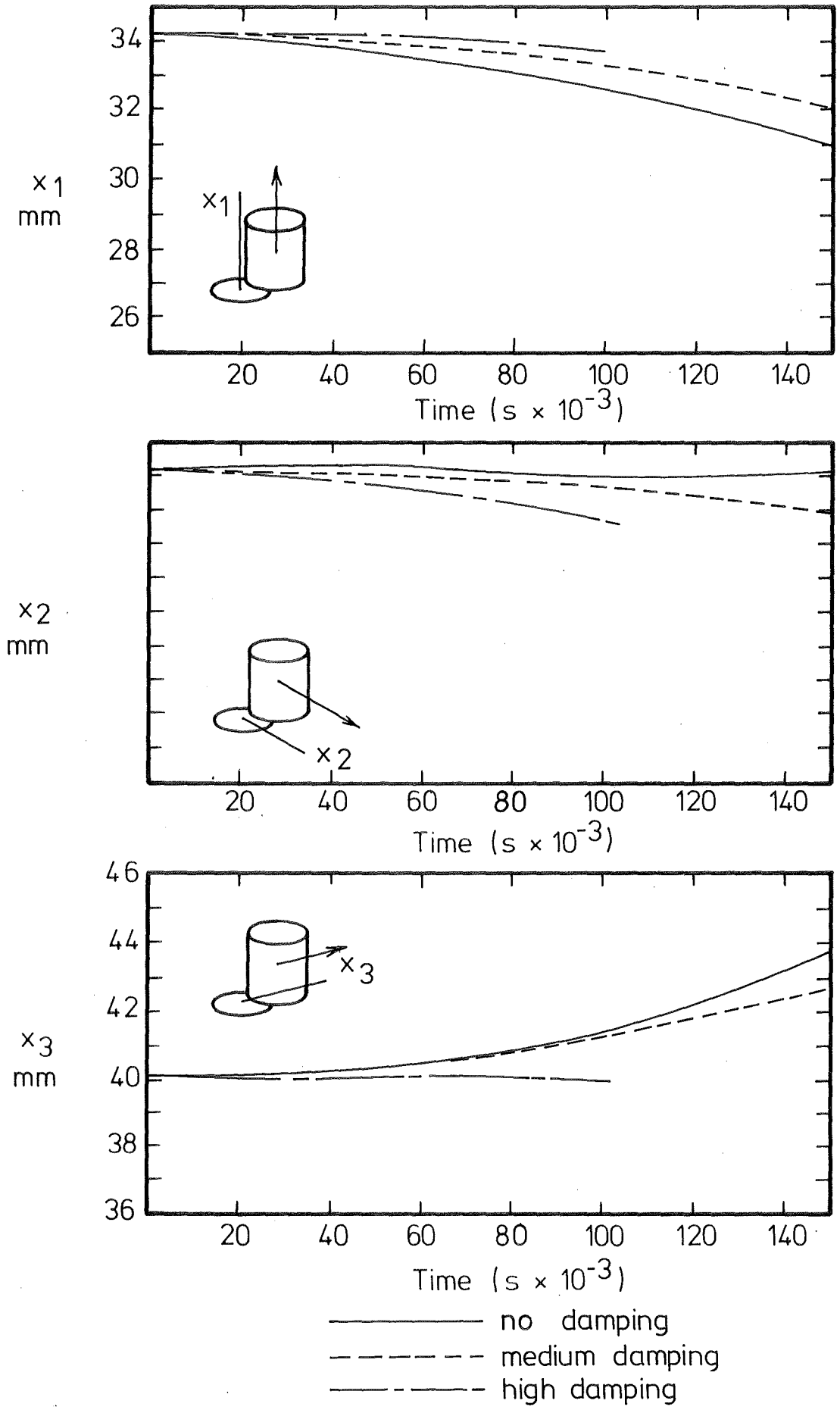

FIG 8.13 VARIATION OF COUPLING DAMPING. DOUBLE POINT CONTACT.

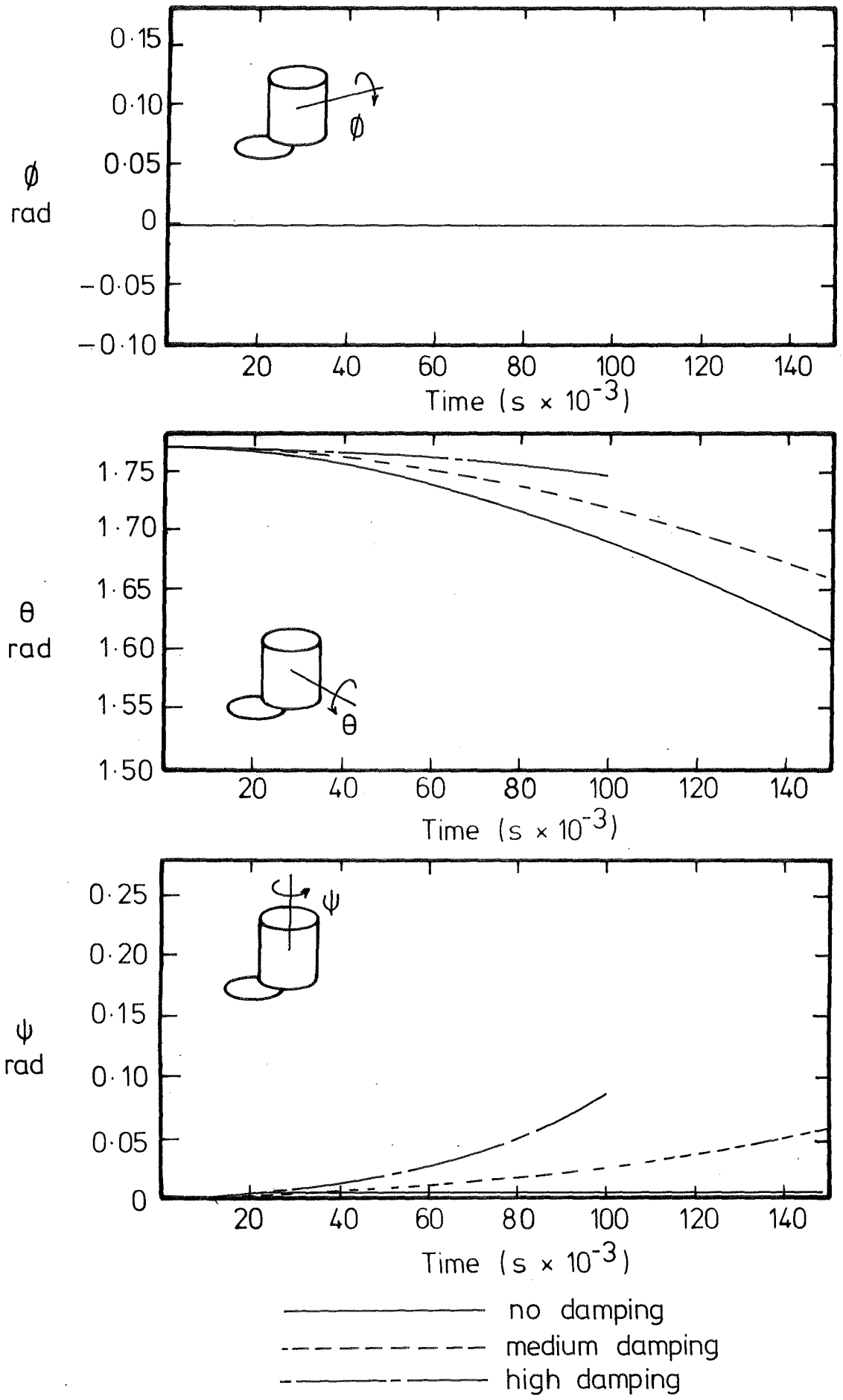

FIG. 8.14 VARIATION OF COUPLING DAMPING. DOUBLE POINT CONTACT.

8.4 EXCITING FORCE MAGNITUDE

An assembly system having high stiffness and medium damping was operated under a range of exciting forces varying from .3 to 10 N.

8.4.1 Results

(i) In single point contact Fig. 8.16 and 8.18 show again the tendency for assembly to occur by rotation about a single contact point. An increase in the exciting force magnitude causes the assembly to be more rapid.

(ii) Two point contact shows again the same behaviour as single point contact.

8.5 CONTACT FORCE

An assembly system having high stiffness and high damping characteristics and subjected to an exciting force of 10 N was simulated. Both high and low axial loads were applied to the peg in an effort to determine the role of sliding.

8.5.1 Results

Simulation was performed for .22 seconds rather than the .15 seconds employed previously.

(i) The Fig's 8.20 and 8.22 show that assembly toward the hole under these conditions is rapid and appears to be independent of either the initial misalignment or the contact force. Assembly seems to be predominantly due to rotation about a single contact point with sliding playing a minor role.

(ii) From Fig. 8.21, it can be seen that the orientation of the peg with respect to the hole plane remains approximately constant. Obviously

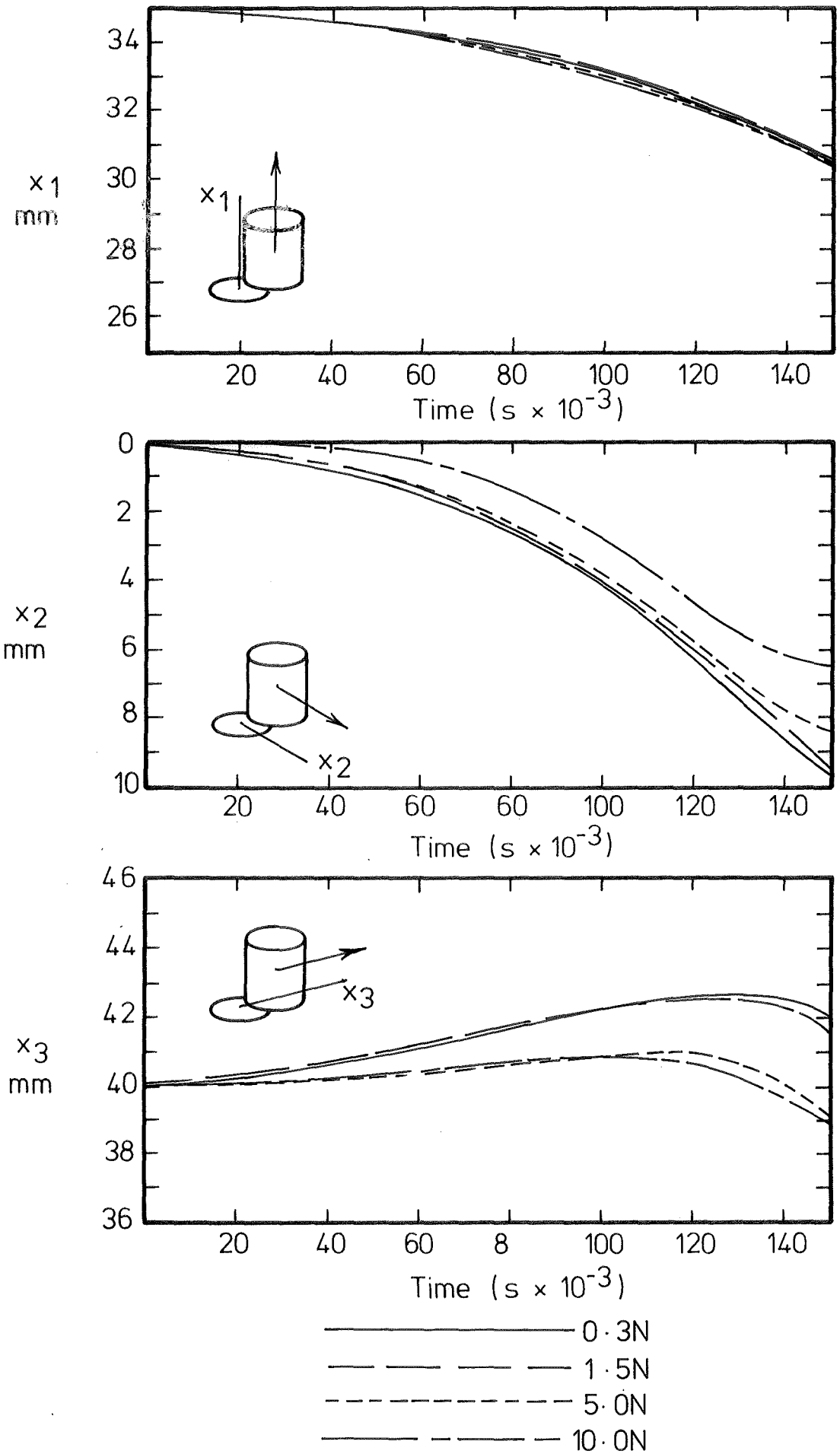

FIG. 8.15 VARIATION OF EXCITING FORCE MAGNITUDE. SINGLE POINT CONTACT.

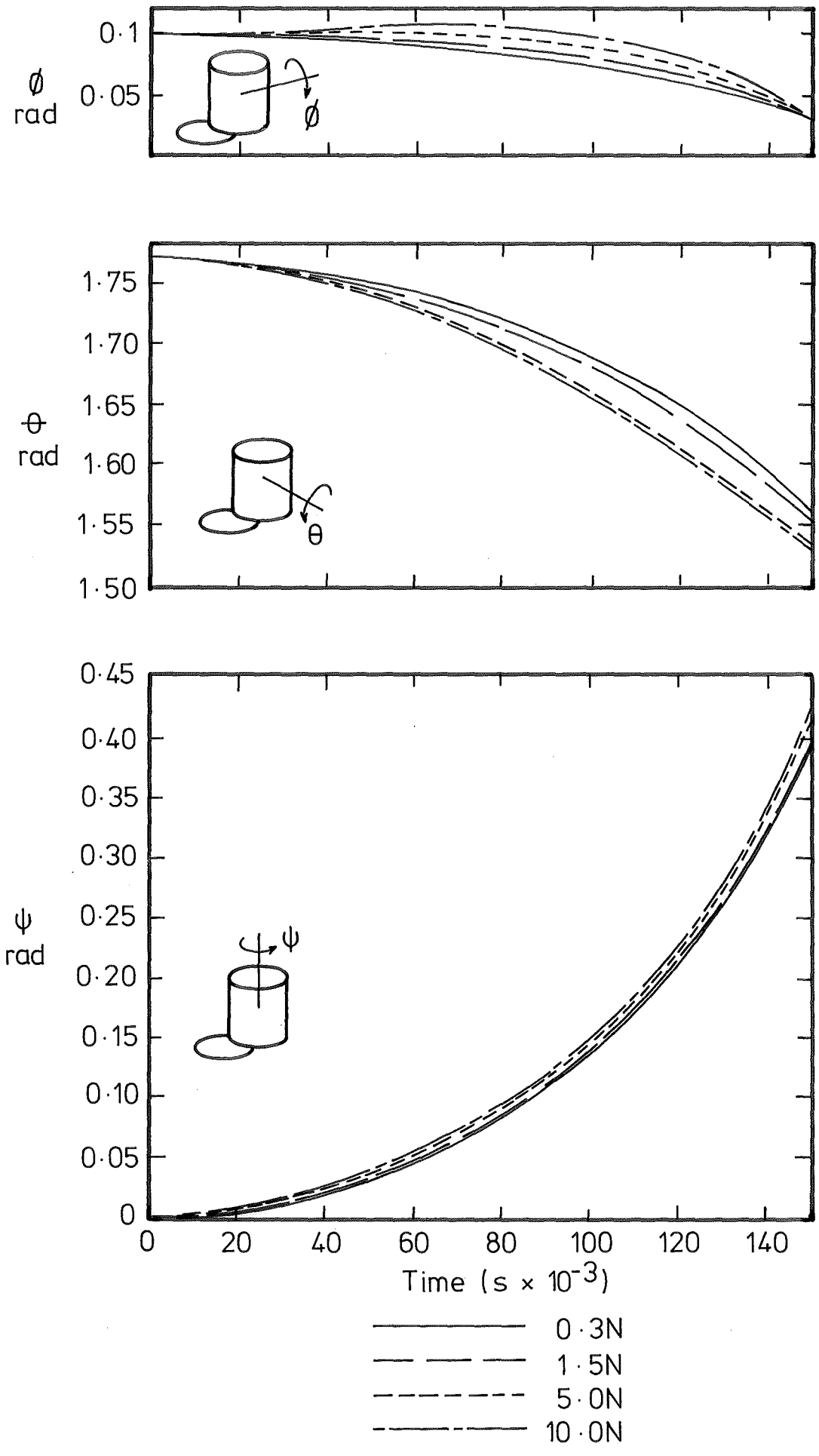

FIG. 8.16 VARIATION OF EXCITING FORCE MAGNITUDE SINGLE POINT CONTACT.

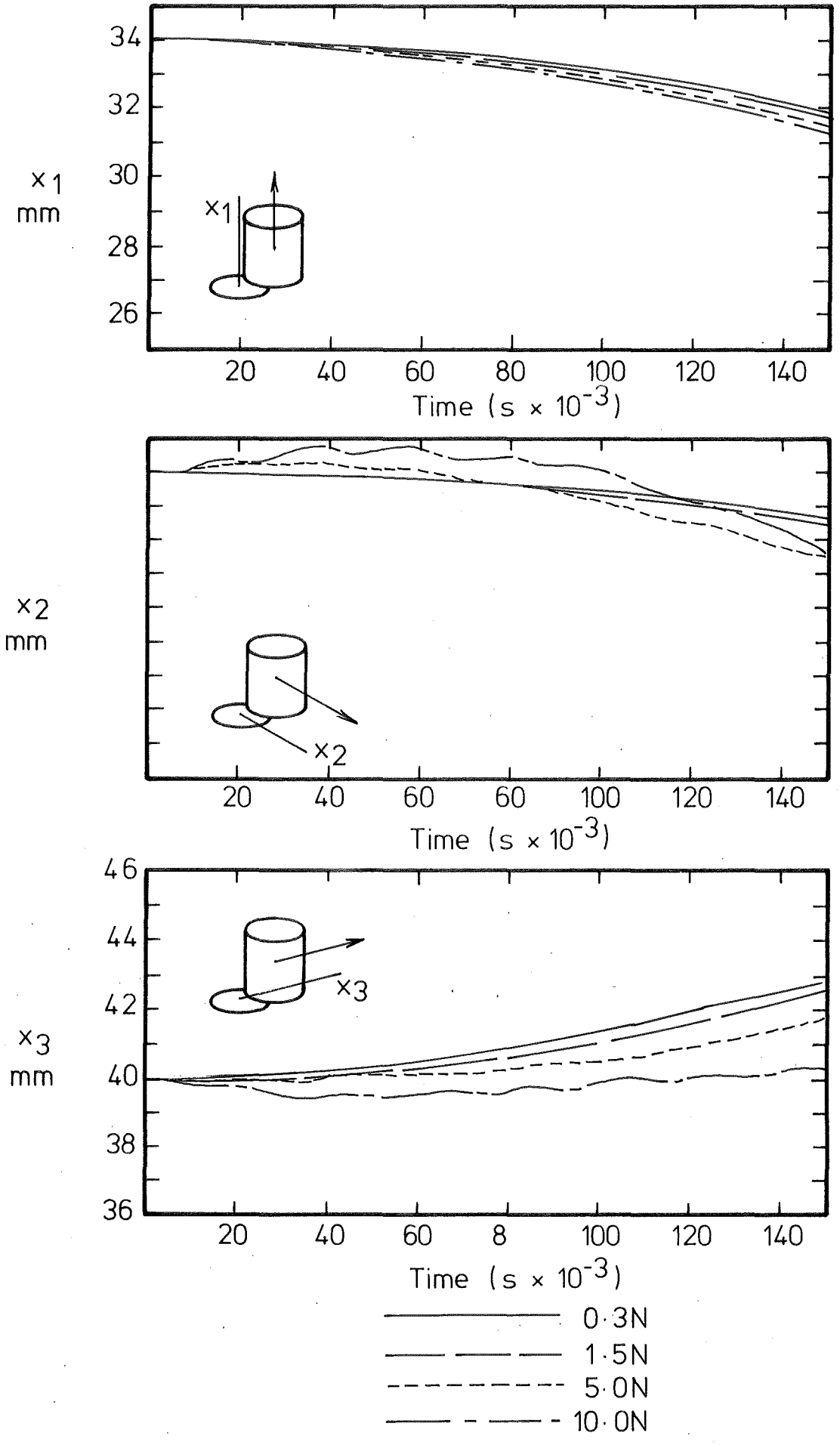

FIG. 8.17 VARIATION OF MAGNITUDE OF EXCITING FORCE. DOUBLE POINT CONTACT.

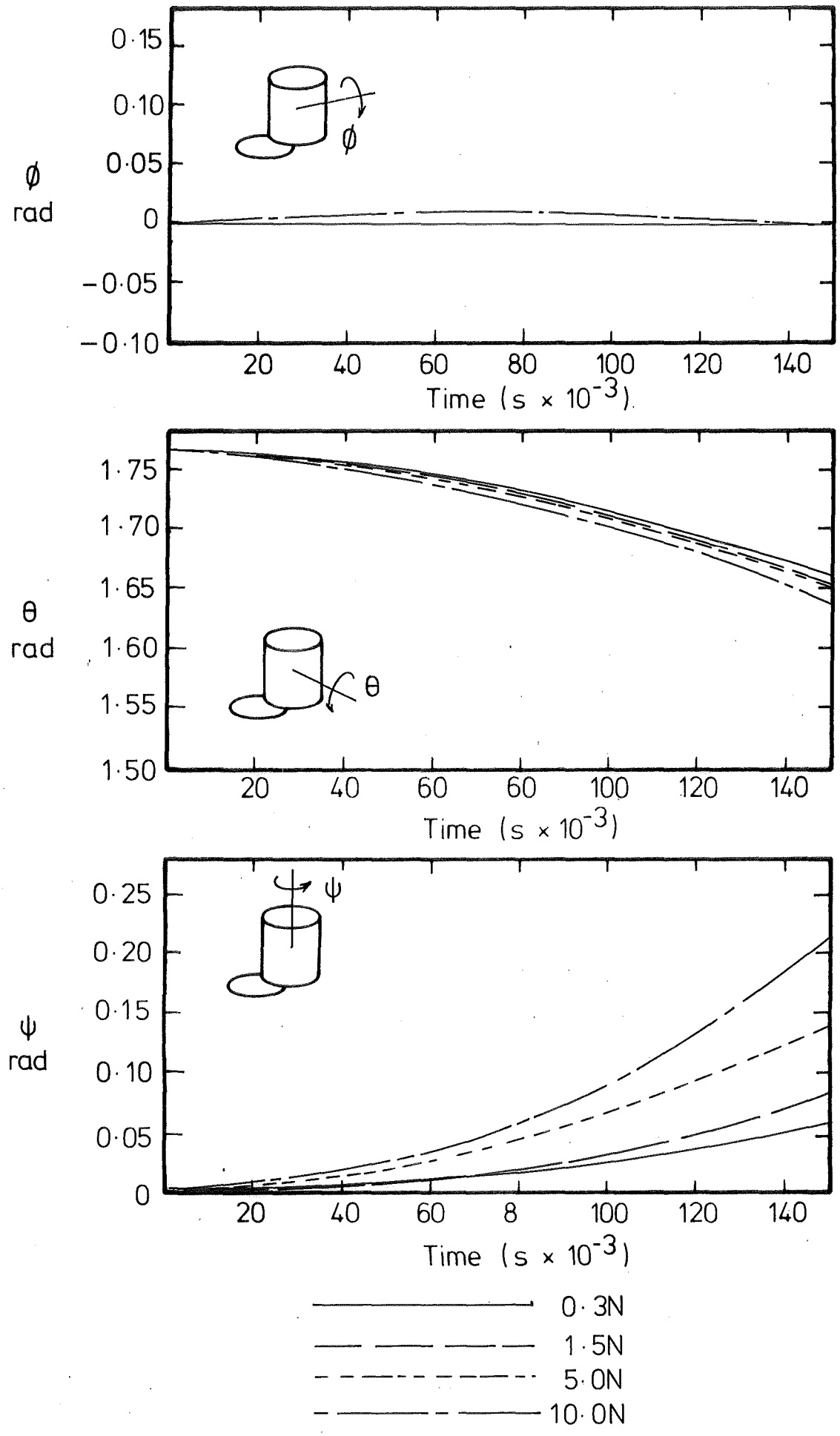

FIG. 8.18 VARIATION OF EXCITING FORCE MAGNITUDE. DOUBLE POINT CONTACT.

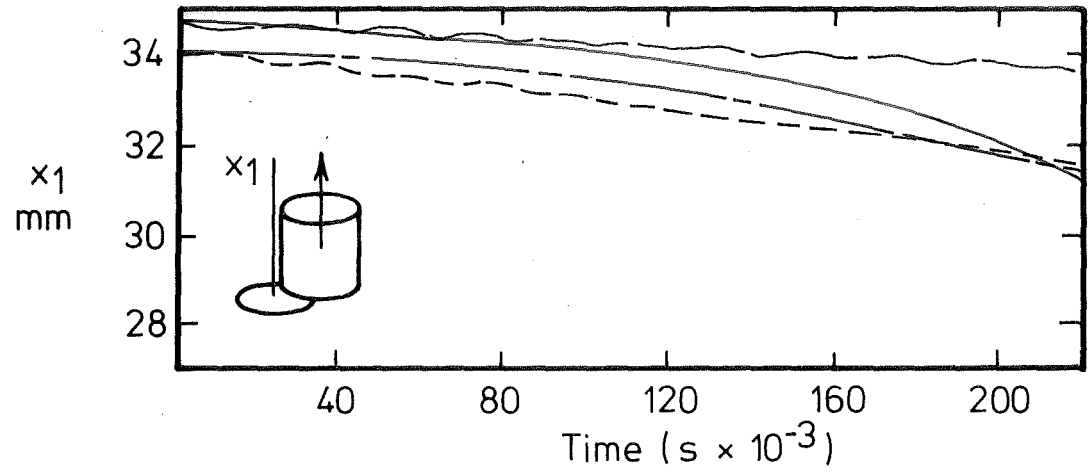

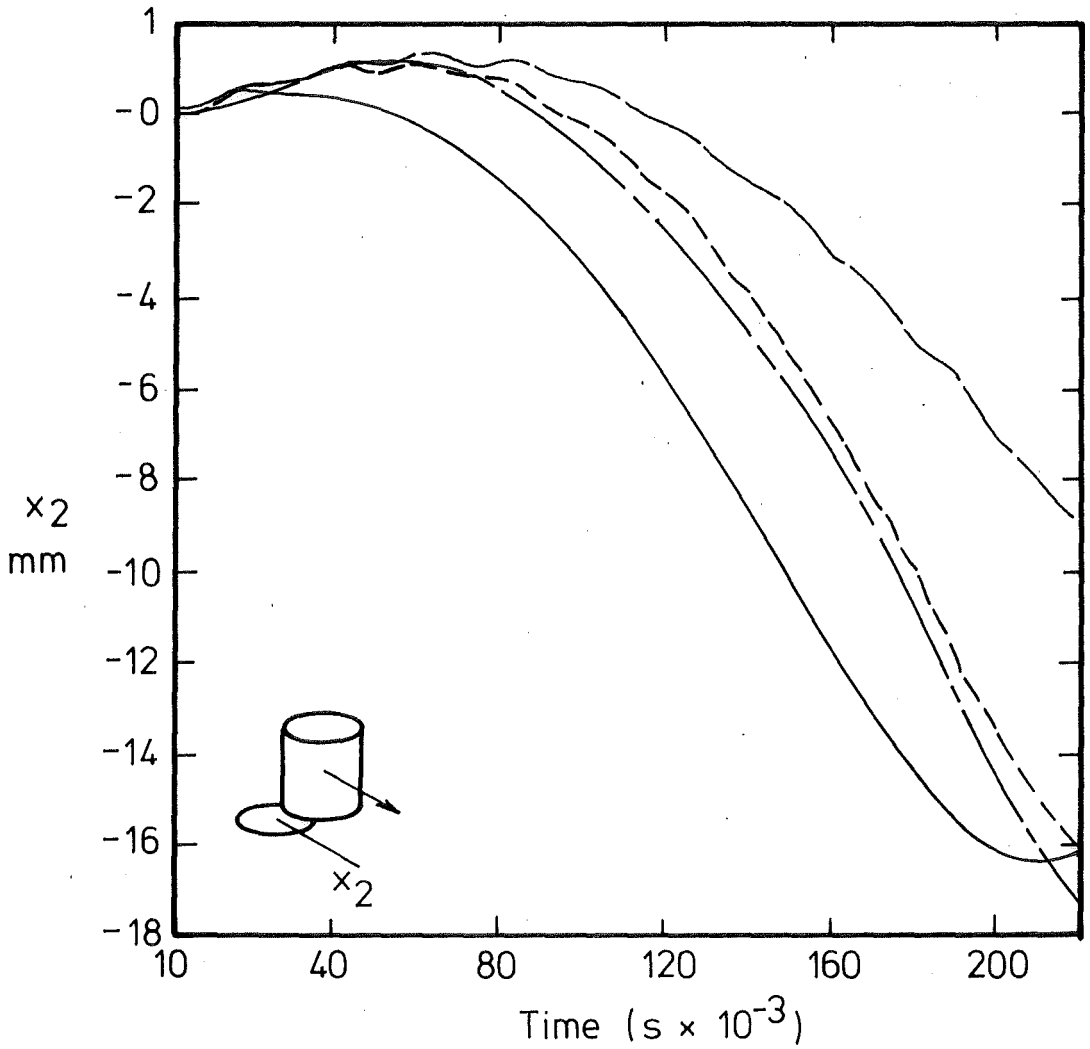

——————— High contact force 1pt. contact
— — — — — — " " " 2pt. "
— — — — — — Low contact force 1pt. contact
— — — — — — — " " " 2pt. "

FIG. 8.19 VARIATION OF CONTACT FORCE MAGNITUDE.

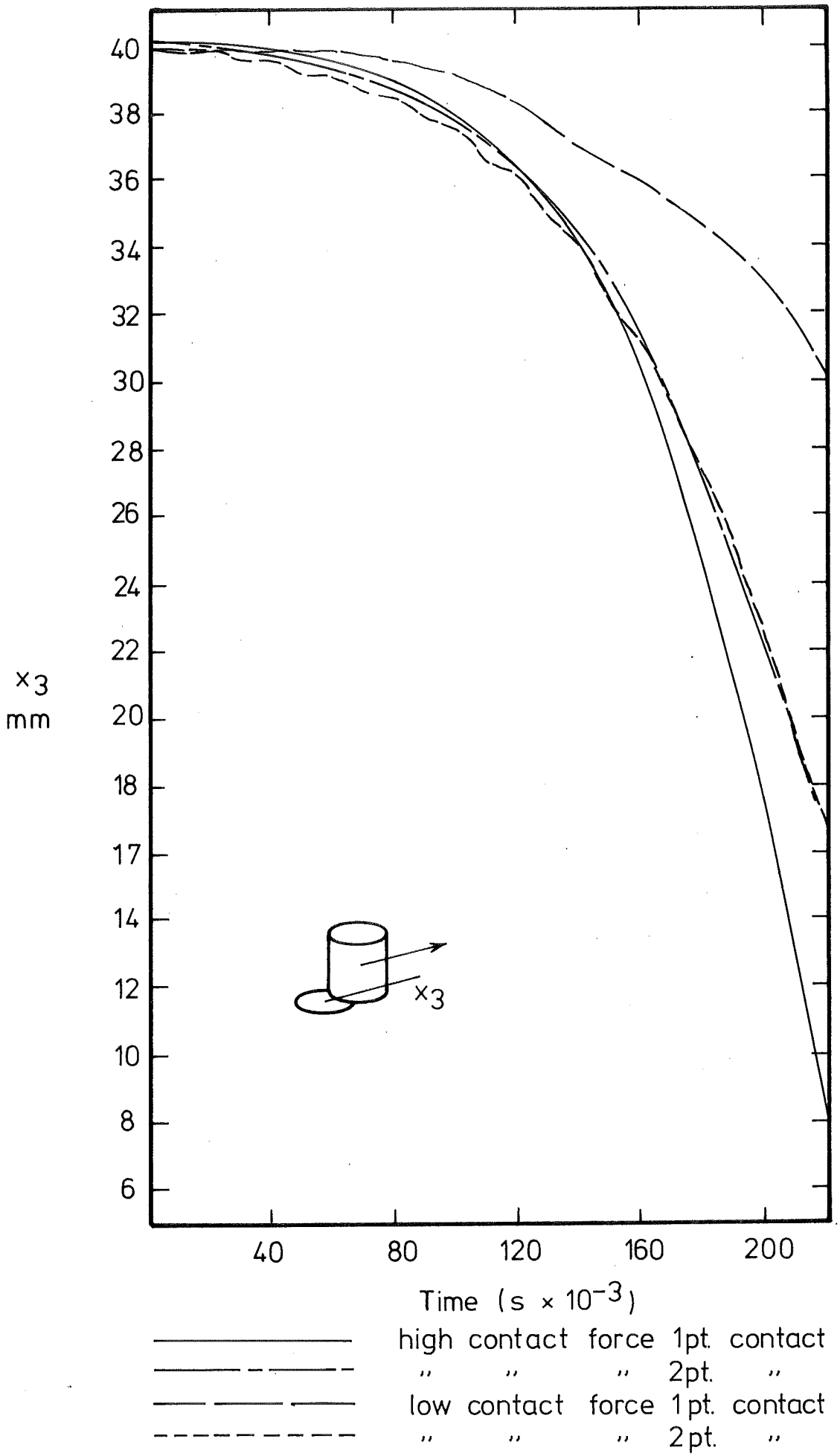

FIG. 8.20 VARIATION OF CONTACT FORCE MAGNITUDE.

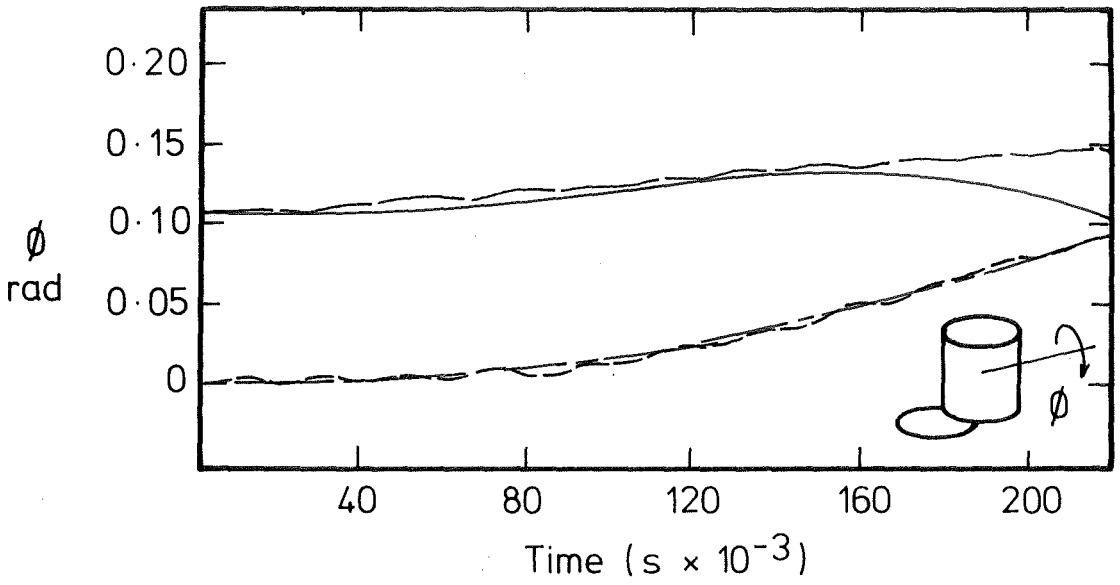

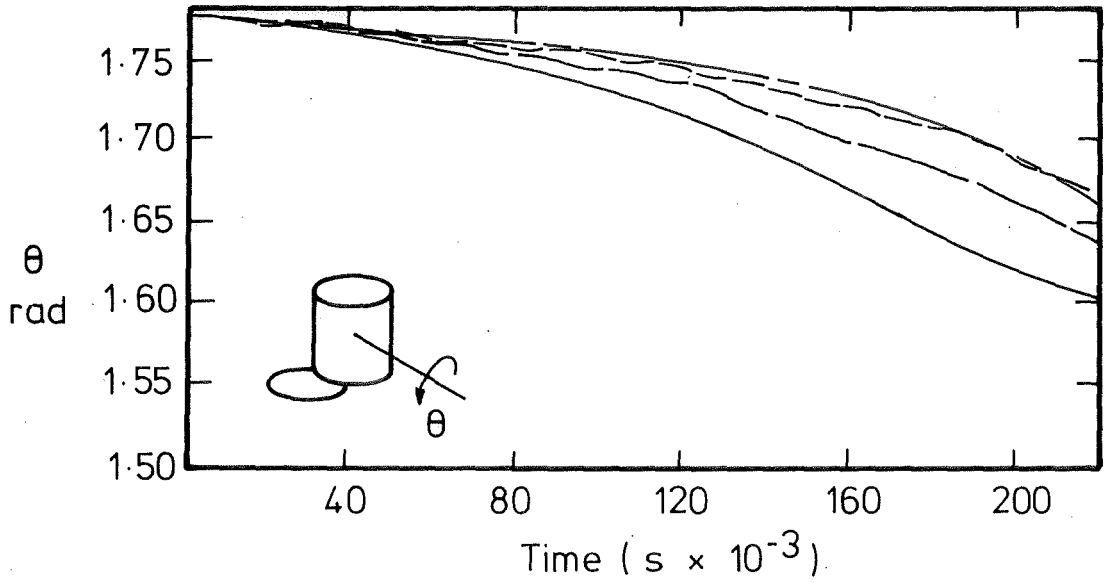

high contact force 1pt. contact
" " " 2pt. "
low contact force 1pt. contact
" " " 2pt. "

FIG. 8.21 VARIATION OF CONTACT FORCE MAGNITUDE.

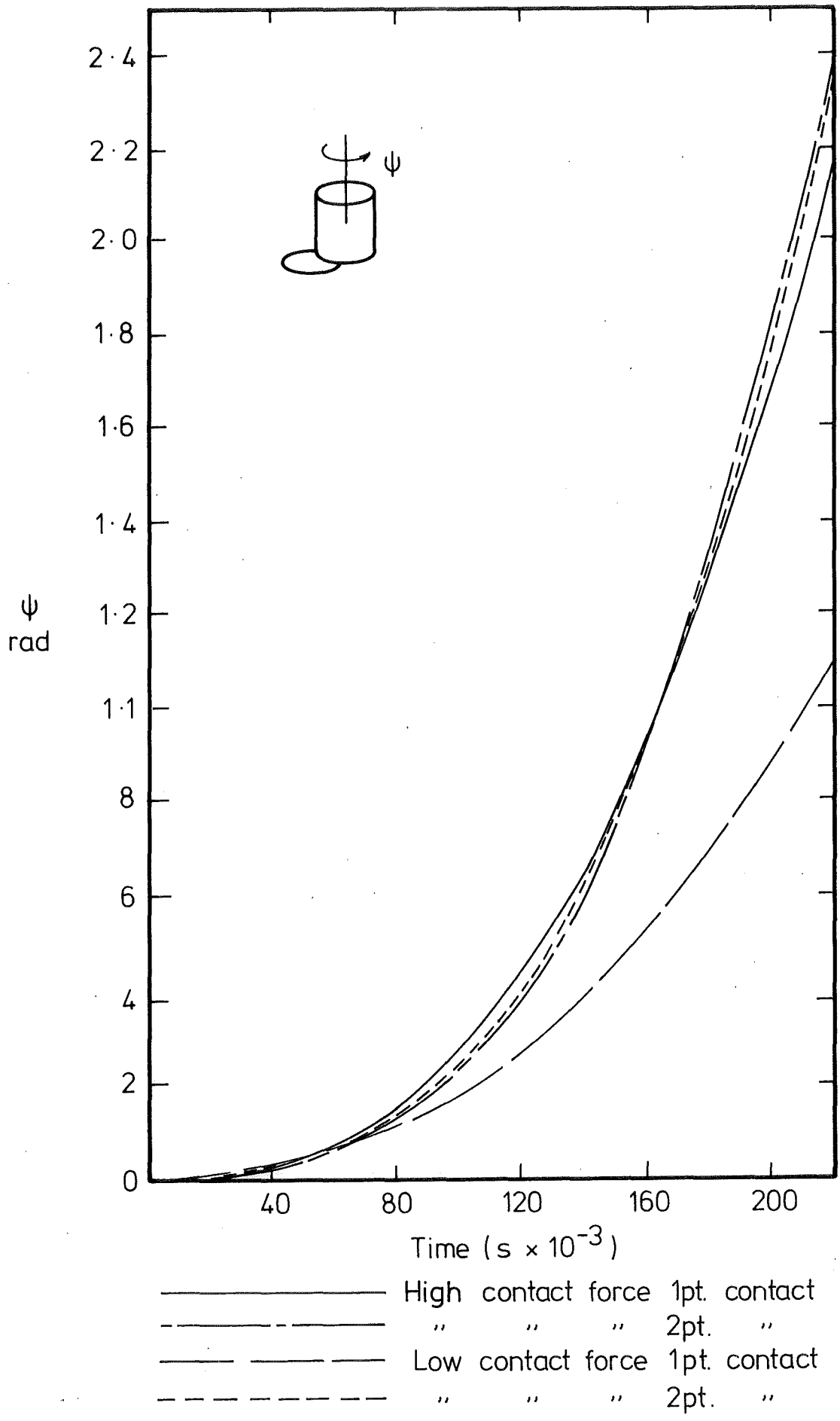

FIG. 8.22 VARIATION OF CONTACT FORCE MAGNITUDE

this means that although the translational misalignment has been largely eliminated the peg is still cocked over as it reaches the mouth of the hole. In this case jamming or wedging could occur.

8.6 ROTATION OF EXCITING FORCE

Finally a check was made to determine the effect of the exciting force's direction of rotation on assembly. A system having the same characteristics as that of Sec. 8.5 with a low contact force was operated under single and double point contact conditions with a clockwise and anticlockwise force of 10 N. Previous runs had been performed using an anticlockwise rotation.

8.6.1 Results

The results shown in Fig's 8.23 - 8.26 demonstrate that assembly occurs regardless of the direction of the contact force's rotation. However, although assembly occurs in both cases, it can be seen in Fig. 8.24 that the resulting motion of the peg is influenced by the direction of rotation, in this case single point contact assembly being achieved more rapidly by a clockwise rotating force.

8.7 SUMMARY

The following trends have emerged in the behaviour of the system studied in this chapter.

(i) A single mode of assembly was dominant. In both single and double point initial contact assembly proceeded by a rotation about a single contact point. The second contact point, in the double point contact case acted merely to retard the peg's motion.

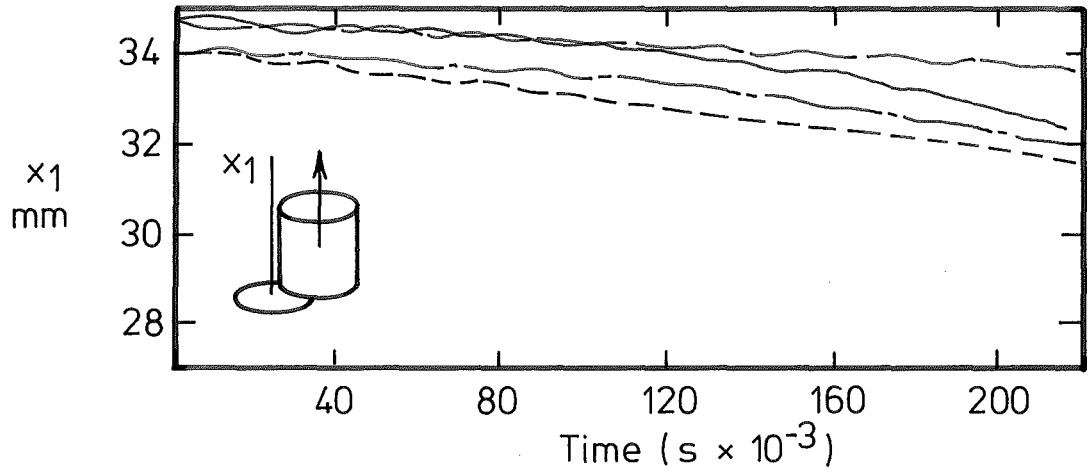

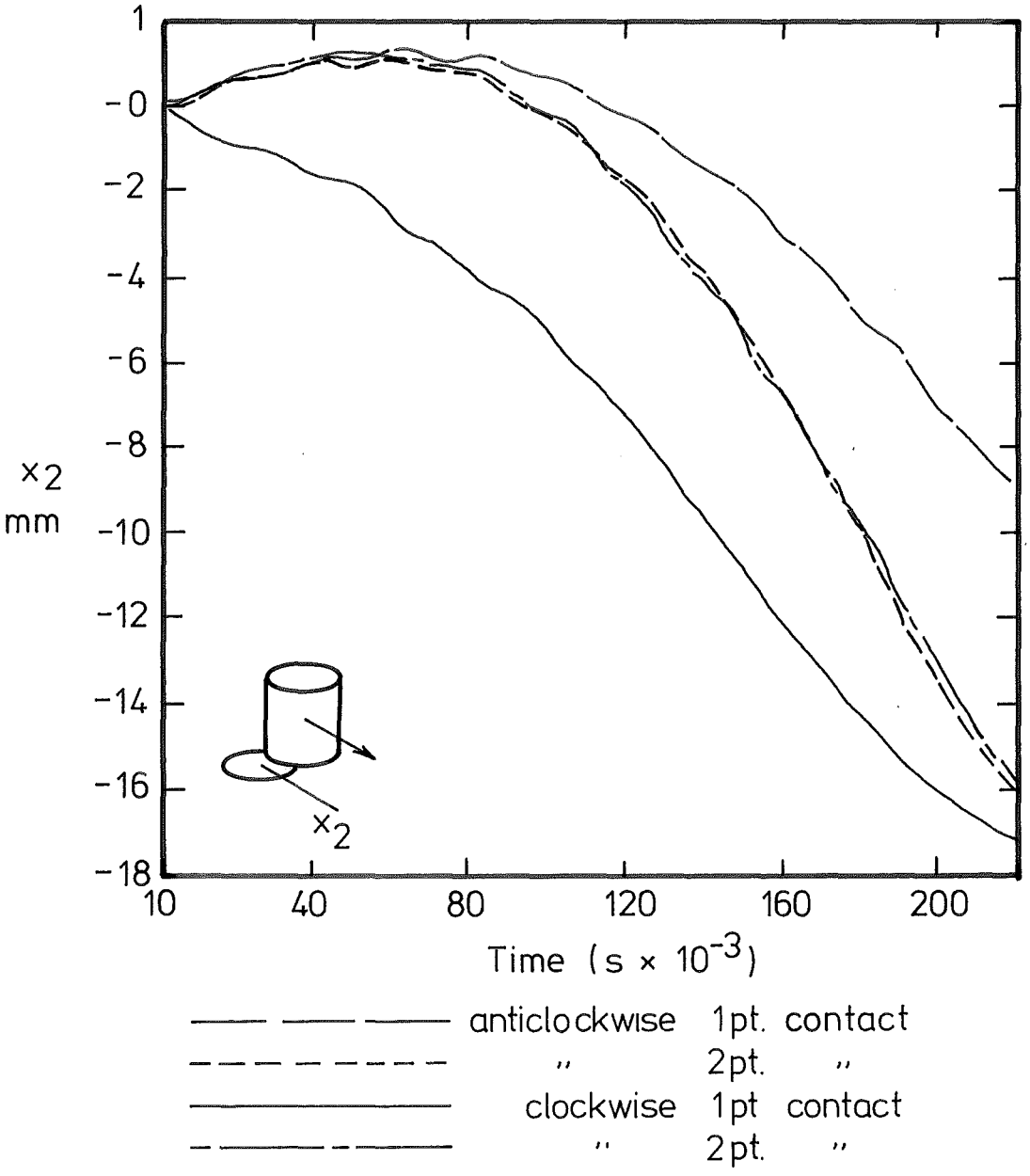

FIG. 8.23 VARIATION OF EXCITING FORCE ROTATION

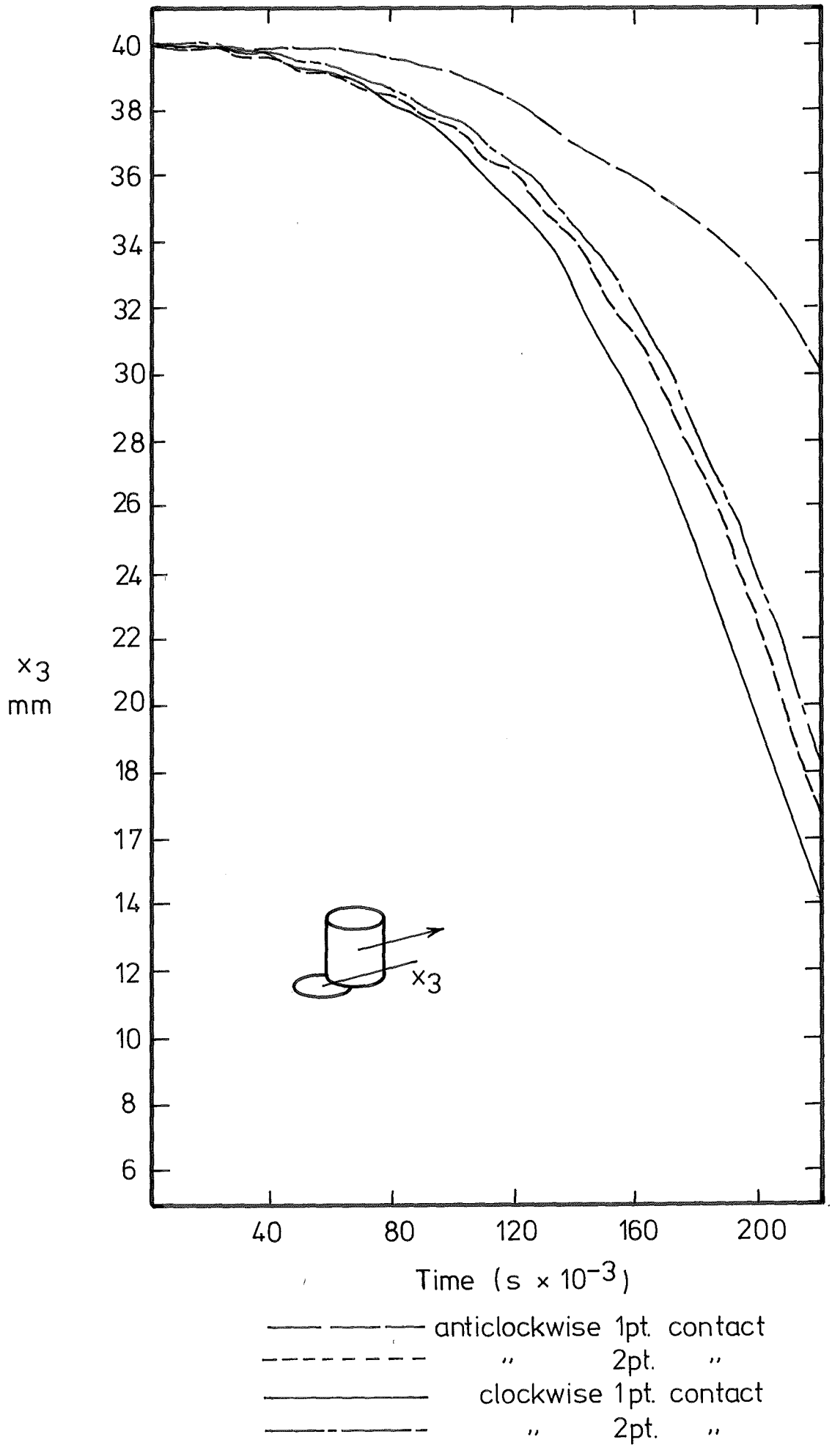

FIG. 8.24 VARIATION OF EXCITING FORCE ROTATION.

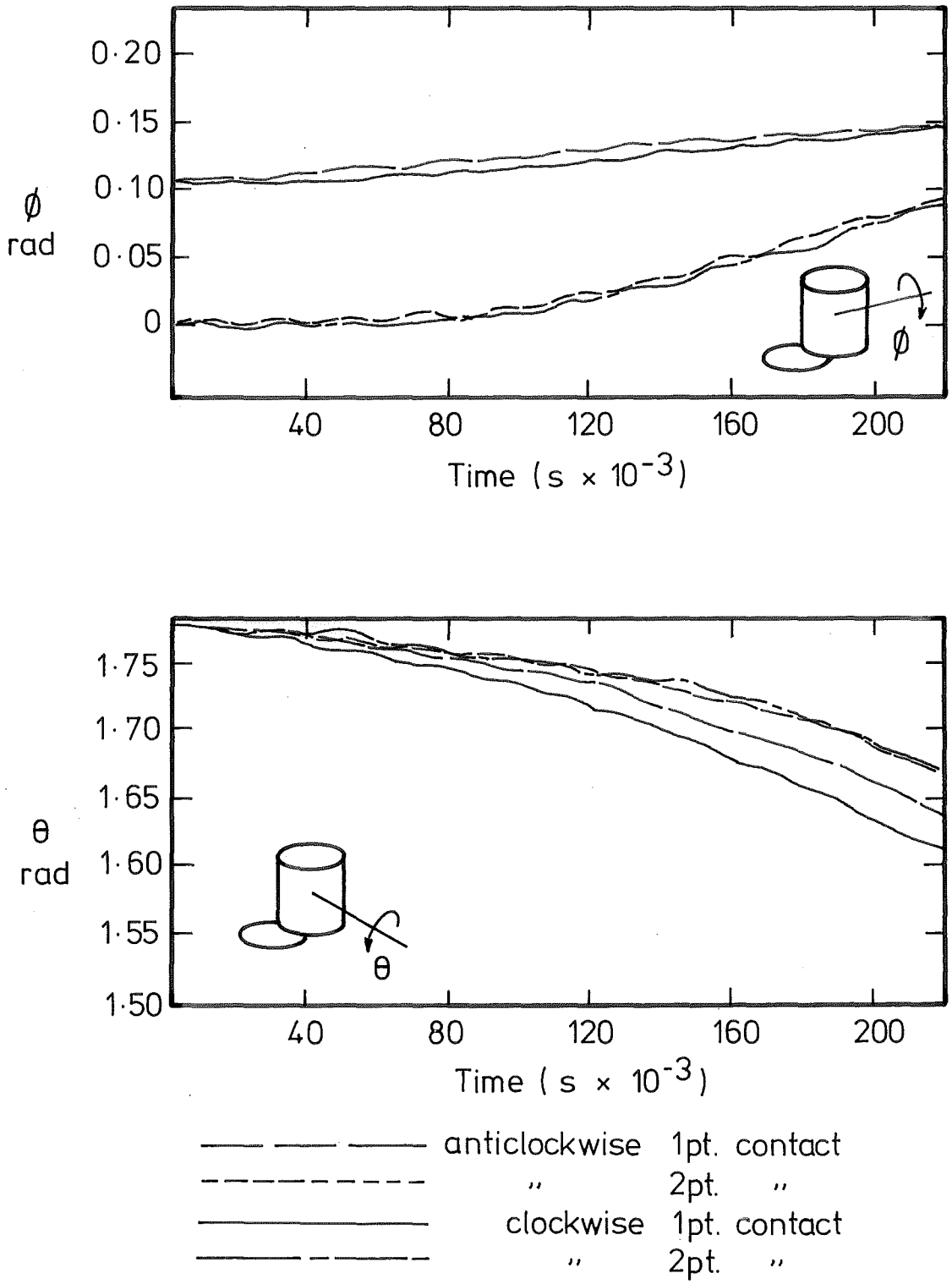

FIG. 8.25 VARIATION OF EXCITING FORCE ROTATION

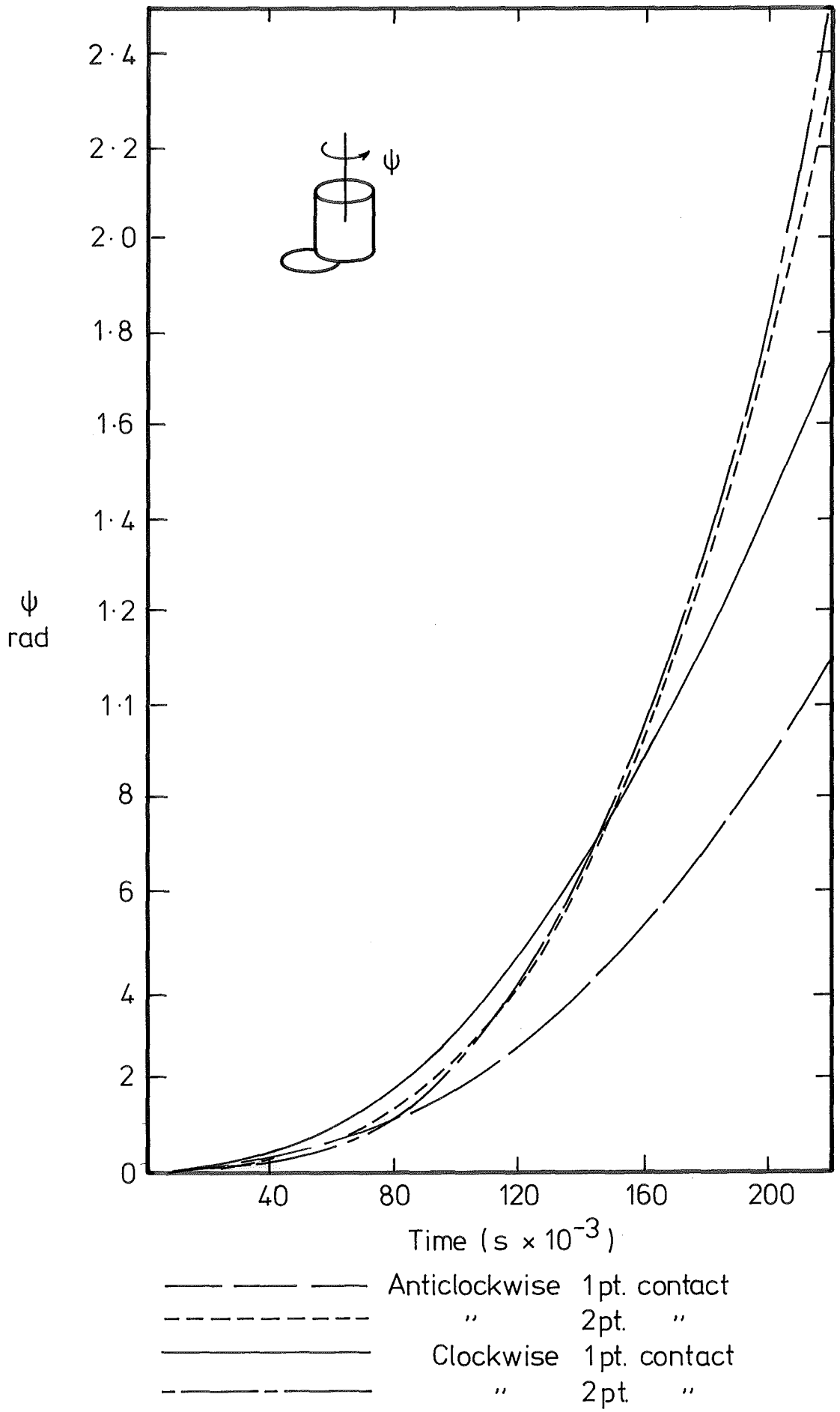

FIG. 8.26 VARIATION OF EXCITING FORCE ROTATION.

(ii) An increase in the stiffness and damping of the flexible coupling supporting the peg caused an increase in the speed of assembly.

(iii) Increasing the magnitude of the exciting force caused the speed of assembly to increase.

(iv) The speed of assembly increased as the contact force between the peg and hole increased.

(v) Assembly was essentially independent of the direction of the exciting force rotation.

Finally the limited work of this chapter appears to indicate that an assembly method based on single point rotation is feasible.

PART TWO

VIBRATORY POSITION

SENSING

CHAPTER 9

VIBRATORY POSITION SENSING

The relative motion of contacting misaligned components, under cyclic excitation, is related to their mode of contact and may be used to provide a feedback signal for manipulator control.

In this chapter the motion of a spring-constrained peg under excitation in different contact modes is studied, and two strategies are developed, by which the monitored movements give an approximation to the rotational and translational misalignments of the peg. Finally a test rig is used to demonstrate the feasibility of the basic sensing method.

9.1 VIBRATORY ASSEMBLY DEVICE WITH MOTION SENSING

The physical system referred to in this chapter, Fig. 9.1, is similar to that described in Sec. 4.2.

Generally the significant misalignments, both rotational and translational, may be described in terms of the manipulator centred XY axes, and it is assumed that the movement of the pegs centre of mass is able to be monitored in these axes. In practice the movement may be detected using strain gauges or accelerometers.

9.2 SINGLE POINT CONTACT WITH NO SLIDING

Single point contact, Fig. 9.2, is possible between the peg-edge and hole edge or hole plane. In either case the approach of Sec. 4.3 is applicable, and we will first direct our attention to the case of symmetrical rotational constraint stiffnesses. The following two special cases will then be studied.

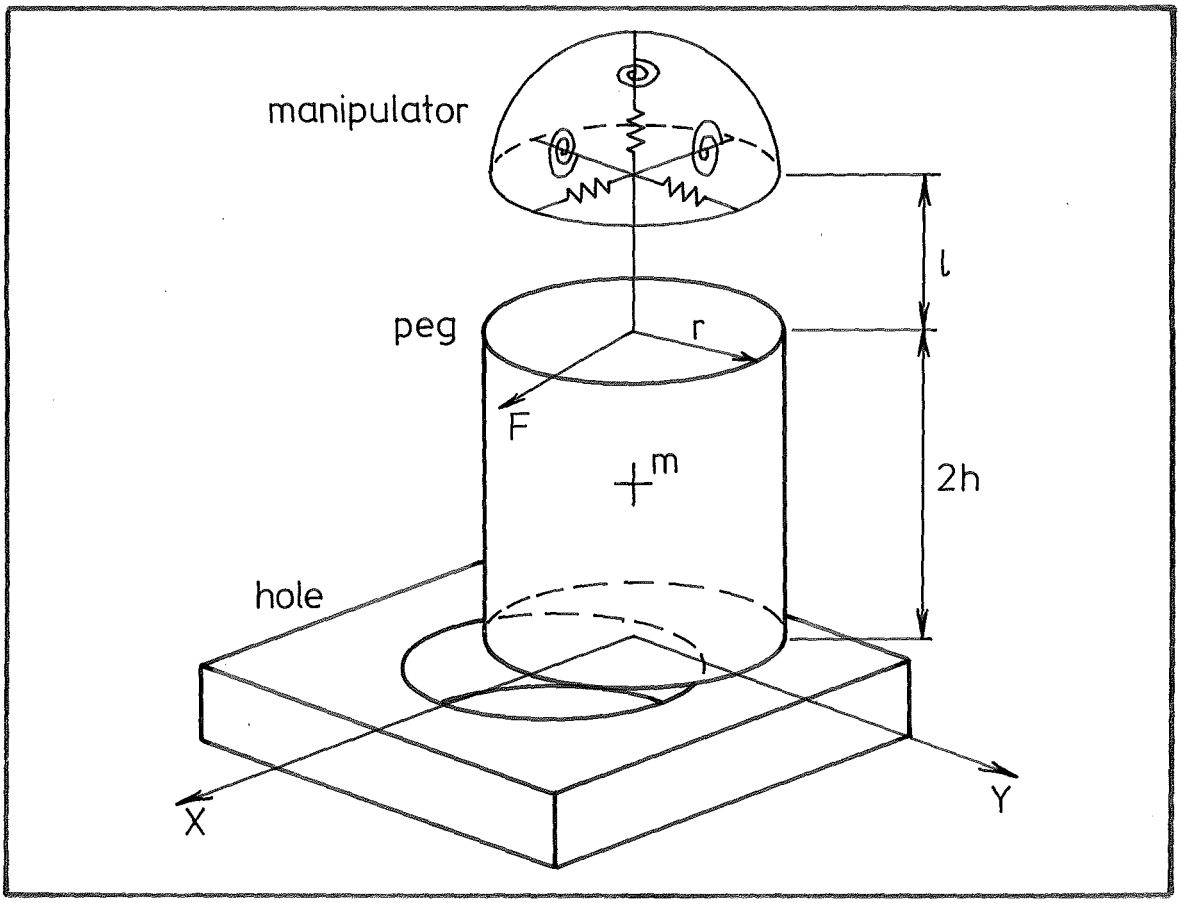

FIG. 9.1 VIBRATORY ASSEMBLY DEVICE

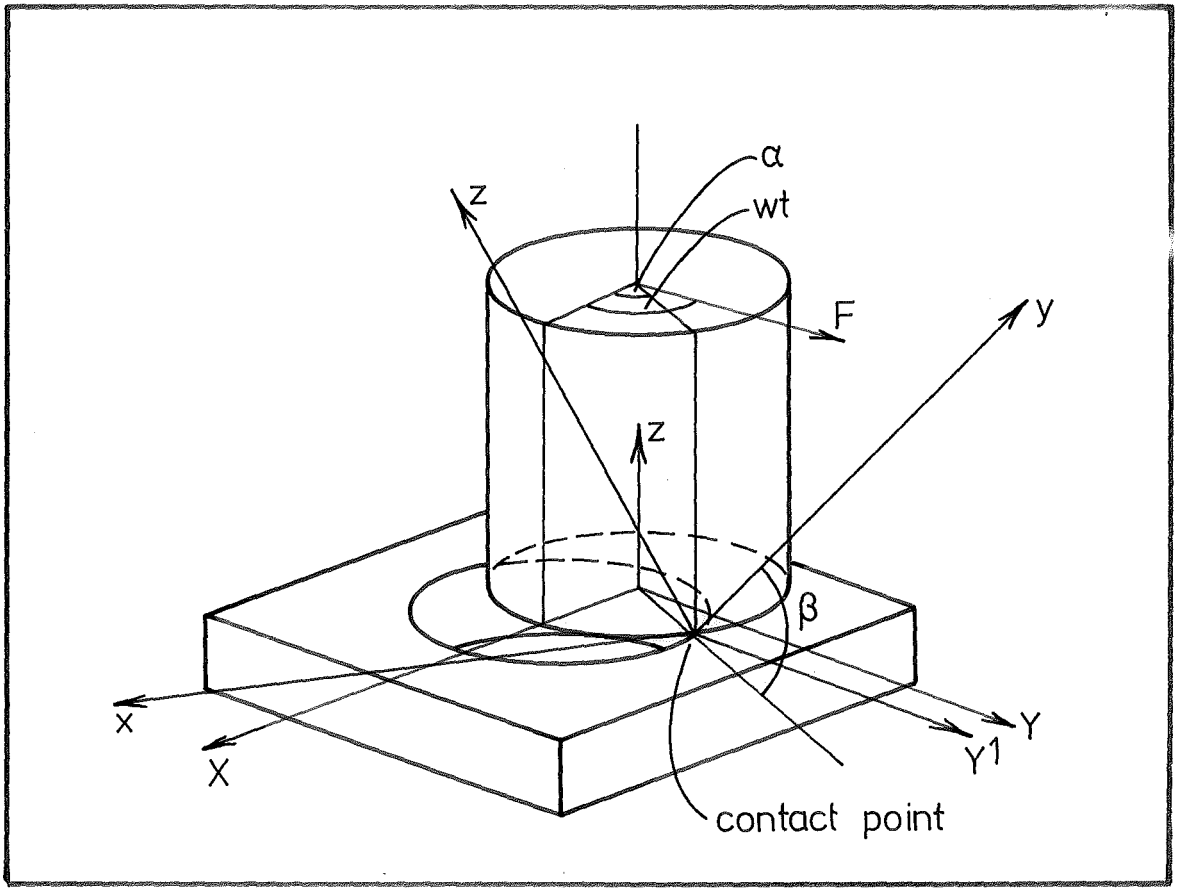

FIG. 9.2 SINGLE POINT CONTACT NO SLIDING

(i) The constraint stiffnesses about the transverse X-Y axes are low and rotations occur mainly about these axes.

(ii) The vertical axis rotational constraint stiffness is low and rotation occurs about this axis.

9.2.1 Symmetrical Constraint Stiffnesses

From Sec. 4.3 we see that the movement of the peg shown again in Fig. 9.2 is described by

$$\theta_x = \frac{-2Fh\cos(\omega t-\alpha)}{K-I_x\omega^2} \tag{9.1}$$

$$\theta_y = \frac{-F(r\sin\beta + 2h\cos\beta)\sin(\omega t-\alpha)}{K-I_y\omega^2} \tag{9.2}$$

$$\theta_z = \frac{-F(r\cos\beta - 2h\sin\beta)\sin(\omega t-\alpha)}{K-I_z\omega^2} \tag{9.3}$$

The overall movement may be thought of as the combination of two rotations θ_x and θ_p where

$$\underline{\theta}_p = \underline{\theta}_y + \underline{\theta}_z$$

With reference to Fig. 9.3 the movement of M in the XY plane is approximately described as

$$X = \sqrt{(r^2 + h^2)}\sin\gamma\theta_p\sin\alpha - h\theta_x\cos\alpha \tag{9.4}$$

$$Y = \sqrt{(r^2 + h^2)}\sin\gamma\theta_p\cos\alpha - h\theta_x\sin\alpha \tag{9.5}$$

where $\gamma = \pi - \beta - \theta_1 - \tan^{-1}\frac{h}{r}$

or more simply, M the mass centre describes an ellipse whose axes are aligned with the x y coordinate system, Fig. 9.4. It can be seen that by oscillating the system near the resonance frequency of θ_x, the major axis of the resulting elongated elliptical locus will lie along the y axis.

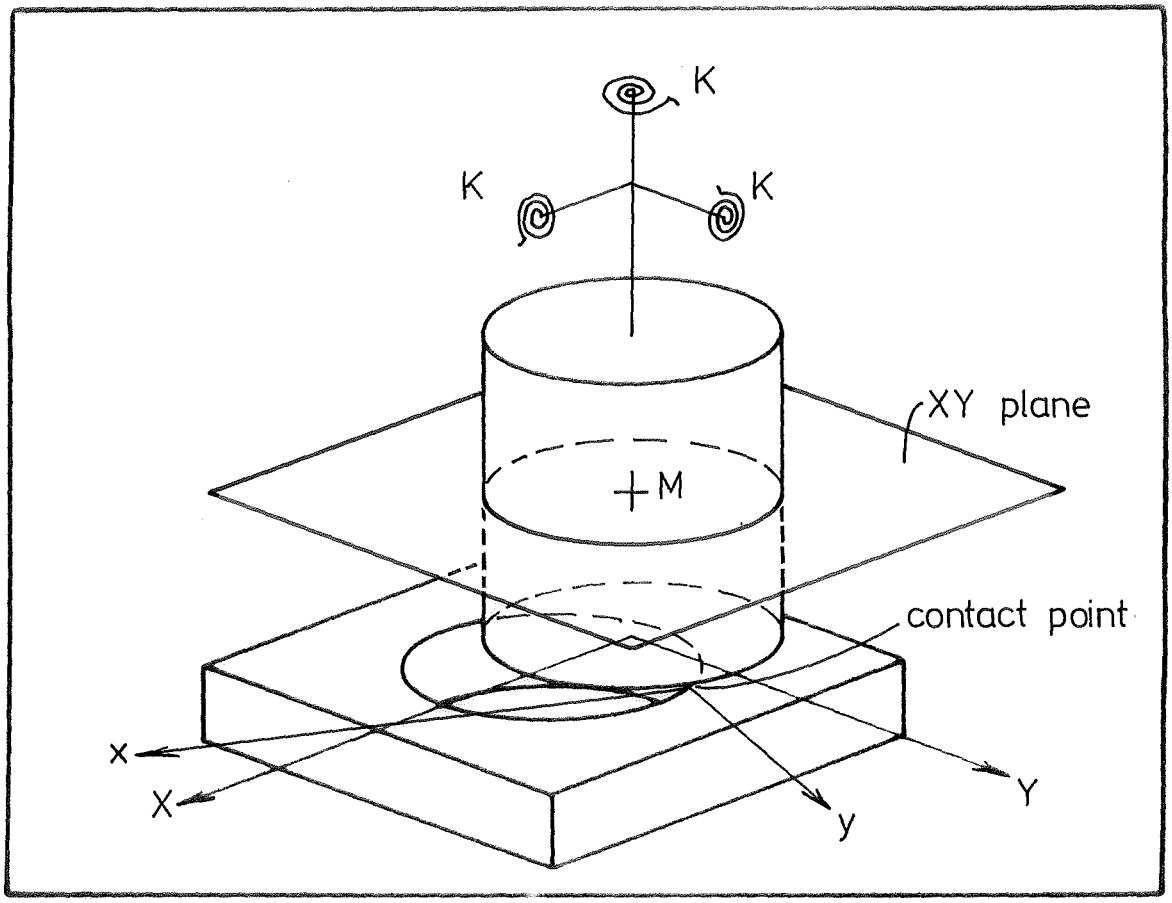

FIG. 9.3 SINGLE POINT CONTACT SYMMETRICAL CONSTRAINT STIFFNESS.

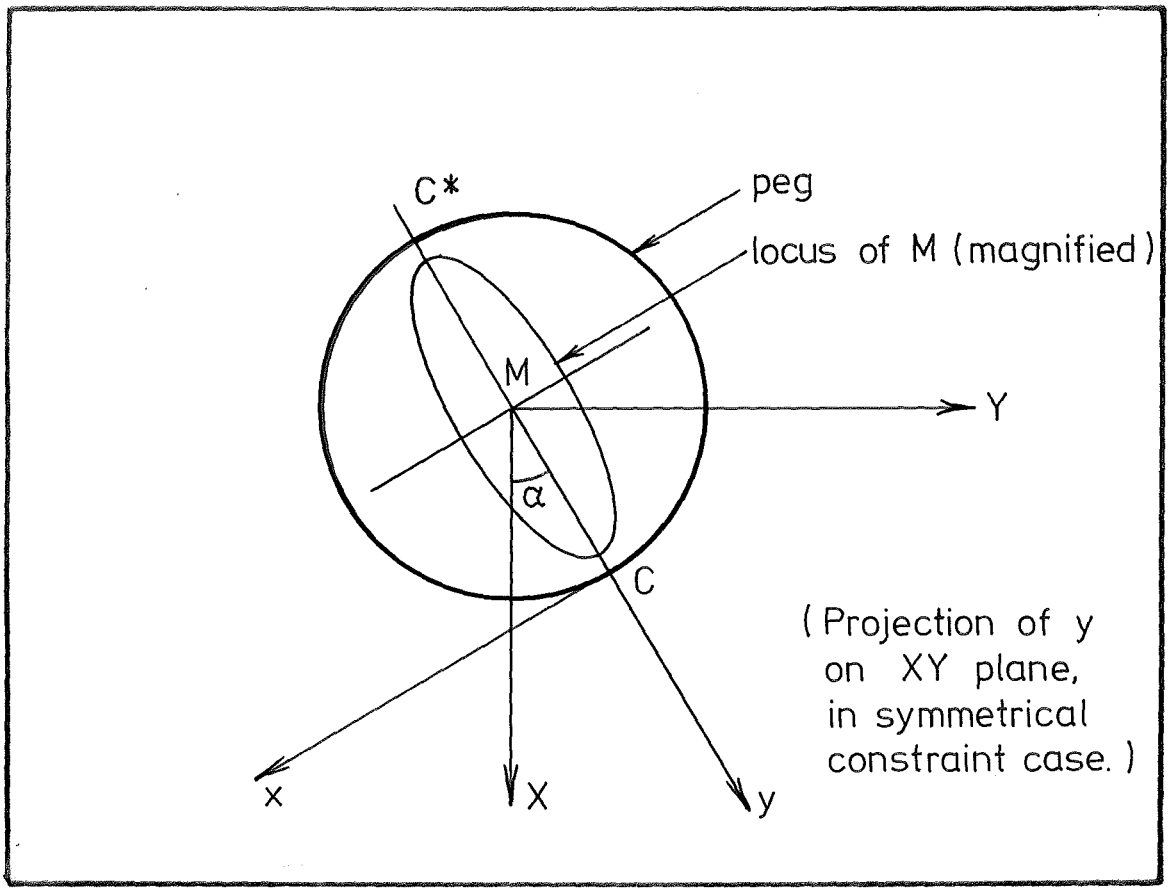

FIG 9.4 LOCUS OF M SYMMETRICAL OR LOW TRANSVERSE CONSTRAINT STIFFNESSES.

Similarly an increase in the amplitude of θ_p, due to exciting either θ_y or θ_z, will cause the major axis to become aligned with the x axis. Referring again to Fig. 9.4 it is apparent, that given this locus information, the contact point lies either at C or C*.

9.2.2 Low Transverse Constraint Stiffnesses

If the rotational stiffness about the vertical axis is high we may treat the system as having two degrees of freedom, movement only occurring about the two transverse principal axes x, y passing through the contact point, Fig. 9.5.

The steady state solution for small movements about these axes are

$$\theta_x = \frac{-2Fh\cos(\alpha-\omega t)}{K_x - I_x\omega^2} \tag{9.6}$$

$$\theta_y = \frac{2Fh\sin(\alpha-\omega t)}{K_y - I_y\omega^2} \tag{9.7}$$

and so

$$X = h\theta_y\sin\alpha - h\theta_x\cos\alpha \tag{9.8}$$

$$Y = h\theta_y\cos\alpha - h\theta_x\sin\alpha \tag{9.9}$$

The movement of M in the XY plane again is approximately described by an ellipse, with its major axis aligned with either x or y axes depending upon the relative amplitude of θ_x and θ_y. The contact point again therefore exists at either C or C*, Fig. 9.4.

9.2.3 Low Vertical Constraint Stiffness

The existence of high transverse stiffnesses allows the peg to be treated as a single degree of freedom system.

The system depicted in Fig. 9.6 rotates about the vertical z axis according to the equation

$$\theta_z = \frac{-Fr\cos(\omega t-\alpha)}{K_z-I_z\omega^2} \tag{9.10}$$

and the motion of M in the XY system is approximately described by

$$X = r\theta_z \sin\alpha \tag{9.11}$$

$$Y = -r\theta_z \cos\alpha \tag{9.12}$$

The locus of M lies on the line segment shown in Fig. 9.7, and as previously, contact occurs at either C or C*.

9.3 SINGLE POINT CONTACT WITH SLIDING

In practice the initial angular misalignments existing between the peg and hole are small. It was shown in Chapter 3, that the contact normals for both peg edge-hole edge and peg edge-hole plane contacts lie almost parallel to the peg vertical axis. Hence the friction force acting on the peg, in sliding contact, is virtually independent of the direction of movement. The expected locus of the peg under these symmetrical conditions is circular, and offers no useful directional information.

9.4 DOUBLE POINT CONTACT WITH NO SLIDING

In the event of double point contact with no sliding, the peg rotates about the contact point chord as described previously, in Sec. 4.5. The movement of M is defined by

$$X = h\theta_{y'} \sin\alpha \tag{9.13}$$

$$Y = h\theta_{y'} \cos\alpha \tag{9.14}$$

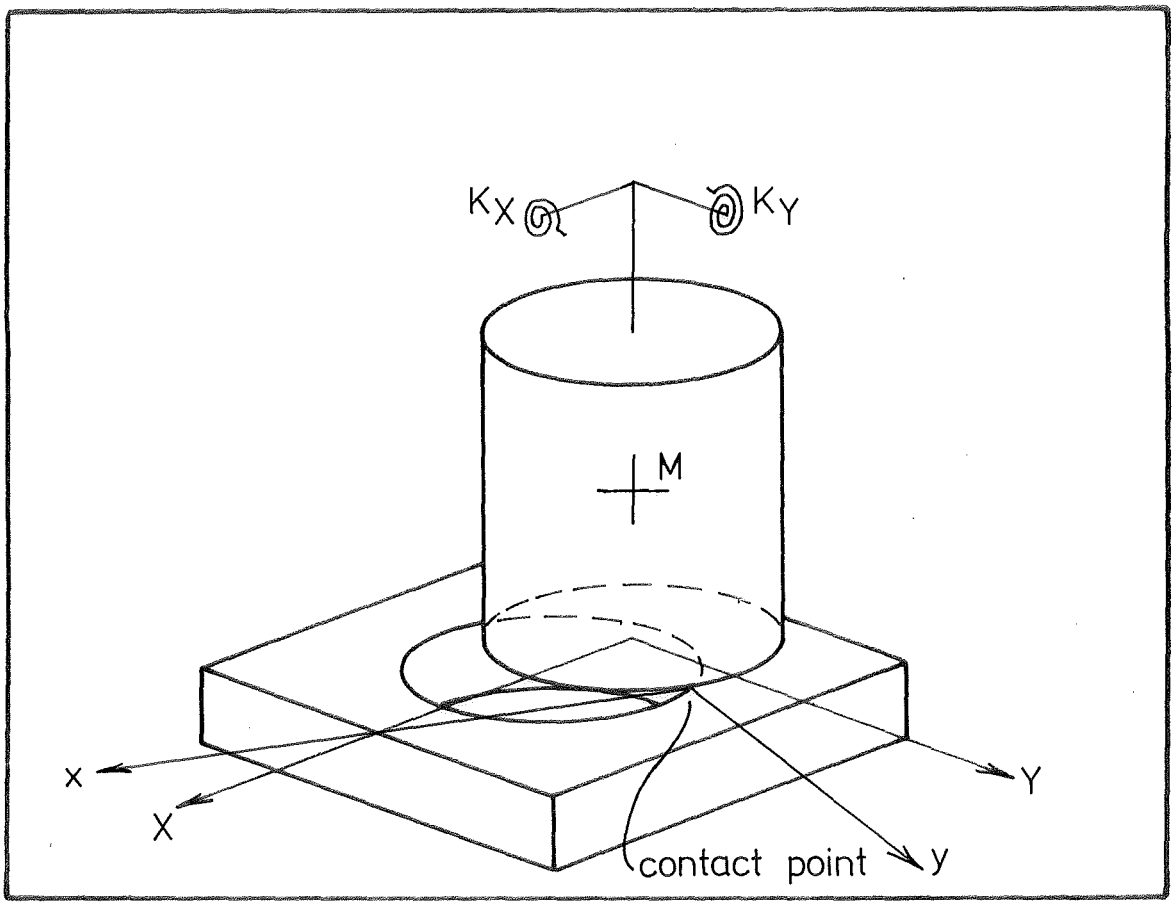

FIG. 9.5 LOW TRANSVERSE CONSTRAINT STIFFNESSES

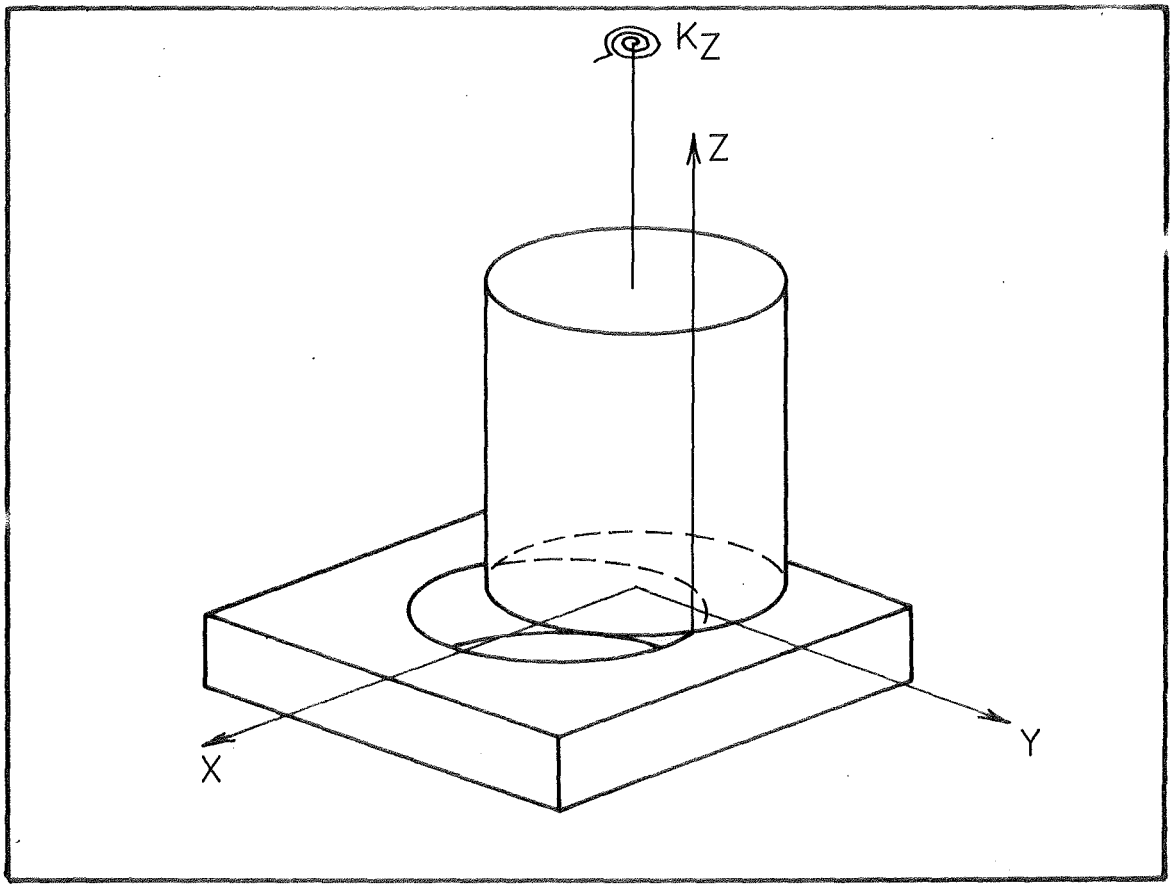

FIG. 9.6 LOW VERTICAL CONSTRAINT STIFFNESS

i.e. M moves on the line segment appearing in Fig. 9.8. The direction of the contact point chord is able to be found from the movement locus, and therefore the axis on which the hole centre lies may be found.

9.5 DOUBLE POINT CONTACT WITH SLIDING

The previous argument applied to the case of single point contact applies here also. The contact normals are again almost parallel to the peg vertical axis, so movement is possible with equal ease in all directions, resulting in a circular locus.

9.6 TRIPLE POINT CONTACT

If the peg contacts the hole edges and hole plane, movement can obviously only occur under sliding conditions.

9.7 SUMMARY, PEG MOVEMENT UNDER VARIOUS CONTACT CONDITIONS

The results of the preceding sections may be summarized into the following conclusions.

(i) In the single point contact non-sliding case, the locus of both a symmetric and non-symmetric elastically supported peg yields information locating the diameter on which the contact point lies.

(ii) Non-sliding double point contact provides us with the direction of the axis on which the hole centre lies.

(iii) As mentioned previously the behaviour of the system under sliding contact yields no information useful for position sensing.

The use of low stiffnesses about the transverse axes of the peg has several advantages.

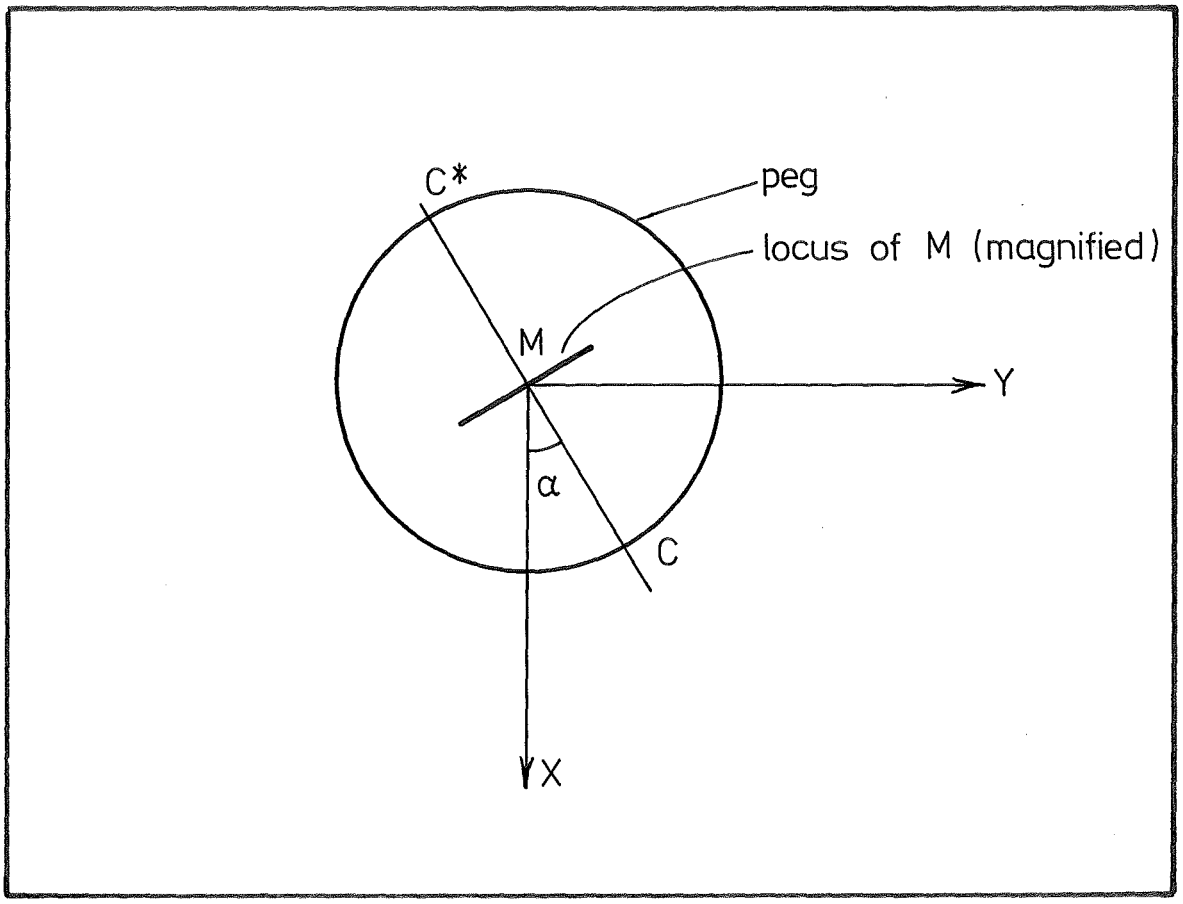

FIG. 9.7 LOCUS OF M LOW VERTICAL CONSTRAINT STIFFNESS.

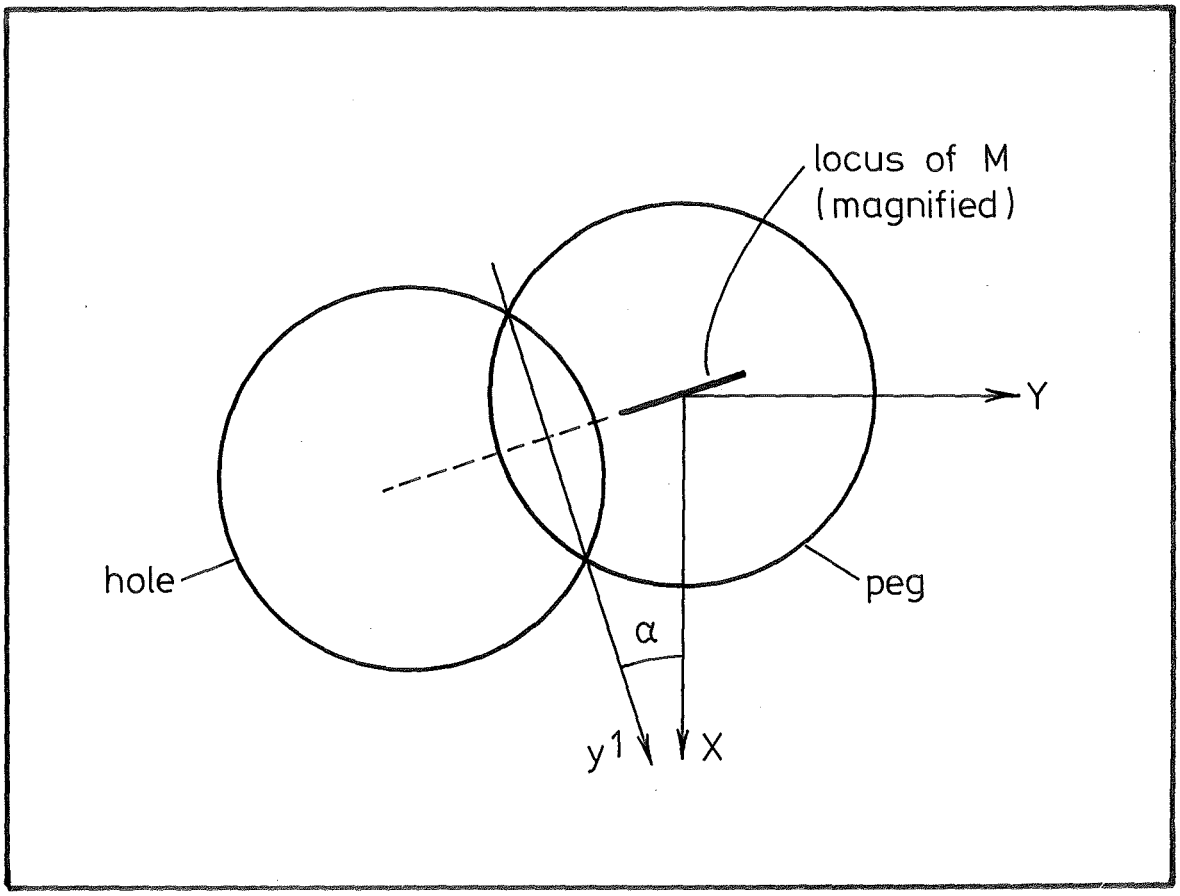

FIG. 9.8 LOCUS OF M DOUBLE POINT CONTACT.

(i) The motion loci of different modes are clearly identifiable under non-sliding conditions, i.e.

(a) single point contact gives an elliptical locus,

(b) double point contact gives a straight line segment,

(c) triple point contact gives no movement.

(ii) Sufficient flexibility exists to allow two point contact rotation.

(iii) As initial contact invariably occurs at the peg edge, a low transverse rotational stiffness provides a safeguard against damage by manipulator movements during assembly.

9.7.1 Assembly Strategies Based on Vibration Loci

The characteristic movements of the peg, supported in low transverse stiffness constraints, may be used in strategies for determining the misalignment of the peg with respect to the hole. Two such strategies are outlined in the following sections.

9.8 SINGLE POINT CONTACT ASSEMBLY STRATEGY

By applying a small wobble to the peg it is possible to determine, approximately, the position of the single contact point, the angular misalignment of the peg, and whether the peg edge contacts the hole edge or hole plane. If the two peg edge-hole edge contacts, possible for a given translational misalignment, can be found the translational misalignment may be deduced.

9,8.1 Single Point, Peg Edge-Hole Plane Contact

The angular misalignment of the peg may be expressed approximately in terms of small rotations θ_{Xh}, θ_{Yh} about the hole centred coordinate

system, Fig. 9.9; X_h and Y_h both lie in the hole plane. For small misalignments the perpendicular distance to the hole plane from any point on the peg edge, defined by α, is

$$h = h_o - \theta_{Yh}\, r\cos\alpha + \theta_{Xh}\, r\sin\alpha \tag{9.15}$$

and at the lowest point where contact if it exists will occur

$$\frac{\partial h}{\partial \alpha} = 0 \tag{9.16}$$

i.e.

$$\tan\alpha = \frac{-\theta_{Xh}}{\theta_{Yh}} \tag{9.17}$$

Obviously for small misalignments, the small angles θ_{Xh} θ_{Yh} approximate the similar angles taken with respect to the manipulator centred XY system.

The angular position of the contact point may be obtained from measurements of the movement locus as outlined in Sec. 9.2.2. Small rotations $\Delta\theta_x$ $\Delta\theta_Y$ are applied about the X, Y axes, Fig. 9.10, and a new value α^1 obtained. We now will designate the new angular position by θ_x θ_Y.

Differentiating Equation 9.17 we get

$$\frac{\partial \alpha}{\partial \theta_x} = \frac{\theta_Y}{\theta_x^2 + \theta_Y^2} \tag{9.18}$$

and

$$\frac{\partial \alpha}{\partial \theta_Y} = \frac{\theta_x}{\theta_x^2 + \theta_Y^2} \tag{9.19}$$

Using the mean value theorem

$$\frac{\Delta\alpha}{\Delta\theta_x} = \frac{-(\theta_Y - \frac{\Delta\theta_Y}{2})}{(\theta_Y - \frac{\Delta\theta_Y}{2})^2 + (\theta_x - \frac{\Delta\theta_x}{2})^2} = k_1 \tag{9.20}$$

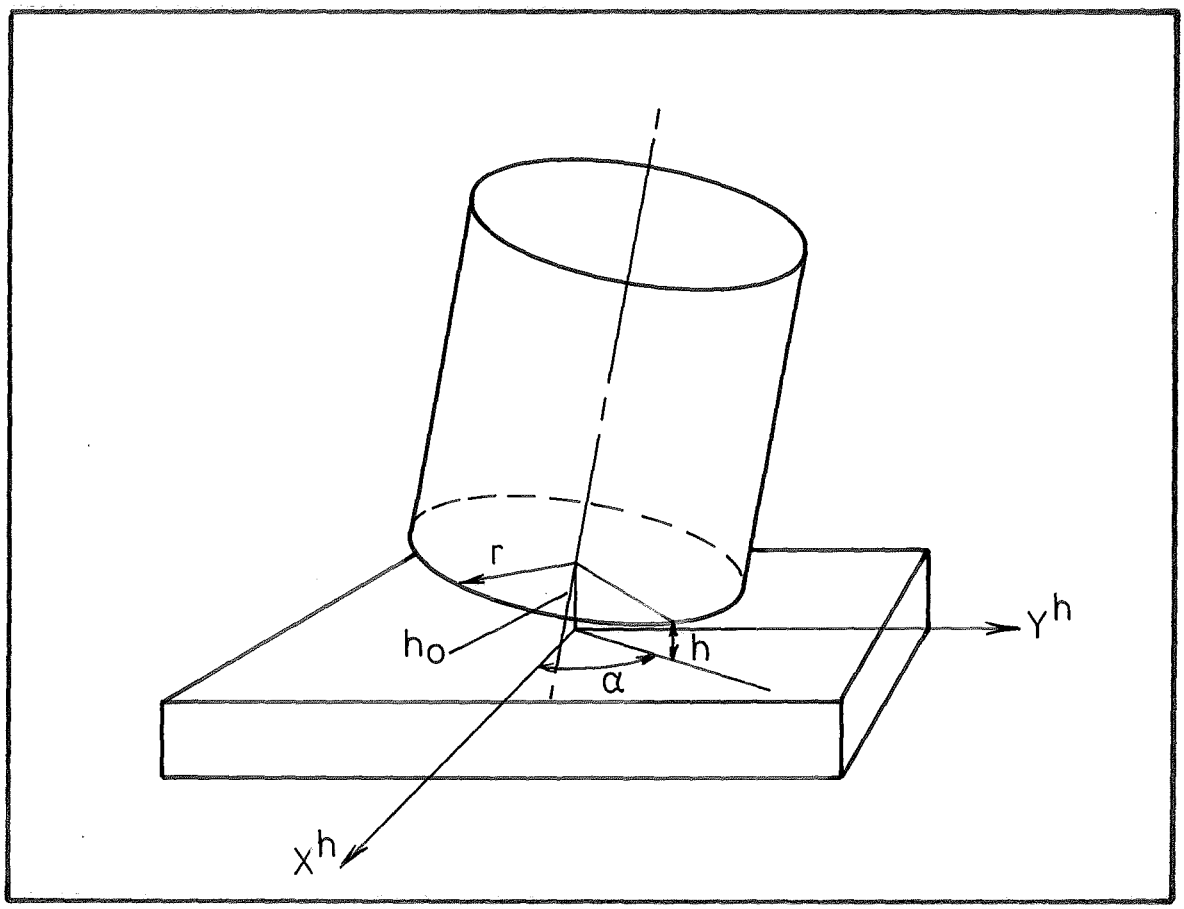

FIG. 9.9 PEG EDGE HOLE PLANE CONTACT

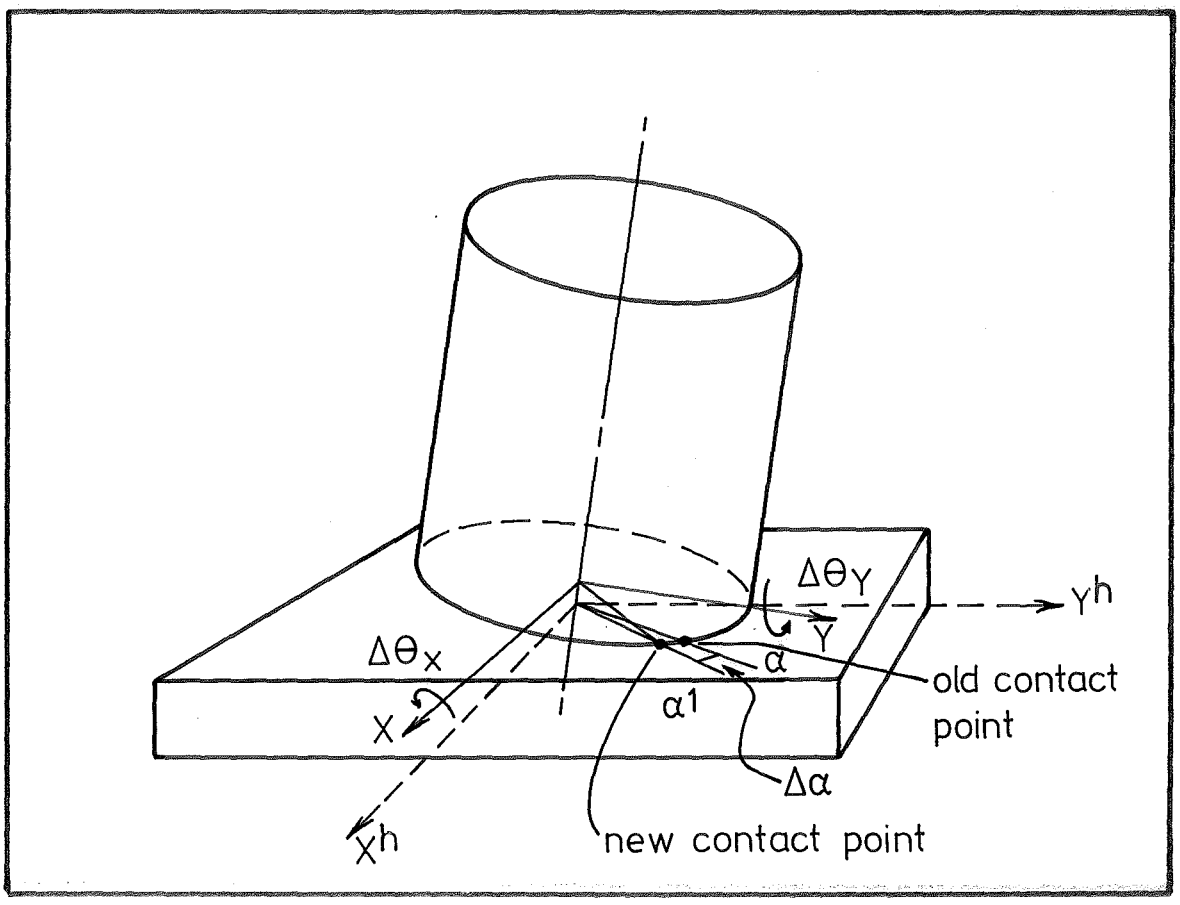

FIG 9.10 EFFECT OF SMALL ROTATION INCREMENTS ('WOBBLE') ON CONTACT POINT.

$$\frac{\Delta\alpha}{\Delta\theta_Y} = \frac{(\theta_x - \frac{\Delta\theta x}{2})}{(\theta_Y - \frac{\Delta\theta_Y}{2})^2 + (\theta_x - \frac{\Delta\theta_x}{2})} = k_2 \qquad (9.21)$$

where $\Delta\alpha = \tan^{-1}\left(\frac{\tan\alpha^1 - \tan\alpha}{1 + \tan\alpha\tan\alpha^1}\right) = \alpha - \alpha^1$

Recalling Equation 9.17 for the final peg position i.e.

$$\tan\alpha^1 = \frac{-\theta_x}{\theta_Y}$$

and eliminating θ_x θ_Y in turn from Equations 9.20, 9.21

$$\theta_x = \frac{\Delta\alpha}{(K_1 - K_2\cot\alpha^1)} \qquad (9.22)$$

$$\theta_Y = \frac{\Delta\alpha}{(-K_1\tan\alpha^1 + K_2)} \qquad (9.23)$$

From geometric considerations, Fig. 9.11 the true contact point position may be found,

if $\theta_Y \geqslant 0$ then $-\frac{\pi}{2} \leqslant \alpha \leqslant \frac{\pi}{2}$

$\theta_Y \leqslant 0$ then $\frac{\pi}{2} \leqslant \alpha \leqslant \frac{3}{2}$

9.8.2 Single Point, Peg Edge-Hole Edge Contact

When contact between peg and hole edges occurs, the condition

$$\frac{\partial h}{\partial\alpha} = 0 \qquad (9.24)$$

does not generally hold at the contact point and clearly a small wobble rotation will not cause movement of the contact point, i.e. variation of α, till the minimum point moves out of the hole area onto the plane, as shown in Fig. 9.12. This fact may therefore be used to determine the type of single point contact, namely, peg edge - hole edge or peg edge - hole plane.

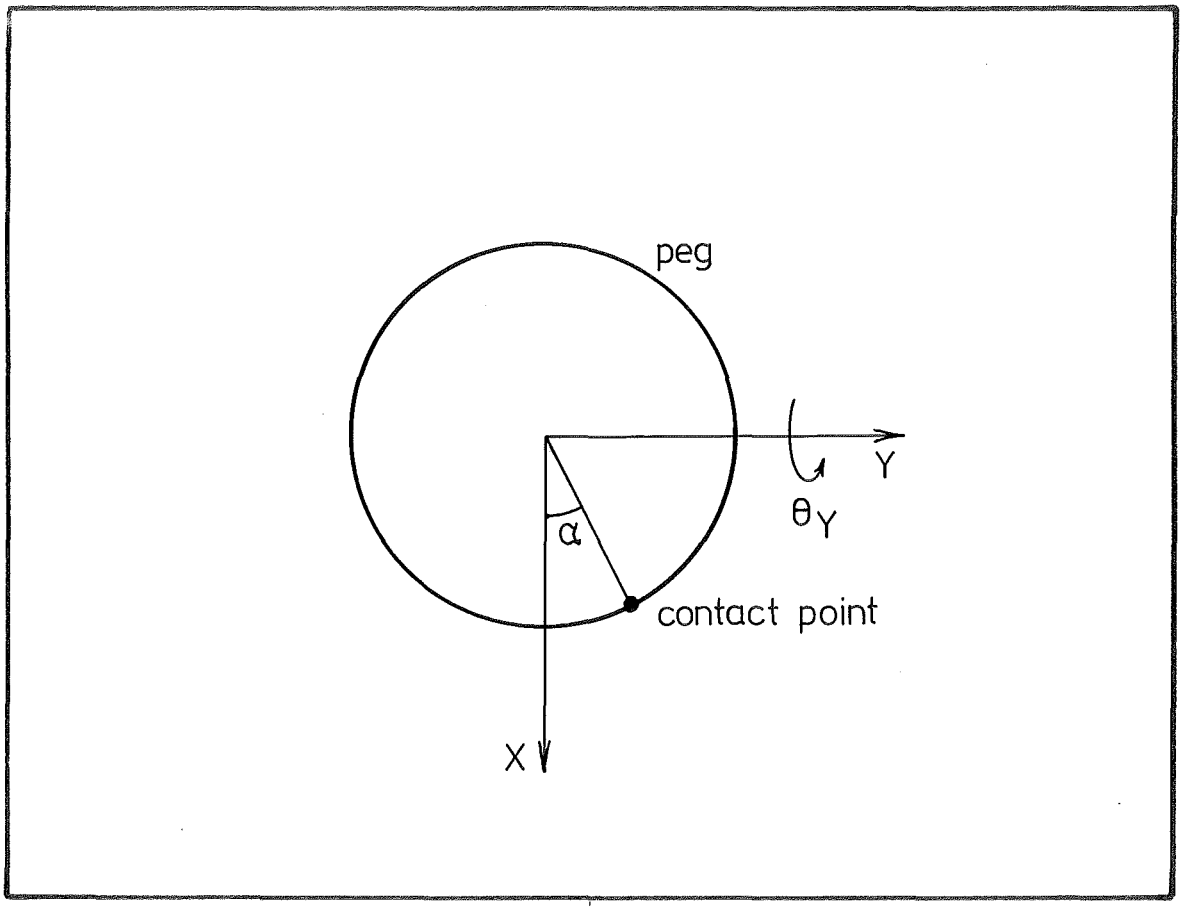

FIG. 9.11 DETERMINING TRUE CONTACT POINT

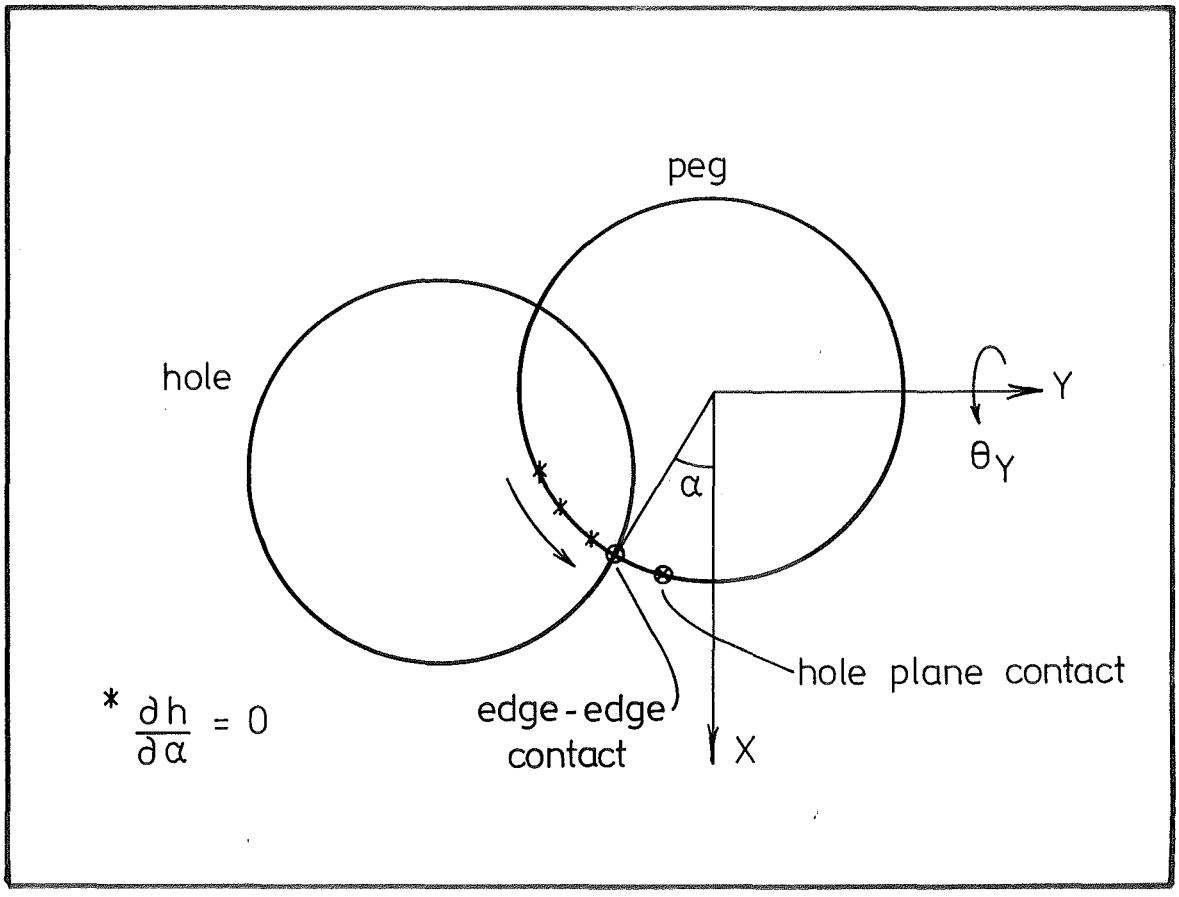

FIG. 9.12 PEG EDGE-HOLE PLANE CONTACT

If both possible peg edge - hole edge contacts are found, Fig. 9.13, the coordinates of the hole centre are approximately given by

$$X = 2r \cos\left(\frac{\alpha_1 - \alpha_2}{2}\right)\cos\left(\frac{\alpha_1 + \alpha_2}{2}\right) \tag{9.25}$$

$$Y = 2r \cos\left(\frac{\alpha_1 - \alpha_2}{2}\right)\sin\left(\frac{\alpha_1 + \alpha_2}{2}\right) \tag{9.26}$$

9.8.3 Single Point Assembly Algorithm

The methods described in the above subsections form the basis of the algorithm shown in Fig. 9.14. Essentially the technique consists of identifying the two edge-edge contact points, by applying small successive rotations about the axis passing through the contact point, and checking whether contact point movement occurs.

Estimates of the angular misalignment are obtained at each step, and the translational misalignment is determined approximately from the position of the two contact points.

9.9 DOUBLE POINT CONTACT ASSEMBLY STRATEGY

If double point contact exists the approximate angular and translational misalignments may be obtained by applying a small wobble rotation to the peg.

9.9.1 Double Point, Peg Edge-Hole Edge Contact

The line on which the hole centre lies is able to be found from the resulting locus of movement of the peg, refer Sec. 9.4. If the peg is subjected to a small rotation $\Delta\theta$ about this axis, Fig. 9.15, the double point contact is destroyed contact now occurring at C. The position of

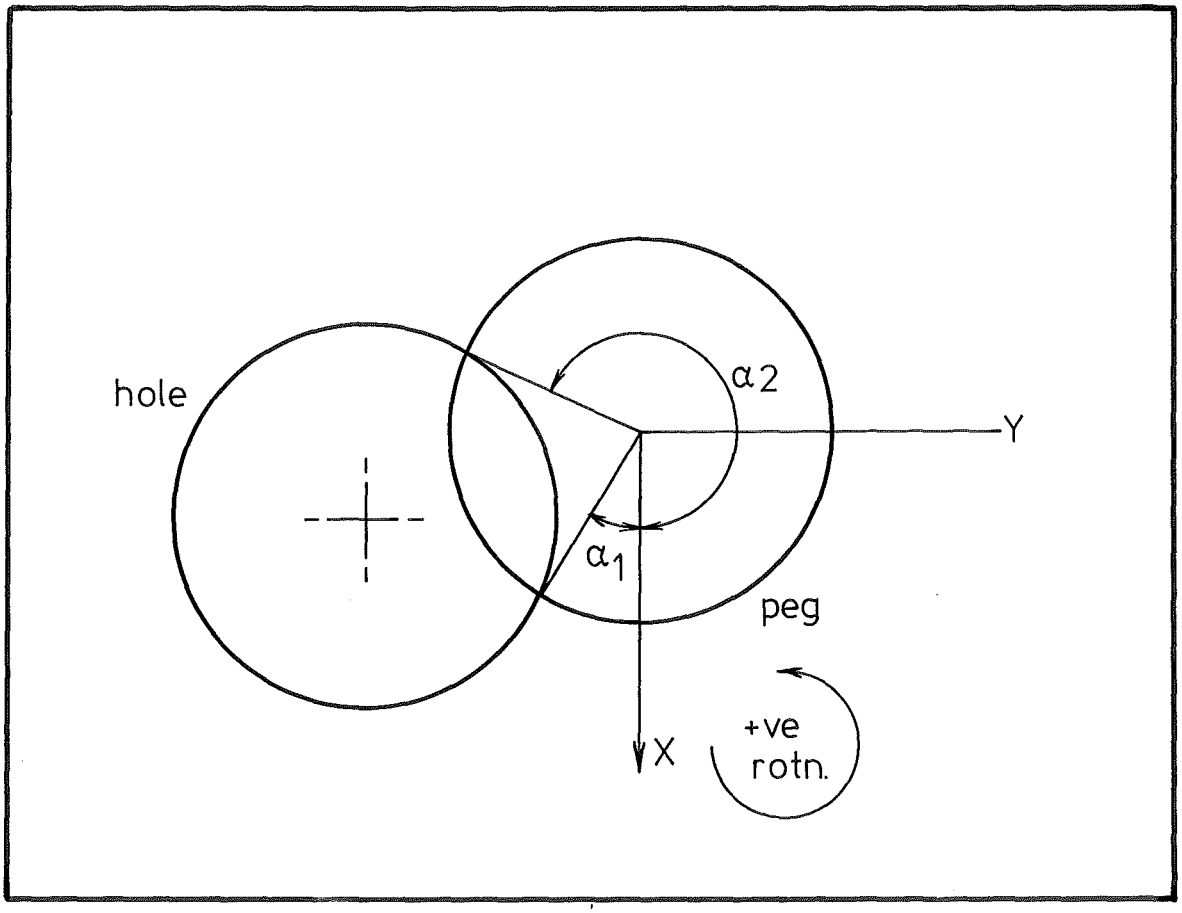

FIG. 9.13 COORDINATES OF HOLE CENTRE IN XY SYSTEM.

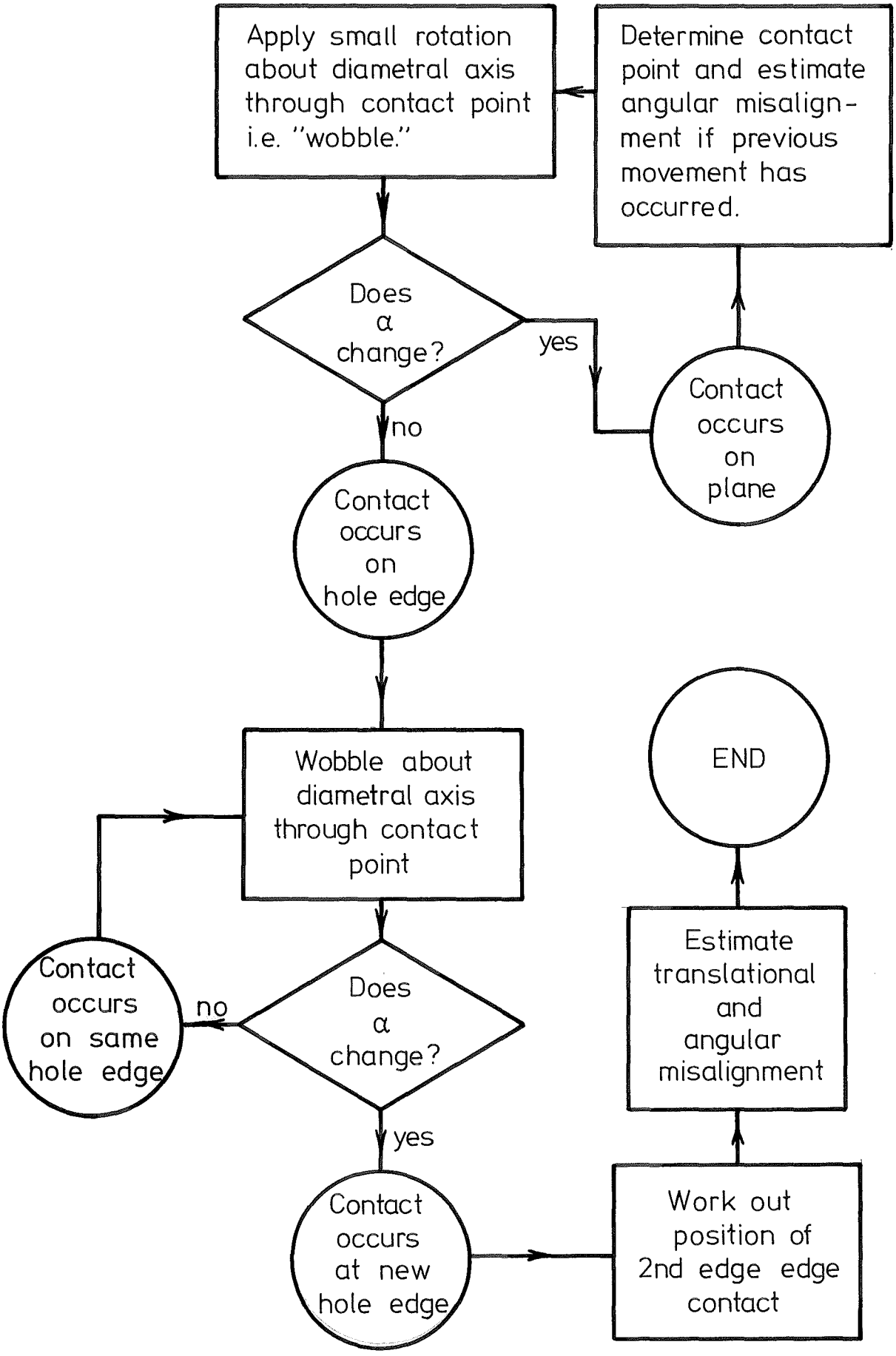

FIG. 9.14 SINGLE POINT CONTACT ALGORITHM

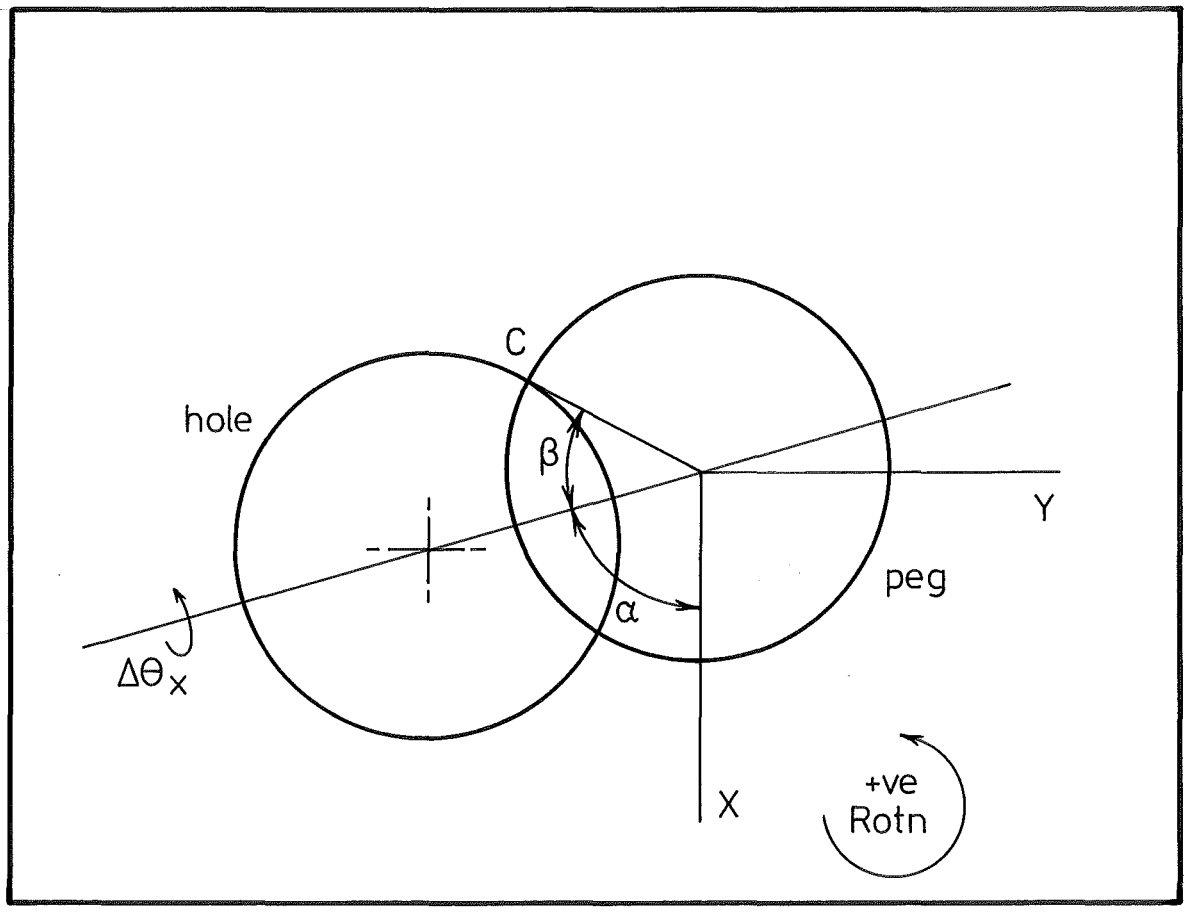

FIG 9.15 TRANSITION FROM SINGLE TO DOUBLE POINT CONTACT

the contact point C may be found from the resulting locus of the peg and using the condition

$0 \leqslant \beta \leqslant \pi$ when $\Delta\theta \geqslant 0$

$\pi \leqslant \beta \leqslant 2\pi$ when $\Delta\theta \leqslant 0$

The position of the hole centre is then simply

$$X = 2r \cos\beta\cos\alpha \tag{9.27}$$

$$Y = 2r \cos\beta\sin\alpha \tag{9.28}$$

If wobble rotation about the $\Delta\theta$ axis is continued till the contact point shifts from peg edge-hole edge to peg edge-hole plane contact the angular misalignments can be found.

i.e. $\tan(\beta-\alpha) = -\frac{\theta_x}{\theta_Y}$

and $\Delta\theta = \theta_x \cos\alpha - \theta_Y \sin\alpha$

so combining

$$\theta_x = \frac{\Delta\theta}{(\cos\alpha + \cot(\beta-\alpha)\sin\alpha)} \tag{9.29}$$

$$\theta_Y = \frac{-\Delta\theta}{(\cos\alpha\cot(\beta-\alpha) + \sin\alpha)} \tag{9.30}$$

9.9.2 Double Point Assembly Algorithm

The above methods are used in the algorithm shown in Fig. 9.16.

9.10 EXPERIMENTAL ASSESSMENT OF VIBRATORY MOTION FEEDBACK

The elastically constrained peg-hole system shown in Plates 9.1 and 9.2 was used to qualitatively demonstrate the possibility of using vibratory movements as a feedback signal.

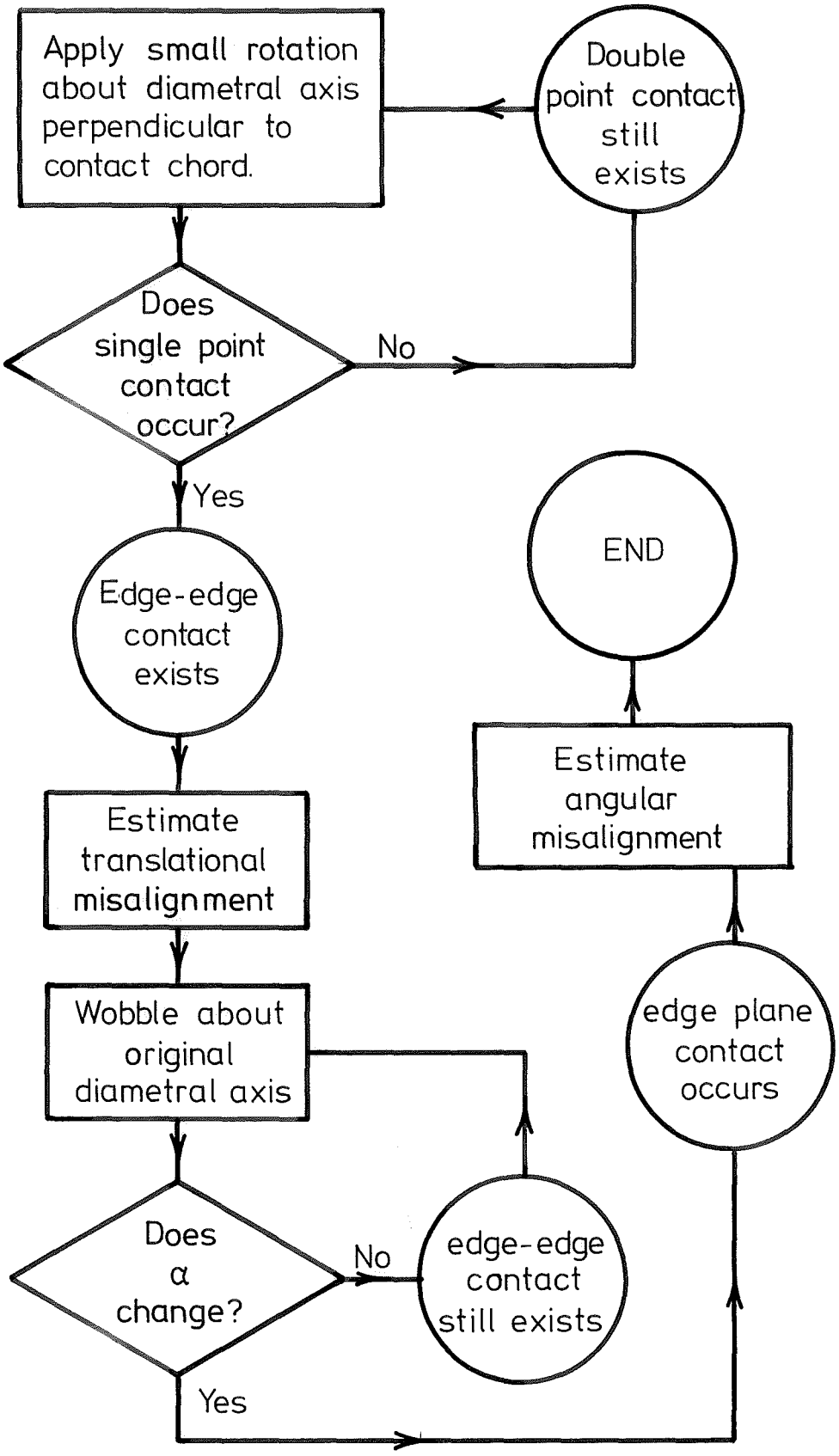

FIG. 9.16 DOUBLE POINT ASSEMBLY ALGORITHM.

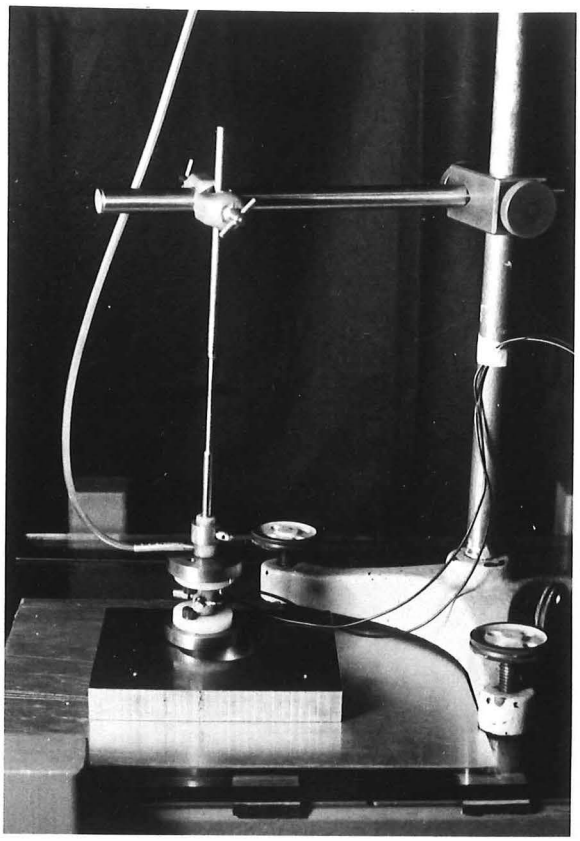

PLATE 9.1

PEG-HOLE VIBRATORY
SENSING TEST RIG

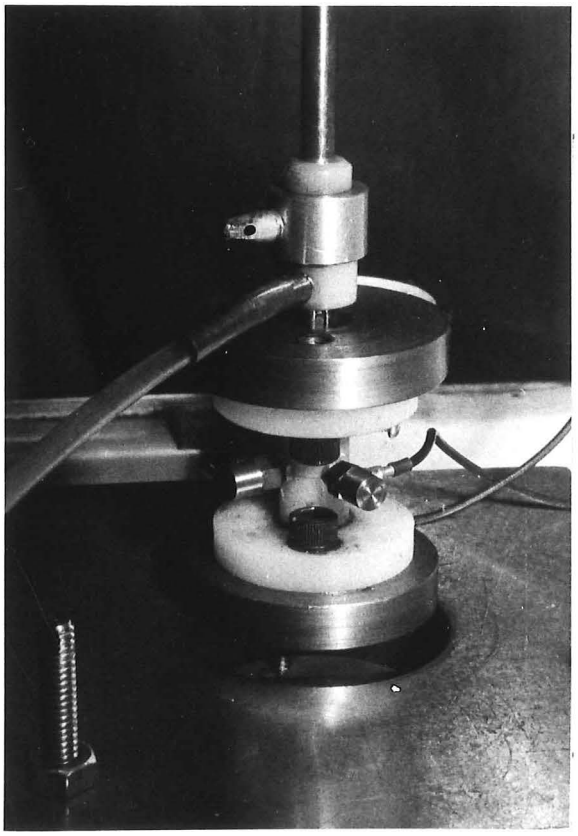

PLATE 9.2

CLOSE-UP OF PEG

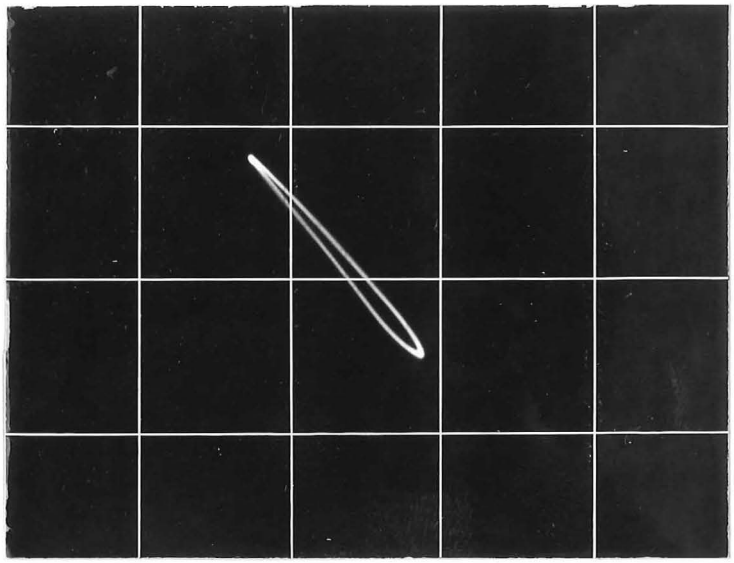

PLATE 9.3 SINGLE POINT CONTACT

1st Resonant Frequency

43 Hz

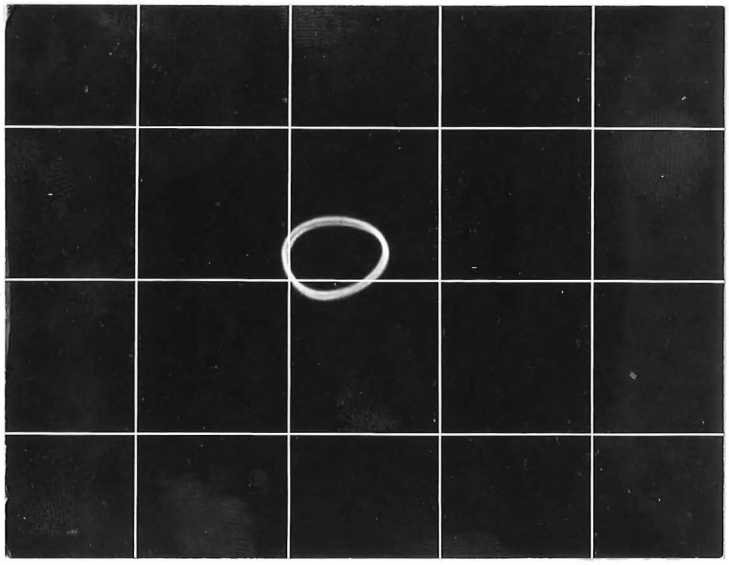

PLAGE 9.4 SINGLE POINT CONTACT

Intermediate Stage

69 Hz

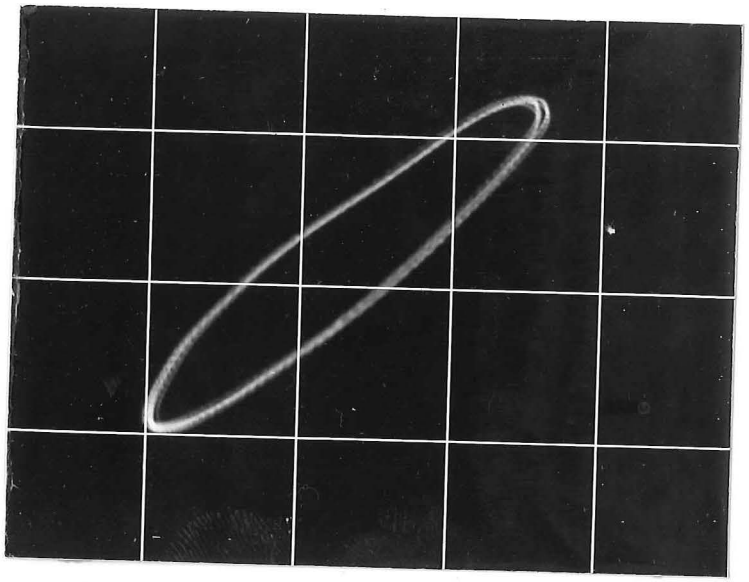

PLATE 9.5 SINGLE POINT CONTACT

2nd Resonant Frequency

86 Hz

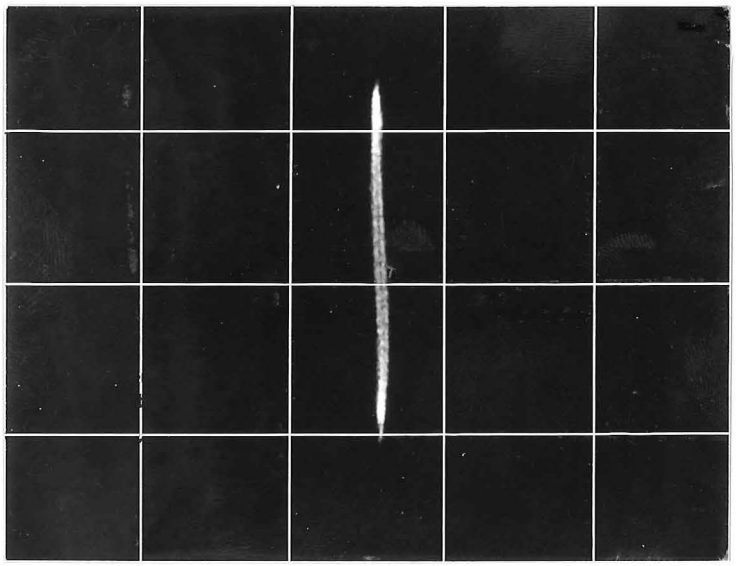

PLATE 9.6 DOUBLE POINT CONTACT

71 Hz

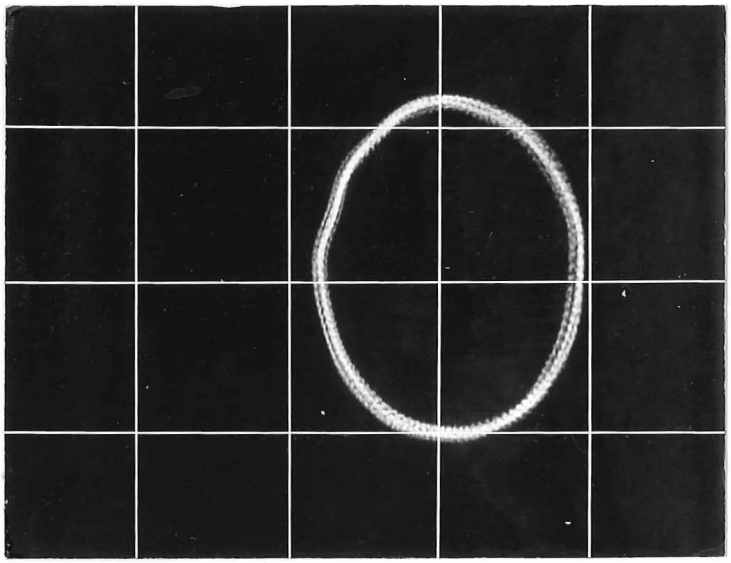

PLAGE 9.7 SLIDING CONTACT

9.10.1 Test Rig

The peg consisting of a nylon spool with attached steel discs is fastened to a flexible steel rod. The exciting force is provided by an out of balance, air driven, Hero's turbine running on a ½" nylon bush coaxial with the peg and support shaft. Frequencies of approximately 100 Hz were attained with this setup. The peg was held in contact with the hole plate so the desired contact modes could be obtained for test purposes.

Bruel and Kjaer Type 4344 miniature accelerometors were fastened to the nylon spool as shown and the resulting signals were amplified and integrated to provide a displacement output. The two outputs were plotted on an XY oscilloscope so giving the approximate locus of the peg in the XY plane.

9.10.2 Experimental Work

The peg and hole were positioned so as to give the three contact modes and the resulting movement loci, shown in Plates 9.3 - 9.7, were obtained.

Plates 9.3 to 9.5 show the locus of the peg in non-sliding single point contact. Plate 9.3 illustrates the locus of the peg at the first resonant frequency and Plate 9.5 shows the second resonant frequency. The shapes of the movement loci agree well with the elliptical paths predicted for this type of contact, Sec's 9.2.1, 9.2.2.

Plate 9.6 shows the movement of the peg in two point, non-sliding contact. Again the line segment obtained agrees well with the predicted result, Sec. 9.4.

Finally Plate 9.7 shows the peg locus under sliding conditions. The circular locus corresponds to the behaviour suggested in Sec's 9.3, 9.5.

9.11 SUMMARY

The limited theoretical and experimental study of vibratory sensing described in this chapter indicates that the method has some potential at least in the general case of a peg and hole.

In contrast to many other tactile sensing techniques, vibratory sensing is quick; small displacements and high frequencies mean rapid information transfer and allow the possiblity of numerical filtering.

PART THREE

TWIN FORCE SENSOR

POSITION SENSING

CHAPTER 10

TWIN FORCE-SENSOR POSITION SENSING

The assembly task may be regarded as a problem of determining the relative orientations and displacements of the components involved. If the contact forces generated during assembly are sensed in the local coordinate system of each component, the spatial relationship between the components may be found. In this chapter a method of position sensing based on this approach is described.

10.1 TWIN FORCE SENSOR POSITION SENSING

Fig. 10.1 shows two objects and their associated coordinate systems prior to assembly. We wish to determine the relationship between the two coordinate systems, so that rotational and translational misalignments may be eliminated.

If contact between the objects occurs the resulting equal and opposite contact force is manifested as direct force and moment components at the 0_A and 0_b coordinate systems. We assume that these components may be sensed, and denote them as the column vectors.

$$[F_{A1}] \quad [M_{A1}] \quad [F_b] \quad [M_b]$$

The object B is now rotated and translated by a known amount to a second contact position as shown in Fig. 10.2, the relationship between the 0_b and 0_B coordinate systems being given as

$$[X_B] = [R_{Bb}][X_b] + [T_{Bb}] \tag{10.1}$$

The second set of contact force and moment components are now found. These are

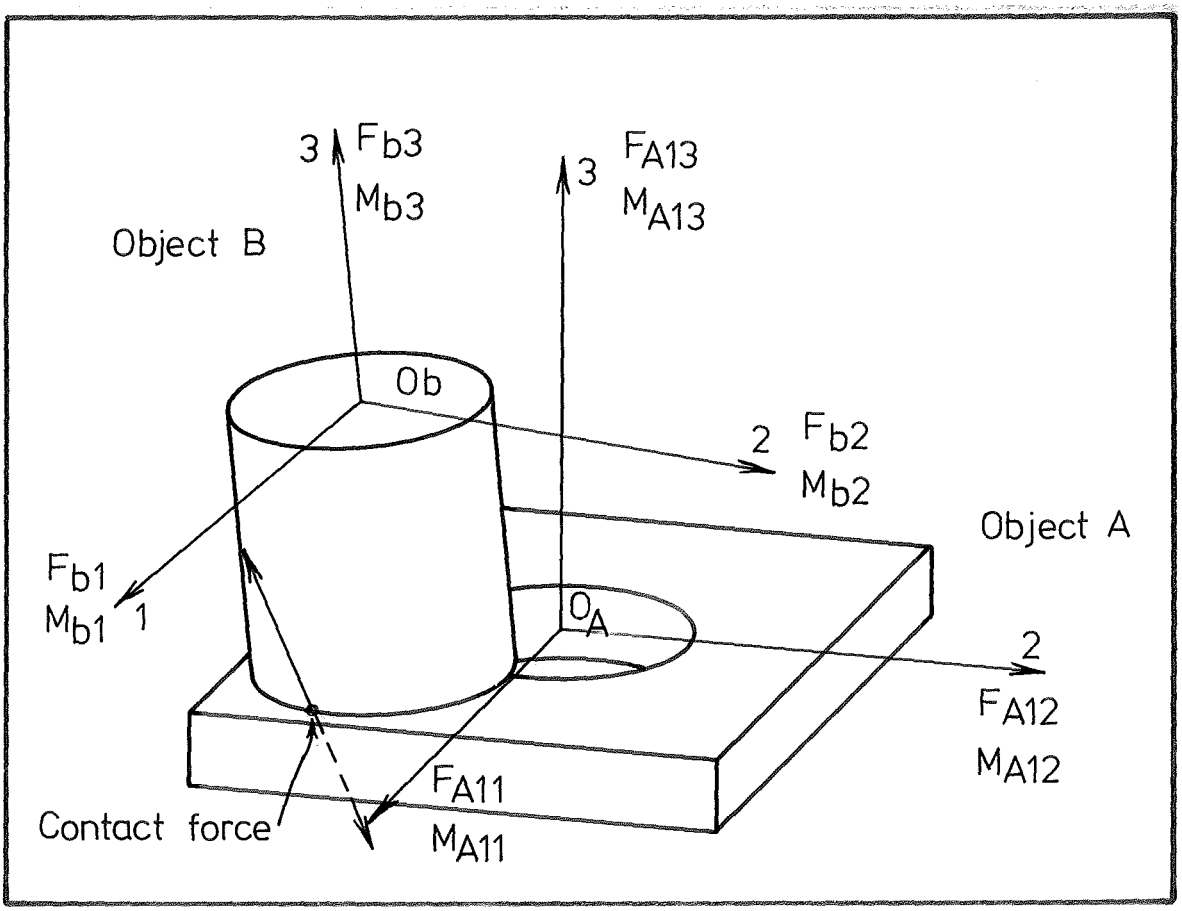

FIG. 10.1 TWO OBJECTS PRIOR TO ASSEMBLY

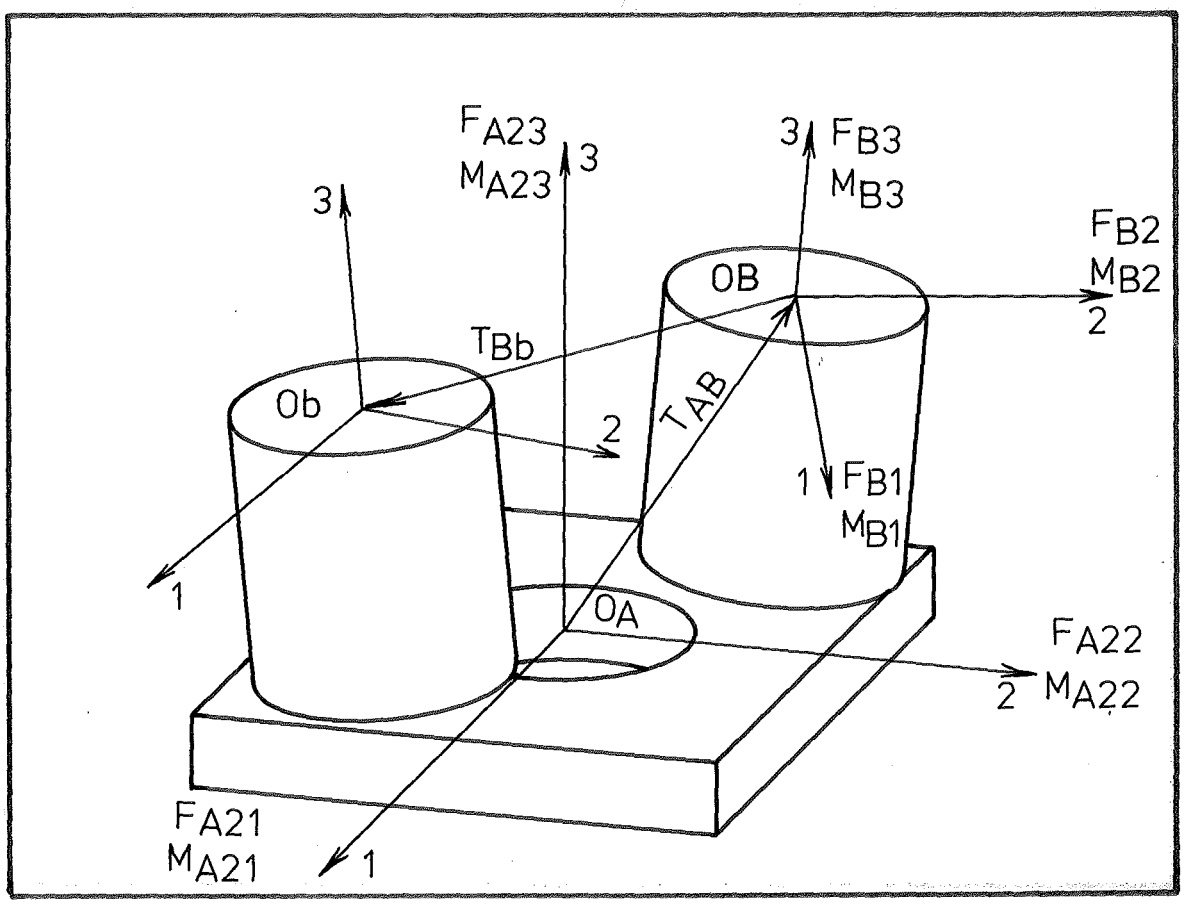

FIG. 10.2 TWO POSITIONS OF OBJECT B

$[F_{A2}]$ $[M_{A2}]$ $[F_B]$ $[M_B]$

The relationship between the two objects may now be found using the force and moment information. Using the form of Equation 10.1, the rotational relationship between the 0_A and 0_B coordinate systems is

$[R_{AB}]$

and the translation is

$[T_{AB}]$

10.2 DETERMINATION OF ROTATION TENSOR

The rotation tensor $[R_{AB}]$ may be found by the application of Rodrigues' formula as outlined by Bisshop [47].

Firstly the vector $[F_b]$ may be described as vector $[F_{b1}]$ in the $[0_B]$system by the transformation

$$[F_{b1}] = [R_{Bb}][F_b] \tag{10.2}$$

It is convenient to define the vectors

$$\underline{a_1} = [FA_1] - [F_{b1}] \qquad \underline{a_2} = [F_{A2}] - [F_B]$$

$$\underline{b_1} = [F_{A1}] + [F_{b1}] \qquad \underline{b_2} = [F_{A2}] + [F_B]$$

Then we may write

$$\underline{W} \times \underline{a_1} = \underline{b_1} \tag{10.3}$$

and

$$\underline{W} \times \underline{a_2} = \underline{b_2} \tag{10.4}$$

which is Rodrigues' formula, where $\underline{W}$ is defined as

$$\underline{W} = \begin{bmatrix} \lambda \\ \mu \\ \nu \end{bmatrix} = \tan\frac{\theta}{2} \begin{bmatrix} k \\ l \\ m \end{bmatrix} \tag{10.5}$$

λ μ ν are three parameters describing the orientation of the 0_B coordinate system with respect to the 0_A system. The 0_A system can be aligned with the 0_B system by performing a rotation θ about an axis with direction cosines k l m with respect to the 0_A system.

Manipulation of Equations 10.3 and 10.4 gives the result

$$\underline{W} = \frac{\underline{b}_1 \times \underline{b}_2}{\underline{a}_2 \cdot \underline{b}_1} = \frac{\underline{b}_2 \times \underline{b}_1}{\underline{a}_1 \cdot \underline{b}_2} \tag{10.6}$$

from which the rotation tensor $[R_{AB}]$ may be obtained [48],

i.e.

$$[R_{AB}] = \frac{1}{\Delta} \begin{bmatrix} 1 + \tfrac{1}{4}(\lambda^2-\mu^2-\nu^2) & -\nu+\tfrac{1}{2}\lambda\mu & \mu+\tfrac{1}{2}\lambda\nu \\ \nu + \tfrac{1}{2}\mu\lambda & 1 + \tfrac{1}{4}(-\lambda^2+\mu^2-\nu^2) & -\lambda+\tfrac{1}{2}\mu\nu \\ -\mu+\tfrac{1}{2}\nu\lambda & \lambda+\tfrac{1}{2}\nu\mu & 1+\tfrac{1}{4}(-\lambda^2-\mu^2+\nu^2) \end{bmatrix}$$

where

$$\Delta = 1 + \tfrac{1}{4}(\lambda^2+\mu^2+\nu^2)$$

10.3 DETERMINATION OF TRANSLATION VECTOR

Taking moments of the contact forces about axes parallel to the 0_A axes but passing through the point 0_B, see Fig. 10.2, the following equations are obtained.

$$\underline{T_{AB}} \times \underline{F_{A1}} = \underline{M_{A1}} + [R_{AB}][M_{b1}] = \underline{M_1} \tag{10.8}$$

$$\underline{T_{AB}} \times \underline{F_{A2}} = \underline{M_{A2}} + [R_{AB}][M_B] = \underline{M_2} \tag{10.9}$$

These are of the same form as Equations 10.3 and 10.4, and therefore

$$\underline{T_{AB}} = \frac{\underline{M_1} \times \underline{M_2}}{\underline{F_{A2}} \cdot \underline{M_1}} = \frac{\underline{M_2} \times \underline{M_1}}{\underline{F_{A1}} \cdot \underline{M_2}} \tag{10.10}$$

10.4 ERROR ANALYSIS

Essential to the above method of position sensing is the determination of the two lines of action of the contact forces in space, on the basis of the force and moment measurements. The effect of errors in these measurements will now be studied.

Force $[F]$ and moment $[M]$ components are measured by sensors as shown in Fig.10.3. The equation of the line of action of the force may be written as

$$x_1 = -\frac{1}{F_3}(M_2 - F_1 x_3) \tag{10.11}$$

$$x_2 = +\frac{1}{F_3}(M_1 + F_2 x_3) \tag{10.12}$$

The absolute errors in the measurement of $[F]$ and $[M]$ are $[\delta F]$ and $[\delta M]$ so the maximum error in the value of x_i is

$$\delta x_i = \sum_{j=1}^{3} \frac{\delta x_i}{\delta F_j} \delta F_j + \sum_{j=1}^{3} \frac{\delta x_i}{\delta M_j} \delta M_j \tag{10.13}$$

Applying Equation 10.13 to Equations 10.11 and 10.12

$$\delta x_1 = \frac{x_3}{F_3}\delta F_1 + \frac{M_2 - F_1 x_3}{F_3^2}\delta F_3 + \frac{-\delta M_2}{F_3}$$

$$\delta x_2 = \frac{x_3}{F_3}\delta F_1 + \frac{-(M_1 + F_2 x_3)}{F_3^2}\delta F_3 + \frac{\delta M_1}{F_3}$$

The force's line of action may therefore lie anywhere within the volume shown in Fig. 10.4. The calculated rotation tensor and translation vector are dependent upon two such contact force measurements. Fig. 10.5a shows the error envelopes of two lines of force in the x_1 x_3 plane. The error in the calculated position may then be thought of as the possible movement of the rigidly connected lines of force within the error envelopes. Qualitatively it may be seen that,

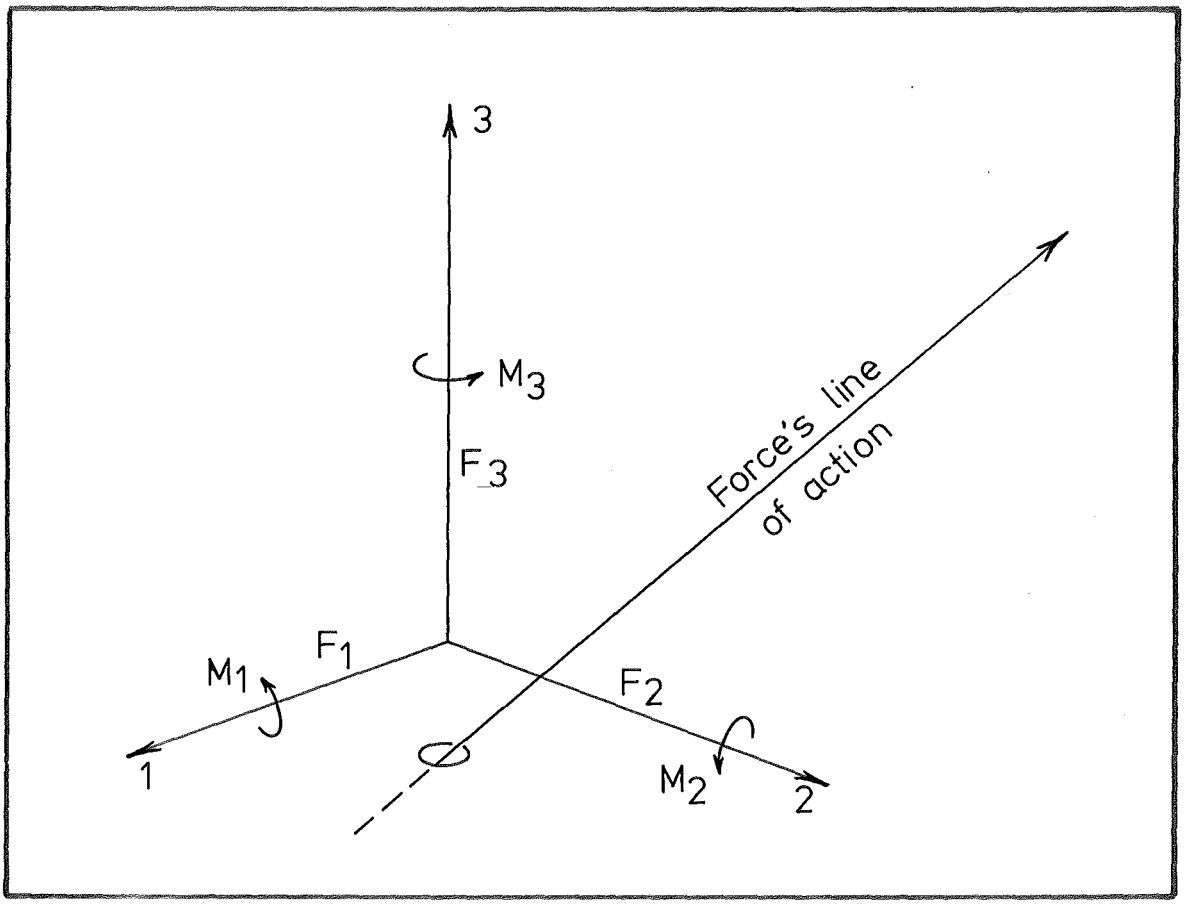

FIG. 10.3 LINE OF ACTION OF FORCE

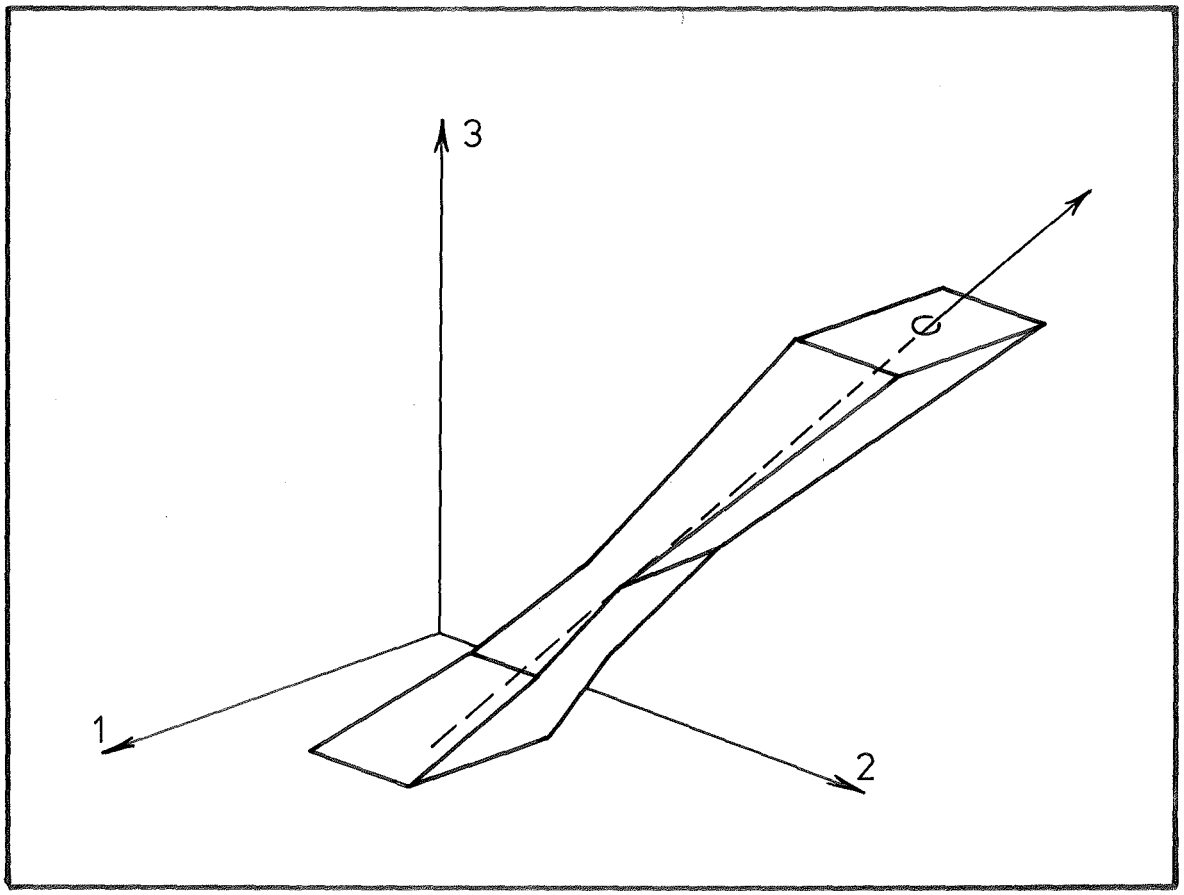

FIG. 10.4 ERROR VOLUME OF LINE OF ACTION.

FIG. 10.5

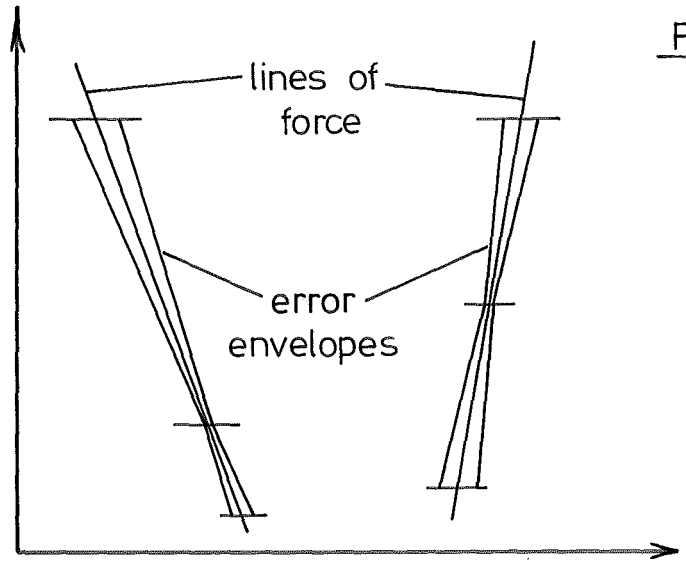

(a)

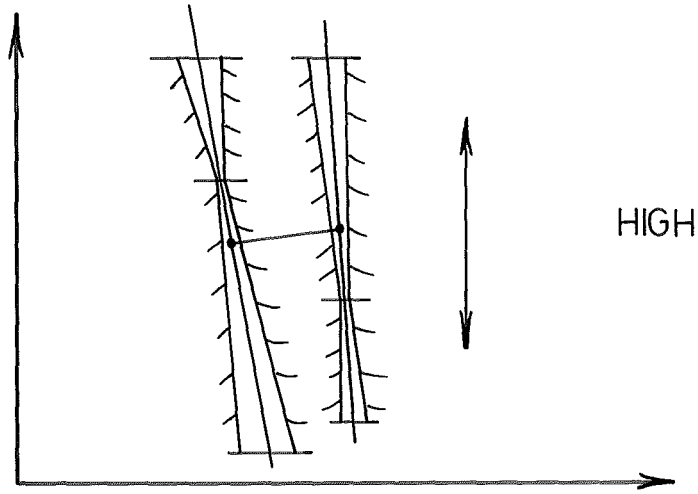

HIGH TRANSLATIONAL ERROR

(b)

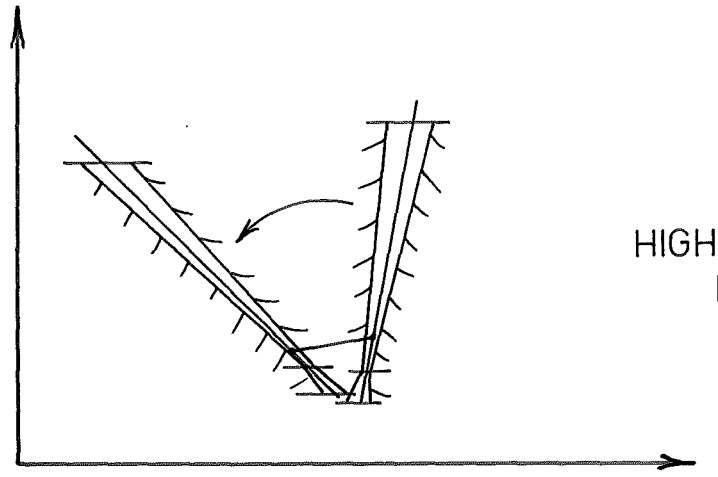

HIGH ROTATIONAL ERROR

(c)

(i) High errors in translational positioning will exist when the measured lines of action approach parallelism, Fig. 10.5b.

(ii) High rotational errors will exist when the constrictions in the constraint envelopes are both positioned close to the point where the lines have a minimum perpendicular distance between them as shown in Fig. 10.5c.

The general effect of the force sensor accuracy on the positioning accuracy may be demonstrated as follows, assuming

$$F_i = 0(F),\ M_i = 0(M),\ x_i = 0(x)$$

and

$$F_i x_j = 0(M)$$

where

0 denotes "of the order of" then Equation 10.13 gives the result

$$\frac{\delta x}{x} = 0\left(\frac{\delta F}{F}\right) = 0\left(\frac{\delta M}{M}\right) \tag{10.14}$$

x's value approximates the length of the moment arm of the contact force, and δx approximates the tolerances involved in fitting. Therefore Equation 10.14 gives the order of the resolution required from the force and moment sensors.

10.5 SUMMARY

Twin force sensor position-sensing is an accurate and deterministic method by which the relative position of two coordinate systems may be found. In assembly applications the coordinate systems are associated with the components undergoing assembly.

The potential of the method however extends beyond assembly, in that it allows flexible handling systems such as robots to be referenced spatially to their environment. Three examples where force sensor positioning could prove useful are shown in Fig. 10.6.

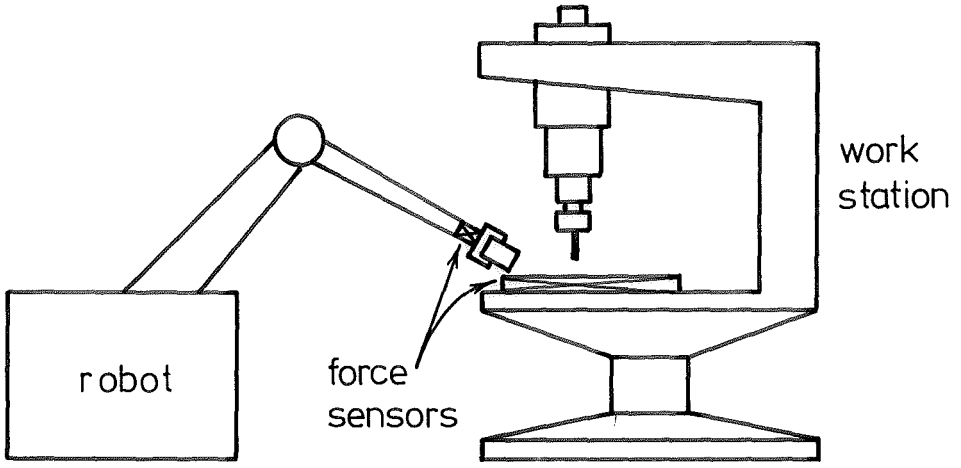

ACCURATE PLACING OF WORK ON WORK STATION.

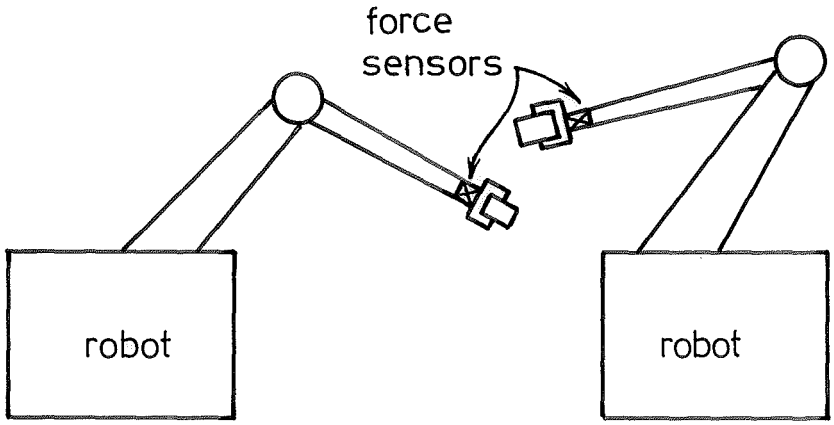

ACCURATE INTERACTION BETWEEN TWO ROBOTS.

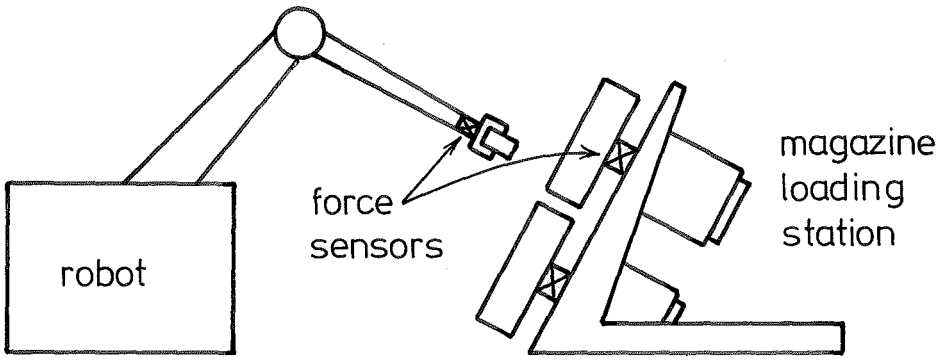

LOADING MAGAZINES

FIG.10.6 APPLICATIONS OF FORCE SENSOR POSITIONING.

PART FOUR

SIX DEGREE OF FREEDOM

FORCE/DISPLACEMENT SENSOR

CHAPTER 11

SIX DEGREE OF FREEDOM FORCE/DISPLACEMENT SENSOR

In this chapter the design and calibration of a 6 d.o.f. force/displacement sensor is outlined. The strain-gauge based sensor is capable of providing either displacement feedback for the vibratory sensing technique described in Chapter 9, or force feedback for the twin force sensor positioning method described in Chapter 10.

11.1 FORCE AND DISPLACEMENT SENSOR DESIGN

The methods described in Chapters 9 and 10 rely on either force or small displacement feedback. These demands suggest the possibility of a combination force/displacement transducer capable of measuring general forces and displacements.

The usual method of force sensing involves the measurement, generally by strain gauge, of deformations induced in the members of the force sensor structure, the structure being so designed that the effects of individual forces are decoupled and then measured by the transducers. This approach has been widely used in the design of machine tool dynamometers [49], friction test rigs [50], and wind tunnel balances.

The demands of assembly work, however, cannot be easily met by the traditional force sensor. Firstly, the deflections under load are generally of the same order of magnitude as the tolerances, thus introducing further errors into the placement task. Secondly, a complex mechanical structure is required to decouple the forces in a 6 d.o.f. sensor.

The sensing of small displacements may be performed by piezo-electric accelerometers, electromagnetic transducers or strain gauges, the latter two only being capable of static measurements. Again, the sensing of general displacements, i.e. 6 d.o.f., is made difficult by problems of cross coupling.

The interfacing of the proposed sensor with a computer has solved these problems by allowing the application of numerical techniques to the strain information.

The force and moment components, ΔF, relative to a given coordinate system, may be extracted from the strain measurements by a transformation of the form

$$[\Delta F] = \sum_{i=1}^{n} [{}_i S^1] \; [\Delta \Sigma^i] \tag{11.1}$$

i.e. each direct force or moment component ΔF is expressed as a polynomial of order n in $\Delta\Sigma$ (the strain increments). $[S^i]$ are the matrices of coefficients.*

Similarly the general displacements of the sensor Δd, may be found by the transformation

$$[\Delta d] = \sum_{i=1}^{n} [{}_i T] \; [\Delta \Sigma^i] \tag{11.2}$$

* This approach has also been used by Watson and Drake at the Stark Draper Laboratories [51] in the design of a 6 d.o.f. force sensor for robotic applications.

11.2 FINAL SENSOR DESIGN

The final design of the sensor is shown in Fig. 11.1 and Plates 11.1 and 11.2. The datum and carrier blocks, both machined to fine tolerances of squareness and parallelism, are linked by a notched bridge.

Loads applied to the carrier block induce relatively high strains at the roots of the notches. These strains are measured using six 500Ω Kyowa temperature-compensated, foil strain gauges arranged in push-pull pairs. Each series - connected pair forms one arm of an initially balanced bridge. The small voltage signals, proportional to the strain, are amplified using Datel Instrumentation amplifiers with a gain of a 1000 X and passed to a DAS.16 10 bit data-acquisition system. The resulting 10 bit digital signal is then passed via a remote terminal to the HP2100 computer for processing. The complete system is shown in Fig. 11.2.

11.3 SENSOR COORDINATE SYSTEM

The coordinate system associated with the sensor, in which the force and moment components as well as the displacements are described, is shown in Fig. 11.3. The rectangular coordinate axes X_1 X_2 X_3 are aligned along the intersections of the three faces of the datum block. The position of the carrier block is defined with respect to the 0_D system by the vector $\underline{d}$

$$[d] = \begin{bmatrix} X_1 \\ X_2 \\ X_3 \\ \lambda \\ \mu \\ \nu \end{bmatrix} \qquad (11.3)$$

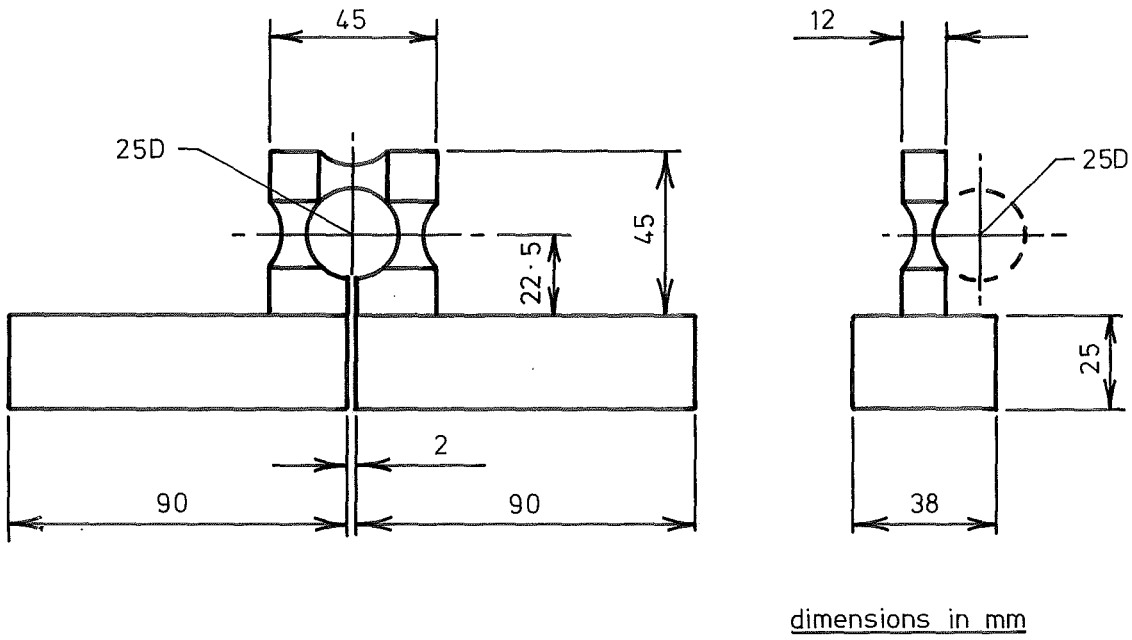

dimensions in mm

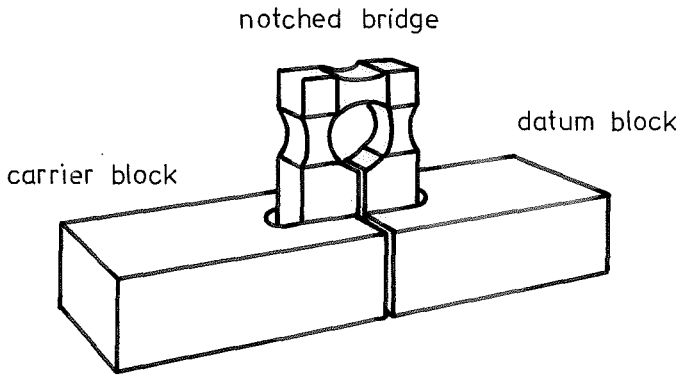

FIG. 11.1 FORCE–DISPLACEMENT SENSOR DESIGN

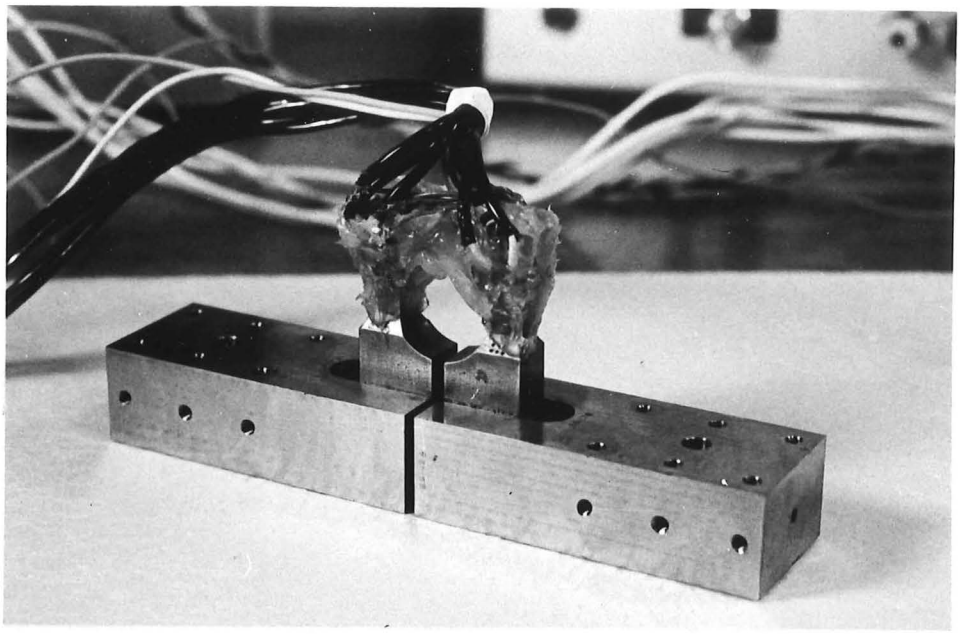

PLATE 11.1

FORCE DISPLACEMENT CENTRE

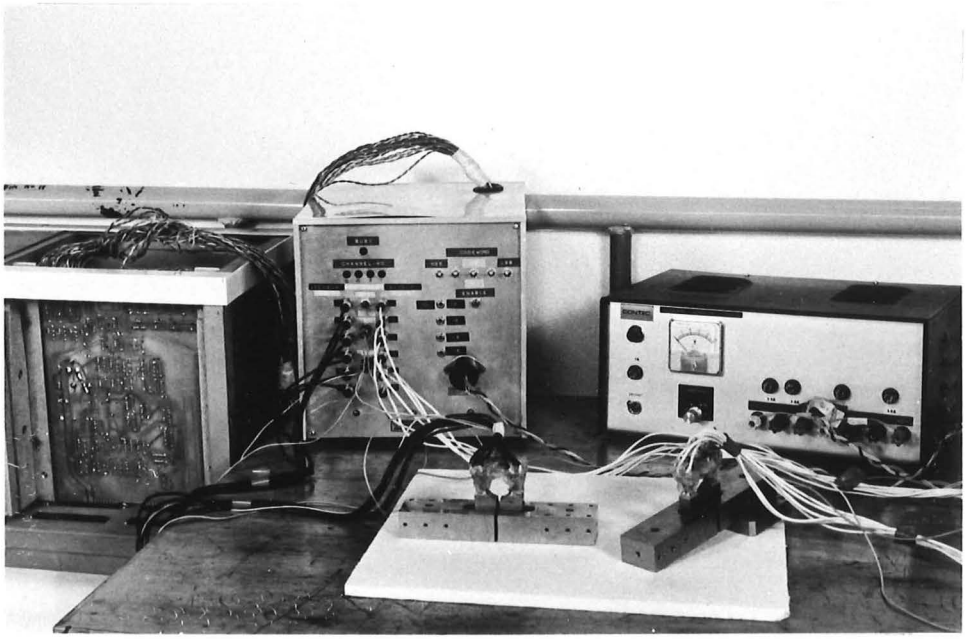

PLATE 11.2

OVERALL SYSTEM

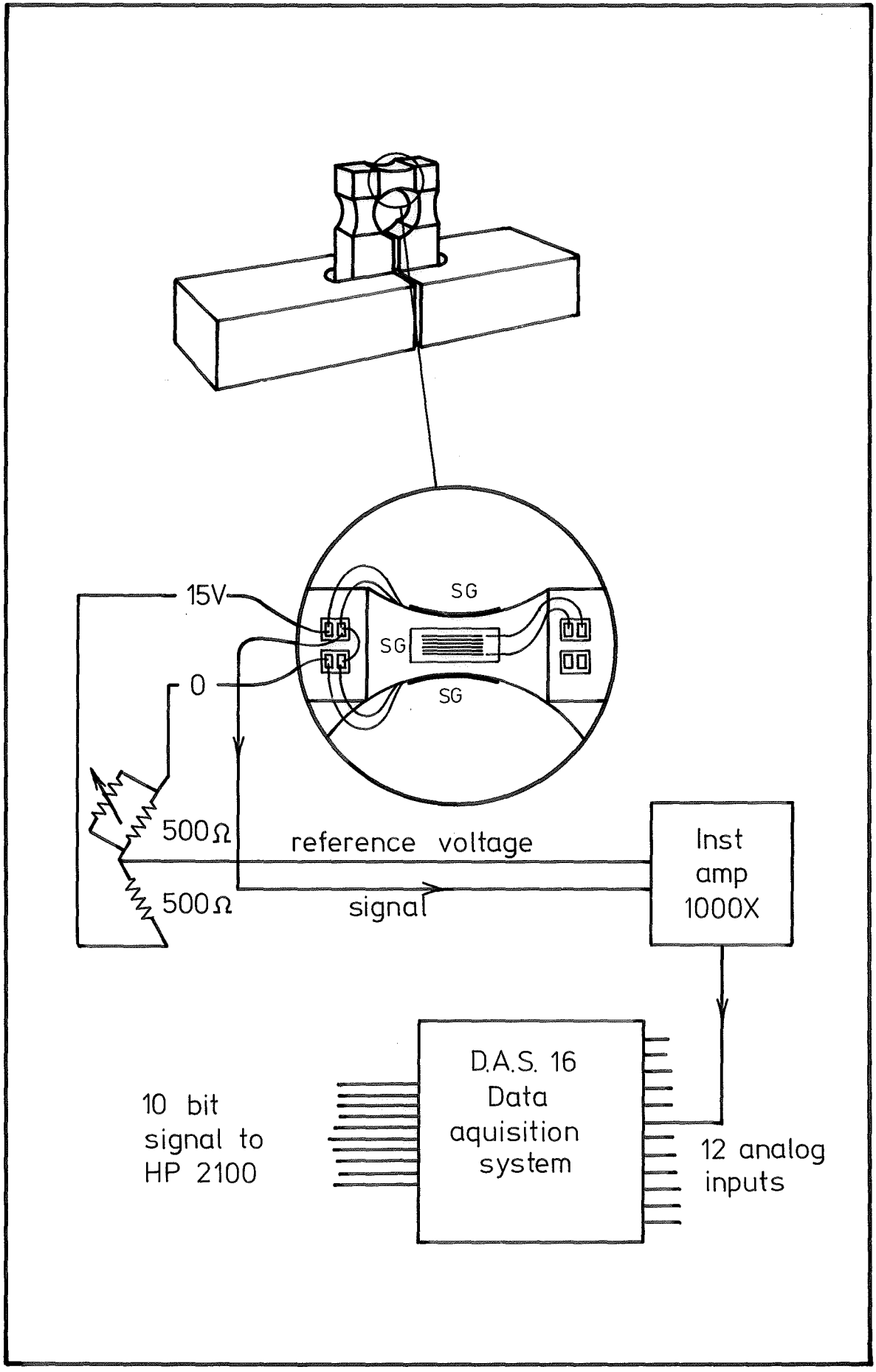

FIG. 11.2 SCHEMATIC DIAGRAM OF SENSOR SYSTEM

where X_1 X_2 X_3 define the origin of the O_C system, and λ μ ν are three parameters describing the orientation of the O_C system with respect to the O_D system. These rotation parameters are defined in Sec. 7.2, and for small values approximate rotations about the O_D axes [48].

11.4 DISPLACEMENT - STRAIN TRANSFORMATION

Small displacements from the equilibrium position due to loading may be approximated by the following second order polynomial equations.

$$\begin{bmatrix} \Delta X_1 \\ \Delta X_2 \\ \Delta X_3 \\ \Delta\lambda \\ \Delta\mu \\ \Delta\nu \end{bmatrix} = [{}_1T] \begin{bmatrix} \Sigma_1 - \Sigma_1^e \\ \Sigma_2 - \Sigma_2^e \\ \Sigma_3 - \Sigma_3^e \\ \Sigma_4 - \Sigma_4^e \\ \Sigma_5 - \Sigma_5^e \\ \Sigma_6 - \Sigma_6^e \end{bmatrix} + [{}_2T] \begin{bmatrix} (\Sigma_1 - \Sigma_1^e)^2 \\ (\Sigma_2 - \Sigma_1^e)^2 \\ (\Sigma_3 - \Sigma_3^e)^2 \\ (\Sigma_4 - \Sigma_4^e)^2 \\ (\Sigma_5 - \Sigma_5^e)^2 \\ (\Sigma_6 - \Sigma_6^e)^2 \end{bmatrix} \tag{11.4}$$

i.e.

$$[\Delta d] = [{}_1T]\,[\Delta\Sigma] + [{}_2T]\,[\Delta\Sigma^2]$$

or $$[\Delta d] = [{}_1T\,;\,{}_2T] \begin{bmatrix} \underline{\Delta\Sigma} \\ \Delta\Sigma^2 \end{bmatrix} = [T]\,[\underline{\Delta\Sigma}]$$

The elements of ${}_1T$ and ${}_2T$ are best found by experimental calibration. The calibration procedure involves applying general but known displacements to the carrier block, to produce strains which are measured. Equation 11.4 then yields 6 linear equations with the elements of $[{}_1T]$ and $[{}_2T]$ as unknowns, and the experimental strain increments as their coefficients. Performing 12 tests therefore allows us to write 72 equations.

$$\left[\underline{\underline{\Delta\Sigma}}_{\text{exp}}\right]\begin{bmatrix} {}^{1}T_{11} \\ \vdots \\ {}^{1}T_{66} \\ {}^{2}T_{11} \\ \vdots \\ {}^{2}T_{66} \end{bmatrix} = \left[\Delta d_{\text{exp}}\right] \tag{11.5}$$

from which the unknown elements of T may be obtained,

i.e.

$$\begin{bmatrix} {}^{1}T_{11} \\ \vdots \\ {}^{1}T_{66} \\ {}^{2}T_{11} \\ \vdots \\ {}^{2}T_{66} \end{bmatrix} = \left[\Delta\Sigma\right]^{-1}_{\text{exp}} \left[\Delta d\right]$$

The displacements were measured using a method suggested by McEntire [52] and revised by McCallion and Pham [52]. The method is described below.

The datum block is set in the equilibrium position, with the X_3 axis vertical, and three pairs of dial gauges, aligned parallel with the 0_p axes as shown in Fig. 11.4, measure the coordinates of points G_{11} - G_{33}, on the x_2x_3, x_3x_1, x_1x_2 planes, with respect to the translated coordinate system 0^1_D. The coordinates of G_{11} may be written as $(X^1_{11} - D, 0)$ where X^1_{11} is obtained from the adjusted dial gauge reading and D is constant. The coordinates of the other five points may be similarly specified.

By substituting these results into the equations of the three orthogonal planes forming the 0_C coordinate system, McEntire has obtained the rotation matrix $[R]$ relating the coordinate systems.

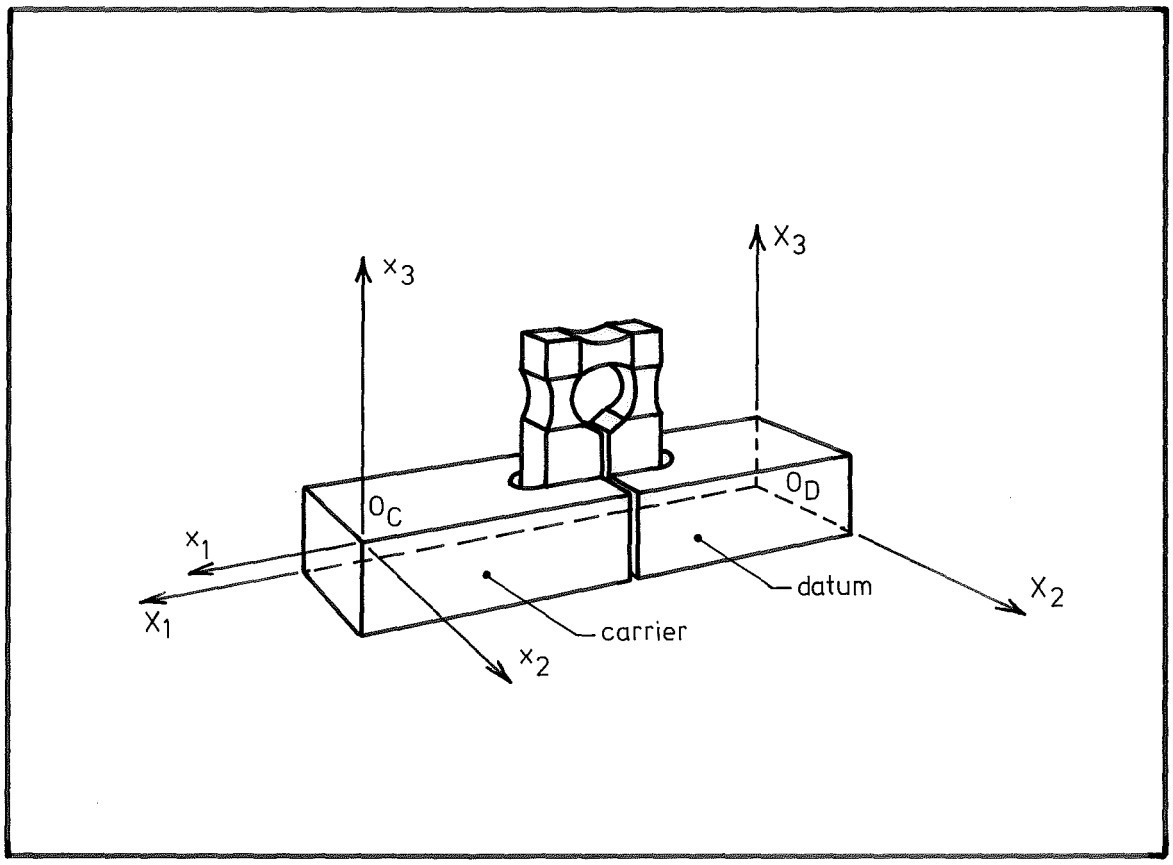

FIG. 11.3 SENSOR COORDINATE SYSTEM

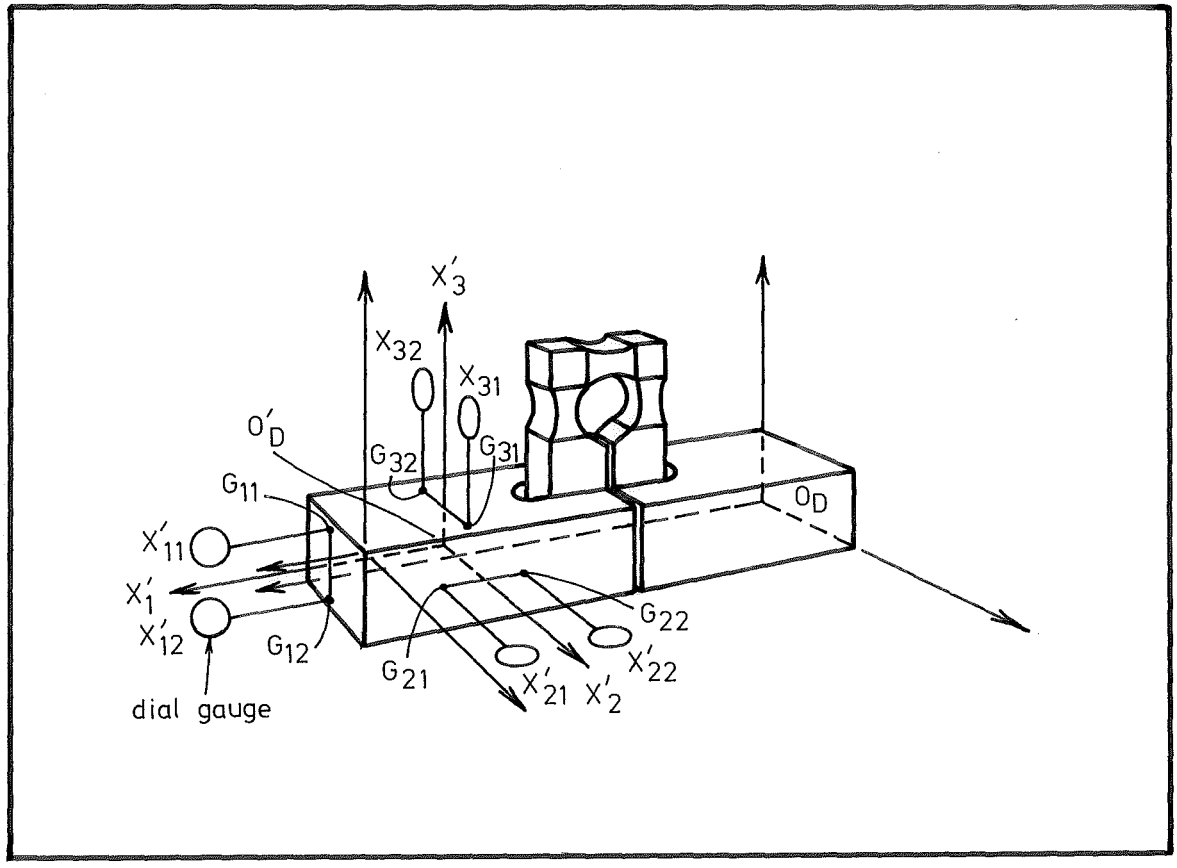

FIG. 11.4 DIAL GAUGE ARRANGEMENT

i.e. $$R_{11} = \sqrt{\left(\frac{1}{1 + D^2 + U^2}\right)}$$

$$R_{12} = ER_{11}$$

$$R_{13} = UR_{11}$$

$$R_{21} = VR_{22}$$

$$R_{22} = \sqrt{\left(\frac{1}{1 + F^2 + V^2}\right)}$$

$$R_{23} = FR_{22}$$

$$R_{31} = GR_{33}$$

$$R_{32} = WR_{33}$$

$$R_{33} = \sqrt{\left(\frac{1}{1 + G^2 + W^2}\right)}$$

and

$$E = \frac{X_{12} - X_{11}}{2D} \qquad G = \frac{X_{32} - X_{31}}{2D} \qquad V = \frac{FG - E(F^2+1)}{EFG + 1}$$

$$F = \frac{X_{22} - X_{21}}{2D} \qquad U = \frac{EF - G(E^2+1)}{EFG + 1} \qquad W = \frac{GE - F(G^2+1)}{EFG + 1}$$

The parameters λ μ ν may be obtained from the diagonal elements of $[R]$

$$\begin{bmatrix} \lambda \\ \mu \\ \nu \end{bmatrix} \qquad 2 \tan \frac{\theta}{2} \qquad \begin{bmatrix} k \\ l \\ m \end{bmatrix}$$

where

$$\theta = \cos^{-1}\left[\frac{R_{11} + R_{22} + R_{33} - 1}{2}\right]$$

$$k = \frac{R_{32} - R_{23}}{2 \sin\theta}$$

$$l = \frac{R_{13} - R_{31}}{2 \sin\theta}$$

$$m = \frac{R_{21} - R_{12}}{2 \sin\theta}$$

The position of point 0_c with respect to 0_D^1 is given by

$$\begin{vmatrix} X_1^1 \\ X_2^1 \\ X_3^1 \end{vmatrix} = [R] \begin{vmatrix} R_{11} X_{11}^1 + R_{12} D \\ R_{22} X_{21}^1 + R_{23} D \\ R_{33} X_{31}^1 + R_{31} D \end{vmatrix}$$

The displacements $[\Delta d]$ may therefore be obtained from the dial gauge readings.

11.5 FORCE-STRAIN TRANSFORMATION

For small strains, on the basis of a linearity test carried out and described in Appendix 2, it is assumed that

$$\begin{bmatrix} \Delta F_1 \\ \Delta F_2 \\ \Delta F_3 \\ \Delta M_1 \\ \Delta M_2 \\ \Delta M_3 \end{bmatrix} = [{}_1S] \begin{bmatrix} \Sigma_1 - \Sigma_1^e \\ \Sigma_2 - \Sigma_2^e \\ \Sigma_3 - \Sigma_3^e \\ \Sigma_4 - \Sigma_4^e \\ \Sigma_5 - \Sigma_5^e \\ \Sigma_6 - \Sigma_6^e \end{bmatrix} = [{}_1S] \quad [\Delta\Sigma] \qquad (11.6)$$

Again the elements of $[{}_1S]$ are best found experimentally. In this section only the elements of the first three rows of $[{}_1S]$, those relating the strains to the direct force components, will be determined.

Two sensors are aligned as shown in Fig. 11.5 in the equilibrium position with their datum block coordinate systems parallel. If contact occurs between the carrier blocks and no external forces act, then the components of the contact force in each system may be equated

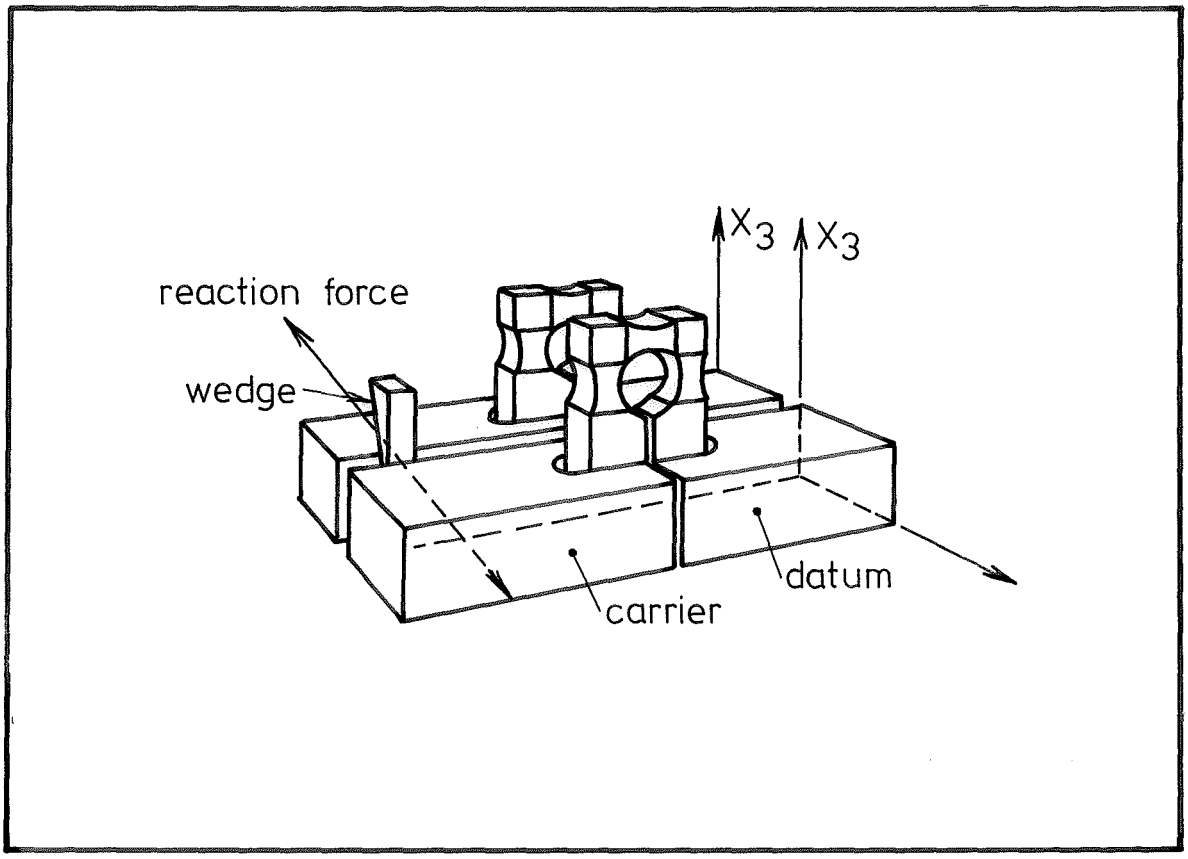

FIG. 11.5 REACTING SENSORS TO OBTAIN STRAIN MEASUREMENTS.

$$\left[\begin{matrix}\Delta F_1\\ \Delta F_2\\ \Delta F_3\end{matrix}\right]_A + \left[\begin{matrix}\Delta F_1\\ \Delta F_2\\ \Delta F_3\end{matrix}\right]_B = \left[\begin{matrix}0\end{matrix}\right] \qquad (11.7)$$

Substituting from Equation 11.6 we may rewrite Equation 11.7 in terms of the unknown transformation matrix elements of sensors A and B, and the measured strain increments $[\Delta\Sigma]_A$ $[\Delta\Sigma]_B$. Each test allows us to write 3 equations and performing a total of 11 tests allows us to write 33 homogenous equations for the 36 unknown coefficients, $[{}_1S_{11}]$ to $[{}_1S_{33}]$ in the A and B matrices. In order to convert the equations to a non-homogenous system the final three equations are obtained by applying a dead weight to sensor A as shown in Fig. 11.5. The set of 36 equations is solved to give the elements of the first three rows of the $[{}_1S]_A$ $[{}_1S]_B$ matrices.

i.e.

$$\left[\begin{matrix}1\ S_{11}\\ \vdots\\ 1\ S_{33}\\ \vdots\\ 1\ S_{33}\end{matrix}\right] = \left[\Delta\Sigma\right]^{-1}_{exp} \left[\begin{matrix}0\\ \vdots\\ 0\\ \vdots\\ Mg\\ Mg\\ Mg\end{matrix}\right] \qquad (11.8)$$

11.6 MOMENT-STRAIN TRANSFORMATION

The remaining elements of the $[{}_1S]$ transformation matrices were found by applying a series of known moments to each sensor and solving the resulting linear equations.

In practice, although the application of direct forces may be achieved without difficulty by weights, the application of a calibrating

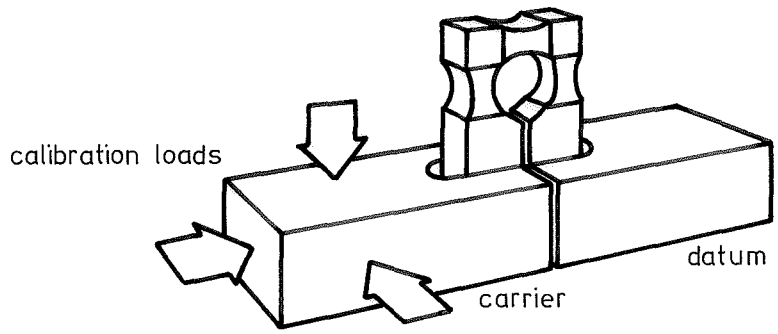

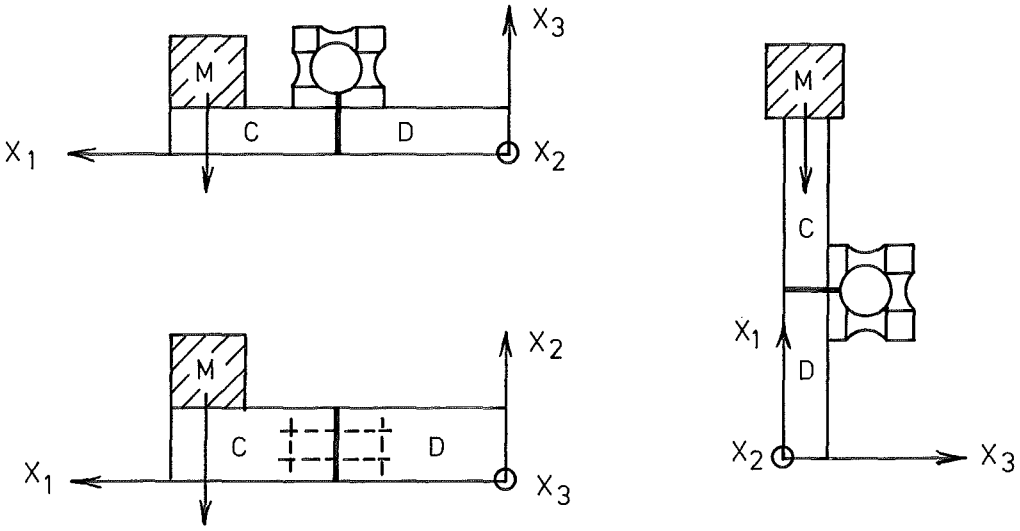

FIG. 11.6 DEAD WEIGHT CALIBRATION OF SENSOR

moment is difficult. The determination of the moment arm of the applied force is the key to the problem; in practical cases this dimension must be known to an accuracy of .01 mm. The usual methods of applying moments by means of weights on arms or pulley systems are of insufficient accuracy [51] and the following method is proposed.

Several fine indentations, P_i, are made on the carrier block, their position relative to the carrier block coordinate system being measured using a toolmakers microscope. The position of these points relative to the O_D system, P_i, may therefore be found using the transformation

$$[P_i] = [R]\,[p_i] + [X]$$

where the rotation tensor $[R]$ and vector $[X]$ may be expressed in terms of the strain increments $[\Delta\Sigma]$ corresponding to a particular loading.

A load is then applied through the indentation as shown in Fig. 11.7, and the resulting strain increments measured. The position of the point P_i under the load may be determined from Equation 11.4 and the magnitude and direction of the applied force ΔF_j may be found from Equation 11.6, using the transformation matrix elements ${}_1S_{11} - {}_1S_{33}$ already obtained. The applied moment therefore is

$$\underline{P_i} \times \underline{F_j} = \underline{M_j} \tag{11.9}$$

Eighteen such tests are carried out to provide equations which may be solved to give the unknown elements

$$\begin{bmatrix} {}_1S_{41} \\ \vdots \\ {}_1S_{66} \end{bmatrix} = [\Delta\Sigma]^{-1}_{exp} \begin{bmatrix} M_j \end{bmatrix} \tag{11.10}$$

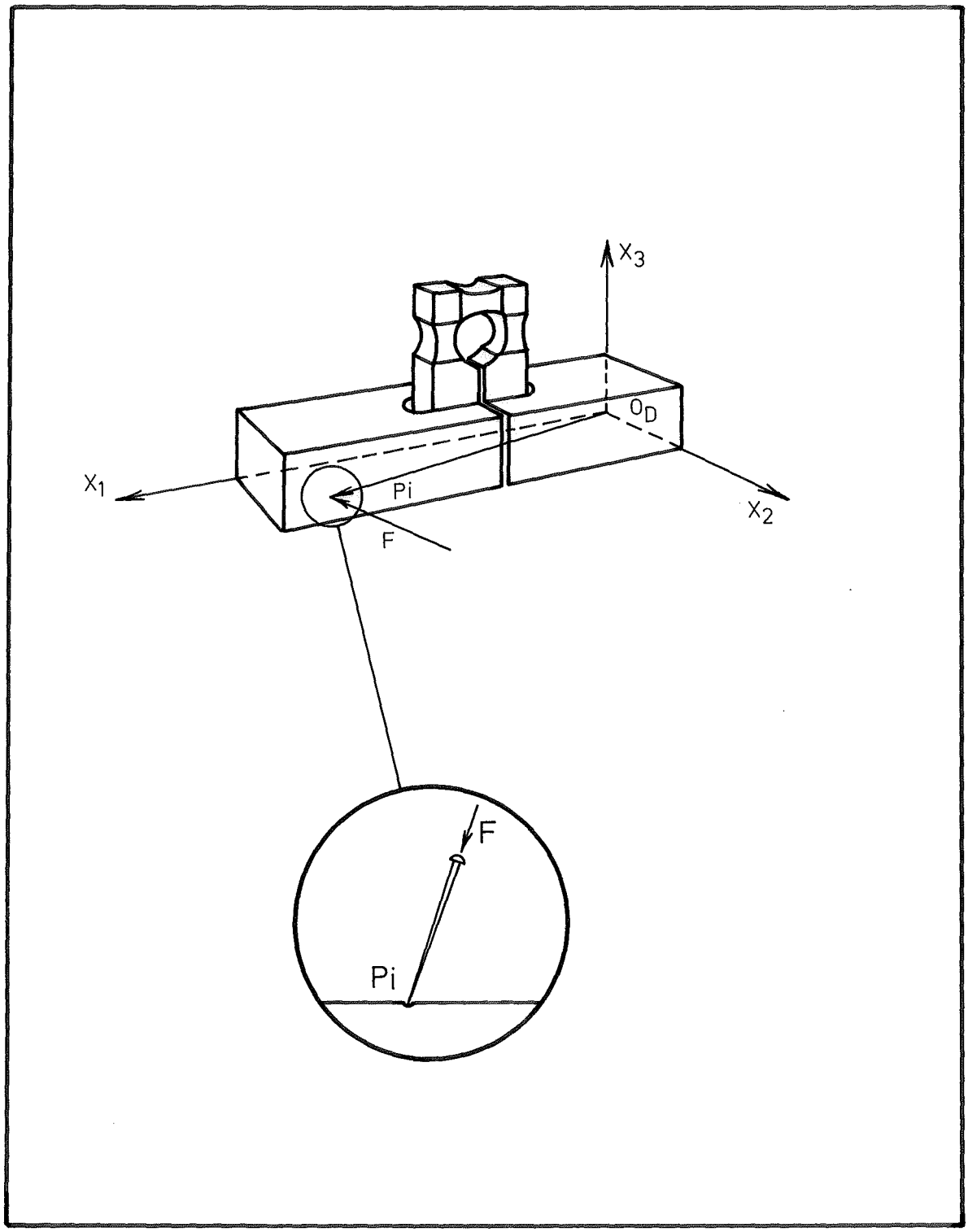

FIG. 11.7 APPLICATION OF MOMENT

11.7 SUMMARY

The force/displacement sensor described in this section avoids many of the problems associated with more conventional sensors such as deflection, cross-coupling, and inaccurate moment calibration. Actual testing is still required to prove its worth however.

CHAPTER 12

SUMMARY OF WORK

In this concluding chapter the initial goals of the research work and the main conclusions are reiterated, finally some guidelines as to future work are provided.

12.1 SUMMARY OF WORK

The aim of the research carried out was the development of techniques which would permit the use of industrial robots in assembly tasks.

In Chapter 3 it was suggested, on the basis of published work, that the assembly problem could well be generalized into the problem of fitting a peg into a hole. This restatement of the assembly task allowed a more rigorous definition of its various stages to be made. The second stage, in which the peg is moved from initial edge - edge contact with the hole to the position where its lower edge lies entirely within the projected hole cylinder, was chosen as an area for study. The remainder of the work was directed toward the resolution of this closely defined problem.

In Part 1 vibratory assembly was studied. Initially an analytical approach was taken, this involving the study of a variety of highly simplified situations. The main conclusions of this chapter of work were that:

(i) For all but excessively misaligned cases two point contact between the peg and hole edges affords the most predictable behaviour, sliding occurring toward the hole under a variety of constraint stiffnesses and exciting forces.

(ii) Single point contact between the peg and hole edges does not necessarily lead to assembly and intermittent contact at two single contact points can cause the peg to walk out of the hole.

(iii) Peg edge - hole plane contacts appear to have little effect on the translational misalignment of the peg.

These conclusions were translated into the following design features of an experimental assembly rig:

(i) The rig was designed to operate in the two point contact sliding mode, the required "tilt" being provided by a rotating moment.

(ii) Single point contact was eliminated by embodying low transverse rotational stiffnesses which ensured the pegs weight would cause it to seat squarely on the hole plane. Single point peg edge - hole plane contacts were avoided by limiting the magnitude of the applied moment.

(iii) Peg edge - hole plane contact around the peg edge, allowed by the low transverse rotational stiffnesses, was used as a "rest" mode during the cyclic assembly process.

The simple theoretical model developed to describe the behaviour of the rig agreed reasonably well with the experimental results and the following conclusions emerged:

(i) Increasing misalignment causes a marked increase in assembly time.

(ii) Increasing the magnitude of the rotating moment decreases the assembly time.

The complexity of the problem supported the adoption of a simil-ation approach, and a model of a mechanically more realistic vibratory assembly system was developed. Two computer programs based on two different sets of assumptions about contact conditions emerged, however subsequent testing showed only one of the approaches to be satisfactory.

The effects of variations in the stiffness and damping of the peg support coupling, the exciting force magnitude, and the contact force, on a typical system were found using the simulation program.

The following trends emerged in both single and double point initial contact cases.

(i) Assembly proceeded by a rotation about a single contact point, the second contact point in the double contact point case merely acting to retard the assembly.

(ii) Increasing the stiffness and damping of the flexible coupling supporting the peg increased the speed of assembly.

(iii) Increasing the magnitude of the rotating exciting force again caused the speed of assembly to increase.

(iv) An increase in contact force caused an increase in assembly speed.

(v) The assembly movement was relatively independent of the direction of rotation of the force.

Part 1 therefore describes two reasonably useful methods of achieving the second assembly stage without the use of feedback.

The major thrust of research into automated assembly at Canterbury however, has been aimed toward the development of "active" methods for assembly, i.e. those involving feedback. The initial work in this direction falls into either of the following two categories:

(i) The invention and development of assembly algorithms operating on information from displacement, force or tactile sensors.

(ii) The creation of a general purpose facility, involving computer interfaced sensors and a computer driven 6 d.o.f. manipulator, to serve as a tool for testing the methods devised in (i).

The work in the remainder of the thesis covered both these areas. In Parts 2 and 3 two assembly algorithms, based on displacement and force feedback respectively, are described. Part 4 deals with the construction and calibration of a combination 6 d.o.f. force/displacement sensor.

Unfortunately the concurrent pursuit of paths (i) and (ii) above, within this thesis meant that the experimental verification of Parts 2 and 3 could not be performed.

The use of vibratory motion as a source of feedback was investigated in Part 2. It was found that the motion of the centre of mass of a spring constrained peg acted on by a rotating force could be used to determine the mode of contact existing between the peg and hole. The most useful case was that where relatively flexible rotational constraints exist. Under these circumstances the following relationships hold between the contact mode and the peg locus.

(i) Single point contact - Elliptical locus with major or minor axis passing through the contact point.

(ii) Two point contact - Straight line segment perpendicular to the contact chord.

(iii) Three point contact - No movement.

(vi) Sliding - Circular locus.

These relationships were then combined to give two algorithms whereby an approximation to the Stage 2 misalignments could be obtained.

Although the lack of hardware prevented these overall strategies from being developed and tested, preliminary experimentation employing double integrated accelerometer measurements gave encouraging results. These tests verified the above contact mode - locus relationships.

Part 3 describes a method of position sensing based on contact force measurements made in the coordinate systems of both the peg and the hole. An error analysis of this method indicated good positioning accuracies however as with Part 2 the method was unable to be tested.

A combination force/displacement sensor was developed in response to the methods described in Parts 2 and 3. This system whose construction and calibration is set out in Part 4 ultimately will form part of the general purpose test rig described earlier.

Here again the lack of interfacing with the computer meant that calibration could not be performed. Off-line testing however indicated the performance of the system to be satisfactory.

12.2 FUTURE WORK

Future work arising out of this thesis lies in the following areas:

(i) The development of sophisticated hardware for "passive" assembly, based on the two-point-contact sliding, and single-point rotational assembly modes demonstrated in Part 1.

(ii) The methods described in Parts 2 and 3 clearly demand experimental work. The development of the "active" assembly test rig should firstly permit an evaluation of their feasibilities, and secondly allow development work in hardware and software if any potential exists.

(iii) The force/displacement sensors require calibration and testing. Work in this area could possibly extend to the development of special purpose sensors such as wrist force sensors, platform sensors etc.

Hopefully work along the lines suggested will result in the emergence of practical solutions to the assembly problem.

APPENDIX 1

LISTING OF PROGRAM B

Fortran

for use on Burroughs 6700

```
C*****************************************************
C*                                                   *
C*           PEG HOLE ASSEMBLY                       *
C*                                                   *
C*     THIS PROGRAM SIMULATES THE BEHAVIOUR OF       *
C*     A NINE-DEGREE-OF-FREEDOM PEG-HOLE             *
C*     ASSEMBLY SYSTEM.                              *
C*                                                   *
C*****************************************************
C
C
C*****************************************************
C*                                                   *
C*                  NOTES                            *
C*                                                   *
C*     1) MATRIX INVERSION SUBROUTINE "INVERT"       *
C*        MUST BE PROVIDED.                          *
C*     2) OUTPUT SUBROUTINE MUST BE PROVIDED.        *
C*                                                   *
C*****************************************************
C
      COMMON AC1,AC2,AC3,AC4,AC5,AC6,AC7,AC8,AC9,
     1AD1,AD2,AH,AI,AI3,AI4,
     2AK1,AK2,AK3,AK4,AK5,AK6,AK7,AK8,AK9,AKC,
     3AK26,AK35,AK53,AK62,ALF(3,3),
     4AM,AM1,AMUSL,AMUST,ANRM(2,3),ARH,ARP,
     5CY8,CY10,CY12,DIRT(2),GRAV,H,HLST,
     6MODE,NDIM,NUC,NUMODE,NUNUC,PERP(2,3),
     7PRLL(2,3),PRMT(5),SLIDE(2),SY8,SY10,SY12,
     8THINC,THOLD(2),XC(2,3),
     9YE2,YE8,YE10,YE14,YE16,YE18
      COMMON/DR/NUM
      DIMENSION Y(18),DERY(18)
C
CCC   READ DATA IN FREE FORMAT
C
      READ/,AC1,AC2,AC3,AC4,AC5,AC6,AC7,AC8,AC9

      READ/,AD1,AD2,AH,AI,AI3,AI4
      READ/,AK1,AK2,AK3,AK4,AK5,AK6,AK7,AK8,AK9,AKC
      READ/,AK26,AK35,AK53,AK62
      READ/,AK1,AK2,AK3,AK4,AK5,AK6,AK7,AK8,AK9,AKC
      READ/,AM,AM1,AMUSL,AMUST,ARH,ARP,GRAV,HLST
      READ/,MODE,NUMODE,NDIM
      READ/,PRMT(1),PRMT(2),PRMT(3),PRMT(4),PRMT(5)
      READ/,THINC,THOLD(1),THOLD(2)
      READ/,YE2,YE8,YE10,YE14,YE16,YE18
      READ/,Y(1),Y(2),Y(3),Y(4),Y(5),Y(6),Y(7),Y(8),Y(9)
      READ/,Y(10),Y(11),Y(12),Y(13),Y(14),Y(15),Y(16),Y(17),Y(18)
      READ/,DERY(1),DERY(2),DERY(3),DERY(4),DERY(5),DERY(6),DERY(7),
     1DERY(8),DERY(9)
      READ/,DERY(10),DERY(11),DERY(12),DERY(13),DERY(14),DERY(15),
     1DERY(16),DERY(17),DERY(18)
C
CCC   WRITE OUT DATA
C
      WRITE(6,100)
  100 FORMAT(" ******************************"/
     1       " *                            *"/
     2       " *     SYSTEM PARAMETERS      *"/
     3       " *                            *"/
     4       " ******************************"/////)
      WRITE(6,101)AD1,AD2,AH,AI,AI3,AI4,AM,AM1,
     1AMUSL,AMUST,ARH,ARP,GRAV
  101 FORMAT(" SYSTEM DIMENSIONS MASSES AND INERTIAS"/
     1       " ********************************"//
     2       "     AD1=",E14.4,"     AD2=",E14.4,"      AH=",E14.4,
     3       "      AI=",E14.4,"     AI3="/E14.4,"     AI4=",E14.4,
     4       "      AM=",E14.4,"     AM1=",E14.4,"  AMUSL=",E14.4,
     5       "  AMUST=",E14.4/"     ARH=",E14.4,"    ARP=",E14.4,
     6       "    GRAV=",E14.4///)
      WRITE(6,102)AK1,AK2,AK3,AK4,AK5,AK6,AK7,AK8,AK9,
     1            AK26,AK35,AK53,AK62
  102 FORMAT(" SYSTEM STIFFNESSES"/
     1       " ******************"//
     2       "     AK1=",E14.4,"     AK2=",E14.4,"     AK3=",E14.4,
     3       "     AK4=",E14.4,"     AK5=",E14.4/"     AK6=",E14.4,
     4       "     AK7=",E14.4,"     AK8=",E14.4,"     AK9=",E14.4,
     5       "   AK26=",E14.4/"   AK35=",E14.4,"   AK53=",E14.4,
```

```
     6         "    AK62=",E14.4///)
      WRITE(6,103)AC1,AC2,AC3,AC4,AC5,AC6,AC7,AC8,AC9
103   FORMAT(" SYSTEM DAMPING"/
     1         " ***************"//
     2         "     AC1=",E14.4,"     AC2=",E14.4,"     AC3=",E14.4,
     3         "     AC4=",E14.4,"     AC5=",E14.4/"     AC6=",E14.4,
     4         "     AC7=",E14.4,"     AC8=",E14.4,"     AC9=",E14.4,
     5        ///)
      WRITE(6,104)(Y(I),I=1,18)
104   FORMAT(" INITIAL CONDITIONS"/
     1         " ******************"//
     2         "      Y1=",E14.4,"      Y2=",E14.4,"      Y3=",E14.4,
     3         "      Y4=",E14.4,"      Y5=",E14.4/"      Y6=",E14.4,
     4         "      Y7=",E14.4,"      Y8=",E14.4,"      Y9=",E14.4,
     5         "     Y10=",E14.4/"     Y11=",E14.4,"     Y12=",E14.4,
     6         "     Y13=",E14.4,"     Y14=",E14.4,"     Y15=",E14.4/
     7         "     Y16=",E14.4,"     Y17=",E14.4,"     Y18=",E14.4///)
      WRITE(6,105)YE2,YE8,YE10,YE14,YE16,YE18
105   FORMAT(" EQUILIBRIUM POSITIONS"/
     1         " *********************"//
     2         "     YE2=",E14.4,"     YE8=",E14.4,"    YE10=",E14.4,
     3         "    YE14=",E14.4,"    YE16=",E14.4/"    YE18=",E14.4///)
      WRITE(6,106)AKC,HLST,MODE,NDIM,NUMODE,(PRMT(I),I=1,5),
     1            THINC,THOLD(1),THOLD(2)
106   FORMAT(" PROGRAM PARAMETERS"/
     1         " ******************"//
     2         "     AKC=",E14.4,"    HLST=",E14.4,"    MODE=",E14.4,
     3         "    NDIM=",E14.4," NUMODE=",E14.4/"   PRMT1=",E14.4,
     4         "   PRMT2=",E14.4,"   PRMT3=",E14.4,"   PRMT4=",E14.4,
     5         "   PRMT5=",E14.4/"   THINC=",E14.4," THOLD1=",E14.4,
     6         " THOLD2=",E14.4///)
      CALL HPCG(Y,DERY)
      WRITE(6,110)
110   FORMAT("    END OF RUN    ")
       STOP
      END
006:01F8:4   IS THE LOCATION FOR EXCEPTIONAL ACTION ON THE I/O STA
006:01FA:0   IS THE LOCATION FOR EXCEPTIONAL ACTION ON THE I/O STA
006:01FB:2   IS THE LOCATION FOR EXCEPTIONAL ACTION ON THE I/O STA
006:01FC:4   IS THE LOCATION FOR EXCEPTIONAL ACTION ON THE I/O STA
006:01FE:0   IS THE LOCATION FOR EXCEPTIONAL ACTION ON THE I/O STA
006:01FF:2   IS THE LOCATION FOR EXCEPTIONAL ACTION ON THE I/O STA
006:0200:4   IS THE LOCATION FOR EXCEPTIONAL ACTION ON THE I/O STA
006:0202:0   IS THE LOCATION FOR EXCEPTIONAL ACTION ON THE I/O STA
006:0203:2   IS THE LOCATION FOR EXCEPTIONAL ACTION ON THE I/O STA
006:0204:4   IS THE LOCATION FOR EXCEPTIONAL ACTION ON THE I/O STA
006:0206:0   IS THE LOCATION FOR EXCEPTIONAL ACTION ON THE I/O STA
006:0207:2   IS THE LOCATION FOR EXCEPTIONAL ACTION ON THE I/O STA
006:0208:4   IS THE LOCATION FOR EXCEPTIONAL ACTION ON THE I/O STA
006:020A:0   IS THE LOCATION FOR EXCEPTIONAL ACTION ON THE I/O STA
```

```
      SUBROUTINE HPCG(Y,DERY)
C
C*****************************************************
C*                                                   *
C*      SUBROUTINE HPCG SOLVES A SYSTEM OF           *
C*      FIRST ORDER ORDINARY GENERAL DIFFERENTIAL    *
C*      EQUATIONS WITH GIVEN INITIAL VALUES          *
C*                                                   *
C*****************************************************
C
C
      COMMON AC1,AC2,AC3,AC4,AC5,AC6,AC7,AC8,AC9,
     1AD1,AD2,AH,AI,AI3,AI4,
     2AK1,AK2,AK3,AK4,AK5,AK6,AK7,AK8,AK9,AKC,
     3AK26,AK35,AK53,AK62,ALF(3,3),
     4AM,AM1,AMUSL,AMUST,ANRM(2,3),ARH,ARP,
     5CY8,CY10,CY12,DIRT(2),GRAV,H,HLST,
     6MODE,NDIM,NUC,NUMODE,NUNUC,PERP(2,3),
     7PRLL(2,3),PRMT(5),SLIDE(2),SY8,SY10,SY12,
     8THINC,THOLD(2),XC(2,3),
     9YE2,YE8,YE10,YE14,YE16,YE18
      DIMENSION AUX(16,18),Y(18),DERY(18)
C
C
      N=1
      IHLF=0
      X=PRMT(1)
      H=PRMT(3)
      PRMT(5)=0.
      DO 1 I=1,NDIM
      AUX(16,I)=0.
      AUX(15,I)=DERY(I)
    1 AUX(1,I)=Y(I)
      IF(H*(PRMT(2)-X))3,2,4
C
C     ERROR RETURNS
    2 IHLF=12
      GOTO 4
    3 IHLF=13
C
C     COMPUTATION OF DERY FOR STARTING VALUES
    4 CALL FCT(X,Y,DERY)
C
C     RECORDING OF STARTING VALUES
      CALL OUTP(X,Y,DERY)
      IF(PRMT(5))6,5,6
    5 IF(IHLF)7,7,6
    6 RETURN
    7 DO 8 I=1,NDIM
    8 AUX(8,I)=DERY(I)
C
C     COMPUTATION OF AUX(2,I)
      ISW=1
      GOTO 100
C
    9 X=X+H
      DO 10 I=1,NDIM
   10 AUX(2,I)=Y(I)
C
C     INCREMENT H IS TESTED BY MEANS OF BISECTION
   11 IHLF=IHLF+1
      X=X-H
      DO 12 I=1,NDIM
   12 AUX(4,I)=AUX(2,I)
      H=.5*H
      N=1
      ISW=2
      GOTO 100
C
   13 X=X+H
      CALL FCT(X,Y,DERY)
      N=2
      DO 14 I=1,NDIM
      AUX(2,I)=Y(I)
   14 AUX(9,I)=DERY(I)
      ISW=3
      GOTO 100
C
C     COMPUTATION OF TEST VALUE DELT
   15 DELT=0.
      DO 16 I=1,NDIM
   16 DELT=DELT+AUX(15,I)* ABS(Y(I)-AUX(4,I))
      DELT=.06666667*DELT
      IF(DELT-PRMT(4))19,19,17
```

```
   17 IF(IHLF-10)11,18,18
C
C     NO SATISFACTORY ACCURACY AFTER 10 BISECTIONS. ERROR MESSAGE.
   18 IHLF=11
      X=X+H
      GOTO 4
C
C     THERE IS SATISFACTORY ACCURACY AFTER LESS THAN 11 BISECTIONS.
   19 X=X+H
      CALL FCT(X,Y,DERY)
      DO 20 I=1,NDIM
      AUX(3,I)=Y(I)
   20 AUX(10,I)=DERY(I)
      N=3
      ISW=4
      GOTO 100
C
   21 N=1
      X=X+H
      CALL FCT(X,Y,DERY)
      X=PRMT(1)
      DO 22 I=1,NDIM
      AUX(11,I)=DERY(I)
   22 Y(I)=AUX(1,I)+H*(.375*AUX(8,I)+.7916667*AUX(9,I)
     1-.2083333*AUX(10,I)+.04166667*DERY(I))
   23 X=X+H
      N=N+1
      CALL FCT(X,Y,DERY)
      CALL OUTP(X,Y,DERY)
      IF(PRMT(5))6,24,6
   24 IF(N-4)25,200,200
   25 DO 26 I=1,NDIM
      AUX(N,I)=Y(I)
   26 AUX(N+7,I)=DERY(I)
      IF(N-3)27,29,200
C
   27 DO 28 I=1,NDIM
      DELT=AUX(9,I)+AUX(9,I)
      DELT=DELT+DELT
   28 Y(I)=AUX(1,I)+.3333333*H*(AUX(8,I)+DELT+AUX(10,I))
      GOTO 23
C
   29 DO 30 I=1,NDIM
      DELT=AUX(9,I)+AUX(10,I)
      DELT=DELT+DELT+DELT
   30 Y(I)=AUX(1,I)+.375*H*(AUX(8,I)+DELT+AUX(11,I))
      GOTO 23
C
CCCCC ***************************************************************
CCCCC THE FOLLOWING PART OF SUBROUTINE HPCG COMPUTES BY MEANS OF
CCCCC RUNGE-KUTTA METHOD STARTING VALUES FOR THE NOT SELF-STARTING
C     PREDICTOR-CORRECTOR METHOD.
  100 DO 101 I=1,NDIM
      Z=H*AUX(N+7,I)
      AUX(5,I)=Z
  101 Y(I)=AUX(N,I)+.4*Z
C     Z IS AN AUXILIARY STORAGE LOCATION
C
      Z=X+.4*H
      CALL FCT(Z,Y,DERY)
      DO 102 I=1,NDIM
      Z=H*DERY(I)
      AUX(6,I)=Z
  102 Y(I)=AUX(N,I)+.2969776*AUX(5,I)+.1587596*Z
C
      Z=X+.4557372*H
      CALL FCT(Z,Y,DERY)
      DO 103 I=1,NDIM
      Z=H*DERY(I)
      AUX(7,I)=Z
  103 Y(I)=AUX(N,I)+.2181004*AUX(5,I)-3.050965*AUX(6,I)+3.832865*Z
C
      Z=X+H
      CALL FCT(Z,Y,DERY)
      DO 104 I=1,NDIM
  104 Y(I)=AUX(N,I)+.1747603*AUX(5,I)-.5514807*AUX(6,I)
     1+1.205536*AUX(7,I)+.1711848*H*DERY(I)
      GOTO(9,13,15,21),ISW
CCCCC ***************************************************************
CCCCC
CCCCC POSSIBLE BREAK-POINT FOR LINKAGE
CCCCC
```

```
C       STARTING VALUES ARE COMPUTED.
C       NOW START HAMMINGS MODIFIED PREDICTOR CORRECTOR METHOD
  200   ISTEP=3
  201   IF(N-8)204,202,204
C
C       N=8 CAUSES THE ROWS OF AUX TO CHANGE THEIR STORAGE LOCATIONS
  202   DO 203 N=2,7
        DO 203 I=1,NDIM
        AUX(N-1,I)=AUX(N,I)
  203   AUX(N+6,I)=AUX(N+7,I)
        N=7
C
C       N LESS THAN 8 CAUSES N+1 TO GET N
  204   N=N+1
C
C       COMPUTATION OF NEXT VECTOR Y
        DO 205 I=1,NDIM
        AUX(N-1,I)=Y(I)
  205   AUX(N+6,I)=DERY(I)
        X=X+H
  206   ISTEP=ISTEP+1
        DO 207 I=1,NDIM
        DELT=AUX(N-4,I)+1.333333*H*(AUX(N+6,I)+AUX(N+6,I)-AUX(N+5,I)+
       1AUX(N+4,I)+AUX(N+4,I))
        Y(I)=DELT-.9256198*AUX(16,I)
  207   AUX(16,I)=DELT
C       PREDICTOR IS NOW GENERATED IN ROW 16 OF AUX MODIFIED PREDICTOR
C       IS GENERATED IN Y. DELT MEANS AN AUXILIARY STORAGE.
C
        CALL FCT(X,Y,DERY)
C       DERIVATIVE OF MODIFIED PREDICTOR GENERATED IN DERY
C
        DO 208 I=1,NDIM
        DELT=.125*(9.*AUX(N-1,I)-AUX(N-3,I)+3.*H*(DERY(I)+AUX(N+6,I)+
       1AUX(N+6,I)-AUX(N+5,I)))
        AUX(16,I)=AUX(16,I)-DELT
  208   Y(I)=DELT+.07438017*AUX(16,I)
C
C       TEST WHETHER H MUST BE HALVED OR DOUBLED
        HMIN=HLST
        IF(NUC.EQ.NUNUC)HMIN=5
        IF((MODE.NE.NUMODE).AND.(H.GT.HMIN))GO TO 222
        DELT=0.
        DO 209 I=1,NDIM
  209   DELT=DELT+AUX(15,I)*ABS(AUX(16,I))
        IF(DELT-PRMT(4))210,222,222
C
C       H MUST NOT BE HALVED. THAT MEANS Y(I) ARE GOOD.
  210   CALL FCT(X,Y,DERY)
        HMIN=HLST
        IF(NUC.EQ.NUNUC)HMIN=5
        IF((MODE.NE.NUMODE).AND.(H.GT.HMIN))GO TO 222
        CALL OUTP(X,Y,DERY)
        IF(PRMT(5))212,211,212
  211   IF(IHLF-11)213,212,212
  212   RETURN
  213   IF(H*(X-PRMT(2)))214,212,212
  214   IF(ABS(X-PRMT(2))-.1*ABS(H))212,215,215
  215   IF(DELT-.02*PRMT(4))216,216,201
C
C
C       H COULD BE DOUBLED IF ALL NECESSARY PRECEEDING VALUES ARE
C       AVAILABLE
  216   IF(IHLF+1)201,201,217
  217   IF(N-7)201,218,218
  218   IF(ISTEP-4)201,219,219
  219   IMOD=ISTEP/2
        IF(ISTEP-IMOD-IMOD)201,220,201
  220   H=H+H
        IHLF=IHLF-1
        ISTEP=0
        DO 221 I=1,NDIM
        AUX(N-1,I)=AUX(N-2,I)
        AUX(N-2,I)=AUX(N-4,I)
        AUX(N-3,I)=AUX(N-6,I)
        AUX(N+6,I)=AUX(N+5,I)
        AUX(N+5,I)=AUX(N+3,I)
        AUX(N+4,I)=AUX(N+1,I)
        DELT=AUX(N+6,I)+AUX(N+5,I)
        DELT=DELT+DELT+DELT
  221   AUX(16,I)=8.962963*(Y(I)-AUX(N-3,I))-3.361111*H*(DERY(I)+DELT
       1+AUX(N+4,I))
        GOTO 201
C
C
```

```
C       H MUST BE HALVED
  222 IHLF=IHLF+1                                                        220
      IF(IHLF-10)223,223,210
  223 H=.5*H
      ISTEP=0
      DO 224 I=1,NDIM
      Y(I)=.00390625*(80.*AUX(N-1,I)+135.*AUX(N-2,I)+40.*AUX(N-3,I)+
     1AUX(N-4,I))-.1171875*(AUX(N+6,I)-6.*AUX(N+5,I)-AUX(N+4,I))*H
      AUX(N-4,I)=.00390625*(12.*AUX(N-1,I)+135.*AUX(N-2,I)+
     1108.*AUX(N-3,I)+AUX(N-4,I))-.0234375*(AUX(N+6,I)+18.*AUX(N+5,I)-
     29.*AUX(N+4,I))*H
      AUX(N-3,I)=AUX(N-2,I)
  224 AUX(N+4,I)=AUX(N+5,I)
      X=X-H
      DELT=X-(H+H)
      CALL FCT(DELT,Y,DERY)
      DO 225 I=1,NDIM
      AUX(N-2,I)=Y(I)
      AUX(N+5,I)=DERY(I)
  225 Y(I)=AUX(N-4,I)
      DELT=DELT-(H+H)
      CALL FCT(DELT,Y,DERY)
      DO 226 I=1,NDIM
      DELT=AUX(N+5,I)+AUX(N+4,I)
      DELT=DELT+DELT+DELT
      AUX(16,I)=8.962963*(AUX(N-1,I)-Y(I))-3.361111*H*(AUX(N+6,I)+DELT
     1+DERY(I))
  226 AUX(N+3,I)=DERY(I)
      GOTO 206
       END
```

```
      SUBROUTINE STATE(Y,DERY)
C
C*************************************************
C*     SUBROUTINE STATE DETERMINES THE MODE      *
C*     CORRESPONDING TO THE NEW PEG POSITION     *
C*                                               *
C*************************************************
C
C
      COMMON AC1,AC2,AC3,AC4,AC5,AC6,AC7,AC8,AC9,
     1AD1,AD2,AH,AI,AI3,AI4,
     2AK1,AK2,AK3,AK4,AK5,AK6,AK7,AK8,AK9,AKC,
     3AK26,AK35,AK53,AK62,ALF(3,3),
     4AM,AM1,AMUSL,AMUST,ANRM(2,3),ARH,ARP,
     5CY8,CY10,CY12,DIRT(2),GRAV,H,HLST,
     6MODE,NDIM,NUC,NUMODE,NUNUC,PERP(2,3),
     7PRLL(2,3),PRMT(5),SLIDE(2),SY8,SY10,SY12,
     8THINC,THOLD(2),XC(2,3),
     9YE2,YE8,YE10,YE14,YE16,YE18
      DIMENSION Y(18),DERY(18)
      DIMENSION A(12,12),G(2),POINT(2),THET(2)
     1,VC(2,3),VCN(2,3),VCP(2,3),XP(2,3),AINV(12,12)
      DOUBLE PRECISION DETERM
C
C
C     SEARCH FOR CONTACT POINTS
C
      CALL TOUCH(G,THET,Y,DERY)
C
C     TRANSFORM COORDINATES
C
      DO 10 I=1,2
      XP(I,1)=-ARP*SIN(THET(I))
      XP(I,2)=ARP*COS(THET(I))
 10   XP(I,3)=-AH
      DO 20 I=1,2
      DO 20 J=1,3
      XC(I,J)=0
      DO 20 K=1,3
 20   XC(I,J)=XC(I,J)+XP(I,K)*ALF(K,J)+Y(2*J)/3
C
C     DETERMINE NUMBER OF CONTACT POINTS
C
      NUMK=0
      IF((G(1).LE.0).OR.(G(2).LE.0))NUMK=1
      IF((G(1).LE.0).AND.(G(2).LE.0))NUMK=2
      IF(NUMK-1.0)110,40,30
C
C     CHECK IF DOUBLE CONTACT OCCURS AT ONE POINT
C
 30   TOL1=.1
      DO 31 J=1,3
 31   SUM=SUM+ABS(XC(1,J)-XC(2,J))
      IF(SUM.LE.TOL1)NUMK=1
      SUM=0
      GO TO 50
C
C     RELABEL SINGLE CONTACT POINT IF REQUIRED
C
 40   IF(G(1).LE.0)GO TO 50
      DO 41 I=1,3
      XP(1,I)=XP(2,I)
 41   XC(1,I)=XC(2,I)
C
C
C     2ND LOOP TO FIND CONTACT NORMAL AND PLANE VECTORS
C
 50   CONTINUE
      DO 110 I=1,NUMK
C
C     FIND CONTACT NORMAL
C
      A(1,1)=XC(I,3)
      A(1,2)=-XC(I,2)
      A(2,1)=XP(I,2)*ALF(1,2)-XP(I,1)*ALF(2,2)
      A(2,2)=XP(I,2)*ALF(1,3)-XP(I,1)*ALF(2,3)
      N=2
      NM=12
      CALL INVERT(NM,N,A,AINV,DETERM)
      C1=-(XP(I,2)*ALF(1,1)-XP(I,1)*ALF(2,1))
      ANRM(I,1)=1
      ANRM(I,2)=AINV(1,2)*C1
      ANRM(I,3)=AINV(2,2)*C1
```

```
      DO 62 J=1,3
 62   SUM=SUM+ANRM(I,J)**2
      SUM=SQRT(SUM)
      DO 63 J=1,3
 63   ANRM(I,J)=ANRM(I,J)/SUM
      SUM=0
C
CCC   FIND CONTACT POINT VELOCITY
C
 70   XC1=XC(I,1)-Y(2)
      XC2=XC(I,2)-Y(4)
      XC3=XC(I,3)-Y(6)
      VC(I,1)=-XC2*Y(7)+XC3*CY8*Y(9)+(XC3*SY8*SY10-XC2*CY10)*Y(11)+Y(1)
      VC(I,2)=XC1*Y(7)+XC3*SY8*Y(9)+(XC1*CY10-XC3*CY8*SY10)*Y(11)+Y(3)
      VC(I,3)=(-XC1*CY8-XC2*SY8)*Y(9)+(XC2*CY8*SY10-XC1*SY8*SY10)*Y(11)
     1        +Y(5)
C
CCC   FIND CONTACT POINT NORMAL AND PLANE VELOCITY
C
      DO 80 J=1,3
 80   SUM=SUM+VC(I,J)*ANRM(I,J)
      DO 81 J=1,3
 81   VCN(I,J)=SUM*ANRM(I,J)
      SUM=0
      DO 82 J=1,3
 82   VCP(I,J)=VC(I,J)-VCN(I,J)
C
CCC   FIND CONTACT POINT PLANE MOVEMENT DIRECTION VECTOR
C
      DO 90 J=1,3
 90   SUM=SUM+VCP(I,J)**2
      SLIDE(I)=SQRT(SUM)
      SUM=0
      IF(SLIDE(I).GT..01)GO TO 93
      PRLL(I,2)=-XC(I,2)
      PRLL(I,3)=-XC(I,3)
      PRLL(I,3)=(XC(I,2)*ANRM(I,2)+XC(I,3)*ANRM(I,3))/ANRM(I,1)
      DO 91 J=1,3
 91   SUM=SUM+PRLL(I,J)**2
      SUM=SQRT(SUM)
      DO 92 J=1,3
 92   PRLL(I,J)=PRLL(I,J)/SUM
      SUM=0
      GO TO 95
 93   DO 94 J=1,3
 94   PRLL(I,J)=VCP(I,J)/SLIDE(I)
 95   CONTINUE
      PERP(I,1)=ANRM(I,2)*PRLL(I,3)-ANRM(I,3)*PRLL(I,2)
      PERP(I,2)=ANRM(I,3)*PRLL(I,1)-ANRM(I,1)*PRLL(I,3)
      PERP(I,3)=ANRM(I,1)*PRLL(I,2)-ANRM(I,2)*PRLL(I,1)
C
CCC   FIND DIRECTION OF TRAVEL IN NORMAL DIRECTION AT CONTACT
C
      DO 100 J=1,3
 100  SUM=SUM+VCN(I,J)*ANRM(I,J)
      DIRT(I)=SUM
      SUM=0
      POINT(I)=0
      IF((DIRT(I).LE.3 ).AND.(SLIDE(I).GT.15))POINT(I)=1
      IF((DIRT(I).LE.3 ).AND.(SLIDE(I).LE.15))POINT(I)=2
 110  CONTINUE
C
CCCC  END OF LOOP
C
CCCCC  DETERMINE NUMODE
C
      GO TO (150,160,170)NUMK+1
C
CC    NUMK=0
C
 150  NUMODE=0
      RETURN
C
CCC   NUMK=1
C
 160  NUMODE=POINT(1)
      RETURN
C
CC    NUMK=2
C
 170  IF((POINT(1).EQ.0).AND.(POINT(2).EQ.0))NUMODE=0
      IF((POINT(1).EQ.1).AND.(POINT(2).EQ.0))NUMODE=1
      IF((POINT(1).EQ.2).AND.(POINT(2).EQ.0))NUMODE=2
      IF((POINT(1).EQ.1).AND.(POINT(2).EQ.1))NUMODE=3
      IF((POINT(1).EQ.2).AND.(POINT(2).EQ.1))NUMODE=4
```

```
      IF((POINT(1).EQ.2).AND.(POINT(2).EQ.2))NUMODE=5
      IF((POINT(1).EQ.0).AND.(POINT(2).EQ.1))NUMODE=6
      IF((POINT(1).EQ.0).AND.(POINT(2).EQ.2))NUMODE=7
      IF((POINT(1).EQ.1).AND.(POINT(2).EQ.2))NUMODE=8
      GO TO (171,171,171,171,171,171,172,172,175)NUMODE+1
  171 RETURN
C
CC     RELABEL CONTACT POINTS
C
  172  DO 173 J=1,3
      XC(1,J)=XC(2,J)
      ANRM(1,J)=ANRM(2,J)
      PERP(1,J)=PERP(2,J)
  173 PRLL(1,J)=PRLL(2,J)
      NUMODE=NUMODE-5
      RETURN
C
  175 DO 176 J=1,3
      VC(1,J)=XC(1,J)
      VCN(1,J)=ANRM(1,J)
      VCP(1,J)=PRLL(1,J)
      XP(1,J)=PERP(1,J)
      XC(1,J)=XC(2,J)
      ANRM(1,J)=ANRM(2,J)
      PRLL(1,J)=PRLL(2,J)
      PERP(1,J)=PERP(2,J)
      XC(2,J)=VC(1,J)
      ANRM(2,J)=VCN(1,J)
      PRLL(2,J)=VCP(1,J)
      PERP(2,J)=XP(1,J)
  176 CONTINUE
      NUMODE=4
      RETURN
      END
```

```
      SUBROUTINE TOUCH(F,THET,Y,DERY)
C
C*****************************************************
C*    SUBROUTINE TOUCH FINDS THE MINIMUM OF THE      *
C*    P/C FUNCTION DESCRIBING THE VOLUMES OF THE     *
C*    PEG AND HOLE ; THIS CORRESPONDS TO THE         *
C*    CONTACT POINT(S). SEARCH IS CARRIED OUT        *
C*    AROUND THE PEG EDGE USING A BISECTION          *
C*    METHOD.                                        *
C*                                                   *
C*****************************************************
C
C
      COMMON AC1,AC2,AC3,AC4,AC5,AC6,AC7,AC8,AC9,
     1AD1,AD2,AH,AL,AI3,AI4,
     2AK1,AK2,AK3,AK4,AK5,AK6,AK7,AK8,AK9,AKC,
     3AK26,AK35,AK53,AK62,ALF(3,3),
     4AM,AM1,AMUSL,AMUST,ANRM(2,3),ARH,ARP,
     5CY8,CY10,CY12,DIRT(2),GRAV,H,HLST,
     6MODE,NDIM,NUC,NUMODE,NUNUC,PERP(2,3),
     7PRLL(2,3),PRMT(5),SLIDE(2),SY8,SY10,SY12,
     8THINC,THOLD(2),XC(2,3),
     9YE2,YE8,YE10,YE14,YE16,YE18
      DIMENSION Y(18),DERY(18)
      DIMENSION F(2),THET(2),XH(3),XP(3)
C
C
      T=1.E-6
      C=.75E-3
      I=0
      DO 5 J=1,2
 5    THET(J)=THOLD(J)
C
 10   I=I+1
      THINK=THINC
      IF(I.EQ.3)GO TO 20
 11   CONTINUE
C
CCC   FIND P/C FUNCTION VALUES
C
      RET=1
      GO TO 30
 12   CONTINUE
      FWUN=F(1)
      THET(I)=THET(I)+.1E-4
      RET=2
      GO TO 30
C
CCC   BISECTION METHOD USING SLOPE CHANGE AS HALVING CRITERION
C
 13   CONTINUE
      GLAST=GRAD
      GRAD=1.E5*(F(I)-FWUN)
      IF(GRAD*GLAST.LT.0)THINK=THINK/2
      IF(GRAD.LE.0)THET(I)=THET(I)+THINK
      IF(GRAD.GT.0)THET(I)=THET(I)-THINK
      IF(THINK.LE..0005) GO TO 10
      GO TO 11
 20    THINC=.01
      DO 25 I=1,2
 25   THOLD(I)=THET(I)
      IF(ABS(THET(1)-THET(2)).GT..05)RETURN
      THINC=.5
      THOLD(1)=0
      THOLD(2)=3.1416
      RETURN
C
CCC   P/C FUNCTION IS WORKED OUT IN THIS SECTION
C
 30    CONTINUE
C
CCC   TRANSFORM TO SUITABLE COORDS
C
      XP(1)=-ARP*SIN(THET(I))
      XP(2)=ARP*COS(THET(I))
      XP(3)=-AH
      DO 35 K=1,3
      XH(K)=0
      DO 35 J=1,3
 35   XH(K)=XH(K)+ALF(J,K)*XP(J)+Y(2*K)/3
C
CCC   CALCULATE INEQUALITIES
C
      GH1=(-XH(2)*XH(2)-XH(3)*XH(3)+ARH*ARH)/ARH
```

```
      GH2=XH(1)
C
CC    CALCULATE P/C FUNCTION VALUE VAL
C
      VH1=SQRT(GH1*GH1+T)
      VH2=SQRT(GH2*GH2+T)
      V=GH1+GH2+VH1+VH2
        F(1)=.5*(V-T/V)+C
      GO TO (12,13)RET
      END
```

```
      SUBROUTINE FCT(X,Y,DERY)
C
CC*****************************************************
C*                                                    *
C*     SUBROUTINE FCT CONTAINS EQUATIONS OF           *
C*     MOTION OF SYSTEM AND CONTACT CONDITIONS.       *
C*     DERY VALUES FOR HPCG ARE OBTAINED HERE         *
C*                                                    *
CC*****************************************************
CCC
C
      COMMON AC1,AC2,AC3,AC4,AC5,AC6,AC7,AC8,AC9,
     1AD1,AD2,AH,AI,AI3,AI4,
     2AK1,AK2,AK3,AK4,AK5,AK6,AK7,AK8,AK9,AKC,
     3AK26,AK35,AK53,AK62,ALF(3,3),
     4AM,AM1,AMUSL,AMUST,ANRM(2,3),ARH,ARP,
     5CY8,CY10,CY12,DIRT(2),GRAV,H,HLST,
     6MODE,NDIM,NUC,NUMODE,NUNUC,PERP(2,3),
     7PRLL(2,3),PRMT(5),SLIDE(2),SY8,SY10,SY12,
     8THINC,THOLD(2),XC(2,3),
     9YE2,YE8,YE10,YE14,YE16,YE18
      DIMENSION Y(18),DERY(18)
       DIMENSION A(12,12),AINV(12,12),AST(6,6),DARY(12),FC(6)

      DOUBLE PRECISION DETERM
C
CCCC
CC
      WORK OUT ROTATION TENSOR RELATING X AND XP SYSTEMS
C
      CY8= COS(Y(8))
      SY8= SIN(Y(8))
      CY10= COS(Y(10))
      SY10= SIN(Y(10))
      SY12= SIN(Y(12))
      CY12= COS(Y(12))
      ALF(1,1)=CY8*CY10*CY12-SY8*SY12
      ALF(1,2)=SY8*CY10*CY12+CY8*SY12
      ALF(1,3)=-SY10*CY12
      ALF(2,1)=-CY8*CY10*SY12-SY8*CY12
      ALF(2,2)=-SY8*CY10*SY12+CY8*CY12
      ALF(2,3)=SY10*SY12
      ALF(3,1)=CY8*SY10
      ALF(3,2)=SY8*SY10
      ALF(3,3)=CY10
      ALF11=ALF(1,1)
      ALF12=ALF(1,2)
      ALF13=ALF(1,3)
      ALF21=ALF(2,1)
      ALF22=ALF(2,2)
      ALF23=ALF(2,3)
      ALF31=ALF(3,1)
      ALF32=ALF(3,2)
      ALF33=ALF(3,3)
      CALL STATE(Y,DERY)
 1     CONTINUE
C
CCC
C
      FIX NUMBER OF CONTACT POINTS
C
      NUNUC=1
      IF(NUMODE.EQ.0)NUNUC=0
      IF(NUMODE.GE.3)NUNUC=2
C
CCC
C
      SET VARIABLE VALUES FROM ARRAY
C
      Y1=Y(1)
      Y2=Y(2)
      Y3=Y(3)
      Y4=Y(4)
      Y5=Y(5)
      Y6=Y(6)
      Y7=Y(7)
      Y8=Y(8)
      Y9=Y(9)
      Y10=Y(10)
      Y11=Y(11)
      Y12=Y(12)
      Y13=Y(13)
      Y14=Y(14)
      Y15=Y(15)
      Y16=Y(16)
      Y17=Y(17)
      Y18=Y(18)
      XC11=XC(1,1)-Y(2)
      XC12=XC(1,2)-Y(4)
```

```
      XC13=XC(1,3)-Y(6)
      XC21=XC(2,1)-Y(2)
      XC22=XC(2,2)-Y(4)
      XC23=XC(2,3)-Y(6)
C
CCC   CALCULATE COUPLING FORCES
C
      FK1=AK1*(AD2*ALF31+Y2-YE2)
      FK2=AK2*(AD2*ALF32+Y4-Y14)
      FOK2=(AK26+AK62)*(Y8-YE8)
      FK3=AK3*(AD2*ALF33+Y6-Y16)
      FOK3=(AK35+AK53)*(Y10-YE10)
      FK4=AK4*(Y12-Y18)
      FOK6=(AK26+AK62)*(FK2/AK2+AD2*ALF31*(Y8-YE8))
      FK5=AK5*(Y10-YE10)
      FOK5=(AK35+AK53)*(FK3/AK3-AD2*SY10*(Y10-YE10))
      FK6=AK6*(Y8-YE8)
      FK7=AK7*(Y14-YE14)
      FK8=AK8*(Y16-YE16)
      FK9=AK9*(Y18-YE18)
      FC1=AC1*(Y1+AD2*(ALF33*Y9*CY8-ALF32*Y7))
      FC2=AC2*(Y3+AD2*(ALF31*Y7+ALF33*Y9*SY8)-Y13)
      FC3=AC3*(Y5-AD2*Y9*SY10-Y15)
      FC4=AC4*(-Y9*SY8+Y11*ALF31-Y17)
      FC5=AC5*(Y9*CY8+Y11*ALF32)
      FC6=AC6*(Y7+Y11*ALF33)
      FC7=AC7*Y13
      FC8=AC8*Y15
      FC9=AC9*Y17
C
CCC   CALCULATE EXCITING FORCES AND MOMENTS
C
      AF1=300*COS(1000*X)
      AF2=300*SIN(1000*X)
      MP1=-AD1*AF2
      MP2=AD1*AF1
C
CCC   EQUATIONS OF MOTION
C
      DARY(1)=(ALF11*AF1+ALF21*AF2+ALF31*AF3-AM*GRAV-FK1-FC1)/AM
      DERY(2)=Y(1)
      DARY(2)=(ALF12*AF1+ALF22*AF2+ALF32*AF3-FK2-FC2)/AM
     1-FOK2/AM
      DERY(4)=Y(3)
      DARY(3)=(ALF13*AF1+ALF23*AF2+ALF33*AF3-FK3-FC3)/AM
     1-FOK3/AM
      DERY(6)=Y(5)
      DARY(4)=((
     1 +(CY12+CY10*CY10*CY12)*MP1+(-SY12-CY10*CY10*SY12)*MP2)/(-SY10)
     2 -FK1*(-AD2*ALF32)
     3 -FK2*(AD2*ALF31)
     4 +FK4*CY10
     6 -FK6
     6 -FOK6
     7 -FC1*(-AD2*ALF32)
     8 -FC2*(AD2*ALF31)
     9 -FC4*(-CY10*ALF31)
     A -FC5*(-CY10*ALF32)
     B -FC6*(1-CY10*CY10)
     C -AI*(2*Y7*Y9*CY10*SY10)
     D -AI3*(-Y7*Y9*CY10*SY10-Y9*Y11*SY10)
     E )/(AI*SY10*SY10)
      DERY(8)=Y(7)
      DARY(5)=((-SY10*SY12*MP1-SY10*CY12*MP2)/(-SY10)
     1 -FK1*(AD2*CY8*CY10)
     2 -FK2*(AD2*SY8*CY10)
     3 -FK3*(-AD2*SY10)
     5 -FK5
     1-FOK5
     7 -FC1*(AD2*CY8*CY10)
     8 -FC2*(AD2*SY8*CY10)
     9 -FC3*(-AD2*SY10)
     A -FC4*(-SY8)
     B -FC5*(CY8)
     C -AI*(-Y7*Y7*SY10*CY10)
     D -AI3*(Y7*Y7*SY10*CY10+Y7*Y11*SY10)
     E )/AI
      DERY(10)=Y(9)
      DARY(6)=((-CY10*CY12*MP1-CY10*SY12*MP2)/(-SY10)
     1 -FK4-FC4*ALF31
     2 -FC5
     2 -FC6
     4-AI3*(DARY(4)*CY10-Y7*Y9*SY10)
     5 )/AI3
      DERY(12)=Y(11)
```

```
      DERY(13)=(FK2+FC2+FOK2-FK7-FC7)/AM1
      DERY(14)=Y(13)
      DERY(15)=(FK3+FC3+FOK3-FK8-FC8)/AM1
      DERY(16)=Y(15)
      DERY(17)=(FK4+FC4-FK9-FC9)/AI4
      DERY(18)=Y(17)
C
      IF(NUMODE.NE.0)GO TO 200
C
CCC   NUMODE=0
C
      DO 11 J=1,6
 11   DERY(2*J-1)=DARY(J)
      RETURN
C
CCC   SET ELEMENTS OF MATRIX A
C
 200  DO 201 I=1,12
      DO 201 J=1,12
 201  A(I,J)=0
      DO 210 I=1,6
 210  A(I,I)=1.0
      A(1,7)=-1/AM
      A(1,10)=-1/AM
      A(2,8)=-1/AM
      A(2,11)=-1/AM
      A(3,9)=-1/AM
      A(3,12)=-1/AM
      A(4,7)=(2*SY8*CY10*XC13+SY10*XC12)/(AI*(SY10**3))
      A(4,8)=(-2*CY8*CY10*XC13-SY10*XC11)/(AI*(SY10**3))
      A(4,9)=(2*CY8*CY10*XC12-2*SY8*CY10*XC11)/(AI*(SY10**3))
      A(4,10)=(2*SY8*CY10*XC23+SY10*XC22)/(AI*(SY10**3))
      A(4,11)=(-2*CY8*CY10*XC23-SY10*XC21)/(AI*(SY10**3))
      A(4,12)=(2*CY8*CY10*XC22-2*SY8*CY10*XC21)/(AI*(SY10**3))
      A(5,7)=(-ALF31*XC13)/(AI*SY10)
      A(5,8)=(-ALF32*XC13)/(AI*SY10)
      A(5,9)=(ALF32*XC12+ALF31*XC11)/(AI*SY10)
      A(5,10)=(-ALF31*XC23)/(AI*SY10)
      A(5,11)=(-ALF32*XC23)/(AI*SY10)
      A(5,12)=(ALF32*XC22+ALF31*XC21)/(AI*SY10)
      A(6,7)=(-SY8*XC13)/(AI3*SY10)
     1  -A(4,7)
      A(6,8)=(CY8*XC13)/(AI3*SY10)
     1  -A(4,8)
      A(6,9)=(-CY8*XC12+SY8*XC11)/(AI3*SY10)
     1  -A(4,9)
      A(6,10)=(-SY8*XC23)/(AI3*SY10)
     1  -A(4,10)
      A(6,11)=(CY8*XC23)/(AI3*SY10)
     1  -A(4,11)
      A(6,12)=(-CY8*XC22+SY8*XC21)/(AI3*SY10)
     1  -A(4,12)
      DO 220 I=1,6
      DO 221 J=1,6
 221  AST(I,J)=A(I,J+6)
      DARY(I+6)=0
 220  FC(I)=0
      GO TO (20,20,60,60,60)NUMODE
C
CCC   NUMODE=1 OR NUMODE=2
C
 20   DO 21 J=1,3
 21   A(7,J)=ANRM(1,J)
      A(7,4)=-ANRM(1,1)*XC12+ANRM(1,2)*XC11
      A(7,5)=ANRM(1,1)*XC13*CY8+ANRM(1,2)*XC13*SY8
     1  -ANRM(1,3)*(XC12*SY8+XC11*CY8)
      A(7,6)=ANRM(1,1)*(XC13*SY8*SY10-XC12*CY10)
     1  +ANRM(1,2)*(XC11*CY10-XC13*CY8*SY10)
     2  +ANRM(1,3)*(XC12*CY8*SY10-XC11*SY8*SY10)
      DARY(7)=-AKC*DIRT(1)-XC11*15
     1 -ANRM(1,1)*XC13*(-Y7*Y9*SY8+Y7*Y11*CY8*SY10+Y9*Y11*SY8*CY10)
     1+ANRM(1,1)*XC12*(-Y9*Y11*SY10)
     2-ANRM(1,2)*XC11*(-Y9*Y11*SY10)
     3+ANRM(1,2)*XC13*(-Y7*Y9*CY8-Y7*Y11*SY8*SY10+Y9*Y11*CY8*CY10)
     4-ANRM(1,3)*XC12*(-Y7*Y9*CY8-Y7*Y11*SY8*SY10+Y9*Y11*CY8*CY10)
     5+ANRM(1,3)*XC11*(-Y7*Y9*SY8+Y7*Y11*CY8*SY10+Y9*Y11*SY8*CY10)
      GO TO (30,40)NUMODE
C
CCC   NUMODE=1
C
 30   DO 31 J=1,3
      A(8,J+6)=AMUSL*ANRM(1,J)+PRLL(1,J)
 31   A(9,J+6)=PERP(1,J)
      N=9
      GO TO 100
```

```
C
CC      NUMODE=2
C
 40     DO 41 J=1,3
 41     A(8,J)=PRLL(1,J)
        A(8,4)=-PRLL(1,1)*XC12+PRLL(1,2)*XC11
        A(8,5)=PRLL(1,1)*XC13*CY8+PRLL(1,2)*XC13*SY8
       1   -PRLL(1,3)*(XC12*SY8+XC11*CY8)
        A(8,6)=PRLL(1,1)*(XC13*SY8*SY10-XC12*CY10)
       1   +PRLL(1,2)*(XC11*CY10-XC13*CY8*SY10)
       2   +PRLL(1,3)*(XC12*CY8*SY10-XC11*SY8*SY10)
        DARY(8)=
       1 -PRLL(1,1)*XC13*(-Y7*Y9*SY8+Y7*Y11*CY8*SY10+Y9*Y11*SY8*CY10)
       1+PRLL(1,1)*XC12*(-Y9*Y11*SY10)
       2-PRLL(1,2)*XC11*(-Y9*Y11*SY10)
       3+PRLL(1,2)*XC13*(-Y7*Y9*CY8-Y7*Y11*SY8*SY10+Y9*Y11*CY8*CY10)
       4-PRLL(1,3)*XC12*(-Y7*Y9*CY8-Y7*Y11*SY8*SY10+Y9*Y11*CY8*CY10)
       5+PRLL(1,3)*XC11*(-Y7*Y9*SY8+Y7*Y11*CY8*SY10+Y9*Y11*SY8*CY10)
        DO 42 J=1,3
 42     A(9,J)=PERP(1,J)
        A(9,4)=-PERP(1,1)*XC12+PERP(1,2)*XC11
        A(9,5)=PERP(1,1)*XC13*CY8+PERP(1,2)*XC13*SY8
       1   -PERP(1,3)*(XC12*SY8+XC11*CY8)
        A(9,6)=PERP(1,1)*(XC13*SY8*SY10-XC12*CY10)
       1   +PERP(1,2)*(XC11*CY10-XC13*CY8*SY10)
       2   +PERP(1,3)*(XC12*CY8*SY10-XC11*SY8*SY10)
        DARY(9)=
       1 -PERP(1,1)*XC13*(-Y7*Y9*SY8+Y7*Y11*CY8*SY10+Y9*Y11*SY8*CY10)
       1+PERP(1,1)*XC12*(-Y9*Y11*SY10)
       2-PERP(1,2)*XC11*(-Y9*Y11*SY10)
       3+PERP(1,2)*XC13*(-Y7*Y9*CY8-Y7*Y11*SY8*SY10+Y9*Y11*CY8*CY10)
       4-PERP(1,3)*XC12*(-Y7*Y9*CY8-Y7*Y11*SY8*SY10+Y9*Y11*CY8*CY10)
       5+PERP(1,3)*XC11*(-Y7*Y9*SY8+Y7*Y11*CY8*SY10+Y9*Y11*SY8*CY10)
        N=9
        GO TO 100
C
CC      NUMODE=3,NUMODE=4 OR NUMODE=5
C
 60     DO 61 I=1,2
        DO 62 J=1,3
 62     A(I+6,J)=ANRM(I,J)
        A(I+6,4)=-ANRM(I,1)*(XC(I,2)-Y(4))
       1   +ANRM(I,2)*(XC(I,1)-Y(2))
        A(I+6,5)=ANRM(I,1)*(XC(I,3)-Y(6))*CY8
       1   +ANRM(I,2)*(XC(I,3)-Y(6))*SY8
       2   -ANRM(I,3)*((XC(I,2)-Y(4))*SY8+(XC(I,1)-Y(2))*CY8)
        A(I+6,6)=ANRM(I,1)*((XC(I,3)-Y(6))*SY8*SY10
       1   -(XC(I,2)-Y(4))*CY10)
       2   +ANRM(I,2)*((XC(I,1)-Y(2))*CY10
       3   -(XC(I,3)-Y(6))*CY8*SY10)
       4   +ANRM(I,3)*((XC(I,2)-Y(4))*CY8*SY10
       5   -(XC(I,1)-Y(2))*SY8*SY10)
        DARY(I+6)=-AKC*DIRT(I)-XC(I,1)*15
       1 -ANRM(I,1)*(XC(I,3)-Y(6))
       2*(-Y7*Y9*SY8+Y7*Y11*CY8*SY10+Y9*Y11*SY8*CY10)
       3+ANRM(I,1)*(XC(I,2)-Y(4))*(-Y9*Y11*SY10)
       4-ANRM(I,2)*(XC(I,1)-Y(2))*(-Y9*Y11*SY10)
       5+ANRM(I,2)*(XC(I,3)-Y(6))
       6*(-Y7*Y9*CY8-Y7*Y11*SY8*SY10+Y9*Y11*CY8*CY10)
       7-ANRM(I,3)*(XC(I,2)-Y(4))
       8*(-Y7*Y9*CY8-Y7*Y11*SY8*SY10+Y9*Y11*CY8*CY10)
       9+ANRM(I,3)*(XC(I,1)-Y(2))
       A*(-Y7*Y9*SY8+Y7*Y11*CY8*SY10+Y9*Y11*SY8*CY10)
 61     CONTINUE
C
CC      CHECK THAT CONTACT NORMALS NOT EQUAL
C
        CANTOL=.99
        CANRM=0
        DO 63 J=1,3
 63     CANRM=CANRM+ANRM(1,J)*ANRM(2,J)
        IF(CANRM.LE.CANTOL)GO TO 65
        DO 64 J=1,6
 64     A(8,J)=0
        DO 66 J=1,3
        A(8,J+6)=ANRM(1,J)
 66     A(8,J+9)=-ANRM(2,J)
        DARY(8)=0
 65     CONTINUE
        GO TO(70,80,90)NUMODE-2
C
CC      NUMODE=3
C
 70     DO 71 J=1,3
        A(9,J+6)=AMUSL*ANRM(1,J)+PRLL(1,J)
```

```
      A(10,J+9)=AMUSL*ANRM(2,J)+PRLL(2,J)
      A(11,J+6)=PERP(1,J)
      A(12,J+9)=PERP(2,J)
 71   CONTINUE
      N=12
      GO TO 100
C
CCC   NUMODE=4
C
C
 80   DO 81 J=1,3
 81   A(9,J)=PRLL(1,J)
      A(9,4)=-PRLL(1,1)*XC12+PRLL(1,2)*XC11
      A(9,5)=PRLL(1,1)*XC13*CY8+PRLL(1,2)*XC13*SY8
     1  -PRLL(1,3)*(XC12*SY8+XC11*CY8)
      A(9,6)=PRLL(1,1)*(XC13*SY8*SY10-XC12*CY10)
     1  +PRLL(1,2)*(XC11*CY10-XC13*CY8*SY10)
     2  +PRLL(1,3)*(XC12*CY8*SY10-XC11*SY8*SY10)
      DARY(9)=
     1 -PRLL(1,1)*XC13*(-Y7*Y9*SY8+Y7*Y11*CY8*SY10+Y9*Y11*SY8*CY10)
     1+PRLL(1,1)*XC12*(-Y9*Y11*SY10)
     2-PRLL(1,2)*XC11*(-Y9*Y11*SY10)
     3+PRLL(1,2)*XC13*(-Y7*Y9*CY8-Y7*Y11*SY8*SY10+Y9*Y11*CY8*CY10)
     4-PRLL(1,3)*XC12*(-Y7*Y9*CY8-Y7*Y11*SY8*SY10+Y9*Y11*CY8*CY10)
     5+PRLL(1,3)*XC11*(-Y7*Y9*SY8+Y7*Y11*CY8*SY10+Y9*Y11*SY8*CY10)
      DO 82 J=1,3
 82   A(10,J)=PERP(1,J)
      A(10,4)=-PERP(1,1)*XC12+PERP(1,2)*XC11
      A(10,5)=PERP(1,1)*XC13*CY8+PERP(1,2)*XC13*SY8
     1  -PERP(1,3)*(XC12*SY8+XC11*CY8)
      A(10,6)=PERP(1,1)*(XC13*SY8*SY10-XC12*CY10)
     1  +PERP(1,2)*(XC11*CY10-XC13*CY8*SY10)
     2  +PERP(1,3)*(XC12*CY8*SY10-XC11*SY8*SY10)
      DARY(10)=
     1 -PERP(1,1)*XC13*(-Y7*Y9*SY8+Y7*Y11*CY8*SY10+Y9*Y11*SY8*CY10)
     1+PERP(1,1)*XC12*(-Y9*Y11*SY10)
     2-PERP(1,2)*XC11*(-Y9*Y11*SY10)
     3+PERP(1,2)*XC13*(-Y7*Y9*CY8-Y7*Y11*SY8*SY10+Y9*Y11*CY8*CY10)
     4-PERP(1,3)*XC12*(-Y7*Y9*CY8-Y7*Y11*SY8*SY10+Y9*Y11*CY8*CY10)
     5+PERP(1,3)*XC11*(-Y7*Y9*SY8+Y7*Y11*CY8*SY10+Y9*Y11*SY8*CY10)
      DO 83 J=1,3
      A(11,J+9)=AMUSL*ANRM(2,J)+PRLL(2,J)
 83   A(12,J+9)=PERP(2,J)
      N=12
      GO TO 100
C
CC    NUMODE=5
C
C
 90   DO 91 I=1,2
      DO 92 J=1,3
 92   A(I+8,J)=PRLL(I,J)
      A(I+8,4)=-PRLL(I,1)*(XC(I,2)-Y(4))
     1  +PRLL(I,2)*(XC(I,1)-Y(2))
      A(I+8,5)=PRLL(I,1)*(XC(I,3)-Y(6))*CY8
     1  +PRLL(I,2)*(XC(I,3)-Y(6))*SY8
     2  -PRLL(I,3)*((XC(I,2)-Y(4))*SY8+(XC(I,1)-Y(2))*CY8)
      A(I+8,6)=PRLL(I,1)*((XC(I,3)-Y(6))*SY8*SY10
     1  -(XC(I,2)-Y(4))*CY10)
     2  +PRLL(I,2)*((XC(I,1)-Y(2))*CY10
     3  -(XC(I,3)-Y(6))*CY8*SY10)
     4  +PRLL(I,3)*((XC(I,2)-Y(4))*CY8*SY10
     5  -(XC(I,1)-Y(2))*SY8*SY10)
      DARY(I+8)=
     1-PRLL(I,1)*(XC(I,3)-Y(6))
     2*(-Y7*Y9*SY8+Y7*Y11*CY8*SY10+Y9*Y11*SY8*CY10)
     3+PRLL(I,1)*(XC(I,2)-Y(4))*(-Y9*Y11*SY10)
     4-PRLL(I,2)*(XC(I,1)-Y(2))*(-Y9*Y11*SY10)
     5+PRLL(I,2)*(XC(I,3)-Y(6))
     6*(-Y7*Y9*CY8-Y7*Y11*SY8*SY10+Y9*Y11*CY8*CY10)
     7-PRLL(I,3)*(XC(I,2)-Y(4))
     8*(-Y7*Y9*CY8-Y7*Y11*SY8*SY10+Y9*Y11*CY8*CY10)
     9+PRLL(I,3)*(XC(I,1)-Y(2))
     A*(-Y7*Y9*SY8+Y7*Y11*CY8*SY10+Y9*Y11*SY8*CY10)
 91    CONTINUE
      DO 93 I=1,2
      DO 94 J=1,3
 94   A(I+10,J)=PERP(I,J)
      A(I+10,4)=-PERP(I,1)*(XC(I,2)-Y(4))
     1  +PERP(I,2)*(XC(I,1)-Y(2))
      A(I+10,5)=PERP(I,1)*(XC(I,3)-Y(6))*CY8
     1  +PERP(I,2)*(XC(I,3)-Y(6))*SY8
     2  -PERP(I,3)*((XC(I,2)-Y(4))*SY8+(XC(I,1)-Y(2))*CY8)
      A(I+10,6)=PERP(I,1)*((XC(I,3)-Y(6))*SY8*SY10
     1  -(XC(I,2)-Y(4))*CY10)
     2  +PERP(I,2)*((XC(I,1)-Y(2))*CY10
     3  -(XC(I,3)-Y(6))*CY8*SY10)
```

```
     4   +PERP(I,3)*((XC(I,2)-Y(4))*CY8*SY10
     5   -(XC(I,1)-Y(2))*SY8*SY10)
      DARY(I+10)=
     1 -PERP(I,1)*(XC(I,3)-Y(6))
     2*(-Y7*Y9*SY8+Y7*Y11*CY8*SY10+Y9*Y11*SY8*CY10)
     3+PERP(I,1)*(XC(I,2)-Y(4))*(-Y9*Y11*SY10)
     4-PERP(I,2)*(XC(I,1)-Y(2))*(-Y9*Y11*SY10)
     5+PERP(I,2)*(XC(I,3)-Y(6))
     6*(-Y7*Y9*CY8-Y7*Y11*SY8*SY10+Y9*Y11*CY8*CY10)
     7-PERP(I,3)*(XC(I,2)-Y(4))
     8*(-Y7*Y9*CY8-Y7*Y11*SY8*SY10+Y9*Y11*CY8*CY10)
     9+PERP(I,3)*(XC(I,1)-Y(2))
     A*(-Y7*Y9*SY8+Y7*Y11*CY8*SY10+Y9*Y11*SY8*CY10)
  93  CONTINUE
      N=12
      GO TO 100
C
CCC   DETERMINING FORCE VALUES
C
 100  CONTINUE
      NM=12
      CALL INVERT(NM,N,A,AINV,DETERM)
      DO 101 I=7,N
      SUM=0
      DO 102 J=1,N
 102  SUM=SUM+AINV(I,J)*DARY(J)
 101  FC(I-6)=SUM
C
CCC   CHECK SIGN OF FORCES
C
      IF(FC(1).GT.0)GO TO 112
      DO 111 I=1,3
 111  FC(I)=-FC(I)
 112  IF(NUMODE.LT.3.)GO TO 115
      IF(FC(4).GT.0)GO TO 115
      DO 114 I=4,6
 114  FC(I)=-FC(I)
 115  CONTINUE
C
CCC   CHECK THAT STATIC FRICTION COEFFICIENT NOT EXCEEDED
C
      GO TO (116,130,116,135,140) NUMODE
 130  FCN1=FC(1)*ANRM(1,1)+FC(2)*ANRM(1,2)+FC(3)*ANRM(1,3)
      FRAT1=(SQRT(FC(1)**2+FC(2)**2+FC(3)**2-FCN1**2))/FCN1
      IF(FRAT1.GT.AMUST)NUMODE=1
      IF(NUMODE.EQ.1)GO TO 1
      GO TO 116
C
 135  FCN1=FC(1)*ANRM(1,1)+FC(2)*ANRM(1,2)+FC(3)*ANRM(1,3)
      FRAT1=(SQRT(FC(1)**2+FC(2)**2+FC(3)**2-FCN1**2))/FCN1
      IF(FRAT1.GT.AMUST)NUMODE=3
      IF(NUMODE.EQ.3)GO TO 1
      GO TO 116
C
 140  FCN1=FC(1)*ANRM(1,1)+FC(2)*ANRM(1,2)+FC(3)*ANRM(1,3)
      FCN2=FC(4)*ANRM(2,1)+FC(5)*ANRM(2,2)+FC(6)*ANRM(2,3)
      FRAT1=(SQRT(FC(1)**2+FC(2)**2+FC(3)**2-FCN1**2))/FCN1
      FRAT2=(SQRT(FC(4)**2+FC(5)**2+FC(6)**2-FCN2**2))/FCN2
      IF((FRAT1.GT.AMUST).AND.(FRAT2.GT.AMUST))NUMODE=3
      IF((FRAT1.GT.AMUST).AND.(FRAT2.LE.AMUST))NUMODE=6
      IF((FRAT1.LE.AMUST).AND.(FRAT2.GT.AMUST))NUMODE=4
      GO TO (1,1,116,141) NUMODE-2
 141  DO 142 I=1,3
      UR1=XC(1,I)
      UR2=ANRM(1,I)
      UR3=PRLL(1,I)
      UR4=PERP(1,I)
      XC(1,I)=XC(2,I)
      ANRM(1,I)=ANRM(2,I)
      PRLL(1,I)=PRLL(2,I)
      PERP(1,I)=PERP(2,I)
      XC(2,I)=UR1
      ANRM(2,I)=UR2
      PRLL(2,I)=UR3
 142  PERP(2,I)=UR4
      NUMODE=4
      GO TO 1
 116  CONTINUE
C
CCC   DETERMINING DERY VALUES
C
      DO 120 I=1,6
      SUM=0
      DO 121 J=1,6
 121  SUM=SUM-AST(I,J)*FC(J)
```

```
  120   DERY(2*I-1)=SUM+DARY(I)
C
        RETURN
        END
```

```
      SUBROUTINE OUTP(X,Y,DERY)
C*****************************************************
C*                                                   *
C*     SUBROUTINE OUTP OUTPUTS VALUES OF             *
C*     Y AND DERY AT TIME X                          *
C*                                                   *
C*****************************************************
C
      COMMON AC1,AC2,AC3,AC4,AC5,AC6,AC7,AC8,AC9,
     1AD1,AD2,AH,AI,AI3,AI4,
     2AK1,AK2,AK3,AK4,AK5,AK6,AK7,AK8,AK9,AKC,
     3AK26,AK35,AK53,AK62,ALF(3,3),
     4AM,AM1,AMUSL,AMUST,ANRM(2,3),ARH,ARP,
     5CY8,CY10,CY12,DIRT(2),GRAV,H,HLST,
     6MODE,NDIM,NUC,NUMODE,NUNUC,PERP(2,3),
     7PRLL(2,3),PRMT(5),SLIDE(2),SY8,SY10,SY12,
     8THINC,THOLD(2),XC(2,3),
     9YE2,YE8,YE10,YE14,YE16,YE18
      DIMENSION Y(18),DERY(18)
C
      RETURN
C
      END
```

APPENDIX 2

LINEARITY TEST OF STRAIN GAUGE IN NOTCH

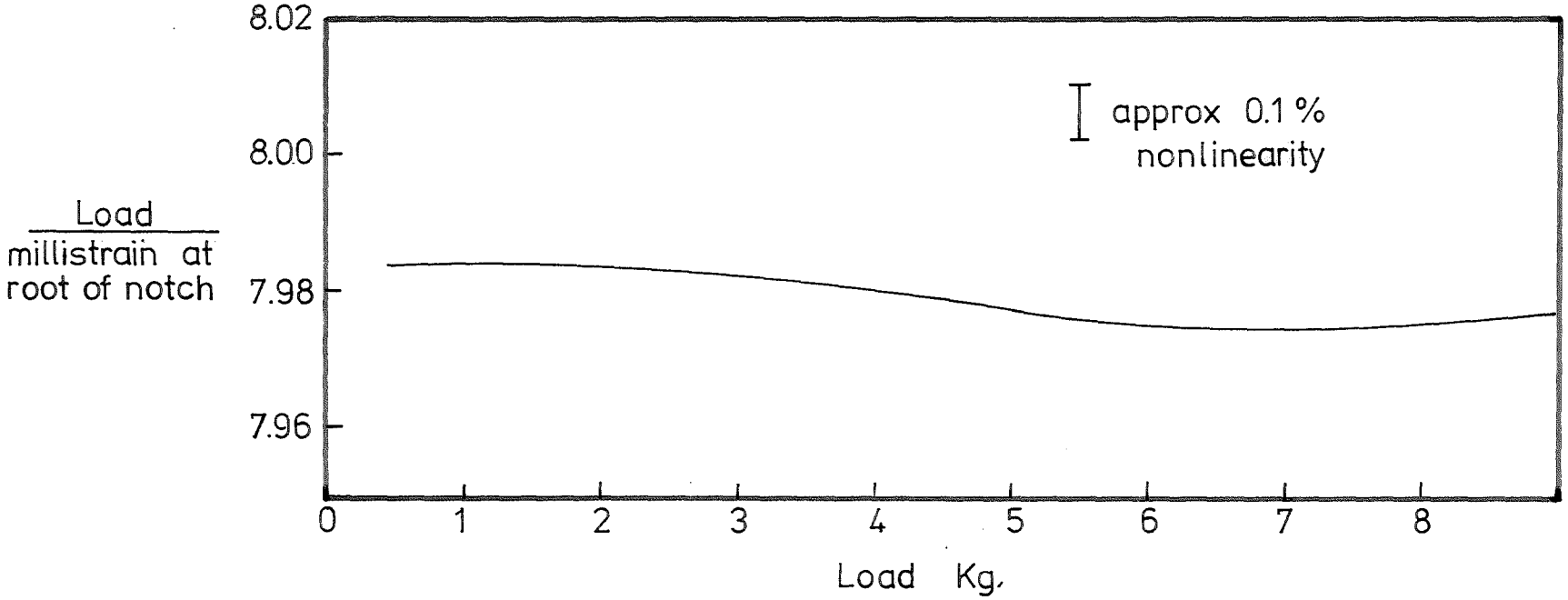

APPENDIX 2

Linearity of strain measurement

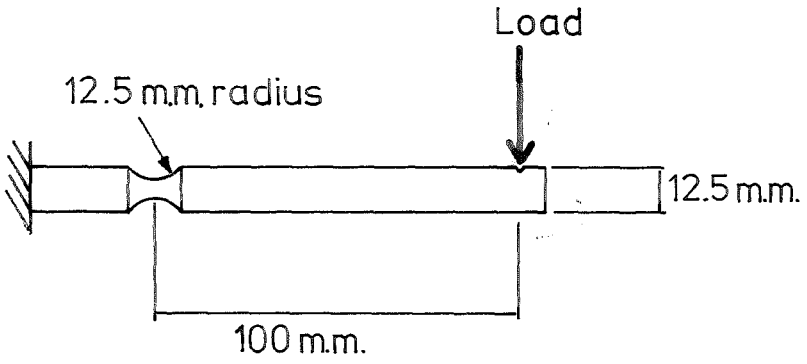

REFERENCES

1. Nitzan D. & Rosen C. A.
   Programmable industrial automation I.E.E.E. Trans. on Computers, Vol. C-25, No.12, Dec. 1976, pp. 1259 - 1270.

2. Seko K. & Toda H.
   Development and application report in the arc welding and assembly operation by the high performance robot. Proc. 4th Int. Symp. on Industrial Robots, Tokyo, Japan, Nov. 1974, pp. 487 - 496.

3. Heginbotham W. B. et al.
   A versatile variable mission assembly machine. Proc. 3rd Conf. on Industrial Robot Technology and 6th Int. Symp. on Industrial Robots, Nottingham, March 1976, pp. 54 - 60.

4. Takeyasu K., Goto T. & Inoyama T.
   Precise insertion control robot and its application. A.S.M.E. Trans., Series B, Journal of Engineering for Industry, Vol. 98, No. 4, Nov. 1976, pp. 1313 - 1318.

5. Olsztyn J. T. et. al.
   An application of computer vision to a simulated assembly task. 1st Int. Joint Conf. on Pattern Recognition, Washington 1973, pp. 505 - 513.

6. Kinoshita G., Aida S. & Mori M.
   A pattern classification by dynamic tactile sense information processing. Pattern Recognition Vol. 7, p.243 - 251.

7. Okada T. & Tsuchiya S.
   Object recognition by grasping. Pattern Recognition, Vol. 9, No. 3, pp. 111 - 119.

8. Stojiljkovic Z. & Saletic D.
   Learning to recognize patterns by Belgrade hand prosthesis. Proc. 5th Int. Symp. on Industrial Robots, Chicago, Sept. 1975, pp. 407 - 413.

9. Ejiri M. etal.
A prototype intelligent robot that assembles objects from plan drawings. I.E.E.E. Trans. on Computers, Vol. C-21, No. 2, Feb. 1972, pp. 161 - 170.

10. Ambler A. P. et. al.
A versatile system for computer controlled assembly. Artificial Intelligence, Vol. 6, No. 2, pp. 129 - 156.

11. Nevins J. L. & Whitney, D. E.
Information and control issues of adaptable programmable assembly systems for manufacturing and teleoperator applications. Mechanism and Machine Theory, 1977, Vol. 12, No. 1, pp. 27 - 43.

12. Simunovic S.
Force information in assembly processes. Proc. 5th Int. Symp. on Industrial Robots, Chicago, Sept. 1975, pp. 415 - 431.

13. Herrman G. & Schraft R.
Industrial robots - requirements vs present situation. Proc. 2nd Conf. on Industrial Robot Technology, Birmingham, March 1974, pp. 15 - 24.

14. Huber R. P. O.
Analysis of the future of robots and artificial intelligence. Proc. 1st Conf. on Industrial Robot Technology, Nottingham, March 1974, pp. 239 - 253.

15. Driscoll L. C.
Projecting blue-collar robot markets and applications. Proc. 2nd Conf. on Industrial Robot Technology, Birmingham, March 1974, pp. F21 - F32.

16. Heginbotham W. G.
Factors influencing economic exploitation of industrial automation. Proc. 1st Conf. on Industrial Robot Technoloby Nottingham, March 1973, pp. 197 - 206.

17. Thulin M. & Kjellberg T.
Design of manufacturing systems with robots. Proc. 2nd Conf. on Industrial Robot Technology, Birmingham, March 1974, pp. A37 - A52.

18. Hanify D. W.
Economic systems analysis - a general purpose approach to the determinations of economic risk. Proc. 2nd. Conf. on Industrial Robot Technology, Birmingham, March 1974, pp. F1 - F8.

19. Bryant S. & Carne E. B.
Some observations on the economics of complex industrial robots. Proc. 2nd Conf. on Industrial Robot Technology, Birmingham, March 1974, pp. F9 - F20.

20. Heginbotham W. B. & Gatehouse D. W.
Programmable assembly machines - have they a future? Proc. 2nd. Conf. on Industrial Robot Technology, Birmingham, March 1974, pp. A1 - A14.

21. Kornfeld J. P. & Magod E. L.
Robotry and automation - key to international competition. Proc. of 2nd Int. Symp. on Industrial Robots, Chicago, May 1972, pp. 31 - 47.

22. Stout K. J., Lee S. F. & Charnley C. J.
Robots - current trends and industrial requirements. Machinery and Production Engineering, 12 May 1976, pp. 440 - 446.

23. Jonsson B.
Labour and technological change. Proc. 1st Conf. on Industrial Robot Technology, Nottingham, March 1973, pp. 231 - 238.

24. Schumacher E. F.
Small is Beautiful.
Blond and Briggs 1973, Great Britain.

25. Peterson R. A.
The Industrial Order and Social Policy, Prentice Hall, 1973.

26. Obenhaus V.
Ethics for an Industrial Age - A Christian Inquiry.
John Wiley and Sons 1967.

27. Cooley, M. J.
Industrial robots - a trade union view of the social and industrial implications.
Proc. 1st Conf. on Industrial Robot Technology, Nottingham, March 1973, pp. 223 - 230.

28. Beer S.
Platform for Change.
John Wiley and Sons, 1975.

29. Bruck H. W.
Technology and urban institutions : a questioning of the great gloppata - gloppata machine.
Technology and Social Institutions, I.E.E.E. Press 1974.
pp. 62 - 74.

30. Ashley J. R.
Mechanization of the assembly process in medium and small batch production.
Proc. Royal Soc. London, A317, pp. 455 - 475 (1970).

31. Whitney D. E.
Robots with sensory feedback.
Proc. Int. Conf. on Systems, Man and Cybernetics, Texas, Oct 1974, pp. 44 - 47.

32. Wong, P. C.
Peg hole assembly; an investigation into tactile methods.
Ph.D. Thesis, University of Canterbury 1975.

33. McCallion H. & Wong P. C.
Some thoughts on the automatic assembly of a peg and a hole.
Proc. of 4th World Congress on The Theory of Machines & Mechanisms.
Univ. Newcastle upon Tyne 1975, pp. 347 - 352.

34. Bowden & Tabor
The friction and lubrication of solids, Part 1.
Oxford University Press 1971.

35. Andrew C., Cockburn J. A. & Wareing A. E.
Metal surfaces in contact under normal forces - some dynamic stiffness and damping characteristics.
Proc. of Conf. - Properties and Metrology of Surfaces.
I. Mech. E. Proc. 67-68, Vol. 182 Part 3K, pp. 92 - 100.

36. Godfrey D.
Vibration reduces metal to metal contact and causes an apparent reduction in friction.
A.S.L.E. Trans. 1967 Vol.10, pp. 183 - 192.

37. Karelin N. M. & Girel A. M.
Automation of component assembly operations in a rotating magnetic field.
Russian Eng. Journal, Vol. 54, No.10, pp. 53 - 56.

38. Andreev G. Ya.
Assembling joints by magnetic methods of orientation.
Russian Eng. Journal, Vol.56, No.4, pp. 68 - 71.

39. Karelin N. M. & Girel A. M.
The accurate alignment of parts for automatic assembly.
Russian Eng. Journal, Vol. 47, No. 9, pp. 73 - 76.

40. Savishchenko V. M. & Bespalov V. G.
The orientation of components for automatic assembly.
Russian Eng. Journal, Vol.45, No.5, pp. 50 - 52.

41. Andreev G. Ha & Laktionov N. M.
Contact stresses during automatic assembly.
Russian Eng. Journal, Vol.49, No.11, pp.57 - 60.

42. Yakhimovich V. A. & Ponomarchuk G. B.
Ultrasonic assembly.
Russian Eng. Journal, Vol.52, No.7, pp. 50 - 54.

43. Bishop R. E. D. & Johnson D. C.
The Mechanics of Vibration.
Cambridge University Press 1960.

44. McCallion H.
Vibration of Linear Mechanical Systems.
Longman, London, 1973.

45. Arnold R. N. & Maunder L.
Gyrodynamics and its Engineering Applications.
Academic Press, New York and London, 1961.

46. Comba P. G.
A procedure for detecting intersections of three-dimensional objects.
Journal of the Association for Computing Machinery, Vol.15, No.3, July 1968, pp. 354 - 366.

47. Bisshop K. E.
Rodrigues' formula and the screw matrix.
A.S.M.E. Trans, Series B, Journal of Engineering for Industry, Vol. 91, No. 1, Feb. 1969, pp. 179 - 185.

48. Thompson E. H.
An Introduction to the Algebra of Matrices with some Applications.
Adam Hilger, London, 1969.

49. Smith J. D. & Welbourn D. B.
A six component dynamometer.
Journal of Mechanical Engineering Science, Vol.12, No.2, 1970, pp. 143 - 145.

50. Mittmann H. M. et al.
A new device for simultaneous measurement of friction force, normal force and friction coefficient.
Wear, Vol.31, 1975, pp. 179 - 184.

51. Watson P. C. & Drake S. H.
Pedestal and wrist force sensors for automatic assembly.
Proc. 5th Int. Symp. on Industrial Robots, Chicago, Sept. 1975, pp. 507 - 511.

52. McEntire R. H.
Three dimension accuracy measurement methods for robots.
The Industrial Robot, Vol.3, No.3, Sept. 1976, pp. 105 - 112.

53. McCallion H. & Pham D. T.
On measuring errors in a placement task - the general spatial relationship between two rigid bodies.
The Industrial Robot, No.4, No.2, June 1977, pp. 86 - 92.